

# NAVAL POSTGRADUATE SCHOOL MONTEREY, CALIFORNIA



## DISSERTATION

**CALIFORNIA SEA BREEZE STRUCTURE AND ITS  
RELATION TO THE SYNOPTIC SCALE**

by

Michael D. Foster

September, 1996

Dissertation Supervisor:

Carlyle H. Wash

Approved for public release; distribution is unlimited.

DTIC QUALITY INSPECTED 3

19970212 096

# DISCLAIMER NOTICE



THIS DOCUMENT IS BEST QUALITY AVAILABLE. THE COPY FURNISHED TO DTIC CONTAINED A SIGNIFICANT NUMBER OF COLOR PAGES WHICH DO NOT REPRODUCE LEGIBLY ON BLACK AND WHITE MICROFICHE.

REPORT DOCUMENTATION PAGE			Form Approved OMB No. 0704-0188	
Public reporting burden for this collection of information is estimated to average 1 hour per response, including the time for reviewing instruction, searching existing data sources, gathering and maintaining the data needed, and completing and reviewing the collection of information. Send comments regarding this burden estimate or any other aspect of this collection of information, including suggestions for reducing this burden, to Washington Headquarters Services, Directorate for Information Operations and Reports, 1215 Jefferson Davis Highway, Suite 1204, Arlington, VA 22202-4302, and to the Office of Management and Budget, Paperwork Reduction Project (0704-0188) Washington DC 20503.				
1. AGENCY USE ONLY (Leave blank)	2. REPORT DATE September 1996	3. REPORT TYPE AND DATES COVERED Doctoral Dissertation		
4. TITLE AND SUBTITLE California Sea Breeze Structure and its Relation to the Synoptic Scale		5. FUNDING NUMBERS		
6. AUTHOR(S) Foster, Michael D.				
7. PERFORMING ORGANIZATION NAME(S) AND ADDRESS(ES) Naval Postgraduate School Monterey CA 93943-5000		8. PERFORMING ORGANIZATION REPORT NUMBER		
9. SPONSORING/MONITORING AGENCY NAME(S) AND ADDRESS(ES)		10. SPONSORING/MONITORING AGENCY REPORT NUMBER		
11. SUPPLEMENTARY NOTES The views expressed in this thesis are those of the author and do not reflect the official policy or position of the Department of Defense or the U.S. Government.				
12a. DISTRIBUTION/AVAILABILITY STATEMENT Approved for public release; distribution is unlimited.		12b. DISTRIBUTION CODE		
13. ABSTRACT (maximum 200 words) <p>The sea breeze structure was examined at several locations along the California coast during the summers of 1993-1995. The sea breeze was objectively classified as three distinct types: gradual, frontal and rapid onset. The sea breeze wind and virtual temperature structure were determined at the surface and the planetary boundary layer. Especially important were the identification of distinct local and regional-scale sea breeze circulations. To examine the role of the synoptic-scale wind patterns on the development of sea breeze type/structure, an objective classification scheme was developed and applied along the West Coast. The synoptic-scale classification scheme identified the long-term position of the eastern North Pacific Ocean anticyclone and significant north/south deviations that determined large-scale wind regimes. Using the classification scheme, the "continental" sea and land breezes, previously only seen in long term statistical analysis, emerged from NOGAPS model analysis fields. The role of the synoptic-scale wind circulation patterns in determining the sea breeze types was explored. The roles of coastline geometry and inland heating sources was determined to be essential in the development and understanding of the sea breeze circulation types.</p>				
14. SUBJECT TERMS Sea-breeze, Marine Atmospheric Boundary Layer, Mesoscale circulations, Thermally-induced circulations, Synoptic classification, Sea-breeze classification.			15. NUMBER OF PAGES 199	
			16. PRICE CODE	
17. SECURITY CLASSIFICATION OF REPORT Unclassified	18. SECURITY CLASSIFICATION OF THIS PAGE Unclassified	19. SECURITY CLASSIFICATION OF ABSTRACT Unclassified	20. LIMITATION OF ABSTRACT UL	





Approved for public release; distribution is unlimited.


**CALIFORNIA SEA BREEZE STRUCTURE AND ITS RELATION TO THE SYNOPTIC SCALE**

Michael D. Foster  
Lieutenant Commander, United States Navy  
B.S., United States Naval Academy, 1982  
M.S., Naval Postgraduate School, 1993

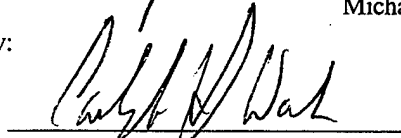
Submitted in partial fulfillment  
of the requirements for the degree of

**DOCTOR OF PHILOSOPHY IN METEOROLOGY**  
from the  
**NAVAL POSTGRADUATE SCHOOL**  
September, 1996

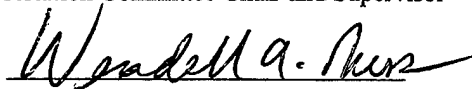
Author:


  
Michael D. Foster

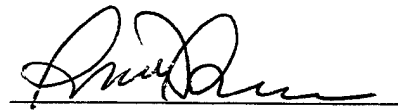
Approved by:

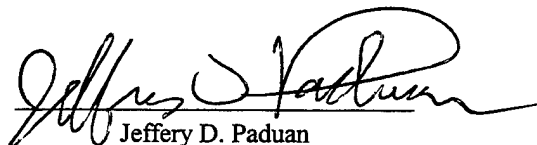
  
Carlyle H. Wash  
Professor of Meteorology

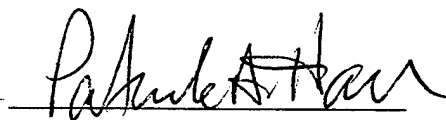
Dissertation Committee Chair and Supervisor

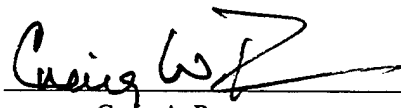
  
Wendell A. Nuss  
Associate Professor of Meteorology

  
Kenneth L. Davidson  
Professor of Meteorology

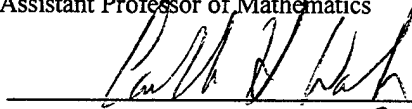
  
Philip A. Durkee  
Associate Professor of Meteorology

  
Jeffery D. Paduan  
Professor of Oceanography

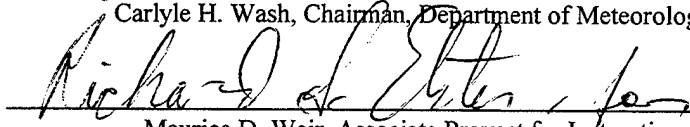
  
Patrick A. Harr  
Assistant Professor of Meteorology

  
Craig A. Rasmussen  
Assistant Professor of Mathematics

Approved by:

  
Carlyle H. Wash, Chairman, Department of Meteorology

Approved by:

  
Maurice D. Weir, Associate Provost for Instruction

DTIC QUALITY INSPECTED 3



## ABSTRACT

The sea breeze structure was examined at several locations along the California coast during the summers of 1993-1995. The sea breeze was objectively classified as three distinct types: gradual, frontal and rapid onset. The sea breeze wind and virtual temperature structure were determined at the surface and throughout the planetary boundary layer. Distinct local and regional-scale sea breeze circulations were identified for each sea breeze classification. To examine the role of the synoptic-scale wind patterns on the development of sea breeze type/structure, an objective classification scheme was developed and applied along the west coast of California. The synoptic-scale classification scheme associated large-scale wind regimes with variability in the position of the eastern North Pacific Ocean anticyclone. Using the classification scheme, the "continental" sea and land breezes, previously only seen in long term statistical analysis, emerged as important large-scale circulation modes. The continental land/sea breeze was previously only seen in long term statistical analysis. The role of the synoptic-scale wind circulation patterns in determining the sea breeze types was explored. The variability in coastline geometry and inland heating sources was determined to be essential in the development and understanding of the sea breeze circulation types.



## TABLE OF CONTENTS

I. INTRODUCTION .....	1
II. THERMALLY-INDUCED SEA BREEZE CIRCULATIONS .....	5
A.    INFLUENCE OF SYNOPTIC-SCALE FLOW ON THE SEA BREEZE .....	8
B.    SEA BREEZE CLASSIFICATION STUDIES .....	11
III. DATA .....	17
A.    AUTOMATIC WEATHER STATION DATA .....	18
1.    Locations .....	18
2.    Data Processing .....	19
B.    RADAR WIND PROFILER .....	20
1.    Locations .....	21
2.    Data Processing .....	21
C.    RASS .....	21
D.    NOGAPS MODEL DATA .....	22
IV. SEA BREEZE STRUCTURE .....	25
A.    LOCAL FACTORS INFLUENCING THE SEA BREEZE .....	25
B.    SEA BREEZE CATEGORIES .....	27
1.    Frontal Sea Breeze .....	28
2.    Gradual .....	30
3.    Rapid Onset (category 12) .....	32

4.	Unclassified .....	32
C.	PROGRAM CHARACTERISTICS FOR SEA BREEZE DEPICTIONS .....	33
D.	CLASSIFICATION RESULTS .....	36
1.	Fort Ord .....	36
2.	Point Mugu .....	43
3.	Point Loma .....	46
V.	SYNOPTIC CHARACTERIZATION .....	51
A.	THEORETICAL BACKGROUND ON EOF'S .....	51
B.	VEOF DECOMPOSITION .....	53
C.	SYNOPTIC DESCRIPTIONS OF THE VEOF MODES .....	58
1.	Southerly Ridge .....	59
2.	Northerly Ridge .....	60
3.	Continental Land/Sea Breeze .....	61
4.	Enhanced/Weakened Alongshore Flow .....	63
5.	Relationships to Monthly Anomalies .....	63
VI.	RELATIONSHIP OF SEA BREEZE TO SYNOPTIC SCALE .....	67
A.	SEA BREEZE FREQUENCY ANALYSIS .....	67
B.	SYNOPTIC INFLUENCES ON SEA BREEZE TYPES .....	73
C.	OTHER FACTORS .....	77
VII.	CONCLUSIONS AND RECOMMENDATIONS .....	79
A.	SUMMARY AND CONCLUSIONS .....	79

B. RECOMMENDATIONS .....	81
APPENDIX. STANDARD DEVIATION AND MEAN WIND ANOMALY PLOTS .....	153
LIST OF REFERENCES .....	171
INITIAL DISTRIBUTION LIST .....	177





## LIST OF FIGURES

- Figure 1.** Diagram of the sea and land breeze circulation (from Moran and Morgan 1986). . . . 83
- Figure 2.** Development of land/sea breeze circulation in an area of complex terrain (from Hsu 1988).  
 ..... 84
- Figure 3.** Wind hodographs for Point Mugu and Fort Ord from the summer of 1993. The hodograph is inscribed by the point of the hourly average wind vector. The speed of the wind is described by the radius from the center in m/s and the times in PST are marked by  $\oplus$ .  
 ..... 85
- Figure 4.** Koschmieder's depiction of frontal sea breeze development induced by off-shore gradient winds (from Wexler 1946, Koschmieder and Hornickel 1936, 1941, 1942). . . . . 86
- Figure 5.** Topography surrounding Monterey Bay. The location of the Fort Ord observing sight is marked with  $\oplus$ . The boundaries for offshore flow and westerly onshore flow are marked with the bold line. Heights are in m. .... 87
- Figure 6.** Topography surrounding Point Mugu observing site. The location of the observing site is marked with a  $\oplus$ . The boundaries for offshore, southerly sea breeze, and westerly sea breeze are diagramed. The local coastline at Point Mugu is east-west as shown in the insert. Heights are in m. .... 88
- Figure 7.** Topography surrounding the Point Loma observing site. The location of the observing site is marked with a  $\oplus$ . The boundaries delineating the offshore, southerly sea breeze, and westerly sea breeze are plotted. The insert is an enlargement of the topography at the observing site. Heights are in m. .... 89
- Figure 8.** Plot of Frontal-Southerly sea breeze at Point Mugu. Plotted are wind direction ( $^{\circ}$ T), wind speed (m/s), temperature ( $^{\circ}$ C) and dew point ( $^{\circ}$ C), and solar radiation (watts/m<sup>2</sup>). The onset

of the sea breeze is plotted with a vertical dash-dot line. The approximate sea breeze end time is shown in the vertical dashed line. Shifts of winds to different sea breeze directions are marked accordingly. Increases in wind speed of 4 kts in 30 min are marked by surges.

.....	90
<b>Figure 9.</b> As Figure 8, except Point Mugu Frontal-Southerly-Westerly sea breeze. ....	91
<b>Figure 10.</b> As Figure 8, except Fort Ord Frontal-Westerly sea breeze. ....	92
<b>Figure 11.</b> As Figure 8, except Fort Ord Gradual-Westerly sea breeze. ....	93
<b>Figure 12.</b> As Figure 8, except Point Loma Gradual-Southerly sea breeze. ....	94
<b>Figure 13.</b> As Figure 8, except Point Loma Gradual-Westerly-Southerly sea breeze. ....	95
<b>Figure 14.</b> As Figure 8, except Point Mugu Gradual-Southerly-Westerly sea breeze. ....	96
<b>Figure 15.</b> As Figure 8, except Fort Ord Rapid Onset sea breeze. ....	97
<b>Figure 16.</b> As Figure 8, except Fort Ord unclassified sea breeze (due to transition). ....	98
<b>Figure 17.</b> Distribution of sea breeze days for summers of 1993-1995 (363 days) at Fort Ord. Numbers in classification categories follows: 1-3 unclassified (missing data, transition, weak sea breeze), 4-7 frontal (southerly, westerly, southerly-westerly, westerly-southerly), 8-11 gradual (southerly, westerly, southerly-westerly, westerly-southerly), and 12 rapid onset. .....	99
<b>Figure 18.</b> Composite of Fort Ord wind and virtual temperature structure for 68 frontal-westerly sea breeze days. ....	100
<b>Figure 19.</b> As Figure 18, except 100 gradual-westerly sea breeze days. ....	101
<b>Figure 20.</b> As Figure 18, except 36 rapid onset sea breeze days. ....	102
<b>Figure 21.</b> Distributions of sea breeze onset times for summers of 1993-1995 at Fort Ord: a) all sea breeze days, b) frontal-westerly days, c) gradual-westerly days , and d) rapid onset days. .....	103

<b>Figure 22.</b> As Figure 21, except time of maximum wind. ....	104
<b>Figure 23.</b> As Figure 21, except maximum wind speed. ....	105
<b>Figure 24.</b> As Figure 21, except wind speed increase associated with sea breeze. ....	106
<b>Figure 25.</b> As Figure 21, except time of sea breeze end point. ....	107
<b>Figure 26.</b> As Figure 21, except duration of sea breeze. ....	108
<b>Figure 27.</b> Distribution of sea breeze days at Fort Ord for summers of 1993-1995: a) all three summers, b) 1993, c) 1994, d) 1995. Classifications as in Figure 17. ....	109
<b>Figure 28.</b> Sea breeze distribution for Point Loma for summer of 1993. Sea breeze classifications as in Figure 17. ....	110
<b>Figure 29.</b> Composite of Point Loma wind and virtual temperature structure for 29 frontal-westerly sea breeze days. ....	111
<b>Figure 30.</b> As Figure 29, except 28 frontal-southerly-westerly sea breeze days. ....	112
<b>Figure 31.</b> As Figure 29, except 36 gradual-westerly sea breeze days. ....	113
<b>Figure 32.</b> Distribution of sea breeze onset times for summer of 1993 at Point Mugu: a) all sea breeze days, b) frontal-westerly days, c) frontal-southerly-westerly, and d) gradual-westerly days. .....	114
<b>Figure 33.</b> As Figure 32, except time of maximum wind. ....	115
<b>Figure 34.</b> As Figure 32, except maximum wind speed. ....	116
<b>Figure 35.</b> As Figure 32, except wind speed increase associated with sea breeze. ....	117
<b>Figure 36.</b> As Figure 32, except time of sea breeze end point. ....	118
<b>Figure 37.</b> As Figure 32, except duration of sea breeze. ....	119
<b>Figure 38.</b> Sea breeze distribution for Point Loma for the summer of 1993. Sea breeze classification as Figure 18. ....	120

<b>Figure 39.</b> Composite of Point Loma winds and virtual temperature structure for 18 gradual-southerly sea breeze days. ....	121
<b>Figure 40.</b> As Figure 39, except 21 gradual-westerly sea breeze days. ....	122
<b>Figure 41.</b> Distribution of sea breeze onset times for summer of 1993 at Point Loma: a) all sea breeze days, b) gradual-southerly days, c) gradual-westerly days, and d) rapid onset days. ...	123
<b>Figure 42.</b> As Figure 39, except 15 rapid onset sea breeze days. ....	124
<b>Figure 43.</b> As Figure 42, except time of maximum wind. ....	125
<b>Figure 44.</b> As Figure 42, except maximum wind speed. ....	126
<b>Figure 45.</b> As Figure 42, except wind speed increase associated with sea breeze. ....	127
<b>Figure 46.</b> As Figure 42, except time of sea breeze end point. ....	128
<b>Figure 47.</b> As Figure 42, except duration of sea breeze. ....	129
<b>Figure 48.</b> NOGAPS 850 mb mean winds for the summers of 1993-1995. One wind barb equals 5 m s <sup>-1</sup> . ....	130
<b>Figure 49.</b> Contribution of VEOF modes 1-8 to the total variance by mode. +/- standard error is plotted as +’s. ....	131
<b>Figure 50.</b> Plot of the VEOF mode 1-3 principal components. ....	132
<b>Figure 51.</b> Histograms of the distribution of the principal components of VEOF modes 1-3 into 90° sectors (phases). The offset represents the amount of rotation of the first sector from 0°. ....	133
<b>Figure 52.</b> Plot of the distributions of the primary phases of VEOF modes 1-3 for every 12 hours. Plots of 2 and 4 in each mode represents principal components in the primary phases, while blanks represent components in the minor 1 and 3 phases. The solid line connects the magnitudes of the largest VEOF mode for each time period. ....	134

<b>Figure 53.</b> Anomaly 850 mb wind composites of the primary VEOF mode 1 phase 2 (southerly ridge regime - 130 members) and mode 1 phase 4 (northerly ridge regime - 131 members).	135
<b>Figure 54.</b> Total 850 mb wind composites of the primary VEOF mode 1 phase 2 (southerly ridge regime - 130 members) and mode 1 phase 4 (northerly ridge regime - 131 members).	136
<b>Figure 55.</b> Anomaly 850 mb wind composites of the primary VEOF mode 2 phase 2 (continental land breeze regime - 77 members) and mode 2 phase 4 (continental sea breeze regime - 79 members).	137
<b>Figure 56.</b> Total 850 mb wind composites of the primary VEOF mode 2 phase 2 (continental land breeze regime - 77 members) and mode 2 phase 4 (continental sea breeze regime - 79 members).	138
<b>Figure 57.</b> Anomaly 850 mb wind composites of the primary VEOF mode 3 phase 2 (reduced alongshore winds regime - 36 members) and mode 3 phase 4 (enhanced alongshore winds regime - 20 members).	139
<b>Figure 58.</b> Total 850 mb wind composites of the primary VEOF mode 3 phase 2 (reduced alongshore wind regime - 36 members) and mode 3 phase 4 (enhanced alongshore wind regime - 20 members).	140
<b>Figure 59.</b> NMC 850 mb height analysis for June 11, 1995, corresponds to southerly ridge regime.	141
<b>Figure 60.</b> DMSP satellite image for 18:06 UTC June 10, 1995 (corresponds to southerly ridge regime in Figure 59).	142
<b>Figure 61.</b> NMC 850 mb height analysis for July 25, 1993, corresponds to northerly ridge regime.	143

<b>Figure 62.</b> DMSP satellite image for 23:43 UTC July 24, 1993 (corresponds to northerly ridge regime in Figure 61).	144
<b>Figure 63.</b> NMC 850 mb height analysis for July 17, 1993, corresponds to continental land/sea breeze regime.	145
<b>Figure 64.</b> DMSP satellite image for 15:41 UTC July 17, 1993 (corresponds to continental land/sea breeze regime in Figure 63).	146
<b>Figure 65.</b> NMC 850 mb height analysis for July 2, 1993, corresponds to enhanced alongshore winds regime.	147
<b>Figure 66.</b> Contribution of strongest mode synoptic regimes by month for a) 1993, b) 1994, and c) 1995.	148
<b>Figure 67.</b> a) Mean monthly (top) and b) anomalous 850 mb winds for July 1993 (CDB 1993b).	149
<b>Figure 68.</b> As Figure 67, except August 1993 (CDB 1993c).	150
<b>Figure 69.</b> As Figure 67, except June 1994 (CDC 1994a).	151
<b>Figure 70.</b> Wind rose of the 12:00 UTC observed NOGAPS anomalous winds at Fort Ord for 1993-1995 from frontal and gradual sea breeze days (directions winds are from).	152
<b>Figure A1.</b> Wind speed standard deviations (m/s) associated with frontal-westerly sea breezes at Fort Ord.	154
<b>Figure A2.</b> Wind direction standard deviations (degrees) associated with frontal-westerly sea breezes at Fort Ord.	155
<b>Figure A3.</b> As Figure A1, except gradual-westerly sea breeze.	156
<b>Figure A4.</b> As Figure A2, except gradual-westerly sea breeze.	157
<b>Figure A5.</b> Plot of eigenvectors associated with VEOF mode 1.	158
<b>Figure A6.</b> As Figure A5, except VEOF mode 2.	159

<b>Figure A7.</b> As Figure A5, except VEOF mode 3. ....	160
<b>Figure A8.</b> a) Mean monthly (top) and b) anomalous (bottom) 850 mb winds for June 1993 (CBD 1993a). ....	161
<b>Figure A9.</b> As Figure A8, except June 1995 (CDB 1995a). ....	162
<b>Figure A10.</b> As Figure A8, except September 1995 (CDB 1995d). ....	163
<b>Figure A11.</b> As Figure A8, except September 1993 (CDB 1993d). ....	164
<b>Figure A12.</b> As Figure A8, except July 1994 (CDB 1994b). ....	165
<b>Figure A13.</b> As Figure A8, except August 1994 (CDB 1994c). ....	166
<b>Figure A14.</b> As Figure A8, except September 1994 (CDB 1994d). ....	167
<b>Figure A15.</b> As Figure A8, except July 1995 (CDB 1995b). ....	168
<b>Figure A16.</b> As Figure A8, except August 1995 (CDB 1995c). ....	169





## ACKNOWLEDGMENTS

I would like to express my sincerest thanks to my advisor, Professor Carlyle H. Wash for working with me on this project. His guidance and support have been instrumental in allowing me to develop, pursue, and accomplish my research goals. He has taught me how to remain focused on the trees and, yet, still see the forest overview. I hope to apply the research and organizational skills learned here to all of life's future challenges. I would also like to thank the members of the doctoral committee, Professors Kenneth L. Davidson, Wendell A. Nuss, Philip A. Durkee, Jeffery D. Paduan, Patrick A. Harr, and Craig A. Rasmussen for their constructive comments regarding this research, which produced a substantially better product. In particular, I would like to thank Patrick Harr for pointing me in the right direction when learning to apply Empirical Orthogonal Functions to meteorological wind data.

I am very thankful for the unselfish support provided by Richard L. Lind in dealing with the variety of surface and radar wind profiler data collected for this study. I would like to thank Mike Cook for his programming expertise in Matlab, who cheerfully helped whenever I sought his assistance. And, I would like to thank Mary Jordan for her timely help in producing some of the final figures used in this study.

Special thanks are due to my wife Bobbi. She endured my long work hours, my absences, and my distracted attention with grace and understanding. Her tremendous support and attention to detail freed my attention from the day-to-day distractions and allowed me to remain focused on the research at hand. Without her support, this research would not have been completed. Therefore, I dedicate this research to my loving wife, Bobbi Jean Foster.

## I. INTRODUCTION

Recently the United States Navy has conducted special relief and local operations in various coastal regions around the world. Coastal regions offer unique challenges for the Navy. Naval operations are vulnerable to short-range, quick-strike weapons (such as low-flying cruise missiles), and rapidly changing coastal meteorological conditions, which affect sensor, aircraft, and weapon performance. Knowledge of the subtle variations in meteorological conditions within the coastal zones will increase the effectiveness and survivability of those units operating there. Consequently, naval meteorologists have increased their focus on mesoscale influences in the coastal zones, especially in the lowest one to two kilometers of the atmosphere known as the planetary boundary layer (PBL).

Understanding the meteorology of the coastal regions of the world is very challenging since the PBL (the part in which most naval operations occur) is governed by both land and ocean influences. The U.S. Navy uses the large-scale NOGAPS (Navy Operational Global Atmospheric Prediction System) model to forecast synoptic-scale meteorological conditions around the world. Large-scale weather models lack the fine-scale resolution needed to depict the atmosphere on mesoscale spatial scales. Also their parameterization of physical processes is based on physical assumptions that describe synoptic-scale processes. The NOGAPS model is hampered by a lack of data, over open oceans and in the coastal zone, to properly initialize model starting fields. Errors in model initialization for coastal regions are due to rapidly changing horizontal and vertical gradients of atmospheric parameters, such as specific humidity and potential temperature, that are not well sampled. Mesoscale models for coastal forecasting are under development but are not operational. Like the larger-scale models, the mesoscale models will be hampered by insufficient data sampling over the oceans and in the coastal zones.

In order to discern meteorological conditions within the coastal regions, it is important to characterize the boundaries of the coastal zone. The coastal zone can be defined as that portion of the atmosphere that is influenced by the presence of a land and water interface. The thermally-induced sea/land breeze circulation is one of the larger coastal mesoscale phenomena and is usually present within the vicinity of the coastline.

The importance of the sea breeze to naval operations was shown as early as 2,400 years ago. In the battle of Salamis in 480 BC, the place and time of battle was chosen by a Greek naval commander so that the increase in wind speed associated with the sea breeze and corresponding building of the wave heights would enable slower, heavier Greek ships, which sat lower in the water, to out-manuever loftier, lighter, and faster Persian ships. The ensuing battle resulted in an overwhelming defeat of the Persian fleet (Simpson 1994).

The sea/land breeze is one of the most recognized atmospheric circulations. There have been many local and field studies of sea breeze behavior, particularly using surface data [see Simpson (1994), Hsu (1988), or Atkinson (1981)]. Also, there have been many numerical modeling studies of sea breeze evolution [see Estoque (1962), Arritt (1993) and others]. But until recently there have been few continuous observations of the PBL sea breeze wind fields and no way to routinely classify sea breeze evolution and explore relationships between local sea/land breeze structure and synoptic-scale circulations.

The need for better understanding of sea/land breeze circulations and the deployment of a new generation of observational tools motivates this research. Continuous surface observation systems and high-resolution vertical wind profilers can sample the coastal PBL frequent enough to routinely measure the rapidly evolving sea/land breeze circulation. Recently three different California coastal locations were equipped with both continuous surface and vertical wind profiler capability.

This study uses these continuous surface and wind profiler observations to objectively examine and characterize the thermally induced sea breeze circulations along the California coast during the summers of 1993, 1994, and 1995. Objective criteria are used to classify and categorize the observed sea breeze structure. Additional criteria are used to delineate summer synoptic-scale circulation patterns during the same time periods. The sea breeze categorization and synoptic-scale delineations provide unbiased mechanisms for linking the synoptic-scale circulation to the mesoscale sea breeze circulation.

The primary goals of this research are to increase the knowledge and understanding about the mesoscale structure and diurnal variations of the sea breeze circulation along the California coast and to objectively relate changes in the sea breeze circulation to changes in prevailing synoptic situation. Although this work is completed for the United States California coast, results can be likely applied to other subtropical west coasts around the world. As essential byproducts of this research, an objective sea breeze classification scheme and a synoptic-scale classification scheme have been developed. The following hypotheses were used as milestones for investigation of the relationship between sea breeze structure and the synoptic scale influences.

- *The sea breeze structure and evolution can be objectively classified and identified using surface measurements and surface-based remote sensing instruments.*
- *The sea breeze circulation is constituted of several scales, one well-know local scale situated about the coastline (~10's km) and a larger regional component (~100 km) driven by larger-scale heating patterns.*
- *Synoptic-scale patterns can be objectively identified through statistical analysis of low-level wind fields.*
- *Synoptic-scale circulation patterns coupled with coastal terrain will influence the vertical structure and diurnal variations in resultant sea breeze circulations.*

Chapter II provides a background on sea breeze circulations. In Chapter III, the various types of data and data processing used for this study are described. In Chapter IV, the sea breeze structure (at the surface and through the PBL) and diurnal variability for different points along the California coast and for several summer seasons are objectively described and compared. In Chapter V, the development of an objective synoptic-scale classification scheme is described. In Chapter VI, the changes in the sea breeze structure under the influence of different synoptic regimes are compared and contrasted. Chapter VI concludes this thesis with a summary and discussion of research results.

## II. THERMALLY-INDUCED SEA BREEZE CIRCULATIONS

The differential heating of the land and ocean produce thermal circulations oriented perpendicular to coastal boundary. In general, it is known that the atmospheric boundary layer will deepen/shallow in response to the diurnal heating/cooling of the boundary layer. While many of the effects of the thermally induced sea/land breeze circulations on boundary layer structure have been identified at discrete points ( $\sim 10$ 's km) in the coastal regions [see Simpson (1994) for many examples], the simultaneous evolution of sea breeze circulations over widely spaced points ( $\sim 100$ 's km) in a coastal region and their relation to the synoptic-scale flow are less well known.

Atkinson (1981) and others describe the thermally-induced circulations that are caused by temperature differences within the PBL. Horizontal temperature gradients naturally occur at the sea/land interface. Solar irradiance is a key factor in producing thermal gradients in the coastal zone. Differences in albedo and specific heat cause land areas to heat much more rapidly than nearby coastal waters. As the land warms, heat is rapidly conducted to the air in the overlying boundary layer (Figure 1). As the air warms, the boundary layer destabilizes, enhancing vertical mixing and producing a deep column of warm air. The warm air within the column expands to form a meso-low pressure cell of less dense air over the land. In the ocean, the high specific heat of the water and the mixing within the surface layer of the ocean combine to produce lower sea surface temperatures than land temperatures. Less heat is transferred from the ocean to the overlying atmosphere and boundary layer mixing over the cooler surface of the water forms a thin, relatively cool pool of air. This cool, relatively dense pool of air above the water forms a weak thermally-induced meso-high pressure cell. There is now a thermal gradient from the ocean to the land, as well as corresponding density and pressure gradient. This pressure gradient produces an onshore flow of air, thus providing a thermally driven wind component near the surface. There is upward motion associated with the heating of the

air over the land in the meso-low pressure cell, and subsidence associated with the meso-high pressure cell over the water. Based on the hydrostatic approximation and conservation of mass, the density and pressure gradients will reverse aloft, creating a return flow towards the ocean as shown in Figure 1a.

The land breeze is simply the reverse case of the sea breeze. At night, the radiative cooling of the land surface produces a meso-high pressure cell over the land. Intense mixing within the surface layer of the ocean produces relatively constant sea surface temperatures and boundary layer air temperatures that are relatively warmer than the air temperatures over the land. This forms a weak and shallow (when compared to daytime meso-low over the land) meso-low pressure cell over the ocean. Flow from the land to the ocean, driven by the pressure and density gradients provide the land breeze as shown in Figure 1b.

From Holton (1979), the acceleration of the land/sea breeze circulation is shown to be directly proportional to the temperature contrast across the sea/land interface and the vertical extent of the circulation as illustrated in the following equation:

$$\frac{dV}{dt} = \frac{R \ln(p_0/p_1)}{2(h+L)} (\bar{T}_2 - \bar{T}_1), \quad (1)$$

where  $V$  represents the mean horizontal velocity in the plane,  $\bar{T}_2$  represents the mean atmospheric temperature over the land,  $\bar{T}_1$  represents the mean atmospheric temperature over the ocean,  $p_0$  represents the pressure at the surface,  $p_1$  represents the atmospheric pressure at the height of the return flow,  $h$  represents the height of the return flow, and  $L$  represents the horizontal extent of the sea breeze circulation. It naturally follows that the acceleration of the surface winds and the intensity of the sea breeze circulation are directly related and proportional to the land/sea temperature differential. The

intensity and acceleration of the winds within the sea breeze would also depend on other factors such as surface friction, background wind flow, and terrain effects which tend to slow, channel, and block the thermal circulations.

Hsu (1988) illustrates the cycle of the sea and land breeze development near a straight coastline, accentuated with small bays, along the Texas coast in Figure 2. The figure depicts the growth and decay of three sea breeze cells closely oriented to one another. It is important to note that the two outside sea breeze cells are located near small bays, where the temperature contrasts between the land and the ocean is smaller than in the vicinity of the central sea breeze cell. The sea breezes begin as small circulations perpendicular to the coast and grow to maximum strength in the late afternoon, about the time of maximum solar heating. As the intensity of solar insolation decreases, the strength of the sea breeze cells also diminish. At night, the greatest temperature differential between the land and ocean is near the previous location of the central sea breeze cell, allowing for the development of a weak land breeze circulation. The land breeze circulation reaches its maximum strength just before sunrise.

Haurwitz (1947) was the first to successfully explain the roles of friction and the rotation of the earth (Coriolis force) as essential forces in the observed veering (clockwise turning) of sea breeze winds throughout the day in elliptical hodographs. This can be shown in most any Northern Hemisphere wind hodograph such shown in the summer of 1993 at Point Mugu or Fort Ord in Figure 3. Succeeding studies have since illustrated that local terrain effects will often overshadow the Coriolis effect, allowing sea breeze wind hodographs to back (turn anticlockwise) throughout the day (Simpson 1995). Zhong and Tackle (1993) stress the importance of frictional forces over Coriolis forces in determining the orientation of the sea breeze circulation; while Coriolis forces are much more important in land breezes.



Simpson's (1994) recent book describes different aspects of the sea breeze, as well as the current knowledge of sea breeze circulations. He includes information on formation, structure, and local winds in relation to the sea breeze. Simpson's book summarizes the wealth of descriptive information on sea breeze behavior. Other factors such as vegetation, cloudiness, irrigation have a direct impact on the strength of the sea breeze circulation and have been summarized by Kondo (1975), McCumber (1980), Segal *et al.* (1986), and Segal and Arritt (1992).

#### **A. INFLUENCE OF SYNOPTIC-SCALE FLOW ON THE SEA BREEZE**

Along the west coast of the United States, a large semi-permanent anticyclone produces subsidence and shallow boundary layer heights (Bridger *et al.* 1993). This shallow boundary layer and associated temperature inversion limit the extent of vertical mixing. The limited mixing provides for increased temperature contrasts in the air over the coastal zone and produces a stronger sea breeze circulation. Conversely, sensible heating associated with the Gulf Stream and warm, shallow waters of the Gulf of Mexico will deepen boundary layers along the east and southeast U.S. coasts. The deeper boundary layers allow for increased vertical mixing, which tends to weaken the temperature difference between the air over the land and ocean. The weaker temperature gradient translate into weak sea breeze circulations on the U.S. east coast.

Elliott and O'Brien (1977) and others have illustrated that the subsidence-producing eastern North Pacific Ocean semi-permanent anticyclone drives a large-scale northerly gradient wind that flows along the Pacific coast. This persistent large-scale wind, when combined with effects of the earth's rotation, tends to produce an offshore flow of surface waters away from the coast. Cold water upwelling replaces the divergent surface waters. The colder surface waters also lead to cooler and shallower boundary layers near the upwelling regions, as was verified by Beardsley *et al.* (1987). In effect, the upwelling tends to strengthen the thermal gradient and to produce stronger sea breeze circulations.

Offshore gradient wind is often related to delayed sea breeze onset. Wexler's (1946) description of Koschmieder's theory (Koschmieder and Hornickel 1936, 1941, 1942) of frontal development of the sea breeze induced by off-shore gradient winds is shown in Figure 4. The morning offshore gradient wind forces the sea breeze circulation to develop offshore as the warm air from the land moves over a cool ocean surface to form a cold surface layer (Figure 4a,b). Turbulent mixing and continued offshore flow causes the cool air to be 'piled up', raising the height of the cold air and the pressure within the column (Figure 4c,d). This will continue until the pressure gradient force associated with the cold layer of air counterbalances the forces producing the offshore gradient wind (Figure 4e). As the land continues to heat, the air above it becomes unstable, which in turn lowers pressure over the land. The lower pressure over land destroys the equilibrium between the pressure gradient force and the gradient wind forces, and allows the pseudo-cold front to move inland (Figure 4f,g). Extensive studies by Intrieri *et al.* (1990), Zhong and Tackle (1993), Schroeder *et al.* (1967), Estoque (1961,1962), and others have confirmed the intensification of thermal gradient and delay of the sea breeze onset by offshore gradient wind flow.

Johnson and O'Brien (1973) conducted a successful field program on west coast sea breeze behavior along the Oregon coast. Specifically, they observed a typical sea breeze circulation under the influence of gradient wind flow parallel to the coast including: 1) the passage of a sea breeze front, 2) a wind maximum in the surface winds behind the front, 3) the surface onshore sea breeze flow, confined below the boundary layer inversion, which deepened the boundary layer at the coast, and 4) a return sea breeze flow above the inversion. They characterized the sea breeze as having a maximum depth of 700 m, a 7.5 m/s surface wind speed maximum, and a 1000-1500 m deep return flow aloft.

Schroeder *et al.* (1967) stress the importance of the Pacific coast monsoon circulation in interpreting west coast sea breeze studies. The monsoon is that part of the flow induced by summer continental inland heating. In general, the air over the western United States is warmer than the air

over the ocean, inducing a continuous large-scale but very weak onshore flow of moist air. This monsoon flow is on the order of 1 m/s on which the coastal sea breeze is superimposed. Schroeder *et al.* (1967) believe this is why eastern North Pacific Ocean coastal sea breezes tend to have less moisture discontinuities than sea breezes in other areas around the world.

Arritt (1993) used two-dimensional non-linear equations to model the large-scale flow characteristics on sea breeze. A series of controlled experiments investigated the effects of ambient winds on the sea breeze. They were: 1) onshore synoptic flow that resulted in a sea breeze that propagated in the same wind direction with a weak thermal perturbation of the large-scale flow; 2) calm to moderate opposing synoptic flow that resulted in the most intense sea breeze with intensity of the thermally induced perturbation increasing for increasing opposing flow; 3) strong opposing synoptic flow that suppressed vertical motions and weakened horizontal wind velocities; and 4) very strong opposing synoptic flow that resulted in very weak vertical velocities and horizontal temperature gradients.

Blanchard and López (1985) studied convection in the Florida panhandle to determine the effect of regional-scale meteorological influences on the sea breeze circulation, and thereby understand the convection associated with the inland extent of the sea breeze circulation. To examine the regional-scale influences, they formed composite convection patterns identified by WSR-57 weather radar, and then constructed streamlines from rawinsonde sites about the southeast United States that were composited based upon times of similar convection. Multi-level regional analyses of temperature, dew point, mixing ratio, and equivalent potential temperature showed no relationship to their convection patterns. However, general wind patterns tended to differentiate between broad types of convective showers. They found that the mean layer vector wind (MLVW) from 1000 ft to 700 mb was the best indicator of the low-level regional wind flow.

Recently, Gould and Fuelberg (1996) and Gould *et al.* (1996) formed a sea breeze climatology by grouping days of similar MLVW in Florida. They formed eleven categories of sea breeze days based on different wind speeds and directions for 52 days. Based upon their limited data, they did find some preferential areas for convection over the Florida panhandle for different synoptic regimes. In particular, they postulated that the thermodynamic differences between the different synoptic regimes will be the key to successfully forecasting sea breeze convection.

## **B. SEA BREEZE CLASSIFICATION STUDIES**

While Haurwitz (1947) was looking at the Coriolis effect on the sea breeze, Wexler (1946) made the first attempt to classify the sea breeze based on prevailing gradient wind conditions. He observed two general sea breeze categories, frontal and gradual. The gradual type was marked by calm or onshore gradient winds prevailing prior to comparatively early sea breeze onset, while the frontal sea breeze was characterized by a delayed onset preceded by a light offshore gradient wind. The frontal sea breeze onset was described by a strong wind shift and discontinuities in temperature and humidity. The gradual sea breeze showed slight changes in wind direction and no significant discontinuities in wind speed, temperature, or humidity, as verified by Fisher (1960), Zhong and Tackle (1993), and others.

Schroeder *et al.* (1967) suggested a third type of sea breeze circulation known as the air mass sea breeze. The air mass sea breeze is very similar to the gradual and frontal sea breeze circulations. Like the gradual sea breeze, it is characterized by prevailing onshore wind flow before sea breeze onset. But, unlike the gradual sea breeze and like the frontal sea breeze, the air mass sea breeze is characterized by sharp increases in wind speed and humidity, and decreases in surface air temperature.

In model studies performed by Estoque (1961, 1962), the effect of the large-scale wind flow on the sea breeze was examined. In particular, Estoque looked at the effects of wind flow parallel to the coast. In modeled wind flow parallel to the coast with an anticyclone over the water, the resultant

sea breeze was reminiscent of a sea breeze normally produced by an onshore gradient wind, the gradual type of sea breeze. In the opposite case with a cyclone located offshore, the slight frictional inflow into the cyclone was enough to produce a sea breeze similar to the frontal types produced by offshore gradient winds.

Fagen (1988) used the combination of acoustic Doppler sodar, Doppler lidar, and conventional observations in the Monterey Bay to determine sea breeze characteristic during LASBEX (Land-Sea Breeze Experiment) in 1987. Specifically, he found that the frontal sea breezes were the easiest to identify, since they are characterized by a sharp wind shift. During the two weeks of the experiment, the sea breeze onset times 1.5 km southeast of Moss Landing occurred near 10:00 PST. The duration of the sea breezes were approximately 8-12 h and the maximum surface wind speeds ranged from 6 to 10 kts. The average height of the sea breeze onshore flow was 659 m, while the average depth of the return flow was twice the depth of the onshore flow.

Intrieri *et al.* (1990), in a lidar study of the sea breeze during LASBEX, confirmed Fagen's results on frontal type sea breezes. A strong wind shift, temperature drop, wind speed increase, and rise in humidity were all found in frontal sea breezes with a depth to 1000 m. The maximum extent of the return flow was 2000 m. The onset of these frontal sea breezes was not characterized by the reversal of the surface winds to an onshore flow, but rather the sea breeze developed beneath a prevailing offshore flow, forcing it aloft.

Banta's (1995) results were also from LASBEX. The results were consistent with previous studies, but keyed on one local, morning sea breeze with a 300 m onshore flow. Banta inferred from the rapid deepening of the onshore sea breeze flow to over 1000 m in the afternoon, that the local-scale sea breeze was absorbed by a deeper sea breeze circulation. Banta hypothesized that the deeper sea breeze circulation was the result of regional or continental-scale influences.

Round (1993) performed a subjective analysis of six different sea breeze types at Fort Ord from April to September 1994. The six types of sea breezes are identified as 1) frontal (which correspond to Wexler's (1946) frontal type of sea breeze); 2) gradual development (corresponding to Fisher (1960) sea breeze); 3) clear onset sea breeze (corresponding to the Schroeder *et al.* (1967) airmass front); 4) double surge sea breeze; 5) no sea breeze; and 6) unclassifiable sea breeze days. Frontal and gradual sea breezes were the most prominent, occurring 29% and 36% of the time, respectively. One interesting result was a correlation between large cloud amount and lighter wind speeds. The most likely time of sea breeze onset was between 8:30 and 11 PST with the most frequent time near 10 PST.

Knapp (1994) also performed a subjective study of synoptic-scale influence on sea breeze in the Monterey Bay from 01 May 1993 to 30 September 1993. The study was limited to the first four main sea breeze categories used by Round (1993): clear onset; gradual; frontal; and double surge. The study used a simple averaging routine, based upon subjective inputs, to determine representative synoptic regimes that occurred along the California coast. Based upon the input surface analysis fields, three synoptic regimes were found: trough, gradient, and ridge regimes. The trough regime is characterized by an inverted low pressure trough whose axis was oriented along the California coast. The trough regime occurred on 52% of the days during spring/summer and was characterized by 10 PST sea breeze onsets, afternoon boundary layer destabilization and significant wind speed increases (11-15 kt wind speed maximums). The gradient regime is characterized by low pressure in eastern Nevada and high pressure offshore, which produced surface isobars roughly parallel to the California coast. The gradient wind regime occurred in 27% of cases, exhibited the strongest associated sea breeze winds, and sea breeze onset times of near 7-8 PST. The ridge regime is the opposite case of the trough regime, with a high pressure ridge centered along the California coast. The ridge regime

contained the fewest number of cases (13%) and exhibited delayed sea breeze onset times of 9-10 PST. Of all of the days of the study, 10 representative sea breeze days were chosen with the following breakdown: 60% were clear onset, 20% gradual, and 20% frontal.

Stec (1996) used radar wind profilers and RASS (Radio Acoustic Sounding System) measurements to examine the sea breeze at four selected sites around the Monterey Bay during June to August 1994. Sea breeze onset times, maximum depths, and virtual temperature distributions were obtained. There was no evidence of return flow aloft associated with the sea breeze. Topography had a significant influence in enhancing or modifying the sea breeze circulations at different locations. Confirming Zhong and Tackle's (1993) assertion that pressure gradient force and surface friction were more important in the daytime surface sea breeze, Coriolis turning was not evident in the surface sea breeze wind field. However, Coriolis turning was observed aloft in the sea breeze circulation in the monthly mean radar wind profiles.

Of particular note is the continuing mention in previous studies of a continental-scale sea breeze by Wexler(1946), Intrieri *et al.* (1990), Banta (1995), Simpson (1995), and Stec (1996). Here the continental sea breeze is defined as a larger-scale sea breeze that is a function of the heating of the interior valleys of California with a delayed, but quite strong sea breeze signal. This research with multi-year data may provide additional insights of the continental sea breeze.

In these studies, it can be seen that the sea breeze circulation will change based upon the prevailing gradient wind conditions. Some sea breeze circulations exhibit fronts that are preceded by offshore gradient winds. With prevailing onshore gradient wind flow, some sea breeze circulations produce gradual changes in the air mass near the surface; while other sea breeze days exhibit frontal characteristics. The role of larger-scale influences has been modeled to produce similar frontal and gradual sea breeze circulations (Estoque 1962, Arritt 1993, and others). Limited subjective studies

have explored the relationship of the gradient wind and synoptic-scale influences on the sea breeze.

A goal of this study is to objectively classify and describe the types of sea breeze structure days and study their relationship to various synoptic-scale influences.





### III. DATA

The data used in this study is unique. This is the first time that continuous measurements of surface variables and continuous measurements of upper-air observations (in the form of radar wind profiles and Radio Acoustics Sounding System [RASS] virtual temperature profiles) have been available at several coastal locations along the California coast for extensive periods of time. This provides the opportunity to make sea breeze measurements and descriptions for both surface and PBL on hourly (or better) time scales.

There are four main types of data to be used in this study: surface automatic weather station data, radar wind profiler data, RASS temperature data, and NOGAPS model analyses. An effort was made to maximize the amount of data available over the widest area and for the longest periods of time in this research. Initial interest focused on the VOCAR (Variability of Coastal Atmospheric Refractivity) Intense Observational Period (IOP) of 23 August to 3 September 1993. It was decided that while the VOCAR IOP would provide intense observations from a wide variety of sources, a period of just 12 days would not provide any significant insight as to sea breeze structure. The data analysis period was expanded to include 1 June to 30 September 1993. Under the auspices of the VOCAR and COVAMP (Coastal Variability Analysis, Measurements and Predictions) programs, additional weather observing sensors were placed at Point Mugu, Point Loma, and San Clemente Island in the Southern California coastal region for the summer of 1993 to collect surface, radar wind profiles, and RASS data (Paulus 1992). While this data will provide for spatial changes in the sea breeze structure along the Southern California coast during the summer of 1993, several summers worth of data would give better indications of the sea breeze structure under more varied synoptic influences. Therefore, 1994 and 1995 were added to the data set by including Fort Ord, since it routinely collects and records the needed data, adding the summers of 1994 and 1995 to the data set.

## **A. AUTOMATIC WEATHER STATION DATA**

### **1. Locations**

Three different automatic weather stations collected surface meteorological data for this study along the California coast. They were located at Fort Ord, Point Mugu, and Point Loma. The Fort Ord automatic weather station is located 4 km inland from the ocean at a height of 51 m near the Marina Airport (formerly known as Fritsche Field and part of Fort Ord) at 36.69 ° N latitude and 121.76 ° W longitude. The station collected near-continuous measurements of surface temperature (° C), surface pressure (mb), wind speed (m/s), wind direction (°), solar radiation (watts/m<sup>2</sup>), downward longwave radiation (watts/m<sup>2</sup>), and relative humidity (%) at 2 minute intervals from 01 June 1993 to 01 October 1995.

The Point Mugu automatic weather station was located at the height of 2 m near the coast at the Pacific Missile Test Range at 34.09 ° N latitude and 119.12 ° W longitude. Point Mugu is southeast of the coastal cities of Oxnard and Ventura, and northeast of Los Angeles. The station collected continuous measurements of surface temperature (° C), surface pressure (mb), wind speed (m/s), wind direction (°), solar radiation (watts/m<sup>2</sup>), net radiation (watts/m<sup>2</sup>), and relative humidity (%) at 1 minute intervals from 01 June 1993 to 01 October 1993.

The Point Loma automatic weather station was located at the height of 20 m near the foot of a long narrow bluff forming the Point Loma peninsula at 32.70 ° N latitude and 117.25 ° W longitude. Point Loma is a coastal peninsula of San Diego. The station collected continuous measurements of surface temperature (° C), surface pressure (mb), wind speed (m/s), wind direction (°), solar radiation (watts/m<sup>2</sup>), net radiation (watts/m<sup>2</sup>), and relative humidity (%) at 1 minute intervals from 01 June 1993 to 01 October 1993.

## 2. Data Processing

The data was obtained on 3.5 inch computer disks and transferred into the Naval Postgraduate School's Indigo Unix IDEA Lab workstations. The surface data was read into working files using Matlab 4.2c1 in the original temporal data resolution.

Using the Clausius-Clapeyron equation, dew point temperature ( $^{\circ}\text{C}$ ), mixing ratio ( $\text{g/kg}$ ), and specific humidity ( $\text{g/kg}$ ) were determined using surface pressure, temperature, and relative humidity values. Wind directions were converted from meteorological format (wind direction = direction from which wind blows) to a more mathematical convention (wind direction = direction to which winds blow), and decomposed into their northward ( $v$ ) and eastward ( $u$ ) components.

### *a. Averaging/Filtering.*

All available data was averaged into 15 minute observations, represented by 00, 15, 30, and 45 minutes past the hour. For example, data in the 00 minute observation represents the averaged data collected from 46 past the hour to the start of the next hour. Fifteen minute time bins were constructed from 0000 UTC 01 June to 23:45 UTC 30 September for each year of the available data. Winds were averaged using  $u$  and  $v$  components and reconstructed into direction and speed. Missing data was flagged appropriately.

Due to the variability in the data, several methods were examined using three different data averaging techniques to minimize the high frequency noise contamination in the data and retain the most representative data possible. Three different filters were used: 1) 15 minute average filter, no further averaging or filtering were performed on the 15 minute observations, 2) 30 minute average filter (represents each 15 minute observation averaged with the preceding 15 minute observation), and 3) 45 minute running filter (average of preceding, proceeding, and each 15 minute observation).

By comparing sea breeze classification results from the above three scenarios, it was concluded that there were no significant advantages gained by using the additional filters. All data used in the surface classification schemes consists of 15 minute temporal resolution.

***b. Wind Accuracies***

The anemometers used on the Point Mugu and Point Loma automatic weather stations are accurate to  $\pm 0.25$  mph (.114 m/s) or 1.5% when above a 1 mph (.45 m/s) threshold. At Fort Ord, the anemometer has similar accuracies with a .9 mph (.405 m/s) threshold. All wind speeds recorded below the anemometer thresholds were considered calm winds and given zero magnitude for the purposes of this study.

**B. RADAR WIND PROFILER**

Three 915-MHZ radar wind profilers were used at three different locations during different times in this study. They were located also at Fort Ord, Point Mugu, and at Point Loma and allowed for nearly continuous vertical wind profile measurements at one hour intervals.

Radar wind profilers observe backscatter from inhomogeneities in the refractive index of the atmosphere created by turbulence and density fluctuations. By using advanced signal processing techniques, signal returns from three to five antenna beams are binned through the use of range gates, and converted into radial velocities. Based on the time of signal return and Doppler shift from each of the transmission beams, computed radial velocities are converted into northward, eastward, and vertical components of wind velocity. These profiles are obtained every 5 minutes and are averaged using consensus algorithms into representative hourly profiles (May and Wilczak 1993). The vertical resolution depends upon the vertical bins determined by the pulse and gate settings of the profiler transmitter/receiver, allowing 105-110 m resolutions at the three sites. A recent comparison study between radar wind profilers and rawinsondes indicated RMS differences of  $\pm 2.5$  m/s between the two measurement systems (Weber and Wurtz 1990).

## **1. Locations**

The radar wind profiler at Fort Ord is collocated with the previously mentioned automatic weather station at  $36.69^{\circ}$  N latitude and  $121.76^{\circ}$  W longitude. Radar wind profiles were collected for the summers of 1994 and 1995. Unfortunately, the 915-MHZ profiler was not present during the summer of 1993. A 404-MHZ radar wind profiler, with less vertical resolution, was available at the Fort Ord observing site during the summer of 1993. The 404-MHZ profiler is more suitable for studies between 1 and 5 km in altitude, instead of the surface to 1500 m needed for this study.

The radar wind profilers at Point Mugu and Point Loma were co-located near the automatic weather stations at  $34.09^{\circ}$  N latitude and  $119.12^{\circ}$  W longitude and  $32.70^{\circ}$  N latitude and  $117.25^{\circ}$  W longitude, respectively. These 915-MHZ profilers provided measurements for the summer of 1993 only.

## **2. Data Processing**

Like the surface station data, the data was read into the Naval Postgraduate School's IDEA Lab Indigo Unix computers using Matlab 4.2c1. The vertical wind and temperature profiles represent the combination of surface data, radar wind profiler data, and RASS data. The individual profiles represent 10 minutes of averaged RASS virtual temperatures, followed by 50 minutes of averaged radar derived wind profiles. The surface data, in this portion of the data processing, was averaged to correspond with the vertical profile measurements. The surface temperature data was averaged for the first ten minutes of the hour to be used with the RASS data. The wind data was averaged for 50 minutes to be used with the vertical wind profiler data. Data significance was determined by using standard consensus algorithms developed for the radar wind profilers and RASS.

### **C. RASS**

During the study, RASS was operated in conjunction with the radar wind profilers to produce hourly vertical profiles of virtual temperature. RASS combines the radar wind profiler with four 2-

kHz acoustic transponders. The radar profiler senses the backscatter of the density fluctuations produced by a projected sound wave, measuring the speed of sound through the atmosphere. Virtual temperature ( $T_v$ ) is calculated by using the measured speed of sound ( $c_s$  in m/s) in the formula  $T_v = (c_s/20.047)^2$  given by May *et al.* (1989). Under normal conditions, the RMS difference between RASS and radiosonde measurements is near 1°C (May *et al.* 1989).

#### **D. NOGAPS MODEL DATA**

In order to determine the relationship of the synoptic-scale to the sea breeze structure, the first requirement was to define objectively synoptic-scale patterns in the atmosphere at a level that was high enough to be free of surface friction near the coast, but yet low enough to influence boundary layer interactions. A second requirement was to use a model analysis field to provide the consistency and mobility required to transport results from one location to another, and also serve a medium for using results to improve forecast results. Therefore, the 850 mb NOGAPS analysis fields, at a typical height of 1500 m, were chosen to represent the synoptic-scale conditions. This height corresponds favorably with the height of the MLVW used by Blanchard and López (1985), Gould and Fuelberg (1996), and Gould *et al.* (1996) to examine wind-influence on the sea breeze.

The NOGAPS 850 mb wind analysis fields were obtained every twelve hours for the months of June, July, August, September 1993 to 1995 for the entire Western hemisphere at 2.5° resolution. The fields were read into Matlab 4.2c1 and pared down to a 25° latitude by 20° longitude grid centered over the Southern California region. The actual limits of the grid were 25°N to 45°N and 130°W to 110°W.

The NOGAPS model used in the summer of 1993 was version 3.3, an 18 level, hydrostatic, primitive equation model in sigma coordinates. Model version 3.3 was limited to 79 waves with triangular truncation, referred to as T79 horizontal resolution (Hogan and Brody 1993). Prior to the

summer of 1994, the model was upgraded to version 3.4, in which the horizontal resolution was increased to 159 waves, also with T159 triangular truncation (Hogan 1996).





#### IV. SEA BREEZE STRUCTURE

The simultaneous near-continuous surface, radar wind profiler, and RASS measurements will be used to objectively classify different types of sea breeze circulations at the three different California coastal sites: Fort Ord, Point Mugu, and Point Loma. Furthermore, analyses using the continuous surface data will determine the frequencies of sea breeze types, their structure and behavior during the summer season. The specification of the sea breeze low-level wind field and thermal structure using the profiler and RASS data is of particular importance.

##### A. LOCAL FACTORS INFLUENCING THE SEA BREEZE

The sea breeze begins when the sun has begun to heat the land surface, and a circulation is initiated perpendicular to the coast. Convex curvature of the coastline would tend to form a stronger onshore flow through the summation of the sea breeze flow perpendicular to the coast throughout the curvature of the coast; while concave coastlines would tend to disperse the onshore sea breeze (Pielke 1984). In areas of complex land heating, such as interior valleys near the coast, there would be an adjustment in the sea breeze circulation towards these larger areas of increased daytime heating, away from the initial cross-coast or local direction (Simpson 1995, and others). Previous studies (Banta 1995, Stec 1996, Round 1993, Knapp 1994, and others) have discussed these complex interactions, but have made no effort to quantify them. With increased thermal contrast produced by the inland heating, one would expect stronger sea breeze wind speeds as predicted in equation (1). Along the California coast, one must consider the geometry of inland heating with respect to the coast to determine the large-scale sea breeze circulation.

Topography will also have a major effect on the sea breeze circulation. Coastal mountains can inhibit the flow of the cool, moist sea breeze inland through flow blocking (Nuss, 1993) and land barrier effects. The Fort Ord site measures the sea breeze evolution along the Monterey Bay.

Topographic features important in understanding the land/sea breeze structure in this location are the Santa Cruz Mountains, Santa Lucia Mountains, and the Salinas and Santa Clara Valleys. The mouth of the nearby Salinas Valley provides a large area for inland heating due east of the observational site as shown in Figure 5. The Santa Clara Valley, to the northeast, also serves as a large region of inland heating. The Santa Cruz Mountains (not shown), to the north, inhibit north-south wind flow in the Monterey Bay which force winds to flow with a west-east wind orientation at the observational site. The Santa Lucia Mountains to the south also serve to block north-south wind flow and funnel west-east winds through the area. The blocking effects by the terrain are more important than the convex shape of the coastline for the Monterey Bay location, since the winds are mostly funneled in a west-east direction.

The Fort Ord site is located near the north-south oriented coastline of Monterey Bay (Figure 5). As a result, the local sea breeze circulation should be generated in the west-east direction at that location. The initial sea breeze on the north (south) side of the bay will develop in a south to north (north to south) direction. This was confirmed by Foster (1993) using data from Santa Cruz (north coast) and Monterey (south coast) locations.

The most intense solar heating occurs inland in the Salinas Valley and Santa Clara Valley, east of the coast. Foster (1993) found that this inland heating develops a larger-scale sea breeze oriented in west to east direction. Consequently, the local sea breezes along the coastlines of Monterey Bay would shift to a west-east oriented sea breeze later in the day. Again results from Foster's (1993) study of four sites around the bay confirmed this evolution. Both the local and larger-scale sea breezes are found at Fort Ord and they are oriented in the same west-east direction. The onset of the larger-scale sea breeze for one case is described by Banta (1995) using LASBEX lidar results. This larger-scale sea breeze structure will be called the *regional* sea breeze to distinguish it from the local sea breeze.

The second measurement location for this research, Point Mugu, has a more complex coastal topography. The immediate coastline at the measurement site is east-west (Figure 6) with extensive agriculture fields located northwest to northeast of the site. A significant mountain ridge is due east of Point Mugu as well. Consequently, the initial sea breeze should develop cross-coast in the coast in the south to north direction. On the larger regional-scale, the coastline of Ventura County runs approximately northwest to southeast, with the highest terrain (greater than 900 m) due north of Point Mugu. The more intense solar heating later in the day will occur in the Ventura Valley northeast of the site as well in the Los Angeles basin to the east. As a result, the regional sea breeze would likely assume a more west-east orientation. One would expect Point Mugu to exhibit two distinct sea breeze orientations, a local north-south sea breeze, which usually occurs in the morning, and an afternoon west-east regional westerly sea breeze as depicted in Figure 6.

The southernmost observational site is located on the Point Loma peninsula in San Diego. Point Loma is actually a small 50 m ridge, guarding the approach to San Diego harbor as shown in Figure 7. Point Loma recorded the lightest wind speeds of all the sites. All observations were taken at an altitude of 20 m near the base of the ridge, slightly in the shadows of the north-south oriented obstruction. The nearness to the ridge is important when considering flow blocking and wind barrier effects at Point Loma. Wind passage into the interior is to the northeast and to the southeast, around the ridge. To separate these two circulations when the sea breeze is directed to the northeast (southeast), it will be labeled southerly (northerly) sea breeze.

## **B. SEA BREEZE CATEGORIES**

Previous studies, reviewed in Chapter II, identified several types of sea breezes. These studies of sea breeze classifications are subjective, where a day of particularly strong sea breeze circulation is selected to determine the overall characteristics of the sea breeze. There are three classical types:

- 1) frontal --- similar to the passage of a cold front (wind shift, temperature decrease, moisture increase,

and wind speed increase), usually produced by an offshore gradient wind flow as indicated by Wexler (1946); 2) gradual --- where there is an existing onshore flow that is enhanced by the sea breeze as indicated by Wexler (1946); and 3) rapid onset --- a sea breeze having the characteristics of sudden increases in wind speed, increases in moisture content, and decreases in temperature. The rapid onset is known by two other names, the air mass front described by Schroeder *et al.* (1967) and the clear onset sea breeze described by Round (1993).

In developing an objective method to determine types of sea breezes, many variables were examined, including wind shifts, wind speed increases, temperature changes, and humidity changes as they related to the sea breeze during times of positive solar insolation. Techniques designed to objectively test for surface wind shifts and wind speed increases were the foundation of the sea breeze classification scheme. While changes in wind direction and speed were the most important, humidity and temperature changes helped to strengthen the classifications for different sea breeze regimes. The humidity and temperature changes were neither sufficient nor consistent enough for sea breeze categorization alone. The variability in these moisture and temperature variables within each day limited their usefulness in sea breeze classification.

Twelve sea breeze classification categories were developed in this study for these three specific locations along the west coast of California. Of the twelve, four different types of frontal and gradual sea breezes are described. Sudden onset plus three reasons for no classification, missing data, transition, and weak sea breeze complete the list. A general description of each category and the specific classification rules follow.

#### **1. Frontal Sea Breeze**

Frontal sea breezes are marked by distinct wind shifts greater than 82 degrees in one hour in the onshore direction with an increase in wind speed. (The eighty-two degree wind shift threshold was determined empirically by graphing the wind shifts for three simultaneous months at Fort Ord, Point

Mugu and Point Loma to see where the natural wind shift break points occurred in the wind records). Often frontal sea breezes were accompanied by increases in dew point temperature and relative humidity and decreases in surface temperature. Increases in relative humidity were difficult to discern, since, with temperatures rising with daytime heating, the relative humidity values were naturally decreasing. Dew point temperature was a more reliable moisture measure, but the changes were often too small to use for classification purposes. There are four subcategories of frontal sea breezes based upon the orientation of the sea breeze circulation at its onset and near its end:

*a. Frontal-Southerly (category 4)*

The frontal-southerly category is defined as a rapid shift of winds confined to a south-north oriented southerly sea breeze and increase in wind speed as illustrated in Figure 8 for Point Mugu. In this figure, the sea breeze onset (front) is characterized by a sharp wind shift near 7 PST, followed by increasing onshore southerly winds. The onshore winds persisted in the southerly direction until they shifted back to northerly winds shortly after midnight. In this example, the frontal onset at 7:00 PST in Figure 8 was marked by a decrease in the rate in which the surface temperature warmed.

*b. Frontal-Southerly-Westerly (category 6)*

The frontal-southerly-westerly category is defined as rapid shift of winds confined to a south-north oriented sea breeze followed by gradually shifting towards the inland direction (westerly winds) in the afternoon as depicted in Figure 9. In this figure, the Point Mugu sea breeze shifted over 100° to form a south-north sea breeze near 7:45 PST. The sea breeze front was marked by an increase in wind speed to 5 kts at the time of onset, while the surface temperature showed an associated sharp temperature decrease. Later in the afternoon, the sea breeze circulation gradually shifted from a south-north orientation to an west-east orientation as the winds became more westerly.

This is a very common occurrence at Point Mugu, where the effects of these two different sea breeze circulations are routinely observed.

*c. Frontal-Westerly (category 5)*

The frontal-westerly category is marked by a rapid shift to westerly winds flowing onto the inland areas to the east and usually marked by a sharp wind speed as illustrated at Fort Ord in Figure 10. In this figure, there are existing light offshore winds (maybe a part of the land breeze) until the wind shifts  $180^\circ$  to westerly winds at 8:30 PST. There is a sharp increase in wind speed and an immediate temperature decrease within minutes of the frontal wind shift. The westerly winds dominate the sea breeze onshore flow throughout this day for Fort Ord.

*d. Frontal-Westerly-Southerly (category 7)*

The final frontal sea breeze category is frontal-westerly-southerly. This category would be appropriate if the local coast was north-to-south with regional-scale heating occurring to the north of the local coastline. This classification is included for completeness and to allow other coastline geometries. This type of sea breeze was not observed at any of the three observing sites.

**2. Gradual**

Gradual sea breezes are marked by prevailing onshore gradient wind flow and by slow gradual changes in wind direction over the course of several hours with corresponding slow increases in wind speeds. Significant changes in the moisture and temperature variables were extremely rare. Again there are four subcategories:

*a. Gradual-Westerly (category 9)*

The gradual-westerly category, defined by persistent westerly winds or slow shifts of the wind towards the east, is illustrated in Figure 11 at Fort Ord. The changes associated with the sea breeze onset are slow and gradual. In this figure, there is a prevailing westerly wind that does not appreciably change wind direction with sea breeze onset, but steadily increases in wind speed. There

are no sudden temperature changes associated with the sea breeze onset. The westerly winds persist through midnight in this case at Fort Ord, only easing in response to decreases solar insolation after 18:00 PST.

***b. Gradual-Southerly (category 8)***

The gradual-southerly category is categorized by persistent southerly winds oriented in response to local forcing mechanisms confining the sea breeze to a south-north oriented sea breeze with slow gradual increases in wind speed as shown in Figure 12. In this figure, at Point Mugu, the southerly winds are associated with a local oriented sea breeze flowing perpendicular to the local coastline. The southerly wind flow increases in direct response to solar heating and shows no tendency for a westerly wind shift towards the Los Angeles basin. The sea breeze decreases in the afternoon, as the solar insolation decreases.

***c. Gradual-Westerly-Southerly (category 11)***

While only included for consistency, the gradual-westerly-southerly sea breeze was observed on a few occasions at Point Mugu and Point Loma. It did not occur enough times to be considered statistically significant (less than 1% of the study). The gradual-westerly-southerly sea breeze exhibited prevailing onshore winds or a slow shift of winds into a westerly wind direction with a gradual shift in winds towards the southerly sea breeze as exhibited in Figure 13. In this figure, the initial sea breeze at Point Loma is oriented towards the southeast. When the winds shift to southwesterly, there is a dramatic increase in the surface temperature, indicating that the southerly portion of the sea breeze circulation is not strong enough to keep the PBL cool. The southwesterly winds gradually shift due to increased nighttime cooling, becoming offshore winds near 21:00 PST.

***d. Gradual-Southerly-Westerly (category 10)***

The gradual-southerly-westerly category exhibits prevailing onshore winds or slow shift of winds (confined to a south-north oriented sea breeze) and then gradually shifts to westerly



winds the afternoon as shown in Figure 14. This category is also statistically small, comprising less than 8% of the days at Point Loma and less than 5% of the days at Point Mugu. In this figure, there is a slow shift to southerly winds near the onset of solar heating. In the afternoon, the southerly wind speed decrease. As the wind direction shifts to westerly at 17:00 PST, the wind speed begins to increase. Onshore winds persist throughout the day, only decreasing below 5 kts after 23:15 PST.

### **3. Rapid Onset (category 12)**

Although very similar to the frontal case with a sudden increase in wind speed (2 m/s or 4 kts in 30 minutes), the rapid onset shows no associated wind shift with sea breeze onset as depicted in Figure 15. The rapid onset in this figure showed a strong surge (increase) in wind speed at 10:45 PST in the onshore direction. The surface temperature shows a sharp decrease associated with the onset of the sea breeze, as well as decreases in solar insolation (indicating increased clouds). Increases in dew point temperature and decreases in temperature variables were commonly detected with this type of sea breeze onset.

### **4. Unclassified**

The rest of the days that could not be classified as frontal, gradual, or rapid onset sea breeze days were classified as unclassifiable sea breeze days. There are three subcategories of unclassified sea breeze days:

#### ***a. Missing Data (category 1)***

If any portion of the surface wind data was missing during the day or night, then this resulted in a missing data classification for that day.

#### ***b. Transition Days (category 2)***

Transition days are unclassified because external events, such as changing synoptic situations, induce two or more distinct sea breeze classifications that coexist in one day. An example

of an unclassified-transition day is shown in Figure 16. In this example, a synoptic-scale frontal passage is clearly shown.

*c. Weak Sea Breeze (category 3)*

Weak sea breeze days are also unclassified days. These are days in which the wind speed does not increase above 2.5 m/s (5 kts) during daylight hours, or the wind speed does not increase by 2.5 m/s (5 kts) from a morning minimum to a morning or afternoon maximum in the onshore direction.

**C. PROGRAM CHARACTERISTICS FOR SEA BREEZE DEPICTIONS**

The objective method used to delineate sea breeze categories has the following characteristics:

- Each day was examined for 24 hours, from 12 UTC to 12 UTC (4 PST to 4 PST) for sea breeze characteristics.
- Daytime was determined from solar radiation measurements. Sunrise and sunset were determined by using a 15 watt/m<sup>2</sup> threshold on the solar radiation measurements. The start of every sea breeze was restricted to begin after sunup.
- Winds were divided into offshore, onshore southerly, and onshore westerly wind components based upon sea breeze orientation sectors described in Table 1 and shown graphically in Figures 5, 6, and 7.
- Maximum wind speeds were determined for daylight hours in the onshore directions.
- Minimum wind speeds were determined for the daylight hours preceding the maximum winds. If the wind flow was offshore, the minimum wind speed included the projection of the offshore component as a negative value.
- Wind shifts were determined by averaging the northward and eastward wind components for each of the preceding 4 observations (1 hour) and subtracted from the current observation, then converted back to polar representations. Calm winds were excluded from the averaging

as well as the immediately preceding observation (for example:  $\text{wind shift}(n) = \{[\text{wd}(n-2) + \text{wd}(n-3) + \text{wd}(n-4)] / \text{number of non-calm observations}\}$ ). Direction changes greater than 82 degrees were starting points to examine for frontal shifts (a wind shift of 82 degrees was chosen empirically). In addition, for a frontal wind shift, the wind speed had to be greater than 1.1 m/s and shift to an onshore direction to be classified as frontal.

- Wind speed surges are wind speed increases of 2 m/s (4 kts) in 30 minutes.
- For rapid onset, the winds had to flow in an onshore direction and surge in wind speed, and not be associated within one hour of a frontal wind shift.
- Missing data, in any portion of the day, classified the day as unclassified.
- Speed increases of less than 2.5 m/s (5 kts) during the day while in an onshore direction, or entire days with winds less than 2.5 m/s, meant the entire day was unclassified.
- Days with multiple sea breeze characterizations were classified as unclassified-transition days.
- Transitions from southerly to westerly directions or vice-versa had to remain in effect for over two hours to be considered important.
- Days in which the sea breeze blew in one onshore direction throughout the day (daylight hours) were classified as westerly or southerly sea breeze days.
- Gradual days were determined by definite daytime increases in wind speed in the onshore direction with slow or no wind shifts. Each 15 minute wind observation was checked for wind shifts greater than 82° in the preceding hour. If no wind shift greater than 82° was detected, and the wind direction was pointing onshore, then the changes in onshore wind speed were examined from sunrise to time of observation to determine the magnitude of the wind increases in the onshore direction. The magnitude of the wind speed increases (in the onshore directions) had to be greater than 5 kts for to be classified as gradual.

- The end of the sea breeze is determined when the wind speed abates to 50% of its maximum value or below 2.5 m/s, whichever occurred first.

Directions (°T) winds flow towards:	Fort Ord	Point Mugu	Point Loma
Offshore	south through west to north	130° through south-west to 313°	150° through west to north
Southerly Sea Breeze	Not Applicable	313° through north to 40°	north to 60°
Westerly Sea Breeze	north through east to south	40° through east to 130°	60° through east to 150°

**Table 1.** Wind direction thresholds defining the boundaries of sea breeze types.

It must be emphasized that the sea breeze classification results in this study are fine-tuned for the local topography, coastline, and nearby inland heating for each observing site at Fort Ord, Point Mugu, and Point Loma. The distribution of sea breeze types are sensitive to local wind-shift thresholds (empirically derived) and wind speed thresholds. Sensitivity studies were conducted to test the validity of the classifications. For example, the effect of wind speed thresholds are compared locally at Fort Ord and Point Loma. At Fort Ord, where the sea breeze is relatively strong compared to Point Loma, a 1 kt increase in the wind speed threshold (from 4 to 5 kts used to define wind speed surges) results in changes in the 1993 sea breeze type distribution of 10% between gradual and rapid onset sea breeze types. At Point Loma, the same 1 kt increase in wind speed threshold results in only a 5% change in sea breeze type distribution between gradual and rapid onset sea breeze types for the summer of 1993. The wind direction and wind shift thresholds were determined empirically by the

examination of months of wind data, the wind direction thresholds are clearly indicative of onshore wind flows. It is with great confidence that the wind shift threshold is large enough to filter out small, random wind shifts and, yet, sensitive enough to classify frontal wind shifts.

#### **D. CLASSIFICATION RESULTS**

##### **1. Fort Ord**

The sea breeze categorization results for the summers of 1993, 1994, and 1995 at Fort Ord are summarized in Figure 17. Since the local sea breeze and the larger-scale regional sea breeze are from the same westerly direction, the distribution of Fort Ord sea breeze days are limited to frontal-westerly (category 5), gradual-westerly (category 9), and rapid onset (category 12) sea breeze circulations. It is important to note that 91% of the days during three consecutive summers at Fort Ord were objectively classified into observable, distinguishable sea breeze categories. Approximately 7% of the days were unclassified due to missing data, while less than 2% of the days were unclassified due to transition events (i.e. synoptic frontal passage). A sea breeze is found to be an almost daily event at the Fort Ord site. Approximately 33% of the days are classified as frontal-westerly, 44% as gradual-westerly, and 15% as rapid onset. This compares favorably to Round's (1993) results of 29% frontal and 36% gradual sea breeze days (however Round's statistics were based upon April to September data). These statistics are not compared to the Knapp (1994) study since his results were limited to ten strong sea breeze cases.

Figure 18 represents an hourly vertical composite of wind and virtual temperature structure of 68 frontal-westerly sea breeze days at Fort Ord in 1994 to 1995. The onset of the sea breeze is easily observed to occur between 9:00 and 10:00 PST with the mean surface wind increasing from calm to 15 kts in 3 hours. The sea breeze winds increase rapidly through the vertical within 2 hours of onset, extending to 1000 m (determined by wind speed increases to 10 kts) to 1500 m (determined by wind shifts in the onshore direction). The end of the sea breeze (classified by 50% drop from peak

wind) is near 19:00 to 20:00 PST. From 1000 to 1800 m, the winds tend to be from the northwest, decreasing from 10 kts at night to 5 kts during the day. The land breeze is not well represented at the surface, but can be seen to extend aloft in the mean winds from 200 to 400 m from 04:00 to 08:00 PST. The variability of these winds in the composite is explored using plots of the standard deviation of the wind speeds (Figure A1) and wind direction (Figure A2). The standard deviation of the wind speed increases with height but remains less than 3 m/s below 800 m. Notice that smaller wind direction standard deviation values (less than  $40^\circ$ ) matches the sea breeze circulation. The wind direction standard deviations are smaller than  $60^\circ$  for nearly all of the winds below 1500 m.

The vertical temperature structure of the Fort Ord frontal-westerly sea breeze is very striking. (The vertical extent of the virtual temperature profiles for the frontal-westerly composite is limited to 900 m. There is a rapid falloff of data collected above this height, due to the drier air mass regime related to frontal-westerly sea breezes). Concentrated heating can be observed in the atmosphere from the surface to 600 m from 10:00 to 12:00 PST, prior to the onset of the sea breeze. Note early maximum temperature occurs before noon. (This concurs with Arritt's (1993) modeling study of the sea breeze thermal perturbation expected with off-shore gradient winds). The sea breeze advects a cool layer of air over the land, extending up to approximately 500 m in response to the onshore flow of oceanic air. The PBL thickness is shallow extending to near 600 m in the afternoon, after the onset of the sea breeze. In addition, there is a cool dome of air which extends from the surface to 400 m in the early morning hours, matching the vertical extent of the land breeze. The standard deviation of the virtual temperatures (not shown) are in the range of 1 to  $4^\circ\text{C}$ . They do indicate larger amounts of temperature variability near the sea breeze onset with decreases in low-level temperature variability in the afternoon associated with the sea breeze circulation.

Comparison of the frontal-westerly sea breeze structure observed at Fort Ord in this study with frontal sea breeze structure observed by Fagen (1988) shows some differences. The onset times for the sea breeze were 90 minutes earlier in Fagen's study (9:42 PST) than observed in the composite plots (Figure 18). The vertical extent of the sea breeze inflow layer was observed to be 659 m in Fagen's study, while in this study it was observed to be over 900 m. The observed maximum sea breeze wind speeds of 6-10 m/s were similar in this study to those observed by Fagen (1988). The onshore sea breeze wind flow observed by Banta (1995) and Banta *et al.* (1993) in single cases compares favorably with this study with similar onset times, growth of the sea breeze inflow layer, height of the sea breeze inflow layer, and associated wind speeds. The offshore wind flow observed by Banta *et al.* (1993) prior to sea breeze onset is of similar strength (~2.5 m/s) and, likewise, extends vertically to over 600 m.

Figure 19 shows the composite vertical wind and virtual temperature structure of 100 gradual-westerly sea breeze days. As is expected with the gradual sea breeze, an onshore wind flow predominates from the surface to 700 m. The onset time is difficult to ascertain with the one hour observations, but the clear increase in speed from 5 to 10 kts at 10:00 PST is present that extends vertically to 300 m. The 10 kt winds extend from the surface to 1000 m in the sea breeze, while associated westerly wind shifts can be observed to a height of 1300 m. The layer of maximum winds (15 kts) extends to 400 m and is shallower than with the frontal case. The increased winds associated with the sea breeze lasts until 01:00 PST at the 200-300 m levels. The sea breeze seems to contain two distinct onshore flows, one confined to below 600 m and the other layered between 700 and 1300 m. The sea breeze return flow is indistinguishable, and no land breeze can be detected. Towards the end of the day, the upper onshore flow seems to change directions, almost orienting itself with the Salinas Valley. This upper-level flow oriented along the Salinas Valley also exists in the frontal-westerly sea breeze (Figure 18), extending from 700 to 1400 m lasting from 21:00 to 04:00 PST. One

possible explanation for this shift is the Coriolis turning of the winds, while another might be a response from the regional-scale heating of the Salinas Valley. This clockwise wind shift was observed by Stec (1996) in monthly wind statistics as well. Note that the mean winds for the gradual sea breeze between 1300 and 1500 m are from the west-southwest, compared to northwest with the frontal type sea breeze. In the lowest layers, the standard deviation of the wind speeds (Figure A3) remain less than 3 m/s and the wind direction standard deviation is less than 60° (Figure A4). Again, the standard deviation of the wind directions within the sea breeze circulation are less than 40°.

The composite virtual temperature structure is considerably different for this sea breeze type. The marine influence of the on-shore flow is very pronounced as there is a 400 m deep layer of cold marine air present over night and only a very shallow surface heating observed during the day. Also at night, there is a slow deepening of the MABL (marine atmospheric boundary layer) until sea breeze onset, at which time the MABL decreases in depth. The extent of the RASS temperature data to 1500 m is an indication of the moister PBL associated with the onshore flow. The marine inversion is found near 1100 m, nearly double the depth found in the frontal sea breeze. The standard deviation of the virtual temperatures in the composite (not shown) are 1 to 4°C.

The rapid onset category occurs less frequently (15%) than the frontal or gradual categories. However, 36 rapid onset days were available for compositing and are presented in Figure 20. Recall that the rapid onset sea breeze type shows characteristics of both gradual and frontal sea breeze types in the surface data. The surface winds are typically on-shore during the day (like the gradual category), but the sea breeze arrival is quite sudden (like the frontal category). The rapid onset sea breeze composite shows attributes of both frontal and gradual type sea breezes. The low-level wind averages show a sudden onset between 10:00 and 11:00 PST with near calm winds increasing to 10 kts through the lowest 500 m, similar to the frontal type shown in Figure 18. However, the thermal



structure for the rapid onset category most resembles the gradual sea breeze with an inversion above 1000 m during the night and cooler marine air dominating the PBL with only shallow surface heating.

During the rapid onset category, the sea breeze winds in the PBL are somewhat weaker than the other two types with winds reaching 15 kts only at the 200 m level. The westerly sea breeze winds extend vertically to 900 m. These winds do shift to northwest between 500 and 1000 m during the evening, like the gradual case. In the 1500-2000 m layer, southeasterly winds are found, in contrast to northwesterly for the frontal and westerly for the gradual composites. During the night, there is a light 500-1500 m layer of winds flowing offshore. The most significant feature in the vertical temperature structure is the shallowing of the MABL after the onset of the sea breeze circulation and the strengthening of the temperature inversion. The thickness of the MABL changes 400 m diurnally.

Surface data show immediate air temperature drops of at least 1°C accompanied 53% of the frontal wind shifts and approximately 87% of the frontal wind shifts were accompanied by immediate dew point temperature increases of 1°C. Approximately 25% of the rapid onset cases included air temperature decreases of 1°C within 30 minutes of onset and 65% of the days contained dew point temperature increases of 1°C within 30 minutes of onset. The average air temperature drop associated with the onset of a frontal or rapid onset sea breeze is 1.4°C.

Using the objective classification program, a set of statistics was derived from the continuous surface data, which provide more details on the behavior of the sea breeze types at Fort Ord. These statistics include sea breeze onset and end point times, duration, maximum wind speed, and time of occurrence.

Figure 21a shows the average sea breeze onset times for Fort Ord for 1993-1995 as well as the distribution of the onset times by category. The most common time interval of sea breeze start is between 8:30 and 9:30 PST, with an average onset time of 9:06 PST. The distribution of onset times by sea breeze category is shown in Figure 21b,c, and d. Frontal-westerly sea breezes on average, show

a 30 minute delay from the average sea breeze onset time, while gradual-westerly sea breezes tend to begin 30 minutes earlier than average. Rapid onset sea breezes tend to begin near the average onset time. The most common time of sea breeze onset for either frontal-westerly or gradual-westerly is between 8:30 and 9:30 PST, while the most common time for rapid onset is shifted later between 9:30 and 10:30 PST. Even though Round (1993) included the months of April and May in his study (which skewed his averages to later in the day), Round's average time of onset was only 30 minutes later than these statistics and with similar most common times of sea breeze onset.

The times of maximum wind and maximum wind speeds are shown in Figures 22 and 23, respectively. The average time of maximum wind is 14:01 PST with an average wind speed of 8.2 m/s. This compares favorably with Round's (1993) time of 14:00 PST and 8 m/s. The dominant range of time of maximum wind is 12:30 to 15:30 PST. The gradual-westerly maximum wind occurs 15 minutes later, while the rapid onset average time of maximum wind is an hour later. Speed of maximum wind by sea breeze category was remarkably similar. This is a surprising result since the coastal temperature gradient should be greater with the frontal type and less with the gradual category. However, this would be consistent with a near constant large-scale cross-coast temperature gradient associated with inland central valley and the coastal ocean.

The maximum sea breeze speed for the different categories is easier to understand if one takes into consideration the ambient flow before sea breeze onset. The ambient wind was determined to be the minimum average speed within one hour of sea breeze onset. Then the sea breeze wind speed increase is computed to be the difference between the maximum and pre-sea breeze average wind speeds, taking into account wind direction. The average increase in surface wind from the start of the sea breeze to the maximum wind is 6.8 m/s (Figure 24). There is a wide variation in surface wind speed increase among the sea breeze categories. The strongest increase is found in the frontal-westerly sea breeze category, with an increase in wind speed an average 8.2 m/s; the most common wind speed

increase is 8.5 to 9.5 m/s. The gradual-westerly sea breeze is the weakest, with an increase in wind speed from 4.5 to 7.5 m/s with an average increase of 5.8 m/s. These sea breeze wind increases are consistent with the frontal (gradual) category having the strongest (weakest) local temperature gradient. The rapid onset sea breeze average was between the two categories with surface wind speed increases from 4.5 to 8.5 m/s, with an average increase of 6.5 m/s.

The end of the sea breeze circulation was also estimated. The winds were analyzed carefully to see what point they dropped below 2.5 m/s or decreased to 50% of their maximum value, and this was determined to be the end point of the sea breeze. Figures 25 and 26 show the times of the end of the sea breeze and its duration. The average time of the end of the sea breeze was 19:52 PST with the most occurrences between 18:30 and 19:30 PST. The frontal-westerly sea breeze average end time was 19:01 PST, while the rapid onset and gradual-westerly sea breezes, with onshore flow, tended to end much later, averaging 20:21 and 21:38 PST, respectively. The durations of the sea breeze averaged 10 hours 46 minutes with most occurrences between 9.5 and 10.5 hours. The durations of the various sea breeze categories followed the sea breeze end times, with frontal-westerly being the shortest and gradual-westerly having the longest durations. This is clearly consistent with expectations.

The year-to-year variation in sea breeze category distribution for Fort Ord is given in Figure 27. The sea breeze distribution changed approximately 12% in 1994 from 1993, 1995, and combined 1993-1995. Some data was missing in September 1995 and this could explain some of the differences in the sea breeze category distribution for that year. But, clearly the distribution of gradual-westerly and frontal-westerly days is different in 1994 from 1993, with 10% more gradual-westerly sea breeze days contained in 1994. Monthly anomalies will be examined in Chapter V to see if there are circulation differences between the years that could possibly explain the variation in the sea breeze distributions.

In comparing surface statistics to the individual years at Fort Ord, the average onset time for 1994 is delayed 30 minutes as compared to 9:14 PST for 1993 and 1995. The most common time of maximum wind occurrence in 1993 is 13:30 to 14:30 PST, an hour later than in 1994 and 1995. The hour delay in 1993 might be explained by the greater number of frontal days in 1993 compared to 1994, the decrease in gradual days in 1995 (probably caused by missing data) compared to 1993-1994, and climatological summer differences as will be discussed in Chapter V. The average maximum wind speeds are very similar, with 0.1 m/s difference separating the years. The sea breeze wind speed increases are also very similar, with a maximum spread of 0.6 m/s for any year and sea breeze category.

## **2. Point Mugu**

One of the goals of this study is to identify and quantify the larger-scale influences on the sea breeze circulation. From observing the sea breeze behavior at Point Mugu for just a few days, obvious separate local and regional-scale effects were present. Point Mugu turned out to be the perfect site to identify both the local and regional-scale influences on the sea breeze circulation. For the frontal cases at Point Mugu, there are definitely two different kinds of onshore wind shifts. One is a local southerly wind shift, while the other is a regional-scale westerly wind shift. In particular, on most mornings the wind shift occurs soon after sunrise from the heating of the extensive agricultural fields north of the observing site. A corresponding 500 m thick sea breeze circulation develops in the same south-north orientation. A few hours later, this circulation shifts towards the Los Angeles basin, clearly indicating a larger-scale influence. In order to better quantify the regional-scale influences, separate frontal categories were used to describe the local effects and the regional-scale effects.

The distribution of the different sea breeze categories for Point Mugu is shown in Figure 28; 13% of the days were unclassified because of missing data, transition, or weak sea breeze days (categories 1,2, and 3). The three largest sea breeze categories at Point Mugu account for 78% of the

sea breeze days. The significant categories of sea breeze circulations are 25% frontal-westerly (category 5), 23% frontal-southerly-westerly (category 6), and 30% gradual-westerly (category 9). At Point Mugu, 48% of the days are frontal, clearly a marked increase from the 33% frontal days at Fort Ord.

Composite wind and virtual temperature profiles for 29 frontal-westerly sea breeze days at Point Mugu in 1993 are shown in Figure 29. The surface sea breeze onset is near 8:00 PST, while the lower PBL shift to onshore winds was delayed until 10:00 PST. The vertical extent of the sea breeze flow is distinguishable to a height of 1300 m. There is no discernable sea breeze return flow. The land breeze is not particularly strong at the surface, but is very evident from 200 to 900 m and lasts until 10 PST at 300 m. The average winds near 1500 m are northwesterly in the early morning but veer to northerly by 10:00 PST. Later in the afternoon, the 1500 m winds back to westerly near 16:00 PST under the influence of the maximum sea breeze circulation and gradually begin to veer to the northwest after 20:00 PST, likely due to Coriolis forces. Near 2000 m, there are average early morning westerly winds that shift to northerly near noontime and back to westerly after 16:00 PST, possibly indicating a larger-scale influence in the 2000 m layer.

The height of the temperature inversion at the top of the PBL is near 900 m during the night with a maximum height near sunrise, and decreases to near 700 m near 16:00 PST. The low-level thermal structure at Point Mugu is different from the Fort Ord site for the same frontal-westerly sea breeze. The sharp thermal perturbation observed at Fort Ord is not present at Point Mugu, possibly due to the earlier sea breeze onset time at Point Mugu, which is 1.5 h earlier than Fort Ord, allowing quicker ventilation of the PBL with cooler marine air.

Composite wind and virtual temperature profiles for 28 frontal-southerly-westerly sea breeze days are shown in Figure 30. There are three main features associated with the frontal-southerly-westerly sea breeze days. The onset of the sea breeze starts with a southerly wind direction (refer to

Figure 6) at the surface near 8:00 PST with an immediate 600 m vertical extent. As the sea breeze at the surface gradually shifts to the inland (westerly wind) direction near noontime (PST), the winds in the 200 to 1500 m layer also shift to westerly winds. There is no obvious return flow. There is a definite land breeze with a vertical extent to over 1500 m. It lasts until 10:00 PST at 500 m and 12:00 PST at 1000 m. The average winds at 1500 m are calm in the early morning hours, becoming northeasterly by 6:00 PST and backing to northwesterly by 16:00 PST. At 2000 m, the winds are generally westerly becoming northerly by noon and backing to northwesterly by 16:00 PST also. The corresponding virtual temperature structure is very similar to the temperature structure in the frontal-westerly sea breeze at Point Mugu.

Composite wind and virtual temperature profiles for 36 gradual-westerly sea breeze days are shown in Figure 31. There is low-level westerly gradient wind flow from the surface to 300 m before sea breeze onset. After sea breeze onset, the onshore (westerly wind) flow extends from the surface to 1200 m. There is no evidence of return flow aloft, nor of a land breeze. From 1500 to 2000 m, the winds are generally westerly throughout the day. In the corresponding virtual temperature fields, there is enhanced mixing within the MABL and the thickness of the MABL decreases to its minimum near 16:00 PST. The temperature inversion is very strong at the top of the MABL. The thermal structure of the gradual-westerly sea breeze composite is very similar to the thermal structure shown in the frontal sea breeze categories at Point Mugu. The most identifiable differences between the frontal and gradual sea breeze composites are 1) the low-level land breeze (easterlies) shown in the frontal cases and westerlies in the gradual case, and 2) the shifting of the 1500 to 2000 m winds to northerly near noon time for the frontal cases, while remaining westerly for the gradual case.

Statistics from four months of surface data on the sea breeze behavior are presented in Figures 32-37. The average surface sea breeze onset time (Figure 32) was 9:40 PST with the frontal-westerly wind shift occurring one hour 27 minutes earlier. The average frontal-southerly-westerly sea breeze

onset occurred even earlier at 8:02 PST. The average gradual-westerly sea breeze onset occurred at 9:28 PST. Point Mugu shows effects opposite to those at Fort Ord with its sea breeze onset times, and the frontal wind shifts at Point Mugu occur earlier than the gradual sea breeze onsets. This is clearly contrary to Wexler's (1946) hypothesis of gradual onsets occurring earlier than frontal type sea breeze onsets.

As shown in Figure 33, there is a wide distribution of the time of maximum winds at Point Mugu. The average time of maximum winds near 15:40 PST is very similar for the frontal-westerly and gradual-westerly categorizes; but, the average time of maximum winds for the frontal-southerly-westerly case is over one hour and 30 minutes earlier at 13:54 PST. The average maximum wind speed is 5 m/s with the averages for each of the categories falling within 0.4 m/s as shown in Figure 34. In Figure 35, there is a large amount of variation in the wind speed that can be attributed to the sea breeze. The average for the Point Mugu is 4.8 m/s with the largest departure from the average in the gradual-westerly sea breeze with an average of 3.8 m/s. The amount of variation is the smallest with the gradual-westerly wind speed increases. Figures 36 and 37 show the end times of the sea breeze with an average near 20:00 PST, 8 minutes later than Fort Ord. The gradual-westerly sea breeze usually lasted an hour longer, ending near 21:45 PST. Interestingly, the significant sea breeze categories all have the same duration of 11 hours 45 minutes, plus or minus 6 minutes.

### **3. Point Loma**

The 1993 distributions for the sea breeze categories for Point Loma for 1993 are shown in Figure 38. Clearly the sea breeze circulations are very complex at Point Loma, where 36% of the days were unclassified. One-half of the unclassified days were due to missing data, while the rest were due to unrecognizable sea breeze events or multiple competing sea breeze events in one day. The three largest sea breeze classification categories at Point Loma account for only 45% of all the 1993 summer days. This is significant when compared to Fort Ord and Point Mugu where the three largest

categories at each site accounted for 91% and 87% of the days, respectively. The most frequent sea breeze categories at Point Loma are 15% gradual-southerly (category 8), 17% gradual-westerly (category 9), and 13% rapid onset (category 12). With only 10% of the days classified as frontal, Point Loma sharply contrasts with its nearest neighbor Point Mugu, where the majority of the days (48%) were classified as frontal. The small percentage of frontal days at Point Loma are most likely due to the local topography at the observing site. Recall that the observing site is located at a 20 m height on the western slope of a 50 m ridge. This ridge inhibits the easterly wind flows that are necessary to compact the temperature gradient and generate the necessary wind shifts associated with frontal sea breeze types.

The vertical composite sea breeze wind and virtual temperature structure for 18 gradual-southerly sea breeze days for Point Loma are shown in Figure 39. Low-level (surface to 1500 m) southerly wind flow dominates throughout the period. Above 1500 m, the winds are more westerly. There is a detectable increase in wind speed only at the surface from 9:00 to 16:00 PST. The 500 m vertical extent of the sea breeze is determined only through the shift in winds to an onshore direction. The only significant temperature features are the formation of a temperature inversion during the day at a height of 1000 m and shallow surface heating.

In averaging the 21 gradual-westerly days at Point Loma, the vertical wind and virtual temperature profiles show north to northwest winds above 200 m (Figure 40). The surface or vertical extent of the sea breeze is not discernable in the composite. The corresponding virtual temperature composite shows a shallow PBL with the temperature inversion at the top of the MABL decreasing 200 m during the day from 800 m at night.

The vertical wind and virtual temperature structure for 15 rapid onset sea breeze days is shown in Figure 41. The sea breeze at the surface begins near 8:00 PST and ends near 20:00 PST. The vertical extent of the sea breeze (500 m) can only be detected by the shift of the winds to a



westerly orientation. The winds are from the northwest from the surface to 1300 m throughout the period. Above 1300 m, the winds are westerly. The remaining low level winds are from the northwest. The vertical composite of the rapid onset sea breeze virtual temperatures shows a well-mixed PBL to 1000 m in the morning. The temperature inversion is weak in the morning but rapidly builds in the afternoon at a height of 800 m.

The average low-level ambient wind structures at Point Loma are drastically different from Fort Ord and Point Mugu. At Point Loma, the average low-level ambient winds for the gradual-southerly, gradual-westerly, and rapid onsets sea breeze categories are oriented from the south-southwest, north, and northwest, respectively. At the other sites, the low-level ambient winds are usually oriented in a more west-east direction. Westerly surface winds associated with the sea breeze are very light at Point Loma, while at the other sites the strongest surface sea breeze winds are westerly. It is important to note that light surface westerly winds are not strong enough to keep the lower 200 m of the atmosphere ventilated with cooler ocean air, and the surface temperature increases rapidly compared to the other two sites. The diurnal changes in the thermal structure (specifically the shallowing and thickening of the PBL) previously shown at Fort Ord and Point Mugu are noticeably absent in the average thermal structures at Point Loma. This provides one mechanism to explain the larger PBL changes observed at the other sites. The stronger sea breezes observed at Fort Ord and Point Mugu may be responsible for the diurnal PBL thickness changes through increased subsidence associated with the seaward end of the sea breeze circulation.

The sea breeze onset times are widely distributed at Point Loma, as shown in Figure 42; where the most common time of occurrence for gradual-southerly sea breeze is between 8:30 and 9:30 PST, and for gradual-westerly between 12:30 and 13:30 PST. As shown in Figure 43, the time of maximum wind is also widely distributed with the most common time of maximum between 11:30 and 12:30 PST for the gradual-southerly case. In Figure 44, the maximum wind speeds are shown to be very

light when compared to the other stations with the majority of the winds speeds being less than 5 m/s. As such, these light winds are reflected in the sea breeze wind speed increases in Figure 45. There is also a wide distribution in the sea breeze end times shown in Figure 46.

The 1993 category frequency distribution for the three sea breeze observing sites can be compared in Figures 27, 28, and 38. Clearly the types of observed sea breeze circulations at the three locations varied widely during the same time period. Local differences in the shape and orientation of the coastline in relation to the regional scale heating effects produce different types of sea breezes. Additionally, the surrounding topography can help to funnel winds in certain directions (as at Fort Ord) or create flow-blocking induced shadow zones that weaken the sea breeze effect (maybe Point Loma). Sea surface temperatures are on the order of 5°C warmer near San Diego than Fort Ord, leading to less intense sea breezes at Point Loma for the same amount of nearby terrestrial heating. And most important, due to the shape of the coastline along the California coast, the same northwesterly wind which produces onshore flow and gradual sea breeze conditions at Fort Ord, produces offshore flow and frontal sea breeze conditions at Point Mugu. It is interesting to note that the occurrence of frontal sea breeze days at Point Mugu is within 5% of the occurrence of gradual sea breeze days at Fort Ord.

Using the sea breeze classification scheme, it is possible to objectively identify the major sea breeze circulations at the various observing sites. The breakdown of the sea breeze circulation into gradual, frontal, and rapid onset sea breeze circulations allows compositing of similar sea breeze circulations to determine wind, temperature, and surface sea breeze structure. The resultant sea breeze wind structures compare favorably to the conceptual models put forth in Chapter II. The temperature structures show a general decrease in MABL thicknesses after sea breeze onset to a minimum in the late afternoon. The 1500 m winds show different wind directions associated with each sea breeze category, suggesting differences in the larger scale synoptic regime.



## V. SYNOPTIC CHARACTERIZATION

Numerical simulations have provided considerable insight on the influence of the synoptic flow on the sea breeze. These modeling studies (e.g. Estoque 1962, Arritt 1993, and others) show that off-shore ambient wind flow enhances the thermal perturbation at the coast, strengthening the sea breeze circulation (frontal type of sea breeze), and that onshore flow weakens the thermal perturbation and the sea breeze circulation (similar to the gradual type of sea breeze). The large-scale winds used in these studies were specified geostrophic winds.

Previous observational studies concerning the relationship of the synoptic-scale influence on the sea breeze circulation have not been comprehensive. These studies focused on days of similar strong sea breeze characteristics. Then the synoptic-scale pattern for those days was examined (Blanchard and López 1985, Knapp 1994, Gould and Fuelberg 1996, Gould *et al.* 1996). The problem with this approach is that it does not completely address the synoptic influence, because days without the same sea breeze characteristics may have also existed under the same synoptic pattern.

As previously discussed, the sea breeze circulation is very important in describing the day-to-day variability of the coastal regions. If one could determine the synoptic regime that controls the flow over the coast, then the type of sea breeze and behavior could be anticipated. Therefore, for better examination of the synoptic influences on the sea breeze, one must objectively characterize the different synoptic regimes, and study the various sea breeze relationships to those regimes. This chapter will develop an objective synoptic classification scheme using Empirical Orthogonal Functions (EOF's), designed to classify days with similar synoptic regimes.

### A. THEORETICAL BACKGROUND ON EOF'S

EOF's have become an increasingly popular analysis tool in meteorology (Harr 1993, Richman 1986 and references therein) since its initial application to meteorology (Lorenz 1956).

EOF's have been determined to be efficient tools for representing the variance in time series of large data sets. In particular, "...an EOF analysis may be used to describe physical attributes of a data set provided adequate examination of the functions indicate a relationship between the structure of the EOF and the characteristic spatial structures of the data set" (Harr 1993). EOF analysis, in this case, is an eigentechnique applied to a covariance matrix. The covariance matrix is computed from data composed of simultaneous time observations over many spatially oriented observation points. A particularly useful feature is that the eigenvalue associated with each eigenvector obtained from the EOF can be used to describe the fraction of the total variance represented by that particular mode.

Two distinct formulations of the EOF technique are discussed by Kutzbach (1967) and Richman (1986), but their procedures are limited to analysis for scalar variables. Klink and Willmott (1989) discovered that EOF analysis based on scalar wind components may lead to biases in the EOF results. Since the data to be used in this study was composed of vector wind fields, the complex form of the EOF analysis (vector EOF or VEOF) was used.

A brief summary of the VEOF analysis using vector data following Hardy (1977) follows. The vector wind is represented by a complex number, where the real part of the wind is the eastward (u) component and the imaginary part is the northward (v) component. The wind vector matrix (V) contains N number of grid points observed over T number of observations. Thus, the wind vector matrix contains NxT complex wind values. The complex covariance matrix (C), which is Hermitian, was formed and served as the input to the diagonalization problem:

$$CE=EA\lambda, \quad (2)$$

where C is the complex covariance matrix,  $\lambda$  contains the eigenvalues, and E contains the complete set of eigenvectors. The trace of the eigenvalue matrix  $\lambda$  is used to determine the percentage of total

$$S=EV \quad (3)$$

variance explained by each eigenvalue. Likewise, the coefficients (principal components) of the relative contribution to the total field variance by each eigenvector to each observation can be computed by where **E** is the matrix that contains all eigenvectors, **V** is the original wind vector matrix, and **S** contains the principal components. A more detailed description can be found in Hardy (1977) and Harr (1993).

## **B. VEOF DECOMPOSITION**

A VEOF decomposition was performed on the NOGAPS 850 mb wind fields described in Chapter III to determine the coherent variability within the anomalous large-scale 850 mb wind fields during the summers of 1993 to 1995. Since the 850 mb level is normally situated near 1500 m, this is an altitude that is low enough to influence the flow in the PBL but high enough to avoid frictional effects and the evolution of the diurnal sea breeze itself. The profiler data shown in Chapter IV has shown the sea breeze influence on the boundary layer below 1500 m. There also were distinct differences in the 1500 m wind in the sea breeze category composites. The wind data was chosen over height data because height gradients are weak in the summer and wind vectors were thought to contain more information about the synoptic regimes.

Because there can be large spatial variability that is latitude dependent, the vector mean wind field (Figure 48) was used to normalize the wind data at all grid points to unit variance. The covariance matrix was determined by taking the product of the complex conjugate transpose of the normalized anomaly field with the normalized anomaly field, divided by the total number of temporal observations. Thus, the covariance matrix contains variances (real numbers) on the diagonal and

covariances (complex numbers) everywhere else. The eigenvalues and eigenvectors were calculated from the covariance matrix.

The percentage of variance explained by each of the first eight VEOF modes is given in Table 2, while the variance and standard errors associated with the eight leading modes are shown graphically in Figure 49. The standard errors (North *et al.* 1982) associated with the eigenvalues determines the statistical significance of the representativeness of each eigenmode and is computed by,

$$\partial\lambda = \lambda(2/N)^{1/2}, \quad (4)$$

where  $\partial\lambda$  is the standard error,  $\lambda$  is the eigenvalue, and  $N$  is the number of independent samples. The number of independent samples was scaled by 14, a common mid-latitude decorrelation factor representing 7 days for observed samples to be independent of one another (Leith 1973). To interpret Figure 49, the eigenmodes are statistically representative if the two adjacent eigenvalues fall outside of the standard error associated with the modes. In this graph, the first four eigenmodes are considered to be well separated. As can be seen in equation (4), increasing the sample size will decrease the standard error associated with the different modes, allowing for increased confidence in the variance explained by each mode. The first three VEOF's account for 48.7% of the total variance. This is a larger amount of variance explained when compared to Harr's (1993) tropical research where 33% of the variance was explained by the first three VEOF modes, and is similar to the 45% explained by the first three VEOF modes in a mid-latitude surface wind study over the United States (Klink and Willmott 1989). The first eight VEOF modes account for 72.5% of the total variance. Because of the rapid decrease in contribution to the total variance, only the first three modes will be considered in this study.

VEOF NUMBER	PERCENT VARIANCE
1	23.5
2	14.6
3	10.6
4	7.5
5	5.4
6	4.2
7	3.6
8	3.0

**Table 2.** Percent of the total variance of the normalized 850 mb NOGAPS wind explained by each VEOF.

The physical interpretation of the spatial patterns associated with the VEOF modes are difficult to understand because the vectors obtained from the VEOF mode at each grid point represent the phase relationships between the grid point and every other grid point. Figures A5-A7 illustrate the phase relationships between the grid points and correspond to VEOF modes one-three, respectively. To facilitate the understanding of the physical interpretations of each VEOF, a compositing technique similar to Harr (1993) was used.

The principal component fields were calculated by multiplying the normalized anomaly wind field by the eigenvector matrix. The principal component fields are plotted in Figure 50 for the first three modes. A close inspection of the plotted principal component fields shows there is a strong tendency for the components of mode one to be either pointing toward  $0^\circ$  or  $180^\circ$ . The same tendency is present in mode three and, to a lesser extent, in mode two.

To determine composite members, vectors in the principal component series were grouped according to the direction in which they pointed. Since the principal components seemed to have



primary directions that were  $180^\circ$  out of phase, the components were divided into four  $90^\circ$  sectors with the centers of the sectors centered on  $00^\circ$ ,  $90^\circ$ ,  $180^\circ$ , and  $270^\circ$ . Since these directions were arbitrarily chosen, the centers of the sectors were rotated in  $5^\circ$  increments until the maximum amount of principal components were contained in two opposing  $90^\circ$  sectors. The amount of rotation needed to maximize the components in opposing sectors is termed the *offset*. The sectors are numbered from one to four, starting with sector one, which is initially centered on  $00^\circ$ . The sector numbers are termed *phases* in this discussion. Figure 51 shows the percentage of principal components contained in each phase for the specified offset, which maximized the number of components in two main opposing sectors. In VEOF mode one, the two phases that contained the largest number of components are two and four. These phases contained approximately 83% of the principal components. For VEOF modes two and three, phases two and four also contained the largest number of principal components, which included 75% of the components.

A plot of the distribution of various VEOF modes and phases by date are shown in Figure 52 so the day-to-day changes of the different VEOF modes can be seen. From Figure 51, it can be seen that the first three VEOF modes are best represented by phases two and four, and so these are plotted in Figure 52. For each day and VEOF mode, the associated phase is plotted if it is two or four, and left blank if the phase is one or three. The solid line in the figure connects the VEOF mode which had the largest principal component magnitude for each 12 hour period (i.e. mode that contributes most to the variance for that time period). In the figure it can be seen that VEOF mode one phases two and four usually occur for extended periods, while the other modes usually occur for just one or two 12 hour periods. In addition, it can be observed that in 1993, there is a strong diurnal signal in VEOF mode two in July and August with 12 h shifts between phases two and four. There is a strong tendency for VEOF mode two phase two to occur at 12:00 UTC and mode two phase four to occur at 00:00 UTC. In 1994 and 1995, the diurnal tendency for 12 h phase shift in VEOF mode two phase

two and four is less pronounced, but still exhibits a preference for phase two at 12:00 UTC and phase four at 00:00 UTC. The changing diurnal signal in VEOF mode two may be indicative of circulation anomaly differences between the summer of 1993 and the summers of 1994 and 1995.

To pick out the strongest contributors in each mode, the vectors in the principal component series that had a magnitude greater than the mean magnitude of the entire series plus one standard deviation of the entire series (to be referred to as mean-plus-sd) were determined. For modes one-three, composites of the 850 mb anomalous and total winds were constructed using mean-plus-sd modes and phases to determine the composition of the averages, and are shown in Figures 53-58.

From Figure 53a, the composite of VEOF mode one phase two (130 periods) illustrates an anomalous anticyclonic turning of the winds in the southeast North Pacific Ocean, which indicates that ridging is stronger there than normal. This is illustrated in the 130 member composite of the total winds (Figure 54a) for the strong mode one phase two days, which shows that the east North Pacific Ocean anticyclone has shifted to the south of the U.S. coast forming a distinctive "southerly ridge." The other phase of mode one, phase four, is presented by Figure 53b and is composed of 131 periods. Phase four defines an area of anomalous cyclonic turning of the winds in the southeast North Pacific Ocean and anomalous anticyclonic turning of the winds in the northeast North Pacific Ocean. This implies that the east North Pacific Ocean ridge is shifted to the north. The composite of the total winds (Figure 54b) describes the wind flow about the North Pacific Ocean anticyclone oriented much farther to the north. Phase four of VEOF mode one is named the "northerly ridge" regime.

From the composite of the anomalous winds in Figure 55a, VEOF mode two phase two (63 periods) defines very weak anomalous wind flow over the ocean, but stronger offshore winds over the continent. The corresponding composite of the total winds Figure 56a shows that the North Pacific Ocean anticyclone has a climatological offshore location, with an offshore wind flow over the continent. Thus VEOF mode two phase two is termed the "continental land breeze." The composite

of the anomalous winds of VEOF mode two phase four (66 periods) also indicates very light anomalous winds over the ocean with strong onshore winds over the land. The corresponding composite of the total winds indicates that the North Pacific Ocean anticyclone is oriented also in climatological central location and strong onshore wind flow is present. VEOF mode two phase four is termed the "continental sea breeze."

Corresponding with the reduction in variance contribution of VEOF mode three, the composites of the anomalous winds in Figure 57 corresponding to VEOF mode three are more difficult to interpret. Phase two (Figure 57a) comprised of 36 members seems to represent northerly winds flowing along the California coast, while phase four (Figure 57b) is comprised of 20 members and represents southerly winds flowing along the California coast. As expected, the corresponding composites of the total winds, show "reduced alongshore winds" for phase two (Figure 58a) and "enhanced alongshore winds" for phase four, as shown in Figure 58b. This mode describes variations in intensity of the North Pacific Ocean anticyclone rather than shifts in location.

### **C. SYNOPSIS DESCRIPTIONS OF THE VEOF MODES**

In this section the various VEOF modes and phases are synoptically described. Physically, the VEOF mode one represents the north-south movement of the east North Pacific Ocean anticyclone. In phase two, the location of the North Pacific Ocean anticyclone is centered to the south near 30°N, forming a large ridge in the vicinity of the southern coast of California, hence the name "southerly ridge." The opposite condition is represented by phase four, where the anticyclone is located much farther to the north, hence the name "northerly ridge." As can be clearly seen in the Figure 52 time series, there are extensive periods of northerly ridge and southerly ridge regimes throughout the three summers. Breaks in the VEOF mode one pattern are common and can be interpreted as transition regimes.

## 1. Southerly Ridge

The location of the southerly ridge (VEOF mode one phase two) is near  $30^{\circ}\text{N}$ . From the 1993 to 1995 data set, when VEOF mode one is greater than the next strongest contributing mode, the southerly ridge occurs approximately 47.1% of the time. When compared to the three dominant VEOF modes, the southerly ridge case accounts for 33.1% of the mean-plus-sd cases. In a year-to-year breakdown of the first three VEOF modes: the southerly ridge case dominates for 8.9 % of the periods in 1993, 53.7% in 1994, and 51.8% in 1995. Figure 59 uses a National Meteorology Center (NMC) 850 mb analysis to illustrate a period that corresponds to a typical southerly ridge classification. The 00 UTC 11 June 1995 850 mb analysis for the southerly ridge falls within a large series of consecutive southerly ridge days (refer to Figure 52). In the analysis, there is a large low pressure system in the east North Pacific Ocean near  $48^{\circ}\text{N}$  with a ridge extending from the west to near  $30^{\circ}\text{N}$ ,  $100^{\circ}\text{W}$ . The wind flow along the coast line of California is onshore in northern California and veering to northerly in Southern California around the ridge. This is very similar to the anomalous wind patterns shown in Figure 53a and is representative of the total wind patterns in Figure 54a.

The coastal cloud patterns are strongly influenced by the synoptic-scale flow. Consequently, it is reasonable to expect distinct cloud patterns associated with the VEOF modes. In the southerly ridge synoptic regime, it is expected that frequent clearing of the coastal stratus will be observed in the Southern California region. It is also expected that there will generally be onshore flow in northern California, Oregon, and Washington associated with a low pressure system. The onshore flow to the north may cause the coastal stratus to be forced against the coast. Figure 60 uses Defense Meteorological Satellite Program (DMSP) satellite imagery to describe cloud distributions associated with the southerly ridge event (depicted by Figure 59) that occurred on 00:00 UTC on 11 June 1995. Shown in Figure 60 is onshore flow and associated coastal cloudiness to the north of San Francisco. The coastal region south of Monterey Bay to Mexico is clear, indicative of offshore low-level wind

flow. The orientation and streaks in the clouds also confirm the direction of the low-level wind flow corresponding to a southerly ridge regime. The southerly ridge wind regime (Figure 54a) produces a northwesterly wind flow through the Southern California coastal region which veers to northeast winds west of the Baja Peninsula. There is distinct clearing of the boundary layer stratus in the Southern California coastal region associated with northwesterly wind flow, and over southern Baja there is offshore flow.

## **2. Northerly Ridge**

The location of the eastern North Pacific anticyclone in the northerly ridge regime is near 40°N. From the 1993 to 1995 data set, the northerly ridge occurs approximately 52.9% of the time when VEOF mode one is significantly greater than the next strongest contributing mode. When compared to the three dominant VEOF modes, the northerly ridge case accounts for 36.6% of the mean-plus-sd cases. In a year-to-year breakdown of the first three VEOF modes: the northerly ridge case comprises 20.0% of the periods in 1993, 6.9% in 1994, and 9.7% in 1995. A typical period of a northerly ridge behavior, which happens to fall within a four day series of northerly ridge cases, is represented by the NMC 850 mb analysis (Figure 61). At 00:00 UTC 25 July 1993, there is a weak low pressure system situated off the coast of Southern California near 30°N, 120°W. In the east North Pacific Ocean, there is a strong high pressure system near 40°N, 140°W. The winds are southerly along the Southern California coast around the low. The rotation and orientation of the wind flow off of the Southern California coast are similar to the anomalous wind composite for the northerly ridge shown in Figure 53b, while the wind flow pattern in the analysis is consistent with the total wind composite in Figure 54b.

For a northerly ridge regime, it is expected that there will be enhanced subsidence and drying of the PBL, and frequent clearing of the coastal stratus along the northern California coast. In addition, over Southern California, there would be north to northwesterly winds turning around Point

Conception that could trap coastal stratus against the Southern California coast. Figure 62, a 23:43 UTC 24 July 1993 visual satellite image, shows strong offshore flow extending from Oregon to Point Conception with extensive coastal clearing as the offshore wind flow pushes the coastal marine stratus out to sea. Figure 62 corresponds to the 00:00 UTC 25 July 1993 northerly ridge event shown in Figure 61. The total wind composite of the northerly ridge event (Figure 54b) shows the same ridging effect in northern California and the onshore flow in the Southern California coastal region, resembling cloud distribution in the satellite image.

Mode one primarily describes the anomalous wind fields associated with propagating synoptic systems during the summer season. As a low pressure center or trough approaches the coast, the subtropical ridge is depressed to the south. This is described by the "southerly ridge" (mode one phase two VEOF). As the trough moves inland and a ridge builds over the eastern North Pacific Ocean behind it, a "northerly ridge" (VEOF mode one phase four) regime occurs. In this pattern with a strong northerly wind flow along the Central California coast, a weak cyclonic flow (like the Catalina Eddy) is common off Southern California.

### **3. Continental Land/Sea Breeze**

As previously mentioned, the two phases of VEOF mode two exhibit a strong diurnal signal. Using the mean-plus-sd criteria, 100% of the periods which have a strong magnitude VEOF mode two phase two, called the "continental land breeze", occur at 12 UTC (04:00 PST) with offshore flow near the coast. In fact, the offshore wind flow for VEOF mode two phase two is perpendicular to the coast along the California and Oregon coastlines. The same applies for VEOF mode two phase four, when 100% of the mean-plus-sd periods occur at 00 UTC. VEOF mode two phase four exhibits onshore wind flow perpendicular to the coast and is described by the name "continental sea breeze."

From the analysis of the data set, the continental land/sea breeze regimes are associated with an anticyclone in the east North Pacific Ocean centered near 35°N. This is near the climatological

position of the east North Pacific Ocean anticyclone. The continental land/sea breeze wind anomalies are small over the ocean, but exhibit a diurnal phase shift of onshore/offshore wind flow over the West Coast land masses. The land/sea breeze's combined VEOF mode is stronger than the other modes in 23.4% of the combined first three VEOF modes. In a year-to-year breakdown of the first three VEOF modes; the continental land/sea breeze regime comprises 39% of the strongest cases in 1993, 12% in 1994, and 7.3% of 1995. Figure 63 is a NMC 850 mb analysis for 12:00 UTC 17 July 1993 during a typical period that contains a series of days when the dominant modes are diurnally varying between continental land and sea breeze regimes (see Figure 52). Figure 63 indicates the east North Pacific Ocean anticyclone in its climatological position near 35°N, 140°W. The winds are northerly over northern California, northeasterly over central California and southwesterly over Southern California. The total wind composite (Figure 56a) is similar to this example with weak troughing over Southern California corresponding to the weak trough present in the analysis shown in Figure 63.

The continental land and sea breezes mode is more difficult to illustrate in satellite imagery. It is not expected that there will be large cloud patterns that can be directly attributed to this mode because the expected pattern is the climatological one consisting of weak northwest winds and stratus along the coast. Figure 64 shows a late morning (15:41 UTC 17 July 1993) satellite image representing the 12:00 17 July 1993 continental land/sea breeze regime. Weak northwesterly winds can be inferred along the coast with expansive areas of coastal stratus from San Francisco to Mexico. The inferred winds from the satellite image correlates well with the expected winds from the continental land breeze total wind composite shown in Figure 56a.

Inferences of a continental sea breeze have been made by using long time series of data (Wexler 1946). In this study, the various synoptic-scale influences are averaged out and the large-scale onshore/offshore continental-scale wind flow remains. In this study, the VEOF modes have identified periods (mode two) where the continental-scale sea breeze dominates as the synoptic-scale

anomalies are weak at the time. The periods of strong mode two VEOF will be very interesting to study with inland data to further investigate this large-scale continent-ocean circulation identified here.

#### **4. Enhanced/Weakened Alongshore Flow**

VEOF mode three comprises only 5.9% of the mean-plus-sd periods in the 1993 to 1995 data. In Figure 52, the enhanced/reduced alongshore flow regime is observed to occur in series of similar phases that usually span several days. From examination of the corresponding total wind composites in Figure 58, the enhanced/weakened alongshore flow regimes are associated with an east North Pacific Ocean anticyclone in its climatological position. The difference between phase two and phase four is the formation of a cyclone near southern Nevada that enhances the gradient flow, creating enhanced alongshore wind flow along the coast of California. This is in agreement with the interpretation of the total wind composites shown in Figure 58. The formation of a synoptic-scale low over southern Nevada is consistent with the slowly changing phase relationships in Figure 52, instead of the diurnal phase shifts associated with VEOF mode two. Figure 65 is a NMC 850 mb analysis for 12:00 UTC 2 July 1993 of a typical period classified as an enhanced alongshore regime. In the analysis there is a low pressure area centered near north-central Nevada with the east North Pacific Ocean High offshore near 37°N, 140°W. The winds are generally northerly near the coast and follow the above description of the enhanced alongshore flow regime.

#### **5. Relationships to Monthly Anomalies**

Since this study has developed synoptic classification schemes and has shown that there are year-to-year variations in the distribution of the different synoptic regimes, there should be corresponding differences in the large-scale circulation patterns over the eastern North Pacific Ocean. In a month-to-month breakdown of the synoptic-scale atmospheric mean 850 mb wind values and monthly departures from the means, the dominant synoptic-scale influences should be visible. Therefore, the monthly averages of the *strongest mode* (for a particular time, this is the VEOF mode



with the largest principal component magnitude) synoptic regimes for 1993 to 1995 are shown in Figure 66. The figure shows clearly that there are large differences in the VEOF patterns each month. These differences can be identified through large-scale circulation statistics.

The sources of the large-scale circulation statistics are the monthly Climate Diagnostics Bulletins published by the Climatic Analysis Center (CDB 1993a-d, 1994a-d, 1995a-d). NMC 850 mb monthly mean winds are given along with the average monthly anomalies from the 1979-1988 10-year base period. These climatic statistics will indicate the representativeness of the 850 mb total and anomalous wind regimes developed in this study.

From Figure 66, there are five months in which the strongest mode VEOF regimes comprise over 33% of all analysis times; they are July 1993 (43%), August 1993 (35%), June 1994 (45%), June 1995 (36%) and September 1995 (37%). Notice that 1993 is comprised of more northerly ridge days, while 1994 and 1995 are comprised of more southerly ridge days.

The CBD 850 mb monthly mean wind analysis for July of 1993 is shown in Figure 67. The mean wind chart shows an area of anticyclonic turning of the winds in the east North Pacific Ocean near 40°N, 140°W. There is a broad area of strong northerly winds along the northern California coast, which is consistent with the winds in the northerly ridge total wind composite previously shown in Figure 54b. This is a departure from June of 1993 (Figure A8), which contained an anticyclone near 30°N, 140°W, and there is more contribution by the southerly ridge regime (Figure 66). The area of anticyclonic winds observed in Figure 67a continues into the month of August 1993 (Figure 68), which clearly corresponds with the dominant northerly ridge regime in August. Notice there is a smaller percentage of northerly ridge days in August 1993 (compared to July) and this compares to lighter mean winds in the 850 mb monthly average. The anomaly for each of these months also shows strong anomalous northerly winds resembling the VEOF mode one phase four in Figure 53b.

The effect of the large percentage of southerly ridge regimes in June 1994 is certainly present in the mean wind chart shown in Figure 69a. The east North Pacific Ocean anticyclone is located near  $30^{\circ}\text{N}$ , which indicates that northwesterly winds dominated along the Southern California coast during the month. This is a close match to the southerly ridge total wind composite shown in Figure 54a. The mean wind charts corresponding to the months of June and September 1995 (Figures A9 and A10) show anticyclonic wind near  $30^{\circ}\text{N}$ ,  $140^{\circ}\text{W}$ . These resulting synoptic patterns are well represented by the southerly ridge regimes.

There is generally even distribution between the different synoptic regimes in the remainder of the summers of 1993, 1994, and 1995 and it is more difficult to draw clear interpretations of the climatological relationship to the synoptic classification regimes. But most of the monthly mean wind fields are well represented by the synoptic regimes developed in this study as can be further seen in the Appendix in Figures A11-A16.

In a climatological sense, the summer of 1993 tended to be dominated by an east North Pacific Ocean anticyclone at 850 mb that was situated near  $40^{\circ}\text{N}$ , as can be seen by the large amount of northerly ridge events in Figure 66 for July and August 1993. September of 1993 was a month in which the east North Pacific Ocean anticyclone was weaker, exhibiting an elongated area of anticyclonic winds that roughly paralleled the coastline along the west coast. There was not any large contribution in the month by the northerly ridge or southerly ridge regimes. It is interesting to note that in this month the continental sea and land breeze regimes were the more frequent (Figure 66).

In this chapter, we have followed Harr (1993) performing a VEOF decomposition on the NOGAPS 850 mb winds for the summers of 1993-1995 for the west coast of the United States. The principal components of the VEOF modes were used to objectively identify the most frequent VEOF mode phases. Total and anomalous 850 mb wind composites were constructed from the strongest of the VEOF mode phases. These VEOF phases and composites were related to the synoptic-scale wind

patterns with NMC 850 mb analyses, satellite images and mean monthly 850 mb wind averages and anomalies (CDB 1993a-1995d). The VEOF synoptic regimes identified were the northerly ridge, southerly ridge, continental land/sea breeze, and enhanced/reduced alongshore wind regimes. The continental land/sea breeze, previously only described using statistical averages from long time series data, emerged as a distinct regime in this analysis.

## **VI. RELATIONSHIP OF SEA BREEZE TO SYNOPTIC SCALE**

One of the goals of this project is to examine the large-scale 850 mb wind circulation influence on the sea breeze. In the past, modeling studies investigated the impact of the large-scale wind flow on the sea breeze with user specified gradient/geostrophic wind inputs (Estoque 1962, Arritt 1993). Studies in Florida by Blanchard and López (1985), Gould and Fuelberg (1996), and Gould *et al.* (1996) and in California by Knapp (1994), discussed earlier, were only partially successful in understanding relationships between the sea breeze and synoptic regimes. These studies started with given sea breeze conditions, and then sought the synoptic-scale circulation influences. In this chapter, the relationships between the synoptic regimes isolated in Chapter V and the different sea breeze types are explored. In addition, evidence of synoptic or larger scale influences on the different sea breeze types are discussed. Finally, other factors influencing these relationships are examined.

### **A. SEA BREEZE FREQUENCY ANALYSIS**

The relationship between the synoptic patterns and the sea breeze are investigated initially by studying the distribution of the types of sea breeze circulations for various VEOF modes. The southerly ridge, northerly ridge, continental land/sea breeze, reduced alongshore flow, and enhanced alongshore flow regimes are examined with data from Fort Ord, Point Mugu, and Point Loma. However, the most emphasis will be placed on relationships at Fort Ord since a longer time series of data is available there and local effects are less important.

First, the sea breeze circulation was objectively classified (this was performed in Chapter IV). Second, a VEOF approach using large-scale NOGAPS wind fields was used to identify objectively synoptic-scale wind circulation patterns (this was performed in Chapter V). It was necessary to objectively classify sea breeze circulations and the synoptic-scale circulation patterns separately to

minimize subjective bias in the results. Now the influence of the synoptic-scale 850 mb wind circulation, as determined from our NOGAPS VEOF approach, can explore some relationships between the sea breeze circulations types and synoptic-scale wind patterns.

Recall that our investigation of sea breeze structure at the Fort Ord site for 1993-1995 isolated the three dominant categories, frontal-westerly, gradual-westerly, and rapid onset (Figure 17). The most frequent classification was that of gradual-westerly, which occurred in 44% of the total sea breeze days (160 days). Frontal-westerly was present approximately one-third of the time, while rapid onset was found 15% of the time. Table 3 summarizes Figure 17 when a NOGAPS 12:00 UTC VEOF dominant regime was available for comparison to a sea breeze type for the summers of 1993-1995 and eliminates missing data. In the 12:00 UTC grouping, the most frequent classification is gradual sea breezes (includes rapid onset) with 64% of the days, while frontal-westerly represents 33% of the days, similar to the complete data set. Table 3 also includes the distributions of the sea breeze categories at Fort Ord in relation to the strongest three eigenmodes and the five most influential synoptic regimes: northerly ridge, southerly ridge, continental land/sea breeze, enhanced alongshore flow, and reduced alongshore flow.

<b>Fort Ord</b>	<b>Frontal (%)</b>	<b>Gradual &amp; Rapid (%)</b>	<b>Other (%)</b>	<b>number</b>
Average	33	64	3	320
Northerly Ridge	37	62	1	65
Southerly Ridge	25	72	3	52
Continental Land/Sea Breeze	36	64	0	77
Enhanced Alongshore Wind	10	90	0	19
Reduced Alongshore Wind	10	80	10	10

**Table 3.** Average distribution of sea breeze type for each synoptic regime at Fort Ord.

At Fort Ord, there is some influence of the VEOF synoptic-scale regimes in the distribution of sea breeze categories. In this discussion, the gradual-westerly and rapid onset sea breeze contributions will be combined into gradual sea breeze days. In the southerly ridge regime (comprising 52 days of the three summers), the distribution of frontal-westerly days decreases by 8% from average to 25%, while the gradual sea breeze days increases by 8% to 72%. From the anomalous wind fields associated with the southerly ridge, it is expected that there will be more days with westerly winds at Fort Ord and thus more gradual sea breeze days, and this is exactly what is shown.

In the northerly ridge regime, it is expected from the anomalous wind fields that there will be more offshore wind days, and thus an increase in the number of frontal sea breeze days. The northerly ridge regime (comprised of 65 days) shows 37% frontal-westerly sea breeze occurrences, about 4% more frequently than the three summer average. The gradual sea breeze occurs 62% of the time, 2% less than average. The increase in frontal sea breeze days within the northerly ridge is consistent with expectations, but small.

The combined continental land/sea breeze regime (77 days) at Fort Ord exhibits a sea breeze distribution that is very close to the three year average. This agrees well with the observation that the continental land/sea breeze regime is found when the large scale pattern is close to climatology.

The number of days with the reduced/enhanced alongshore flow regimes are very small (19 in the enhanced and 10 in the reduced) over a three-summer period at Fort Ord. However, the gradual sea breeze events occur 90% of the time in the enhanced alongshore wind and 80% of the time in the reduced alongshore wind regimes. The frontal sea breezes occurred 10% of the time in both of the alongshore wind regimes. Although the enhanced/reduced alongshore wind regimes define a small portion of the data set, the preference for gradual and rapid onset sea breeze types are consistent with coastline geometry and prevailing onshore flow.

To classify the different synoptic regimes in this portion of the study, the strongest mode was used to define the synoptic regime, thus including the largest number of days. More restrictive criteria were used in defining synoptic regime days to determine if the sea breeze type distribution would relate to the regimes more closely. The mean-plus-sd and *strongest-50* (for each time period, the magnitude of the largest principal component was 1.5 times larger than the next largest contributing mode) were used, as well as some much more stringent separation schemes to determine the most representative wind patterns from the different modes. But the sea breeze type distributions consistently remained within  $\pm 5\%$  of the results given above. This indicates that the sea breeze type distribution is not a function of how the strength of the synoptic wind regime were defined, but rather by the basic VEOF wind regimes themselves. The shift in sea breeze distributions at Fort Ord within the VEOF regimes was modest but consistent with physical expectations for the different VEOF modes.

We now consider the Point Mugu and Point Loma locations. Recall that our investigation of sea breeze structure at Point Mugu was for the summer of 1993 only. It isolated three dominant sea breeze categories: frontal-westerly, frontal-southerly-westerly, and gradual-westerly. In the overall average sea breeze distributions previously shown in Figure 27, the most frequent individual category was the gradual-westerly comprising 30% (36 days) of the year, while the other two categories of frontal days occurred in over 48% of the days. Table 4 shows the sea breeze category distribution corresponding to Figure 27 that is composed of days which correspond to a 12:00 UTC VEOF NOGAPS dominant regime and eliminates missing data. In the table, the contributions for all gradual and rapid onset days combined are 33%, while the contributions of the frontal categories sum to 55%. The table also includes the 12:00 UTC distributions for the sea breeze categories for the synoptic regimes: northerly ridge, southerly ridge, continental land/sea breeze, enhanced alongshore flow and

reduced alongshore flow. Note that all frontal types are grouped together in this table and the rapid onset sea breeze days are combined with the gradual sea breeze days.

Point Mugu	Frontal (%)	Gradual & Rapid (%)	Other (%)	number
Average	55	33	7	109
Northerly Ridge	35	58	7	26
Southerly Ridge	100	0	0	9
Continental Land/Sea Breeze	43	51	6	34
Enhanced Alongshore Flow	54	46	0	13
Reduced Alongshore Flow	0	100	0	1

**Table 4.** Average distribution of sea breeze type for each synoptic regime at Point Mugu.

The 12:00 UTC sea breeze distribution for each synoptic regime at Point Mugu differs from the Fort Ord distributions discussed previously. Under the influence of the northerly ridge, the contribution of gradual sea breezes days increased 15% from average to 58%, while contribution of the frontal sea breeze types decreased 20% from average to 35%. This is easily explained when one takes the total wind composite of the northerly ridge regime (Figure 56b) into account. The wind pattern associated with the northerly ridge regime is from the west at Point Mugu (onshore component), consistent with the gradual sea breeze category.

The southerly ridge 12:00 UTC sea breeze distribution is comprised of 100% frontal sea breeze days. Although, the sample size is very small (9 days), it is interesting that all nine are frontal days. This is extremely different from the average, but not unexpected when the total wind composite for the southerly ridge (Figure 56a) was examined for Point Mugu. The 850 mb NOGAPS wind near Point Mugu is from the north-northwest for this mode, ensuring a strong offshore flow to concentrate the temperature gradient and produce the wind shift changes needed for the frontal classification. The



distribution of the sea breeze days under continental land/sea breeze regime are very similar to the average sea breeze distribution for all modes. The analysis of the Point Mugu sea breeze is limited by the availability of only one year worth of data.

Our previous investigation of sea breeze structure at Point Loma for 1993 isolated three more frequent sea breeze categories, gradual-southerly, gradual-westerly, and rapid onset (Figure 38). The most frequent sea breeze category was gradual-westerly, representing 17% (20 days) of the data. The two other categories, gradual-local and rapid onset, represented 15% and 13% of the days. Table 5 represents the distribution of the sea breeze categories that have corresponding 12:00 UTC VEOF NOGAPS dominant regimes and eliminates missing data for Point Loma. All frontal sea breeze types are summed together, while the rapid onset sea breeze days are summed with all of the gradual sea breeze days. On average the gradual sea breeze types occurred in 66% of the days, while the frontal sea breeze types occurred in 21% of the days. It is important to note that there is a lack of strong individual categories at Point Loma and the distribution of gradual sea breeze days consistently constitute near two-thirds of the days under each VEOF regime. The sea breeze type distribution at Point Loma shows no response to changes in the VEOF mode one.

<b>Point Loma</b>	<b>Frontal (%)</b>	<b>Gradual &amp; Rapid (%)</b>	<b>Other (%)</b>	<b>number</b>
Average	21	66	21	98
Northerly Ridge	0	62	38	19
Southerly Ridge	0	61	39	8
Continental Land/Sea Breeze	16	74	10	35
Enhanced Alongshore Flow	7	57	36	14
Reduced Alongshore Flow	0	100	0	1

**Table 5.** Average distribution of sea breeze type for each synoptic regime at Point Loma.

The influences of the synoptic-scale regimes were not well represented at Point Loma for 1993 for several reasons. First, the sea breeze intensity is weakest at Point Loma (previously identified in Chapter IV) and some surface data were missing. This resulted in one-third of the days in the four months studied being unclassifiable in the study. The effects of the ridge at Point Loma restricted offshore wind flow at the observing site and reduced the amount of frontal sea breezes observed. Finally, the southern Point Loma location is the farthest removed from the changes in mid latitude wind flow.

However, when examining the sea breeze circulations at Point Loma, there is a synoptic-scale influence on the two of the types of sea breezes. Recall from Figure 38 that the two most frequent occurring sea breeze types at Point Loma were the gradual-southerly and gradual westerly sea breezes. In general, it was observed during gradual-southerly sea breeze days, the dominant winds above the PBL were primarily from the south most of the day (Figure 39). And when gradual-westerly sea breezes were observed, the winds near 1000 m were from the north most of the day, and the winds above 1500 m were from the west (similar to the southerly ridge wind regime). These characteristics suggest that the two gradual sea breeze types at Point Loma are influenced by large-scale winds above the boundary layer.

## **B. SYNOPTIC INFLUENCES ON SEA BREEZE TYPES**

Additional information about the synoptic influences on sea breeze categories emerges when considering 850 mb wind anomalies and profiler composites for the different sea breeze types. Using the different sea breeze types as the starting point, all of the 850 mb NOGAPS wind anomalies at Fort Ord from the VEOF analysis (linearly interpolated from the four nearest grid points) were plotted using 15° sectors with 0°T as north as shown in Figure 70. A general preference for easterly anomaly winds for frontal sea breeze days and westerly anomaly winds for gradual sea breeze days is apparent.

More frequent easterly anomalies present with frontal sea breeze occurrences are consistent with the off-shore flow that will occur with a northerly ridge regime. However, there are small numbers of westerly and southerly anomalous winds present as well. Consequently, the northerly ridge regime only explains a portion of the frontal sea breeze events. This is one reason there are only modest shifts in the sea breeze type distributions when the mode one categories are considered. For gradual sea breezes, the primary anomalous wind directions are from northwest and southeast. The west to northwest anomalous winds are consistent with anomalies associated with the southerly ridge VEOF category.

Table 6 presents a contingency table showing the occurrence of frontal and gradual sea breeze types with respect to easterly ( $0^{\circ}$ - $162^{\circ}$  direction) and westerly ( $163^{\circ}$ - $359^{\circ}$ ) anomalous winds. The table illustrates that frontal sea breezes occur more often with easterly anomalous winds and gradual sea breezes are more frequent with the onshore westerly direction. In fact, with westerly anomalous winds, gradual sea breezes occur over three times more often than frontal sea breezes. A Chi-squared test on the contingency table confirmed that the sea breeze type distribution and anomalous 850 mb wind directions at Fort Ord were not independent of one another at the 95% confidence level. This analysis illustrates synoptic-scale winds have an influence on the occurrence of sea breeze types. For additional insight, the sea breeze type composites are examined in more detail.

Number of sea breeze days / percentage of total days	Easterly winds $0^{\circ}$ - $162^{\circ}$	Westerly winds $163^{\circ}$ - $359^{\circ}$	Totals
Frontal Sea Breeze	83 / 32%	22 / 9%	105 / 41%
Gradual Sea Breeze	66 / 26%	86 / 33%	152 / 59%
Totals	149 / 58%	108 / 42%	257 / 100%

**Table 6.** Contingency table of anomalous winds at Fort Ord.

There were clearly some large-scale effects associated with the different sea breeze composites of the gradual-westerly (Figure 19) and frontal-westerly (Figure 18) sea breezes types. Many synoptic attributes of the mode one southerly ridge are found in the gradual-westerly sea breeze composite (Figure 19). The composite of the gradual-westerly sea breeze indicates southwesterly mean winds at 1500 m (near 850 mb). This is an onshore wind flow at Fort Ord and is consistent with the onshore anomalous winds exhibited by the southerly ridge wind regime. The wind flow associated with the entire wind profile during the night and early morning is onshore, indicating lower pressure to north and high pressure to south of Central California. This is the synoptic pressure field associated with the mode one southerly ridge. There is a deeper boundary layer with the inversion located near 1000 m indicating less large-scale subsidence near Fort Ord. This is associated with the southward shift of east Pacific Ocean anticyclone. The deep vertical extent of virtual temperature returns from the RASS indirectly indicates extensive, deep moisture in lower atmosphere because of the consistency of RASS measurements throughout a thick layer (also consistent with the southerly ridge producing moister boundary layers in Central and Northern California). In the composites, the relatively small diurnal temperature changes are indicative of increased low-level cloudiness which would be associated with the gradual sea breeze cases and strong onshore flow. At the 1500 to 2000 m level, southerlies winds imply troughing off-shore, while the subtropical ridge is depressed to the south.

Northerly ridge characteristics are found in the frontal-westerly composites (Figure 18). The frontal-westerly sea breeze exhibits northwesterly mean winds at 1500 m. This is indicative of alongshore to offshore wind flow at 850 mb at Fort Ord and not associated with a strong onshore wind component. This is most likely associated with a nearby high located offshore and is consistent with the anomalous winds of the northerly ridge wind regime. In the composite there are large diurnal temperature changes observed in the virtual temperature profiles, indicative of cool, cloudless nights with strong warming prior to sea breeze onset. The limited vertical extent of the virtual temperature

profiles indicates a dryer PBL and increased subsidence aloft associated with a high pressure area. The low-level easterly winds prior to sea breeze onset are indicative of the land breeze circulation or synoptic offshore flow. The low-level offshore flow suggests clear or minimal cloud coverage over the land.

The composite wind and temperature profiles have strong links to the different mode one regimes and suggest that the profiler vertical structure, as well as the synoptic modes, can be used to explain the types of sea breeze occurrence. While the frequency of sea breeze types does not change dramatically, the vertical structure of sea breeze types do strongly relate to the two different phases of the strongest VEOF mode, northerly ridge and southerly ridge. In fact, a composite of the days from the southerly ridge (which includes different sea breeze types) shows similarities to the gradual sea breeze type, while the composite of days from the northerly ridge (which also includes different sea breeze types) shows similarities to the frontal sea breeze types.

The wind and virtual temperature composite (not shown) of 53 southerly ridge days during 1994 and 1995 shows: westerly winds at 1500 m (near 850 mb), temperature inversion at 1000 m, and strong low-level winds onshore wind within the PBL. All of these observations indicate the gradual sea breeze regime is strongly related to the southerly ridge regime.

The wind and virtual temperature composite (not shown) of 39 northerly ridge days during the summers of 1994 and 1994 exhibit: easterly winds at 1500 m (850 mb), shallow boundary layer (implying enhanced subsidence), strong temperature inversion, and drier air aloft. All of these northerly ridge composite characteristics are consistent with the frontal sea breezes. The wind and virtual temperature composite (not shown) of the continental land/sea breeze regime matched climatology as expected. In summary, encouraging relationships between the sea breeze types and synoptic flow regimes emerged. However, analyses of larger data sets and more sites are needed to confirm the use of the synoptic regimes presented in this study.

### C. OTHER FACTORS

In describing the relationship of the synoptic-scale winds on the sea breeze, this study may have relied too much on the large-scale NOGAPS 850 mb winds. Model analysis errors in the low-level wind patterns will impact the resultant anomaly winds and associated VEOF wind regime. Also the large-scale model analysis resolution ( $2.5^\circ$ ) may be too coarse to accurately define the local low-level wind patterns at specific locations, which are essential in understanding the sea breeze circulation for that location. An analysis from a mesoscale model (like COAMPS) would provide better resolution and allow for finer resolution VEOF regimes to be defined. In turn, this may provide more accurate local wind patterns and allow for better correlation between the VEOF wind regimes and sea breeze types.

The horizontal temperature gradient and distribution of coastal clouds are other factors that may modulate of sea breeze behavior. As the temperature gradient decreases, there is less thermal perturbation necessary to produce a frontal type sea breeze or even a sea breeze at all. An extensive cloud distribution would serve to reduce the temperature gradient across the coast as well. The distribution of coastal clouds is not independent of the synoptic-scale influences. From examination of the sea breeze type composites, there are definite cloud effects apparent in the virtual temperature profiles. In particular, there will be increased coastal cloudiness, which reduces the across coast temperature gradient, associated with synoptic-scale onshore wind flow and gradual sea breeze types. And there will be reduced coastal cloudiness, which increases the across coast temperature gradient, associated with offshore wind flow and frontal sea breeze types.

One of the other factors that may be important in characterizing the day-to-day occurrence of the sea breeze to the 850 mb anomaly winds is the stability of the PBL. During times of high stability, the PBL becomes decoupled from the higher-levels. The winds within the PBL then would be weakly linked to the 850 mb winds and the 850 mb winds may not be indicative of the winds occurring within

the PBL. Thus the sea breeze types developing in the PBL may not be related to the synoptic VEOF wind regimes. The variability of sea breeze types within the northerly ridge regime at Fort Ord may be explained by the stability effects.

In this chapter, as one way to examine the synoptic-scale influences of the sea breeze, the synoptic-scale VEOF wind influences were compared to the occurrence of sea breeze days at Fort Ord, Point Mugu, and Point Loma. The change in sea breeze type distributions due to the different synoptic-scale VEOF regimes were small, but consistent with physical expectations. The location of the observing sites in relation to the synoptic VEOF wind regime is paramount in determining which type of sea breeze circulation to expect. A more detailed study of the 850 mb anomaly winds at Fort Ord indicated that offshore easterly wind anomalies were more associated with frontal sea breeze types. Gradual sea breeze days were most associated with onshore westerly anomalous winds, common to the southerly ridge regime. However, there were some anomalous winds and sea breeze types that did not follow these patterns. Additional large-scale effects were gleaned from the sea breeze type composites developed in Chapter IV. Other influences such as NOGAPS model characteristics, cloud conditions, PBL stability and local temperature gradients may also be factors in determining the type of sea breeze that occurs on any given day.

## VII. CONCLUSIONS AND RECOMMENDATIONS

### A. SUMMARY AND CONCLUSIONS

An extensive atmospheric data set was collected over the summers of 1993-1995 at various California coastal locations. The data set was significant because of the nearly continuous nature of the measurements of surface atmospheric parameters and low-level atmospheric data using the radar wind profiler and RASS systems. Because the observing sites used in this study were widely distributed along the California coast (~100's km separation), this enabled larger-scale analysis of the coastal PBL. The primary goals of this study were to increase the knowledge and understanding about the mesoscale structure and diurnal variations in the sea breeze circulation along the California coast and to objectively relate these changes to the synoptic-scale. To accomplish these goals, the data were analyzed in three distinct steps: 1) the objective classification of sea breeze events at the different observing sites; 2) the objective classification of the major synoptic 850 mb wind regimes that occurred during the study using NOGAPS model wind fields; and 3) the analysis of any relationships between the major synoptic wind regimes and the sea breeze structure.

Based upon initial sea breeze classifications by Wexler (1946) and Schroeder *et al.* (1967) and following the subjective studies of Fagen (1988), Round (1993), and Knapp (1994), an objective sea breeze classification scheme was developed. The classification scheme was designed to work, in general, along the west coast of continents. The classification scheme was fine-tuned for this study's observational sites by accounting for differences in local and regional-scale heating and coastline orientation to define the surface sea breeze circulation characteristics. Evidence of the robust nature of this classification scheme is that it identified sea breeze circulations in over 90% of the days at Fort Ord for the summers of 1993-1995 into three general sea breeze categories, frontal, gradual, and rapid



onset. The same classification scheme identified the same general sea breeze categories at Point Mugu and Point Loma in 87% and 65% of the days in the summer of 1993.

Local and regional-scale heating effects were observed at the surface and through the lower levels in the wind and temperature structures at Point Mugu and Point Loma. Specifically, distinct local and regional-scale sea breeze circulations were identified at Point Mugu that responded to heating from the nearby agricultural fields to the north and the Los Angeles basin to the east. At Fort Ord, the local and regional heating produce a sea breeze circulation consistently oriented along a west-east axis. The PBL temperature structure was strongly influenced by the strength of the sea breeze onshore flow. Stronger wind speeds were generally associated with cooler PBL temperatures, which lessened the effects of daytime heating within the PBL. Large-scale wind and local cloud effects were apparent in the wind and temperature structures of the different sea breeze types in diurnal boundary layer thickness and temperature changes.

Some synoptic-scale wind influences on the sea breeze were identified through VEOF decomposition of NOGAPS 850 mb analysis winds (Harr 1993). Analysis of the principal components provided the necessary information to define periods of similar phase relationships, and thus to develop composite total and anomaly 850 mb winds fields that were representative of five distinct synoptic VEOF wind regimes: northerly ridge, southerly ridge, continental land/sea breeze, enhanced alongshore flow, and reduced alongshore flow regimes. The location of the east Pacific Ocean anticyclone (the dominant summertime feature along the Pacific West Coast) characterized the largest three regimes for the period of this study. These locations were found to be the long term climatic average and shifts to the north and south of the long term average. These regimes corresponded to the first three VEOF modes and accounted for over 48% of the variance in the 850 mb wind fields over the course of this study. The physical relevance of the synoptic VEOF wind regimes were verified by comparison with analysis fields, satellite images, and climatological records.

Using the VEOF classification scheme, the "continental" sea and land breezes, previously only seen in long term statistical analysis, emerged as an important large-scale circulation mode.

Comparison of the sea breeze classifications under the effect of different synoptic VEOF wind regimes showed synoptic-scale wind influences on the type and distributions of sea breeze circulations at Fort Ord. In addition, at Point Mugu, the synoptic-scale VEOF wind regimes consistently produced the expected frontal or gradual sea breeze types in a majority of the cases. Furthermore, there appears to be a general connection between the 850 mb anomalous NOGAPS winds and the type of sea breeze circulation at Fort Ord. Anomalous 850 mb easterly winds are associated more with frontal sea breeze types, while anomalous 850 mb westerly winds are three times more likely to produce gradual sea breeze types. Additional large-scale effects emerged in the sea breeze type composites, indicating that synoptic-scale effects are an important influence on the sea breeze and coastal PBL characteristics. However, there are other factors such as cloud conditions, PBL stability, and local temperature gradients not accounted for in this study that should be addressed in future studies.

## **B. RECOMMENDATIONS**

Recommendations for follow-on research in relating the local sea/land breeze circulation and coastal PBL structure to larger-scale meteorological patterns are:

- VEOF decomposition and compositing of longer periods of data from finer-scale numerical mesoscale models (i.e. COAMPS) may provide more detailed wind patterns that are more representative. This in turn would allow closer investigation of the sea breeze circulations with respect to the larger-scale wind regimes.
- Continued application of the sea breeze classification scheme to long time series of surface measurements will determine the inter-annual and intra-annual variability and distribution of the sea breeze types.
- New principal component coefficients can be determined for analysis and forecast model wind fields by projecting the anomaly wind fields onto VEOF eigenvectors. In this way, new analysis and forecast synoptic wind fields can be classified in relation to the dominant eigenmodes developed in this study. This will provide the ability to objectively relate current analysis fields and forecast wind fields to synoptic-scale VEOF wind regimes.

- Investigation of the stability of the PBL and cross-coast temperature gradients will provide more insight on the development of the different sea breeze types. For example, a stronger cross-coast temperature gradient implies offshore winds and a relatively cloud-free atmosphere in the coastal region. Thus there would be a strong link between frontal sea breeze types, concentrated cross-coastal temperature gradient, and offshore winds. Higher stability in the PBL would inhibit downward momentum transfer into the boundary layer, possibly reducing the representativeness of 850 mb winds in representing the synoptic-scale wind flow within the PBL.

Through the continued analysis of continuous observations of surface and PBL parameters and the exploitation of a new generation of mesoscale models, naval and civilian meteorologists will continue to improve their ability to understand and forecast coastal mesoscale circulations, like the sea breeze, that are of critical importance to local weather analysis and prediction.

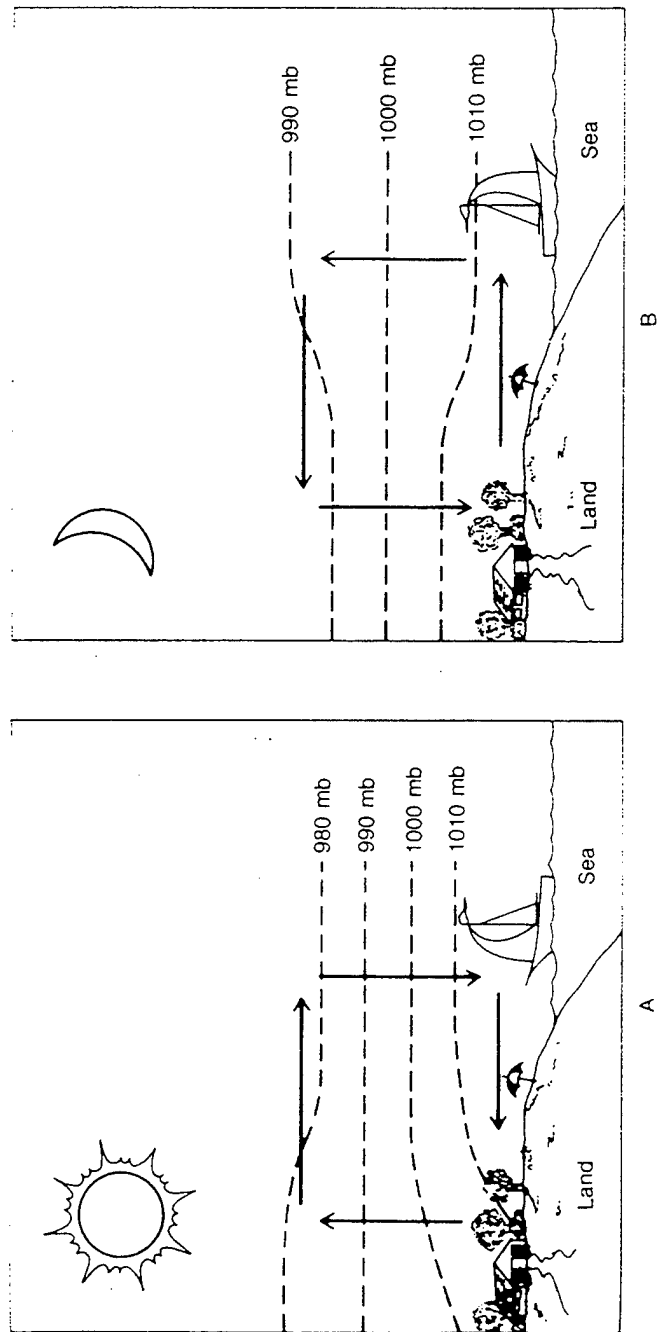


**Figure 1.** Diagram of the sea and land breeze circulation (from Moran and Morgan 1986).

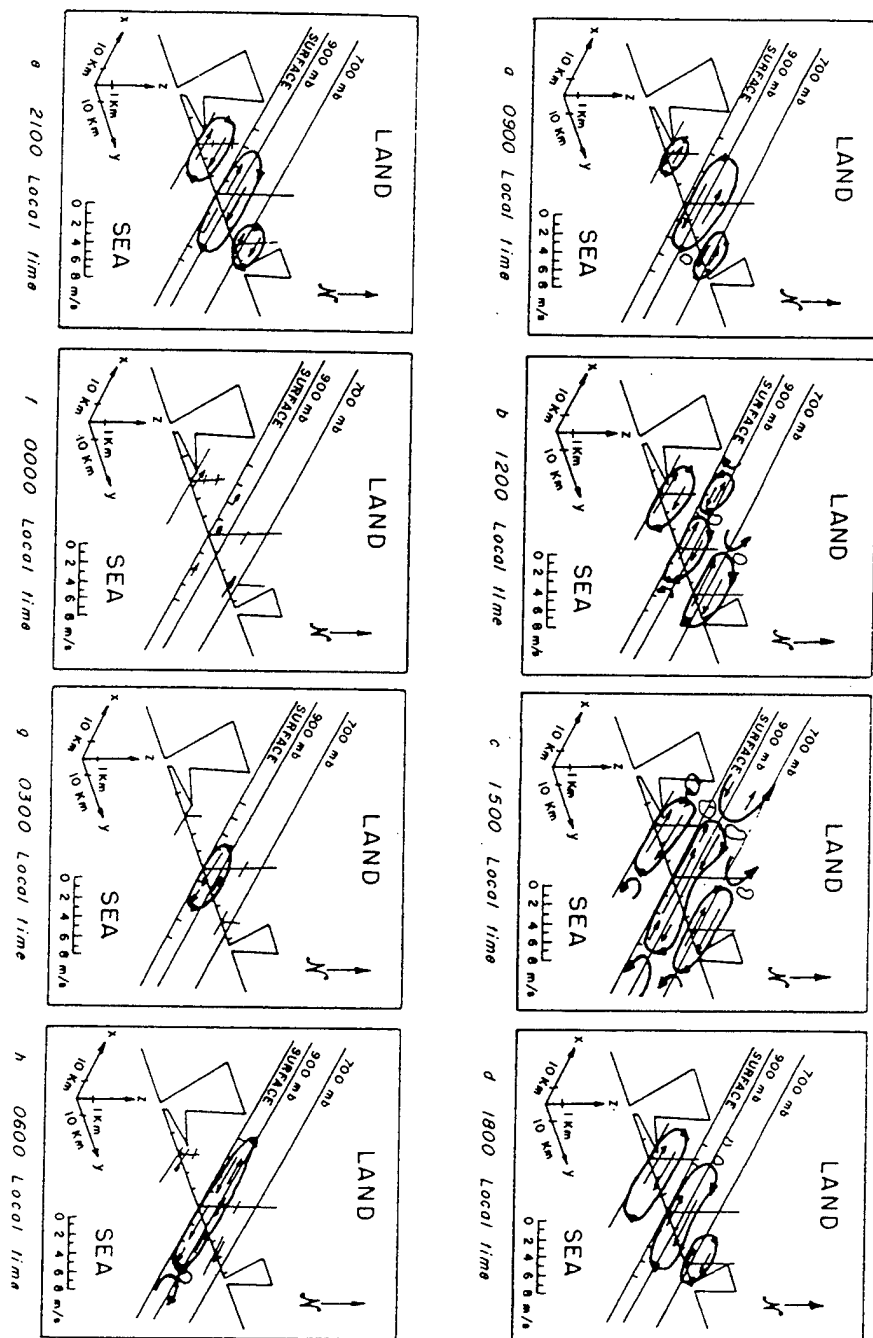
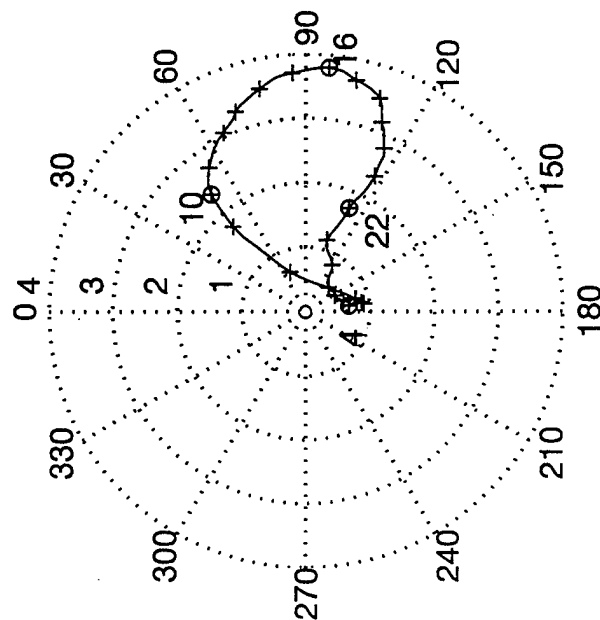


**Figure 2.** Development of land/sea breeze circulation in an area of complex terrain (from Hsu 1988).

PTM 1993



ORD 1993

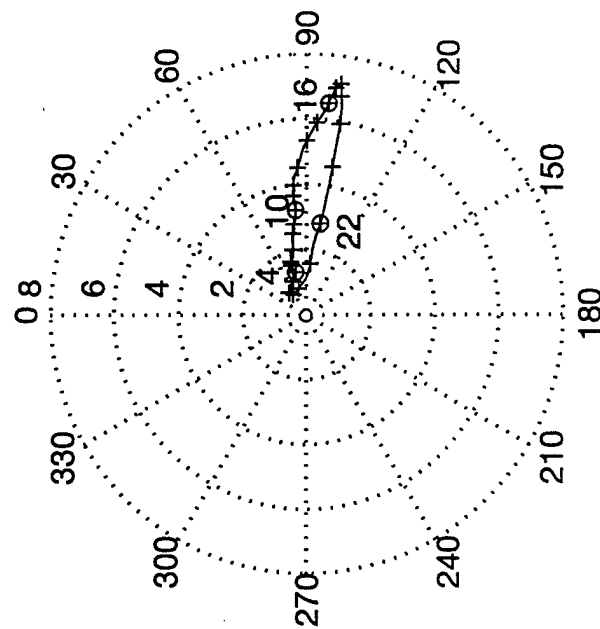


**Figure 3.** Wind hodographs for Point Mugu and Fort Ord from the summer of 1993. The hodograph is inscribed by the point of the hourly average wind vector. The speed of the wind is described by the radius from the center in m/s and the times in PST are marked by  $\oplus$ .

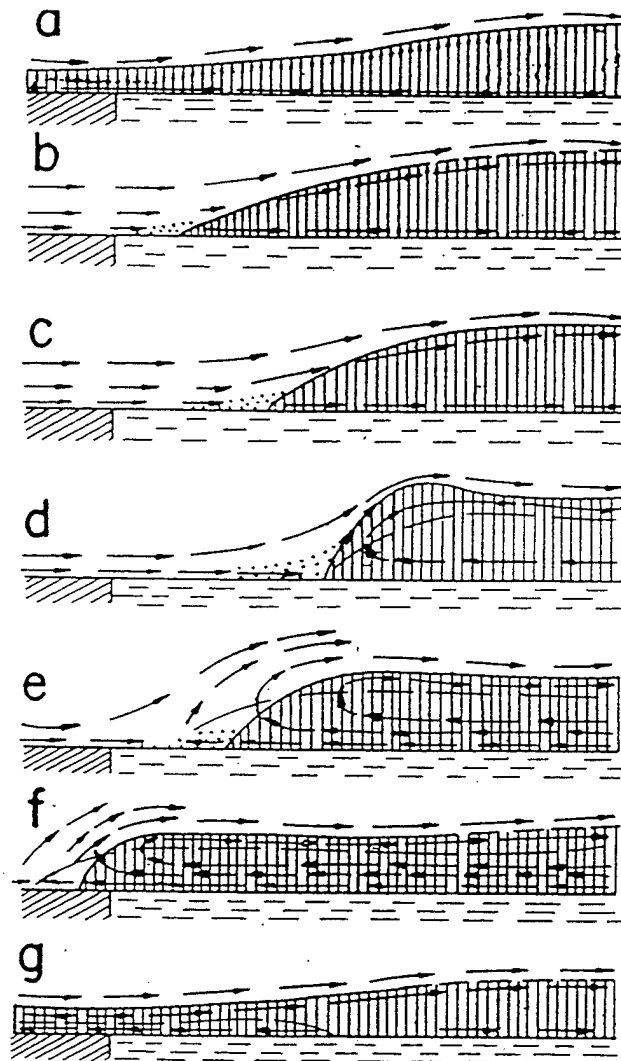


**Figure 4.** Koschmieder's depiction of frontal sea breeze development induced by off-shore gradient winds (from Wexler 1946, Koshchmieder and Hornickel 1936, 1941, 1942).

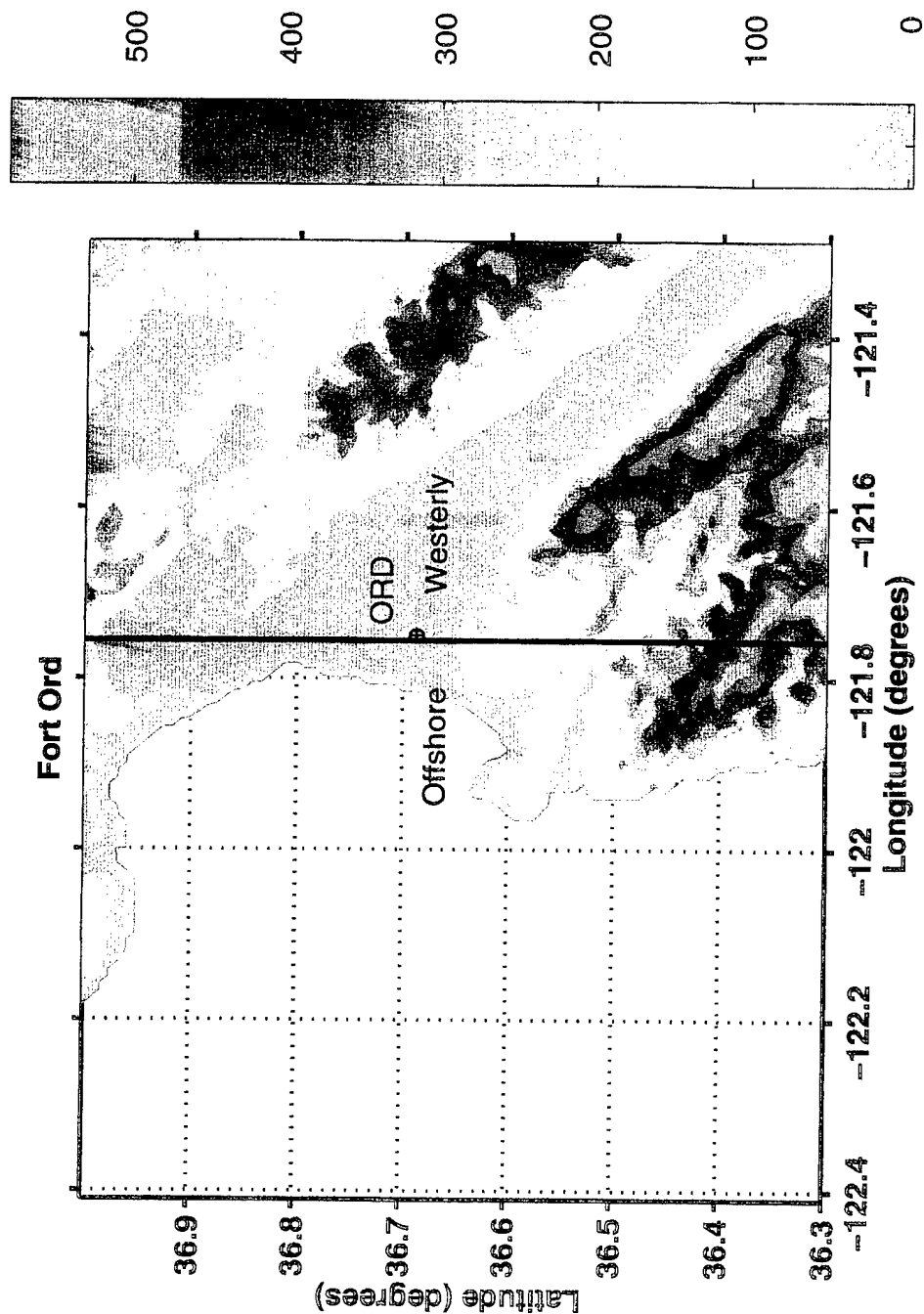
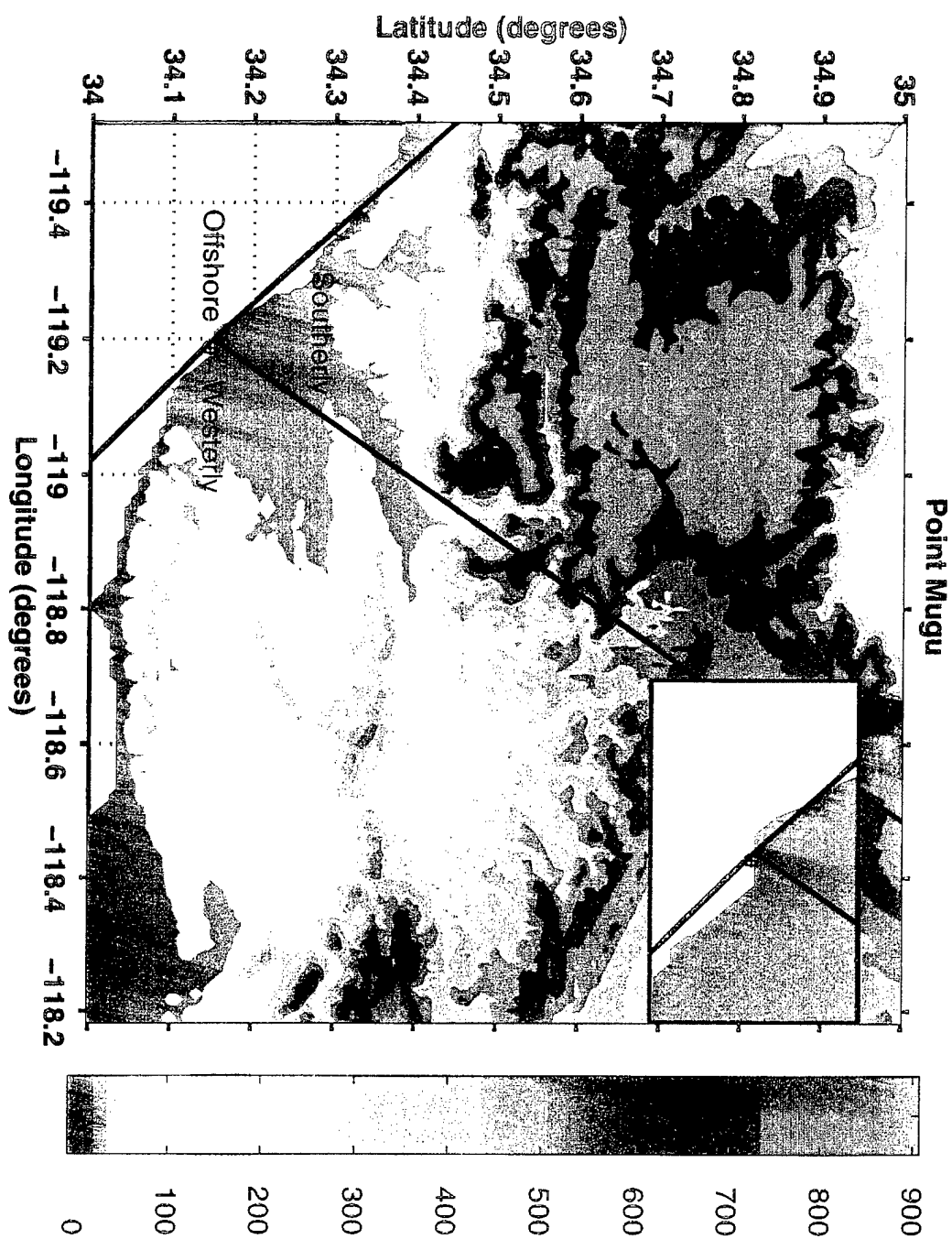
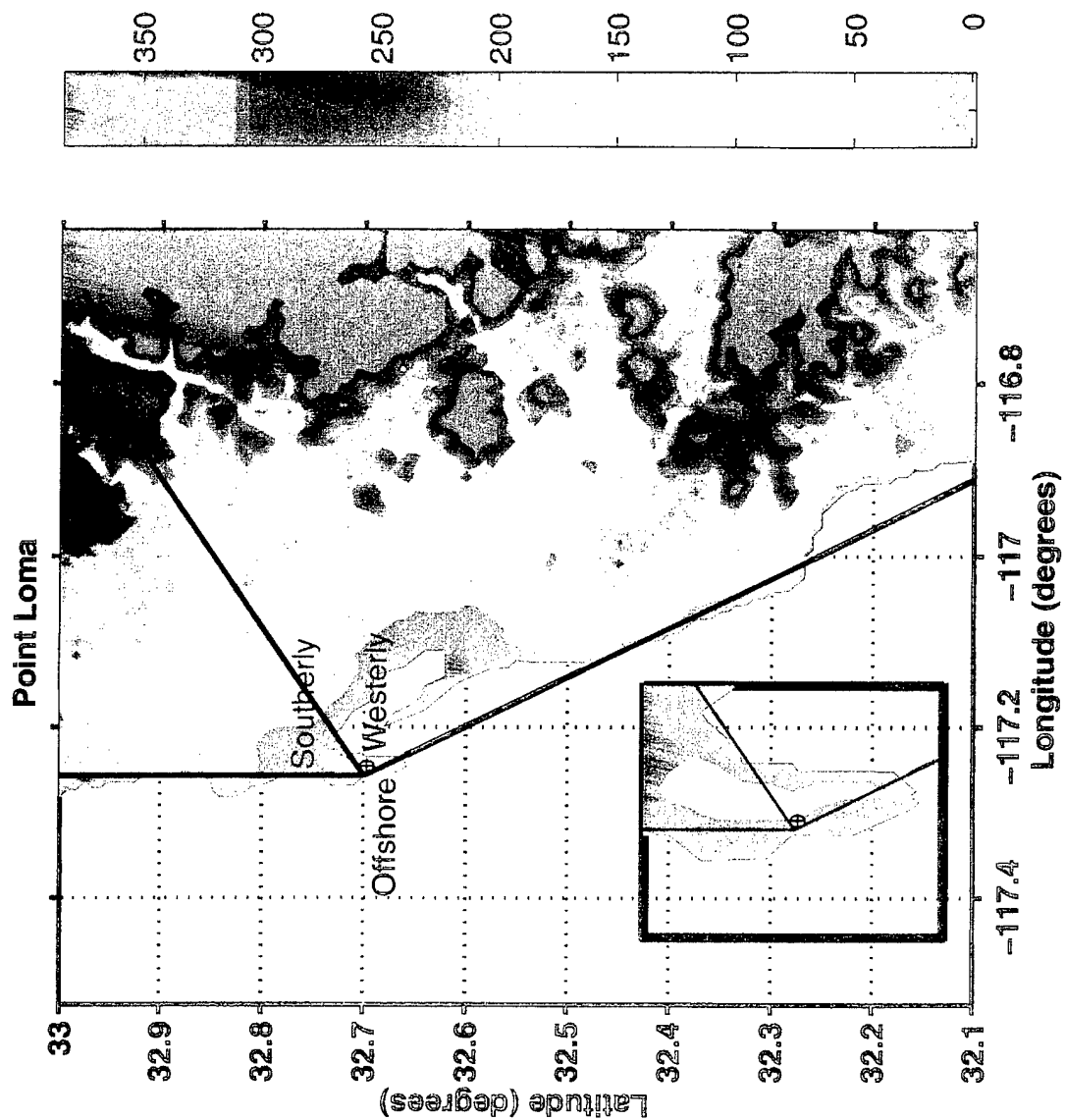


Figure 5. Topography surrounding Monterey Bay. The location of the Fort Ord observing sight is marked with  $\oplus$ . The boundaries for offshore flow and westerly onshore flow are marked with the bold line. Heights are in m.





**Figure 6.** Topography surrounding Point Mugu observing site. The location of the observing site is marked with a  $\oplus$ . The boundaries for offshore, southerly sea breeze, and westerly sea breeze are diagrammed. The local coastline at Point Mugu is east-west as shown in the insert. Heights are in m.



**Figure 7.** Topography surrounding the Point Loma observing site. The location of the observing site is marked with a  $\oplus$ . The boundaries delineating the offshore, southerly sea breeze, and westerly sea breeze are plotted. The insert is an enlargement of the topography at the observing site. Heights are in m.

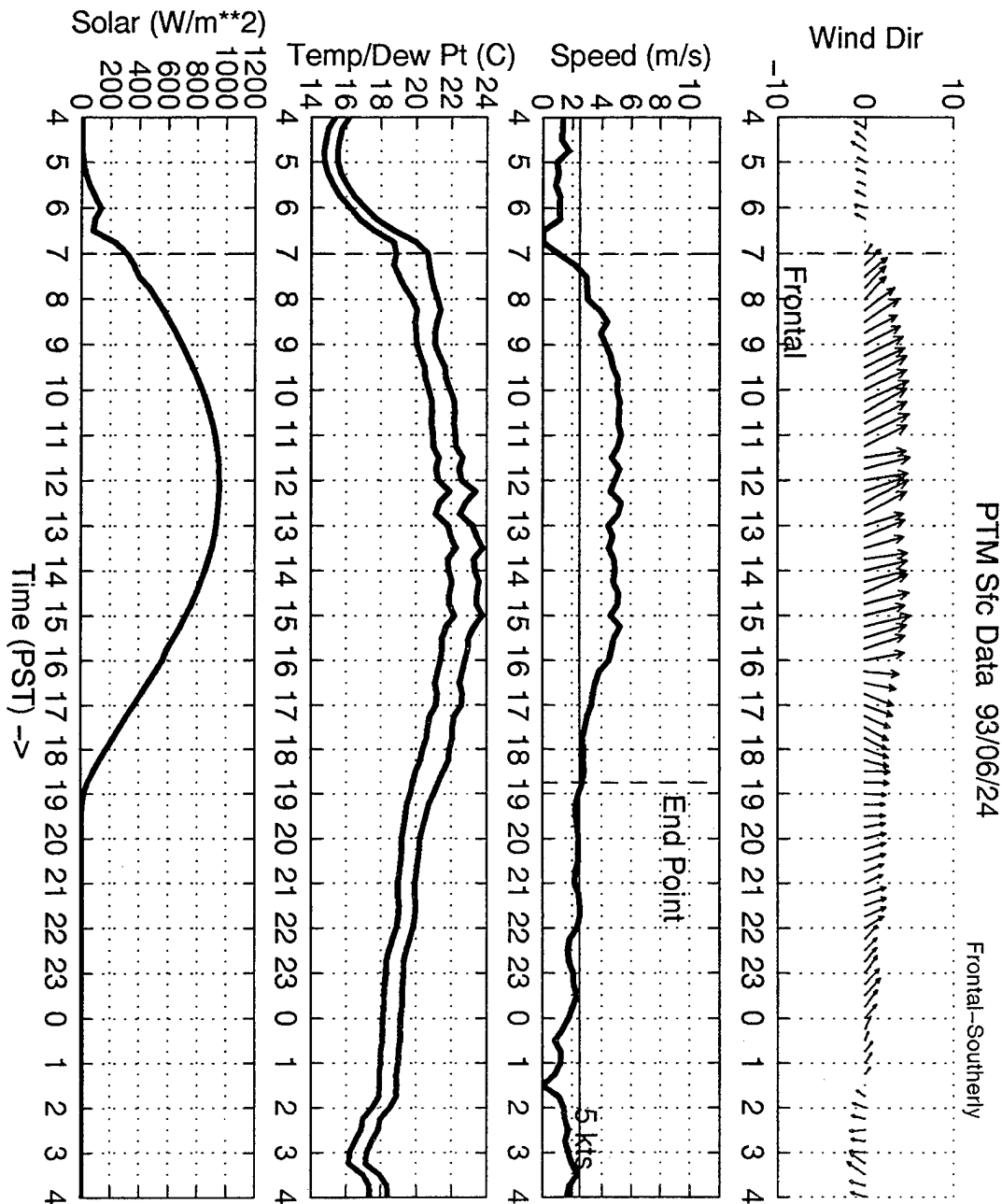


**Figure 8.** Plot of Frontal-Southerly sea breeze at Point Mugu. Plotted are wind direction ( $^{\circ}\text{T}$ ), wind speed (m/s), temperature ( $^{\circ}\text{C}$ ) and dew point ( $^{\circ}\text{C}$ ), and solar radiation (watts/ $\text{m}^2$ ). The onset of the sea breeze is plotted with a vertical dash-dot line. The approximate sea breeze end time is shown in the vertical dashed line. Shifts of winds to different sea breeze directions are marked accordingly. Increases in wind speed of 4 kts in 30 min are marked by surges.

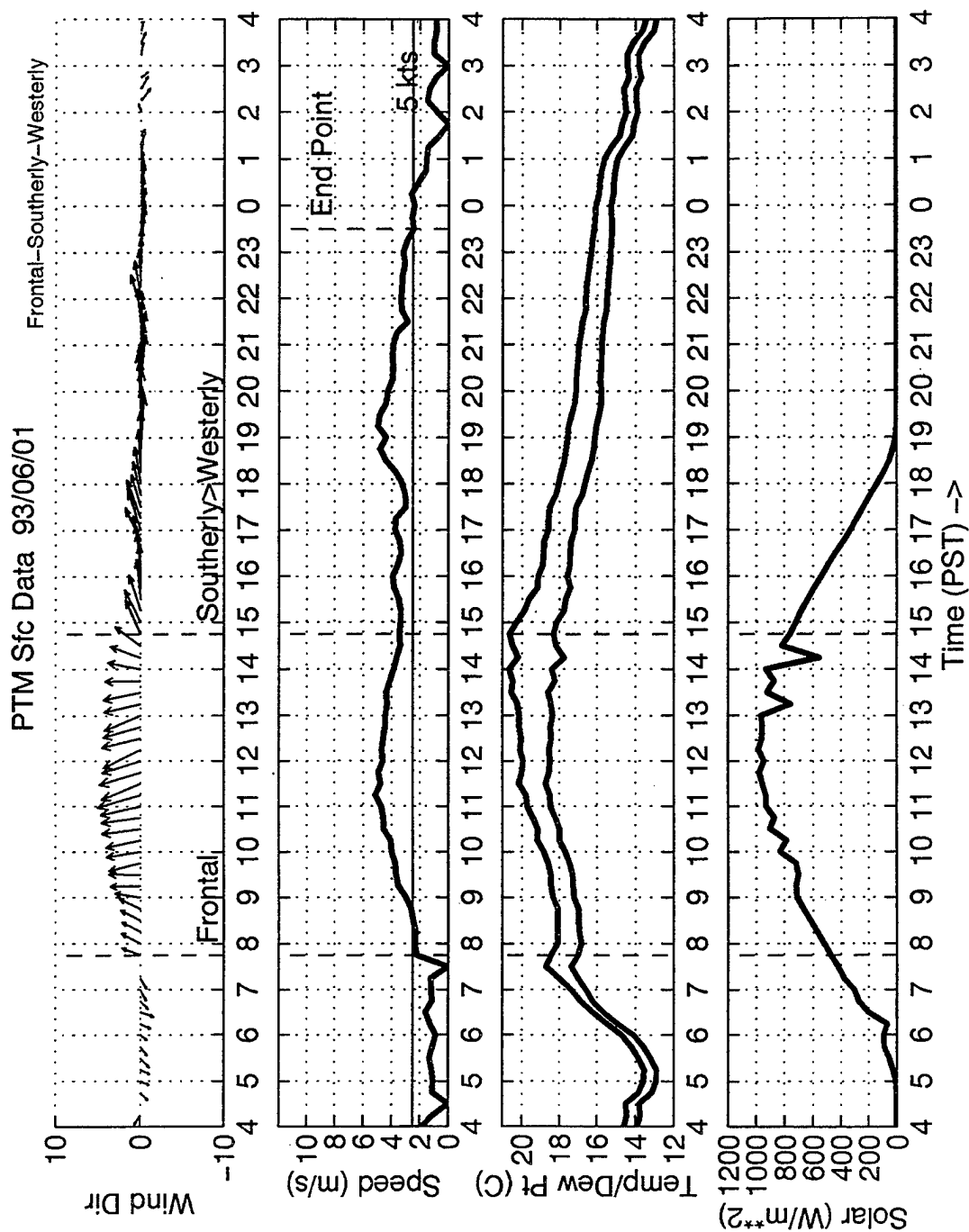


Figure 9. As Figure 8, except Point Mugu Frontal-Southerly-Westerly sea breeze.

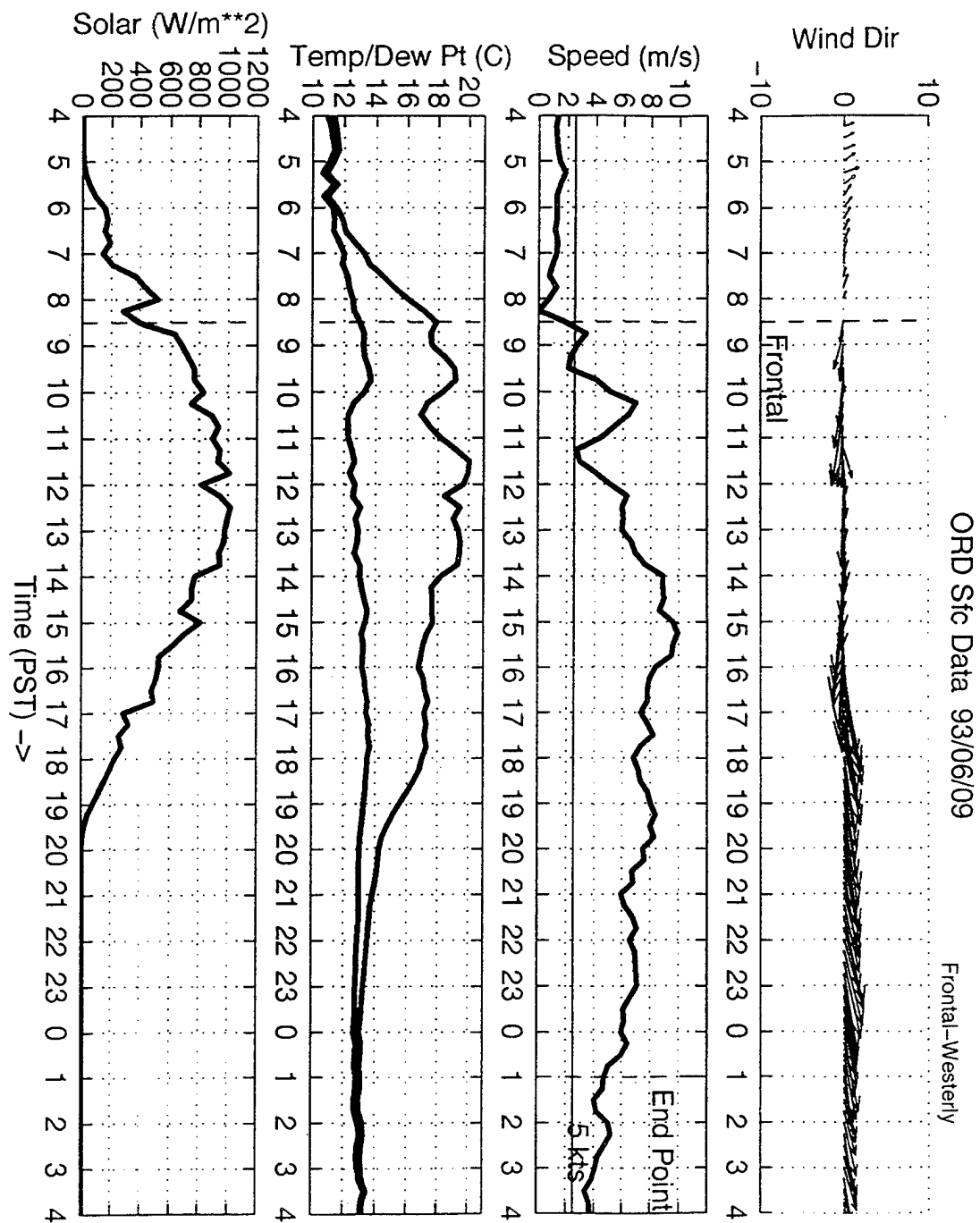


Figure 10. As Figure 8, except Fort Ord Frontal-Westerly sea breeze.

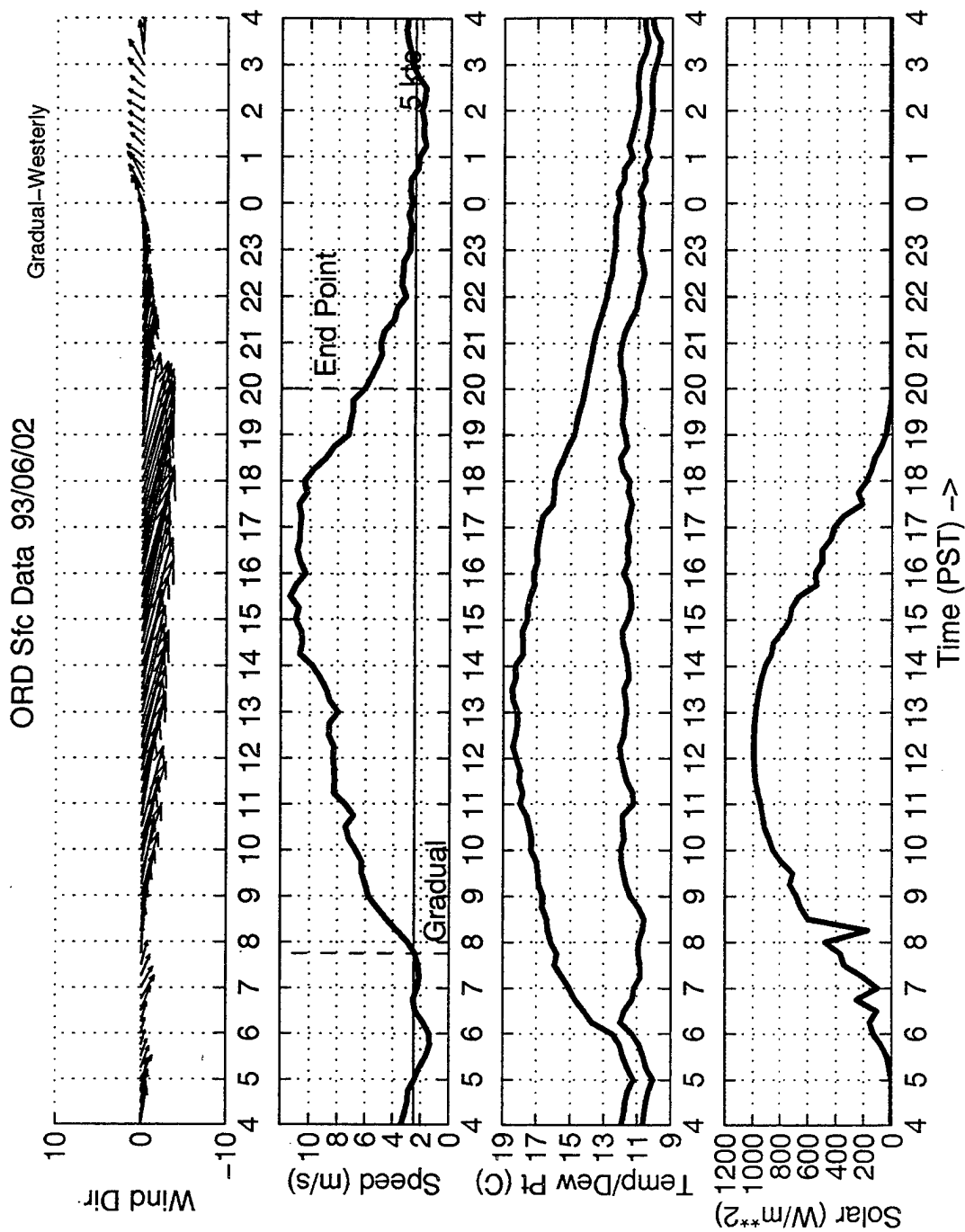


Figure 11. As Figure 8, except Fort Ord Gradual-Westerly sea breeze.

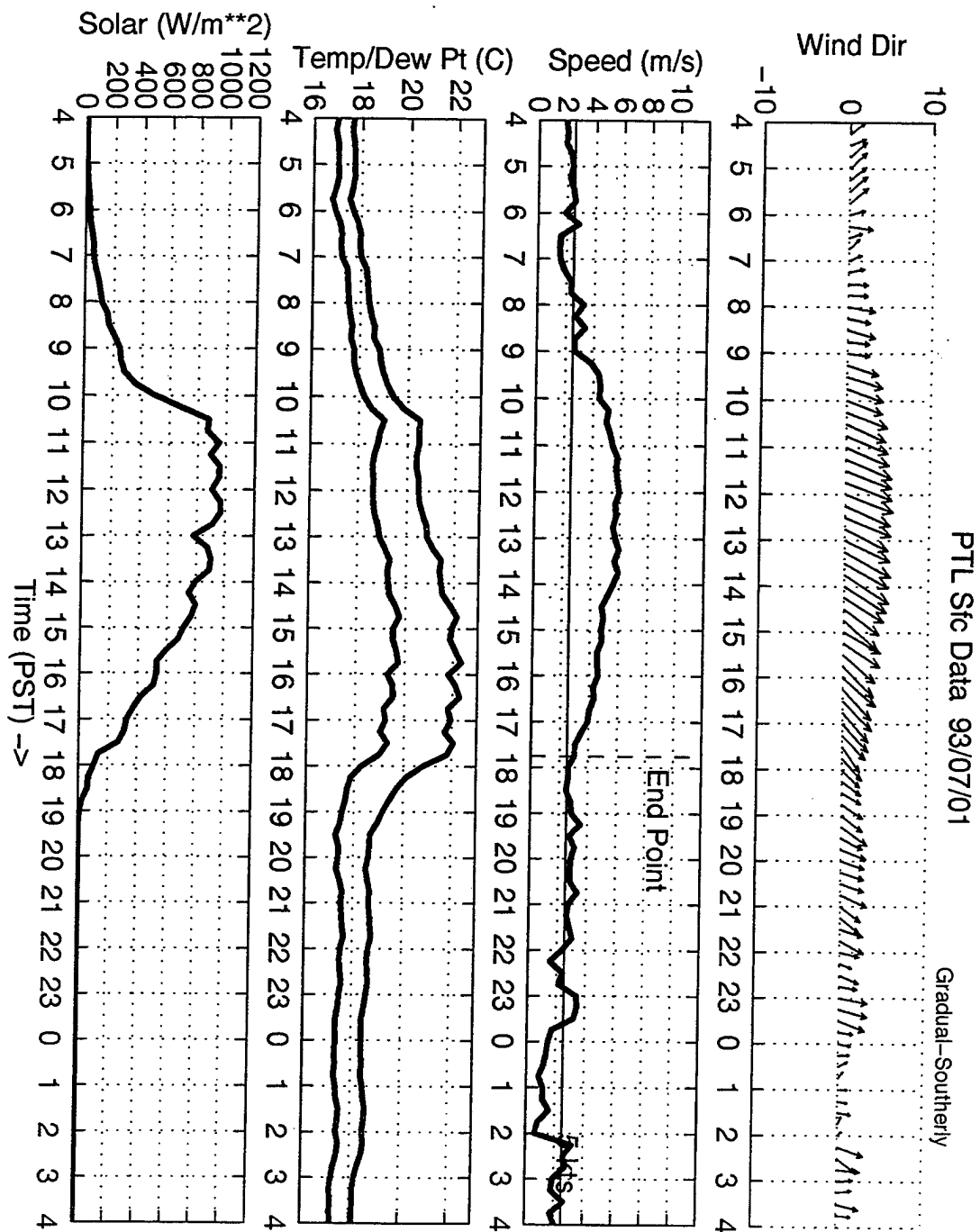


Figure 12. As Figure 8, except Point Loma Gradual-Southerly sea breeze.

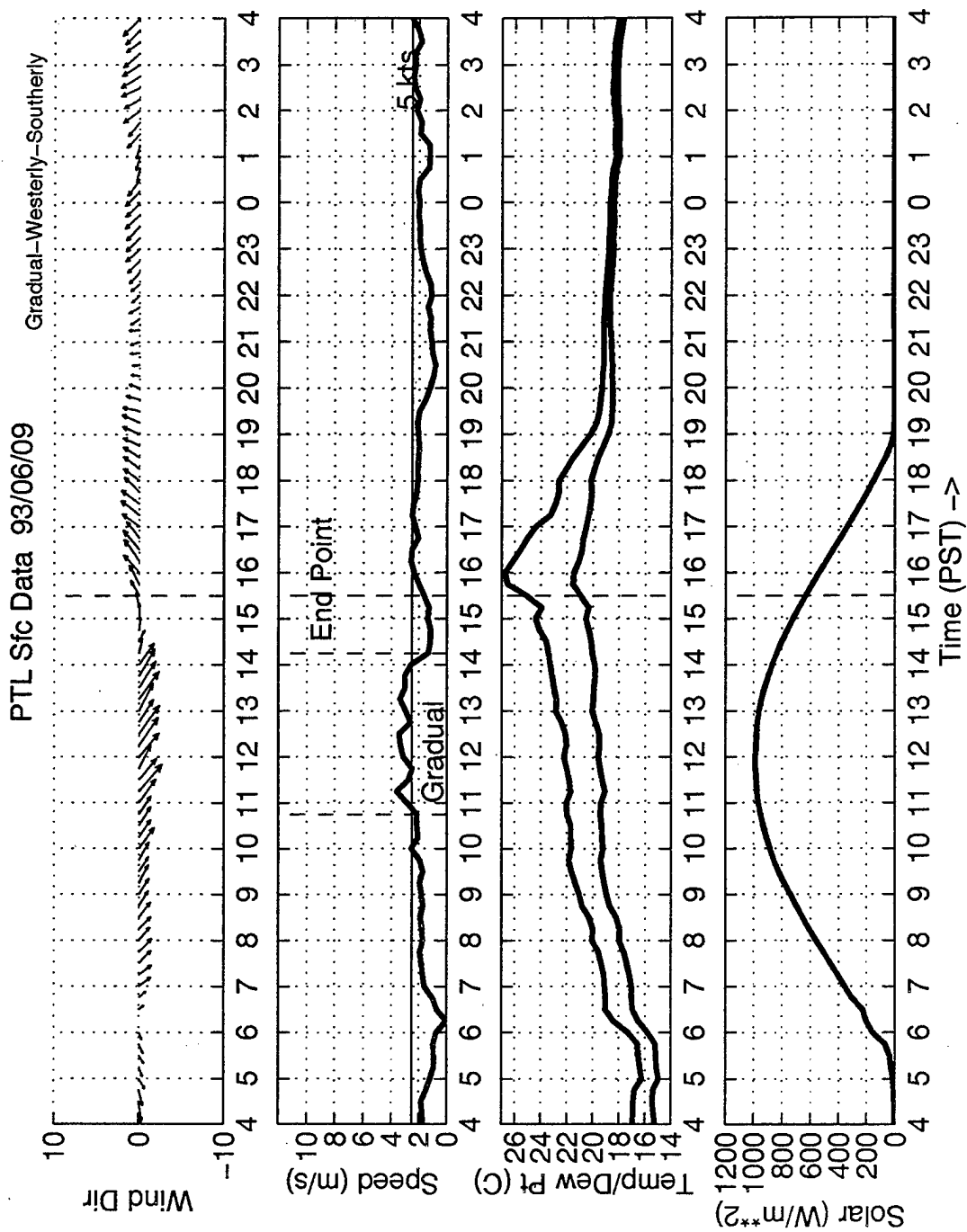


Figure 13. As Figure 8, except Point Loma Gradual-Westerly-Southerly sea breeze.



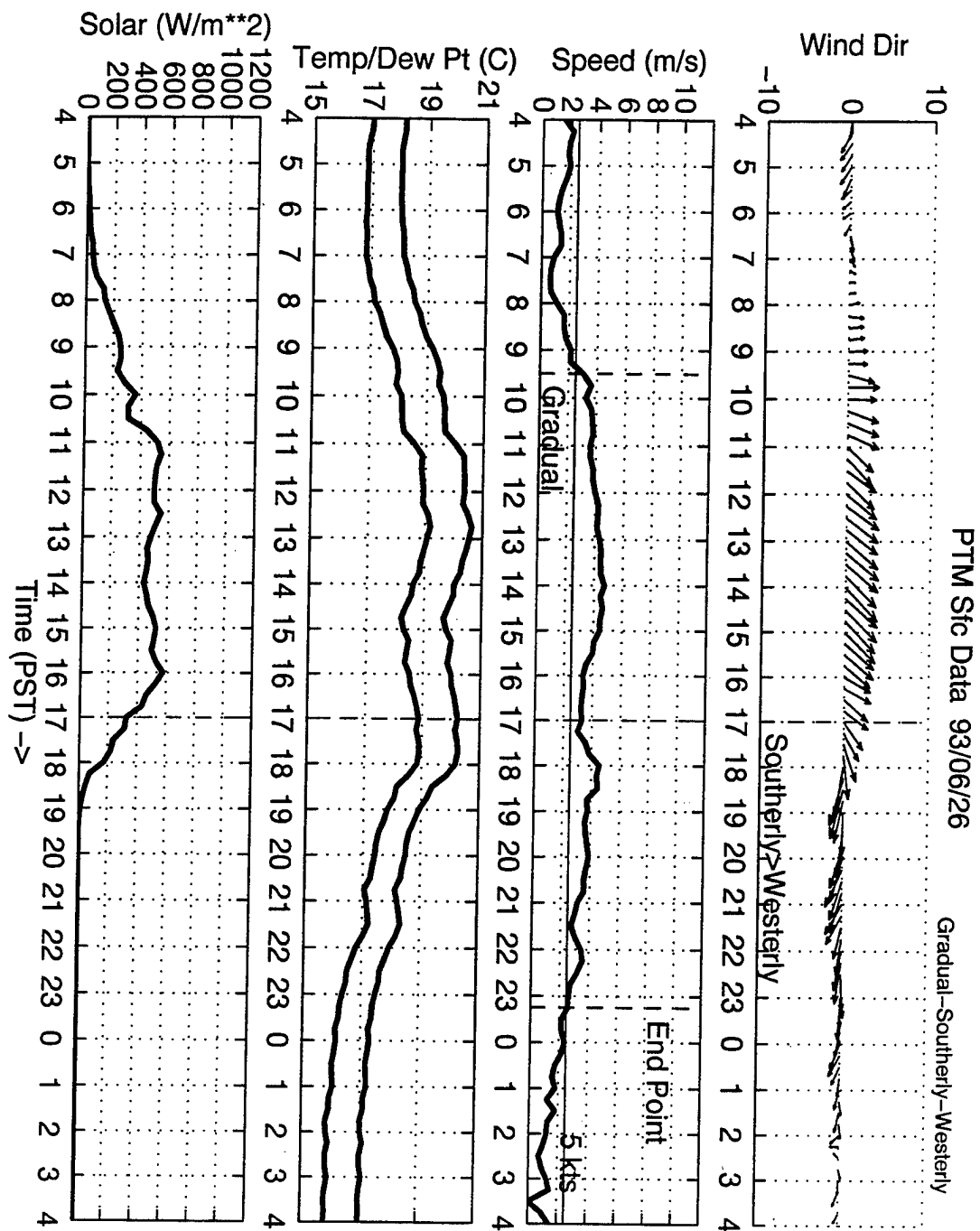


Figure 14. As Figure 8, except Point Mugu Gradual-Southerly-Westerly sea breeze.

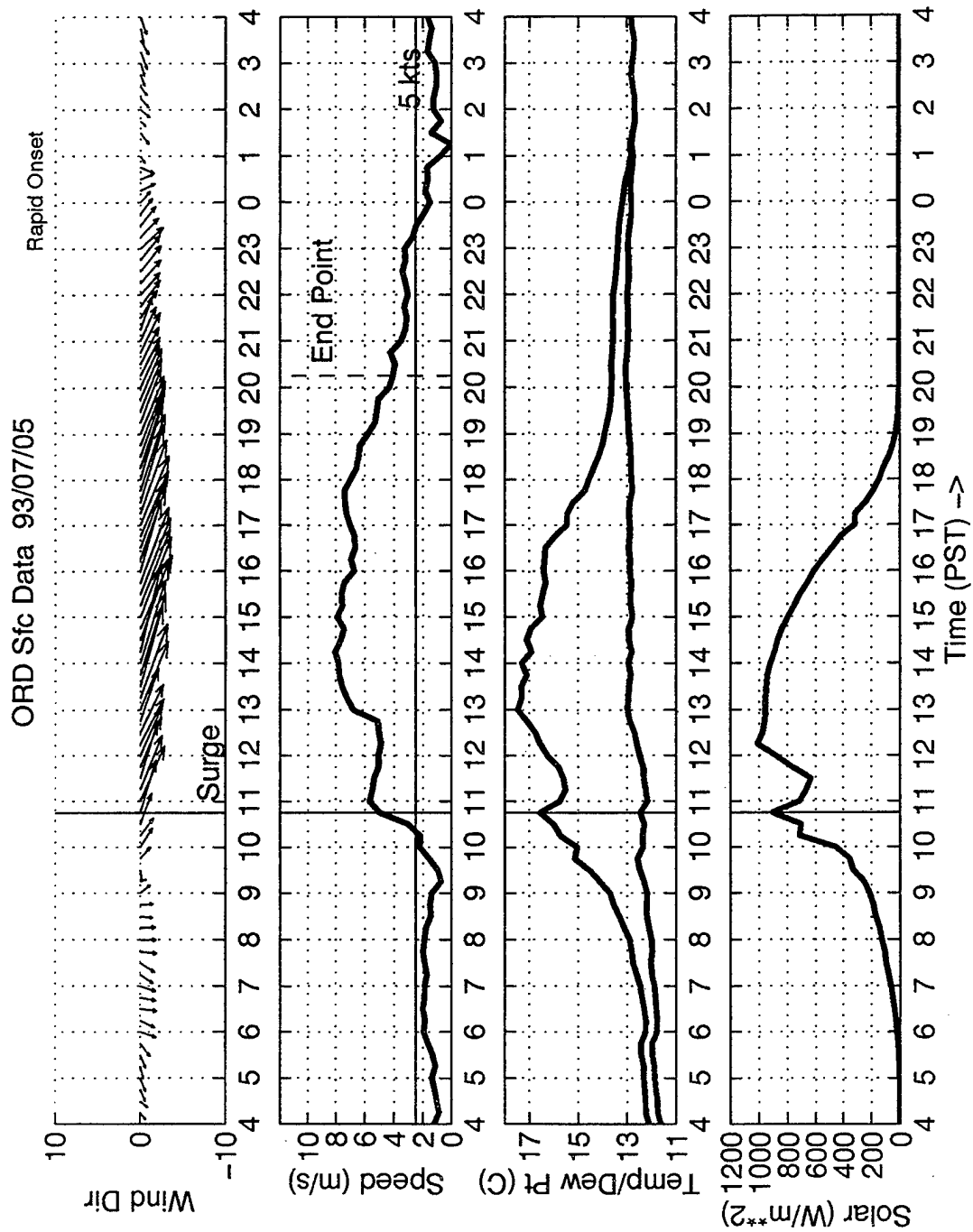
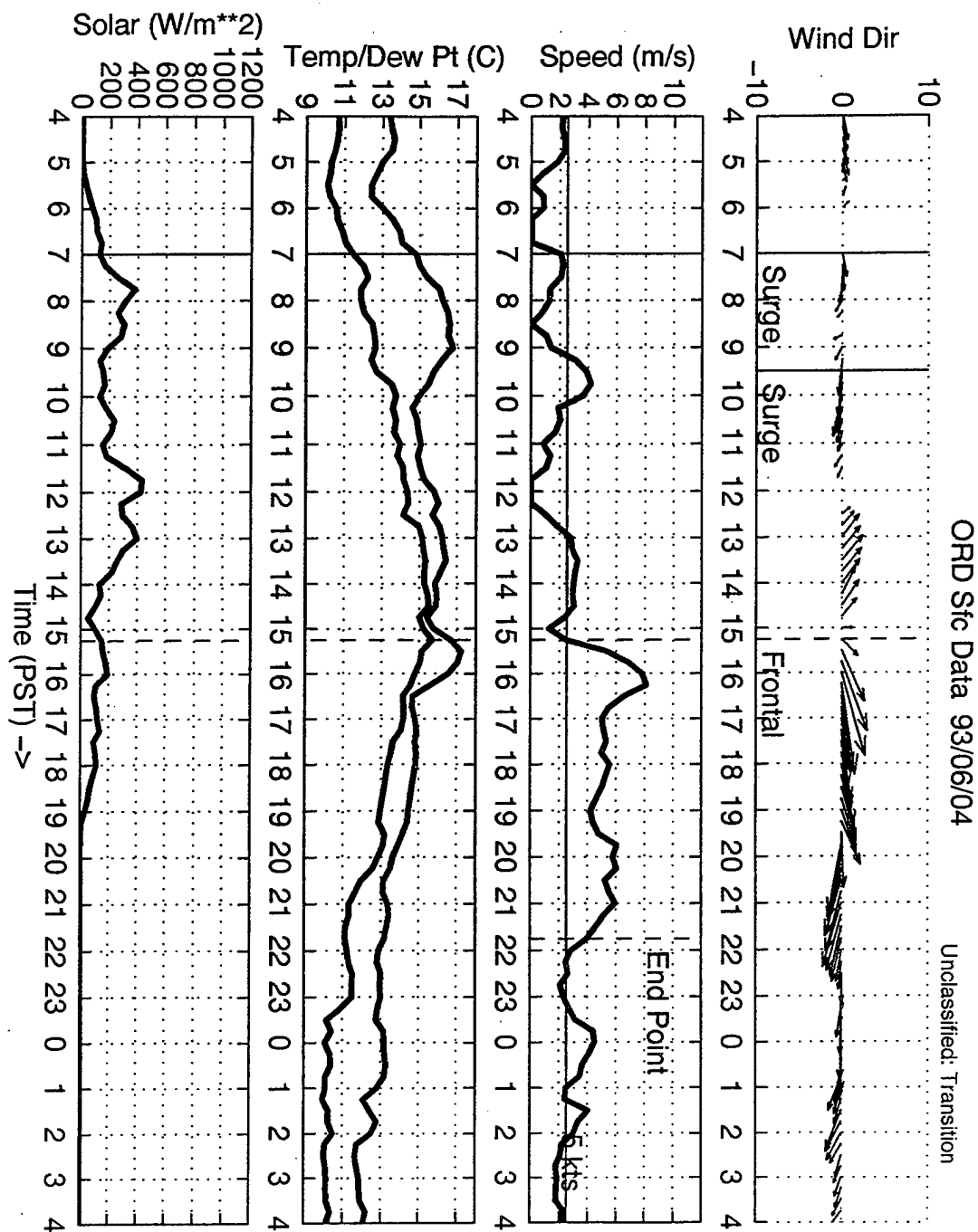
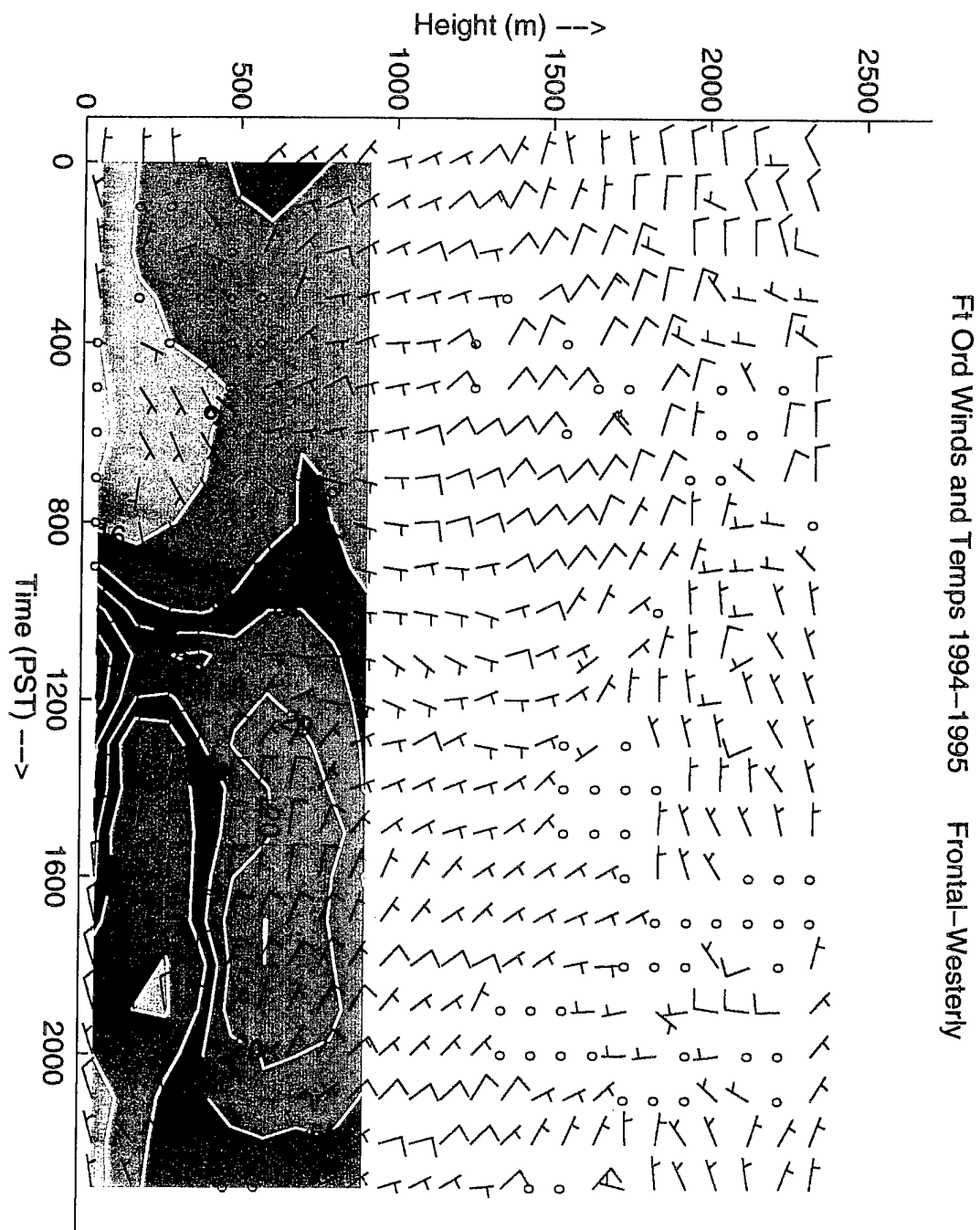


Figure 15. As Figure 8, except Fort Ord Rapid Onset sea breeze.



**Figure 16.** As Figure 8, except Fort Ord unclassified sea breeze (due to transition).





**Figure 18.** Composite of Fort Ord wind and virtual temperature structure for 68 frontal-westerly sea breeze days.

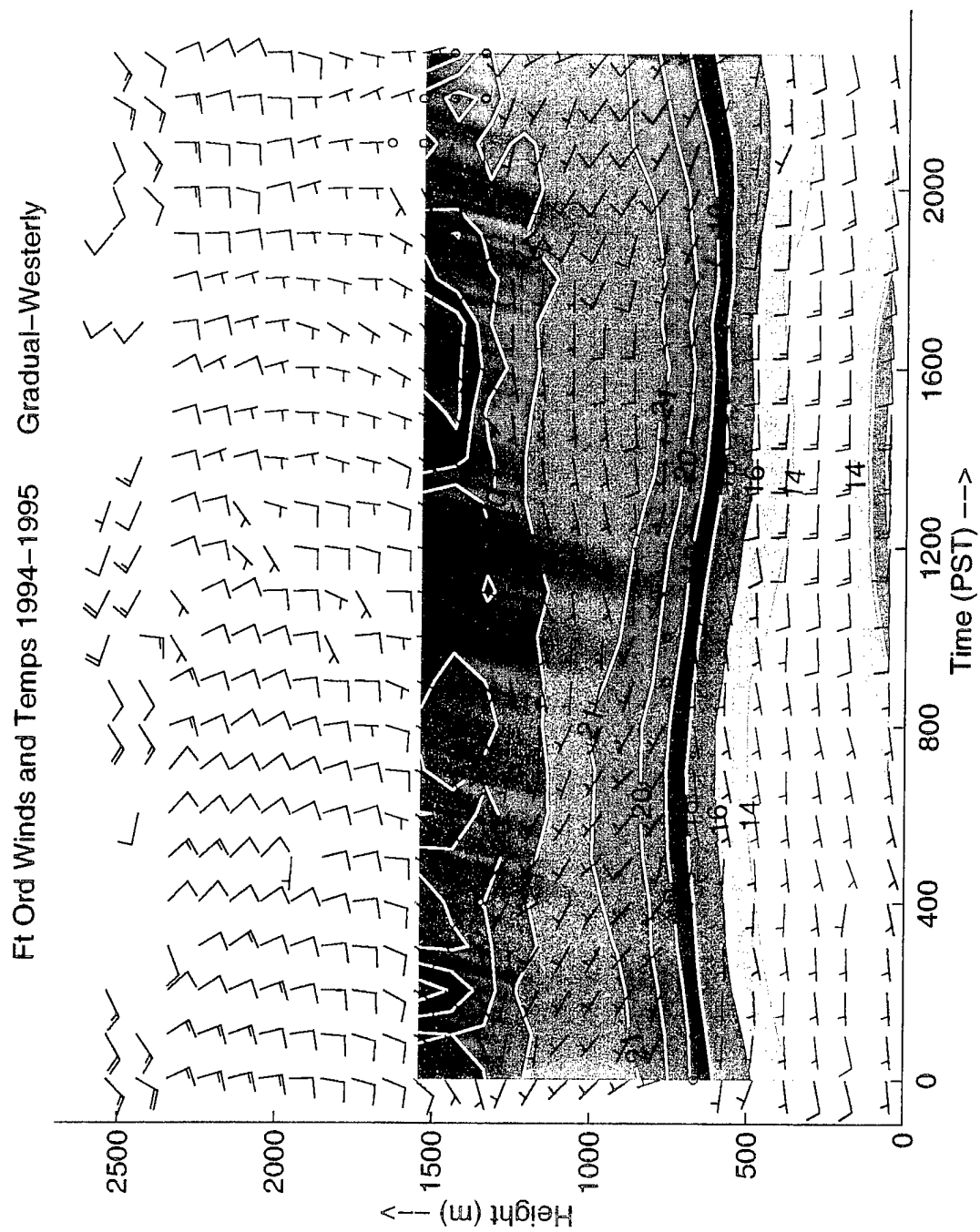


**Figure 19.** As Figure 18, except 100 gradual-westerly sea breeze days.

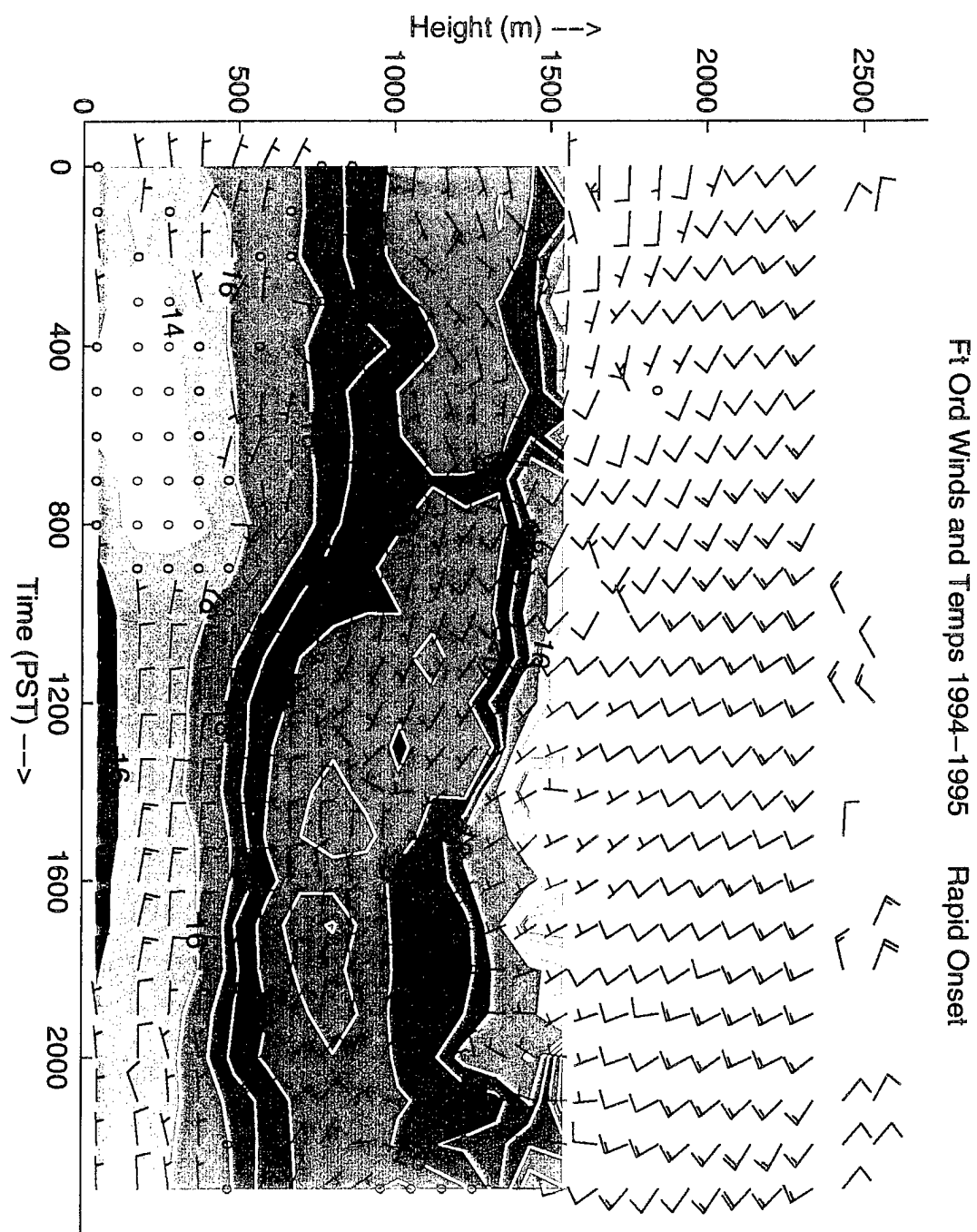
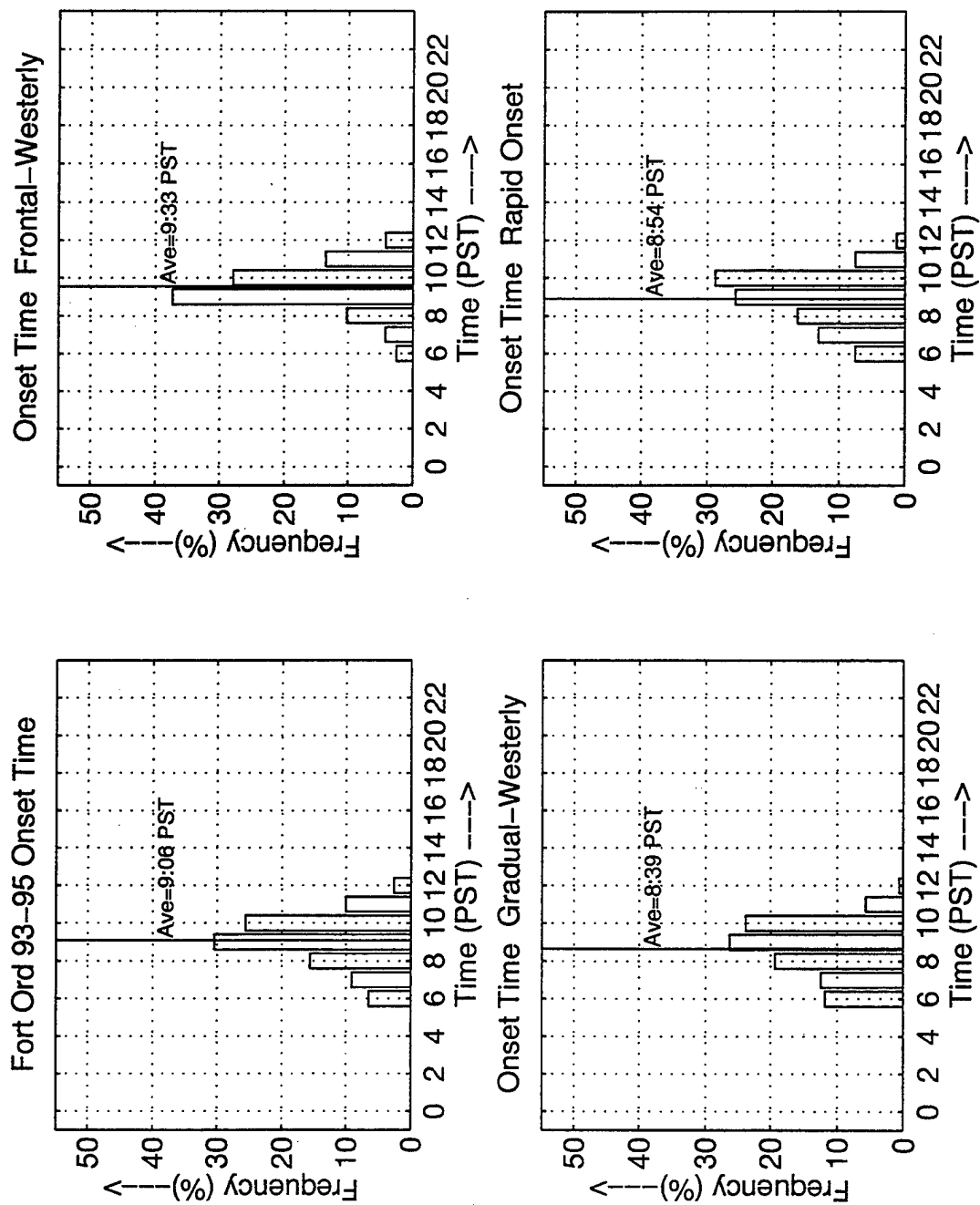


Figure 20. As Figure 18, except 36 rapid onset sea breeze days.



**Figure 21.** Distributions of sea breeze onset times for summers of 1993-1995 at Fort Ord: a) all sea breeze days, b) frontal-westerly days, c) gradual-westerly days , and d) rapid onset days.



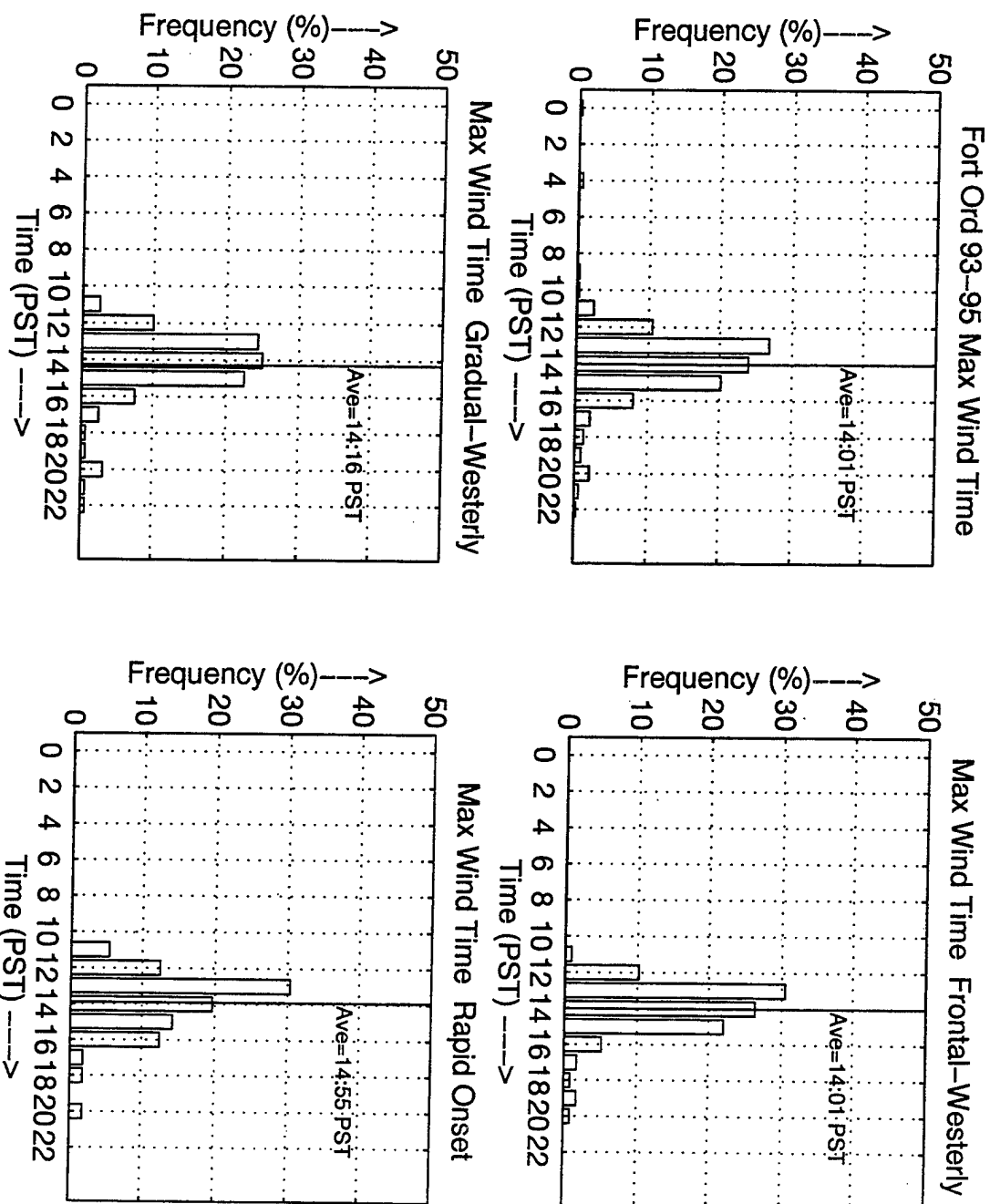


Figure 22. As Figure 21, except time of maximum wind.

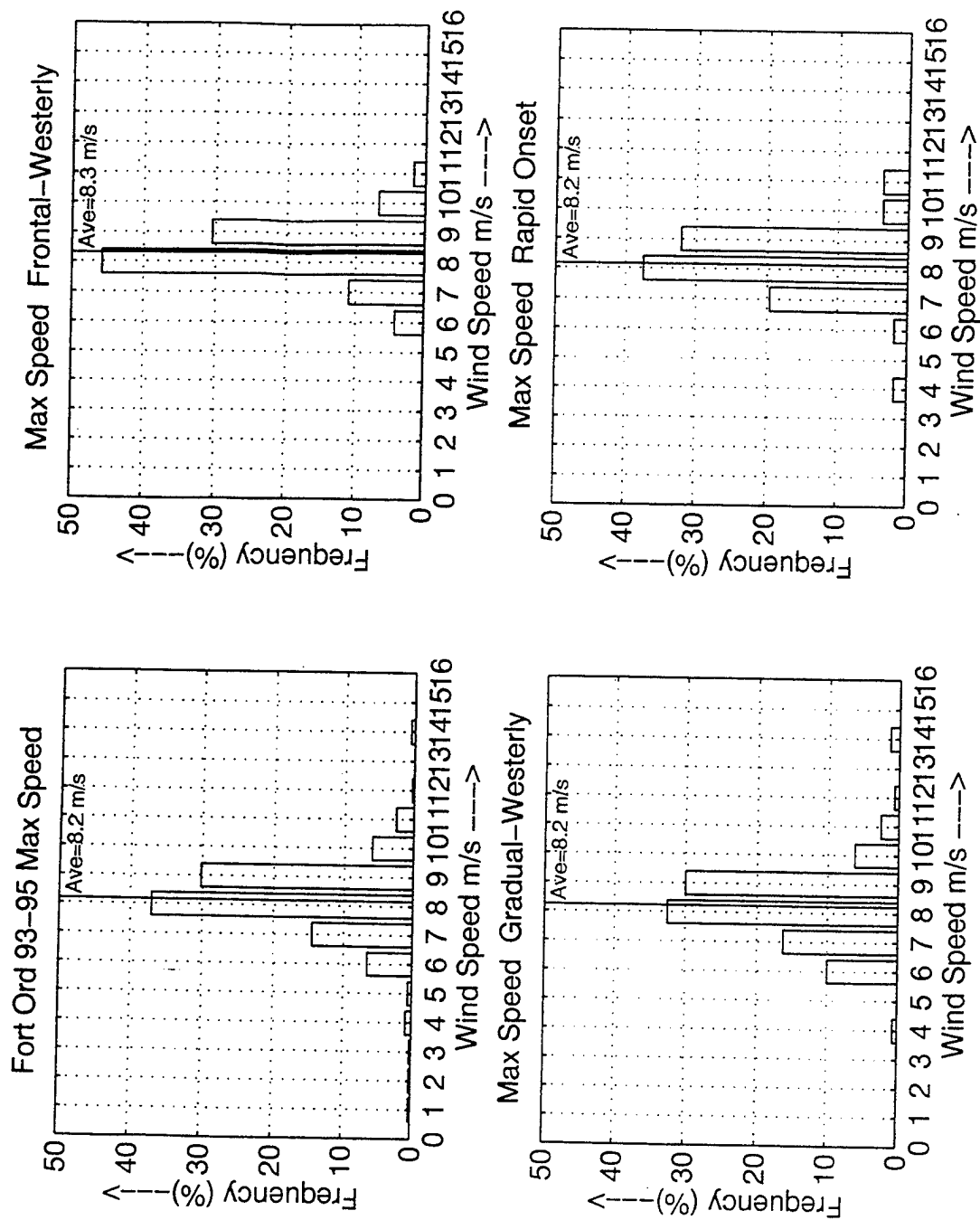


Figure 23. As Figure 21, except maximum wind speed.

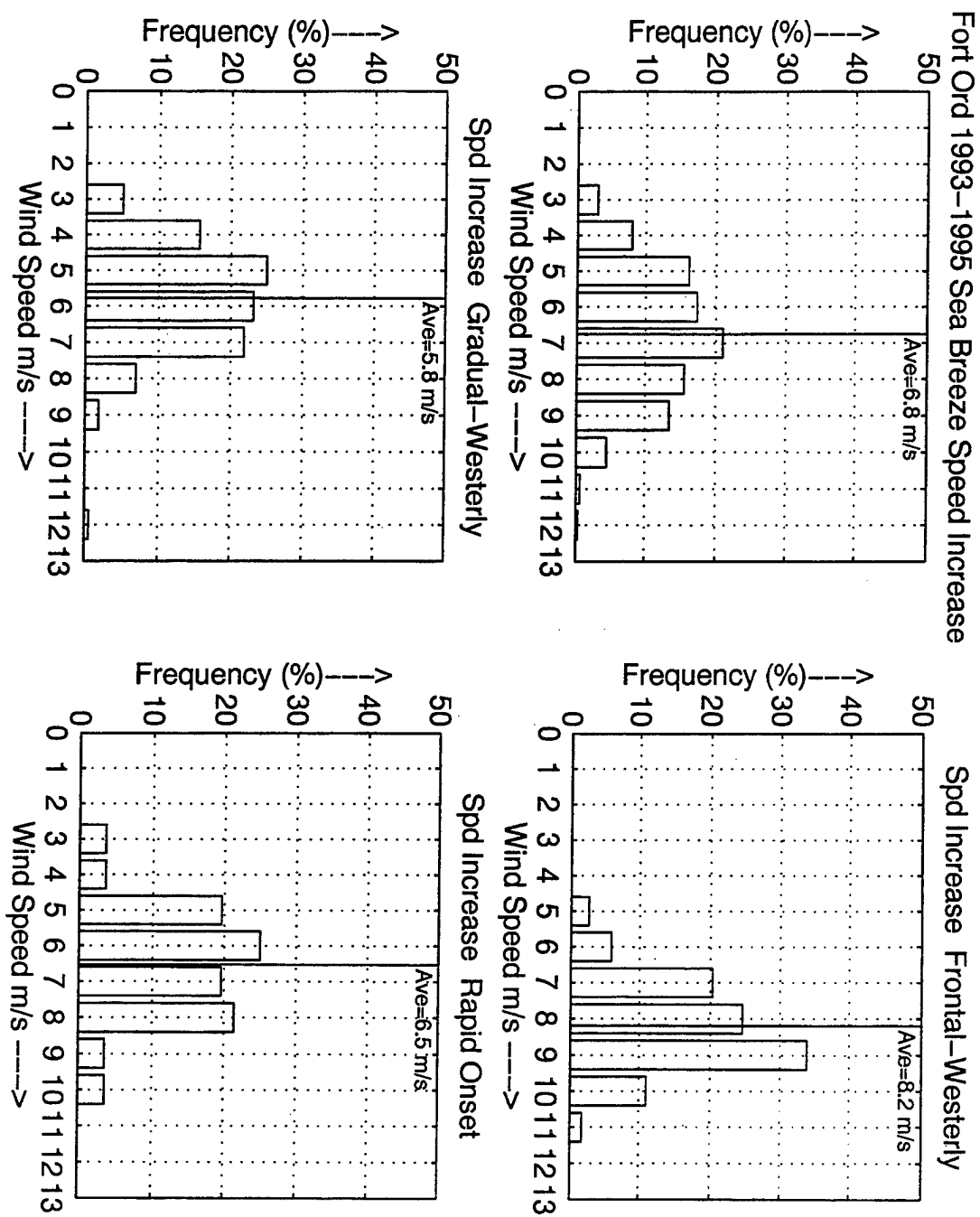


Figure 24. As Figure 21, except wind speed increase associated with sea breeze.

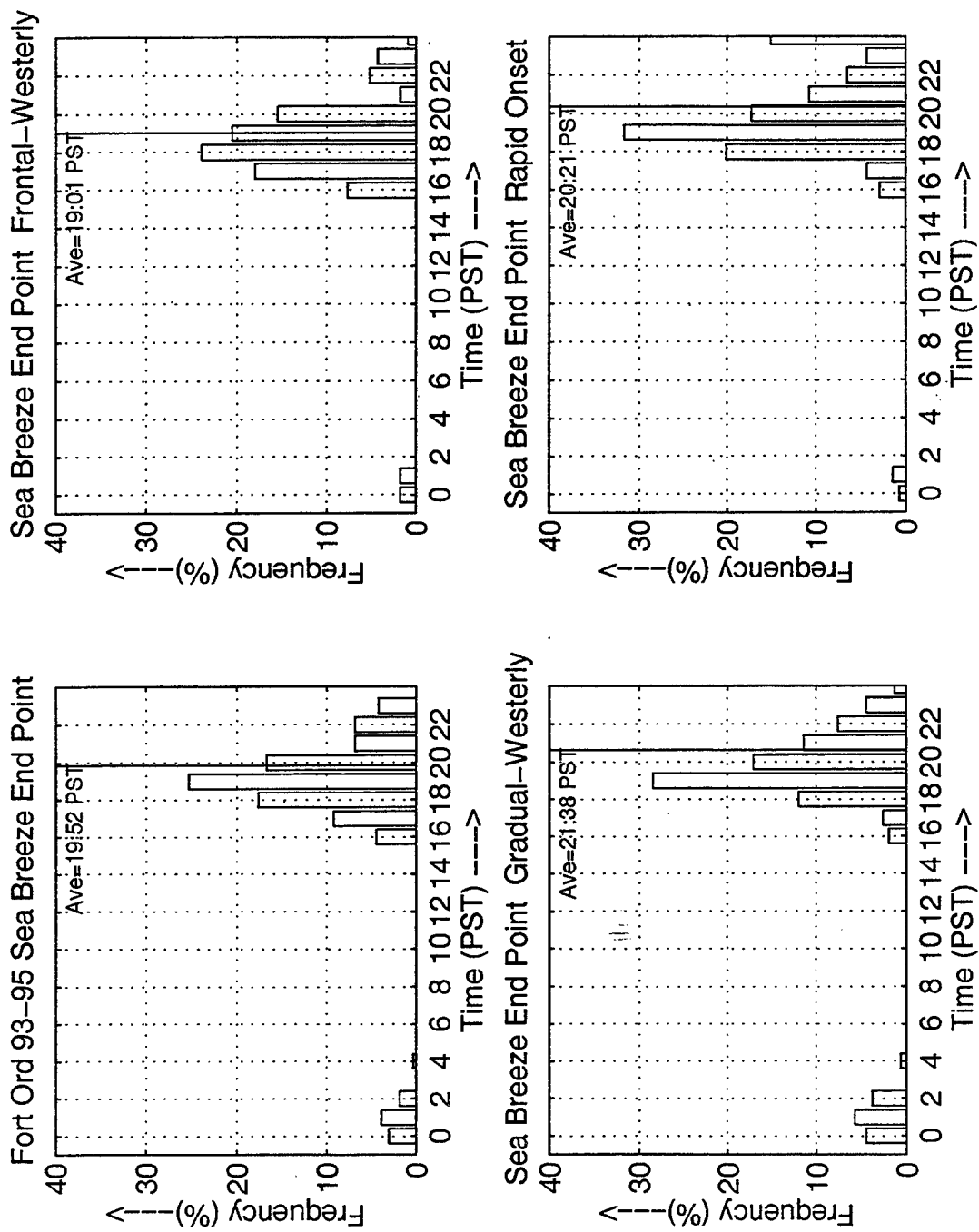


Figure 25. As Figure 21, except time of sea breeze end point.

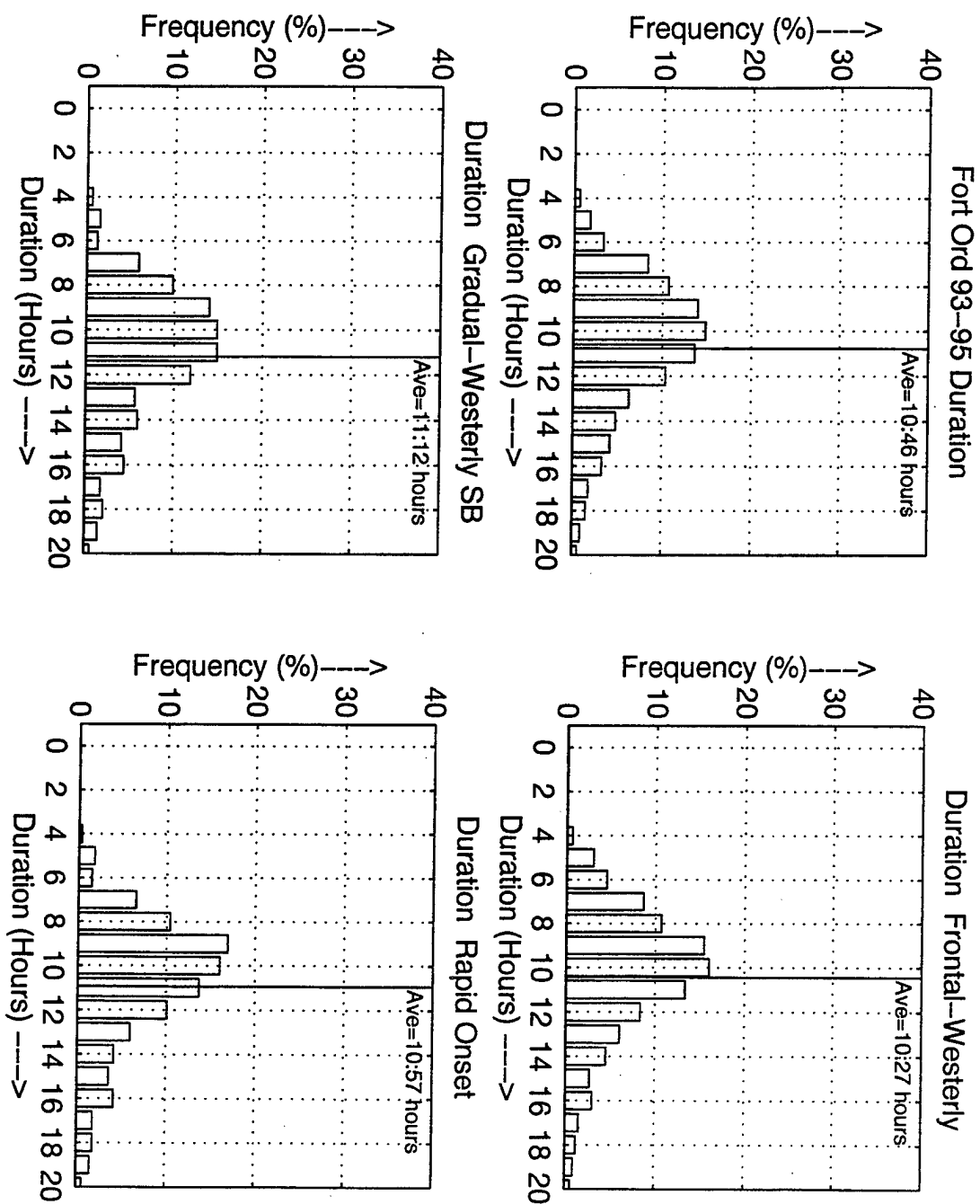
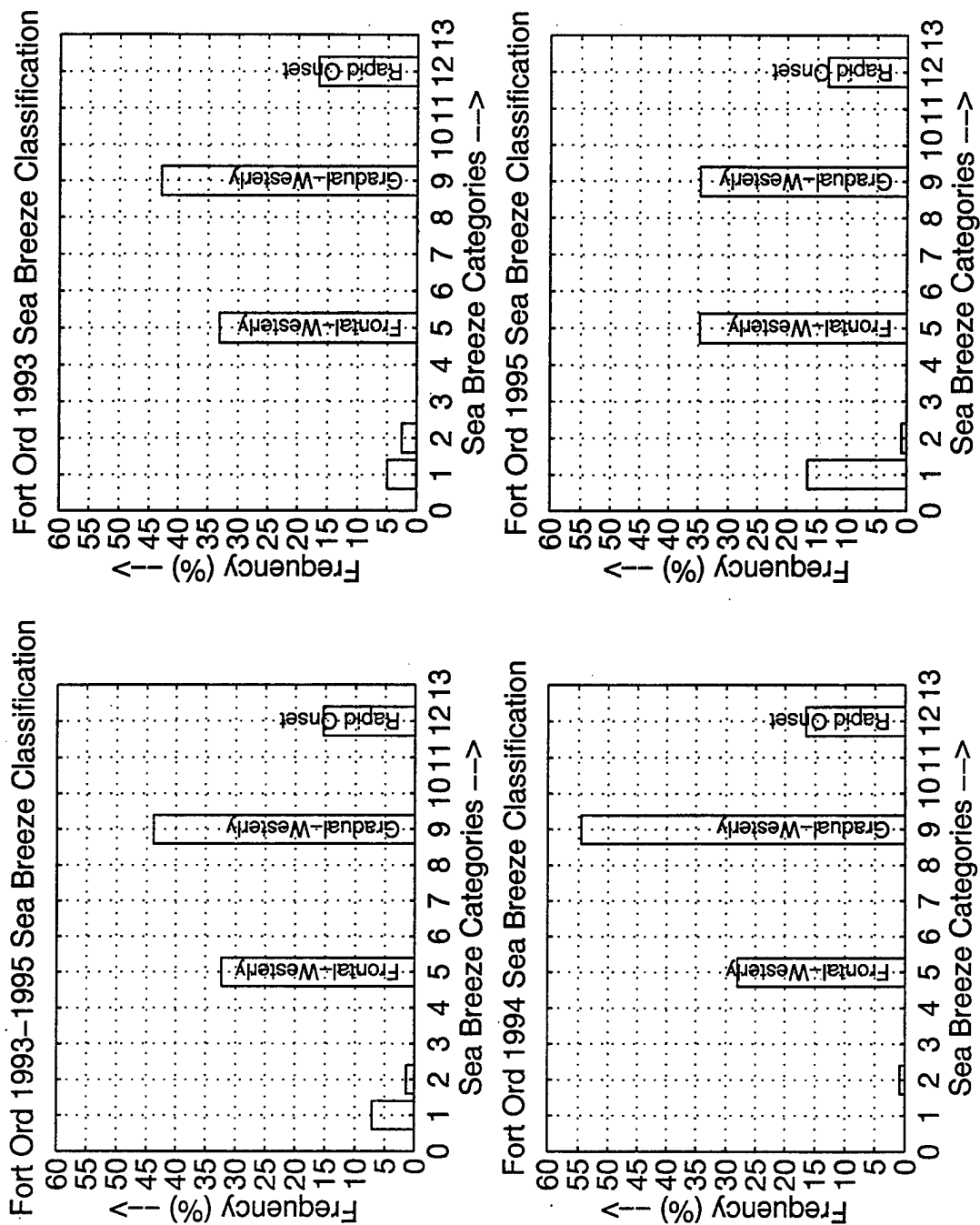
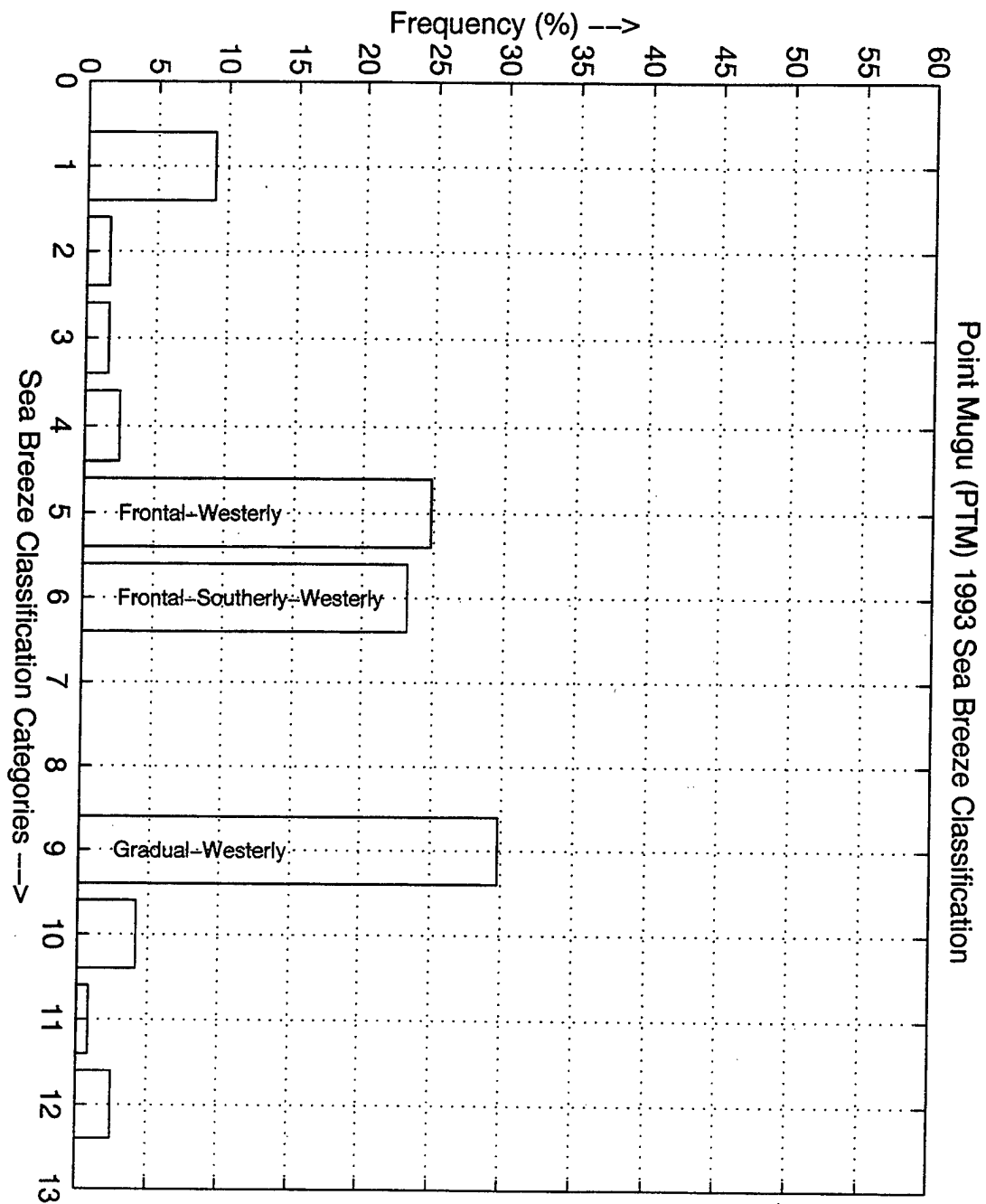


Figure 26. As Figure 21, except duration of sea breeze.



**Figure 27.** Distribution of sea breeze days at Fort Ord for summers of 1993-1995: a) all three summers, b) 1993, c) 1994, d) 1995. Classifications as in Figure 17.



**Figure 28.** Sea breeze distribution for Point Loma for summer of 1993. Sea breeze classifications as in Figure 17.

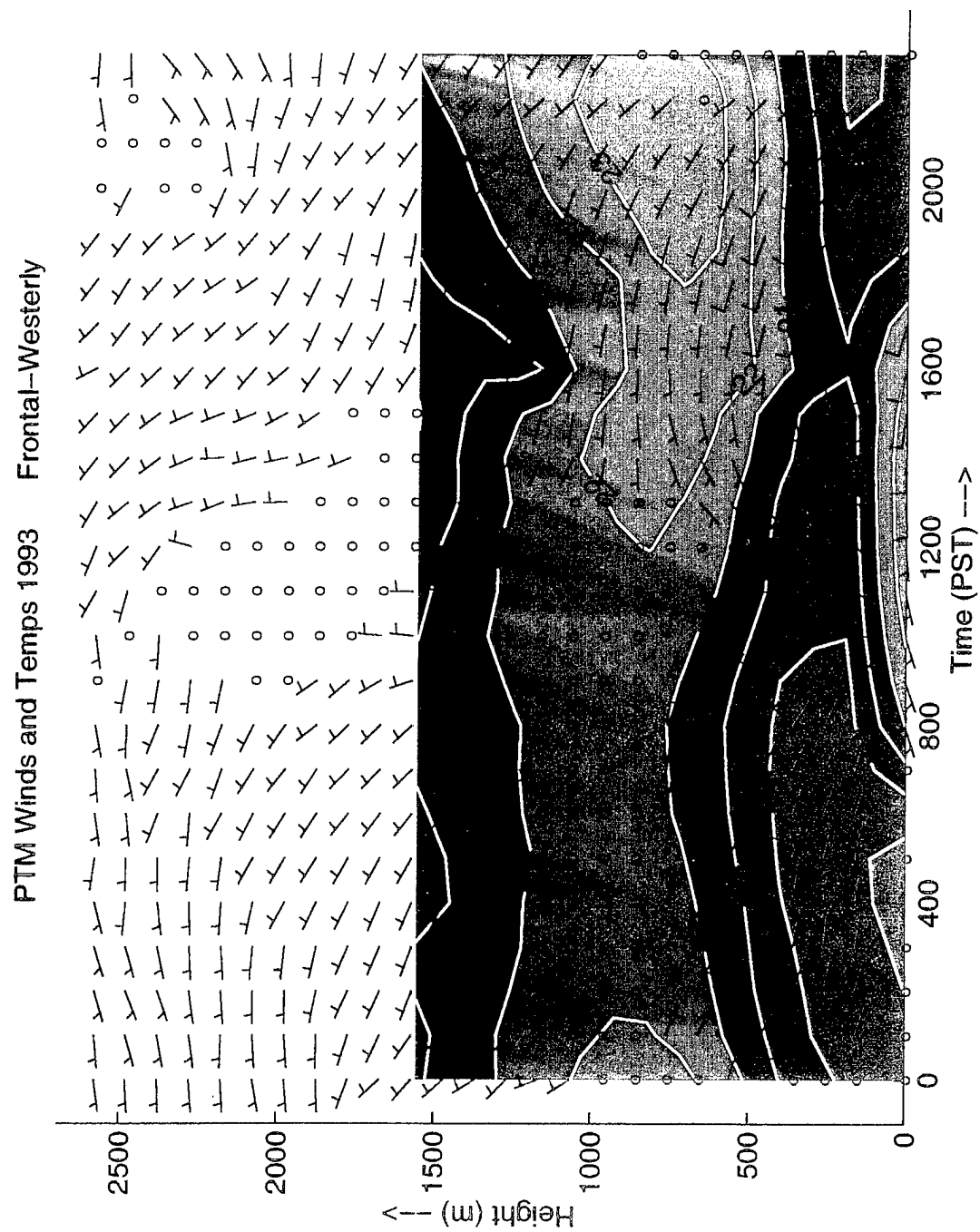


**Figure 29.** Composite of Point Loma wind and virtual temperature structure for 29 frontal-westerly sea breeze days.



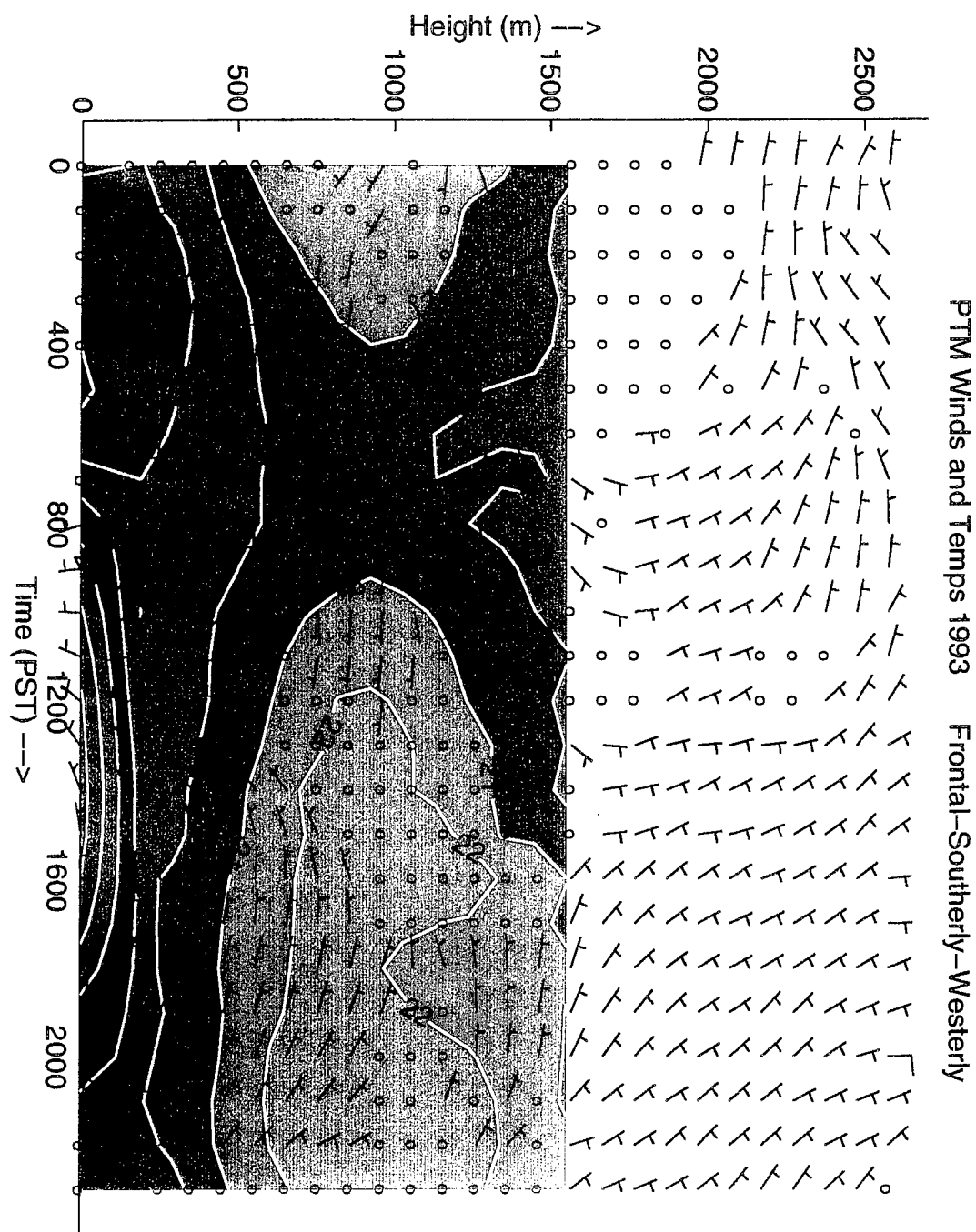


Figure 30. As Figure 29, except 28 frontal-southerly-westerly sea breeze days.

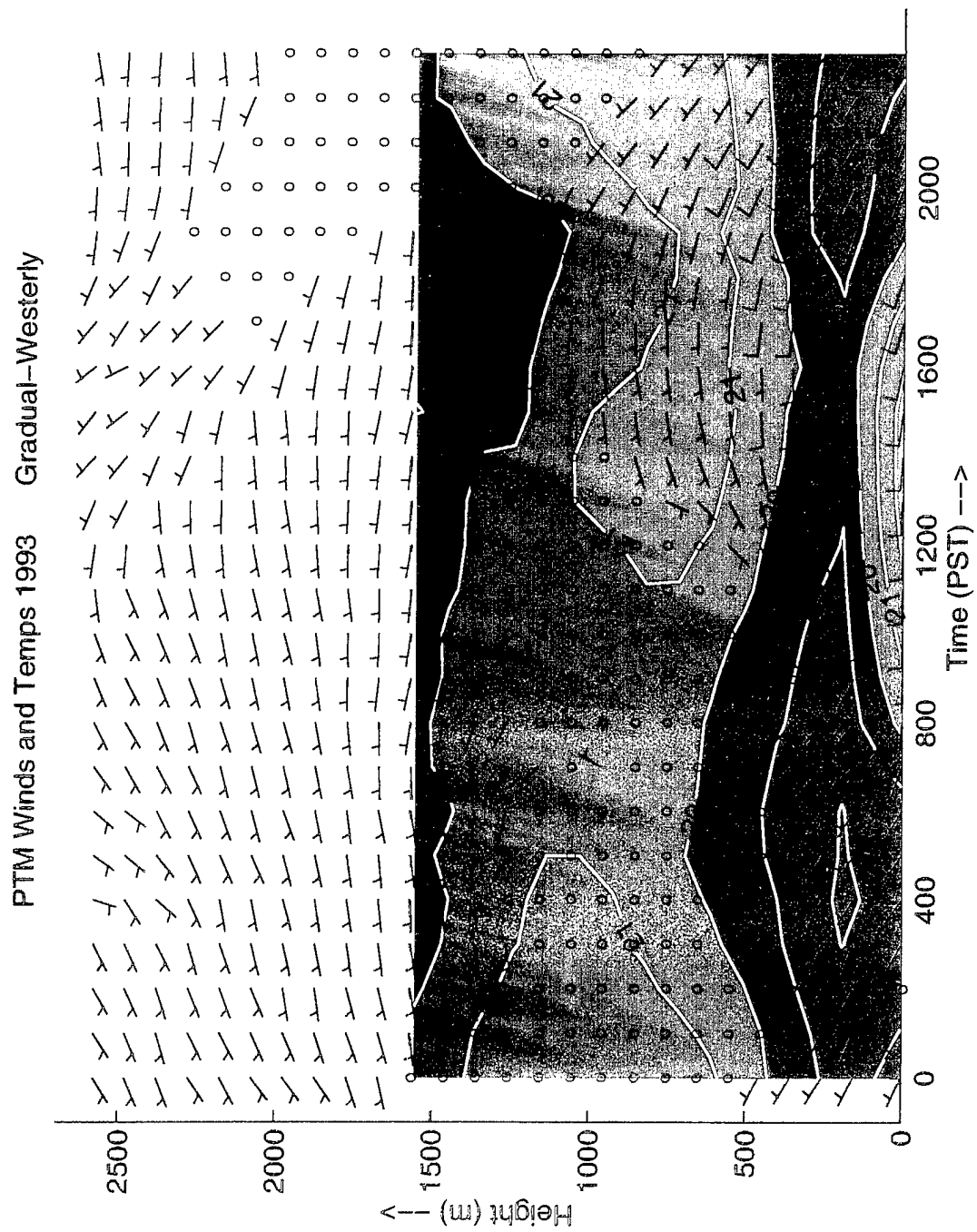
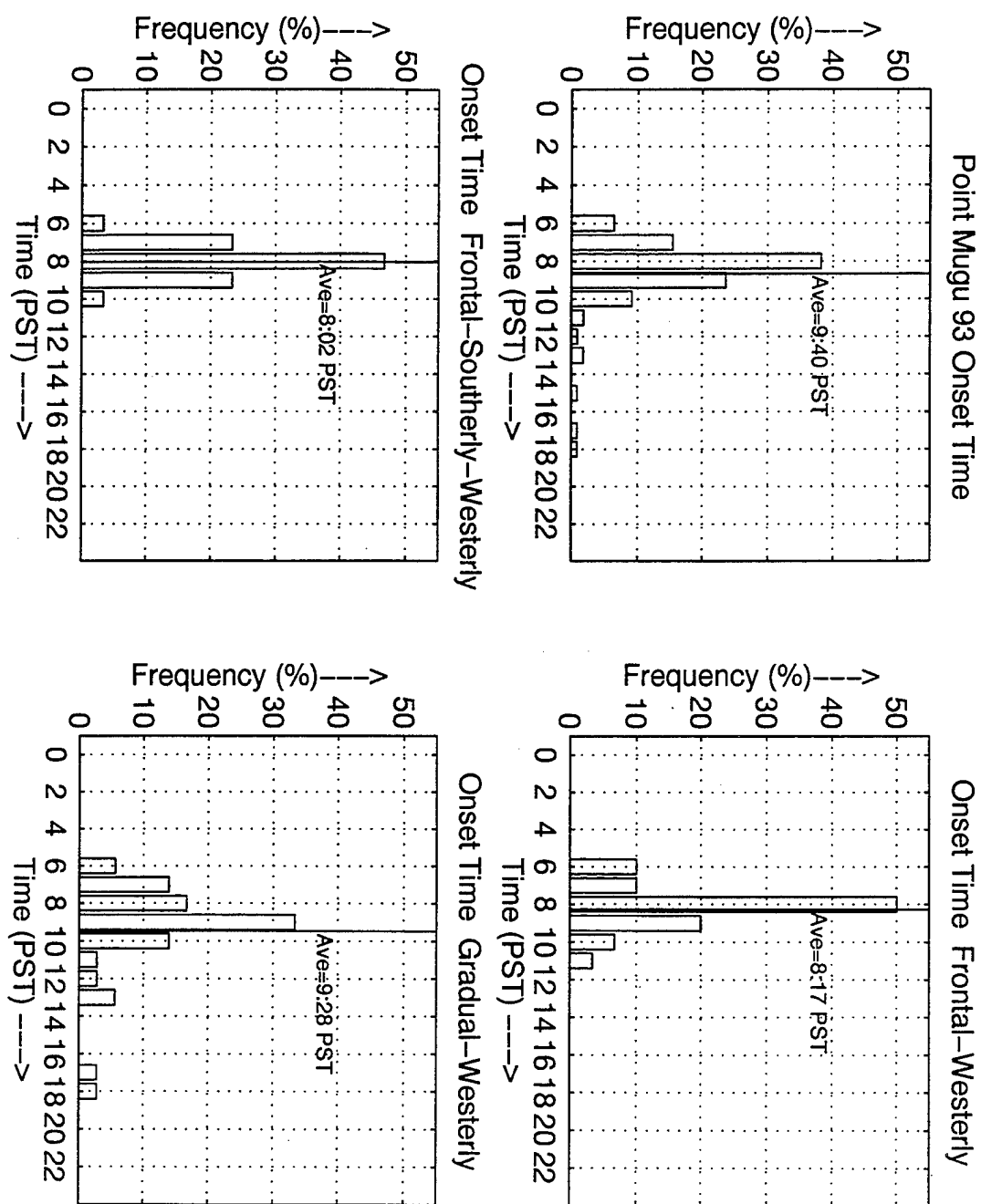


Figure 31. As Figure 29, except 36 gradual-westerly sea breeze days.



**Figure 32.** Distribution of sea breeze onset times for summer of 1993 at Point Mugu: a) all sea breeze days, b) frontal-westerly days, c) frontal-southerly-westerly, and d) gradual-westerly days.

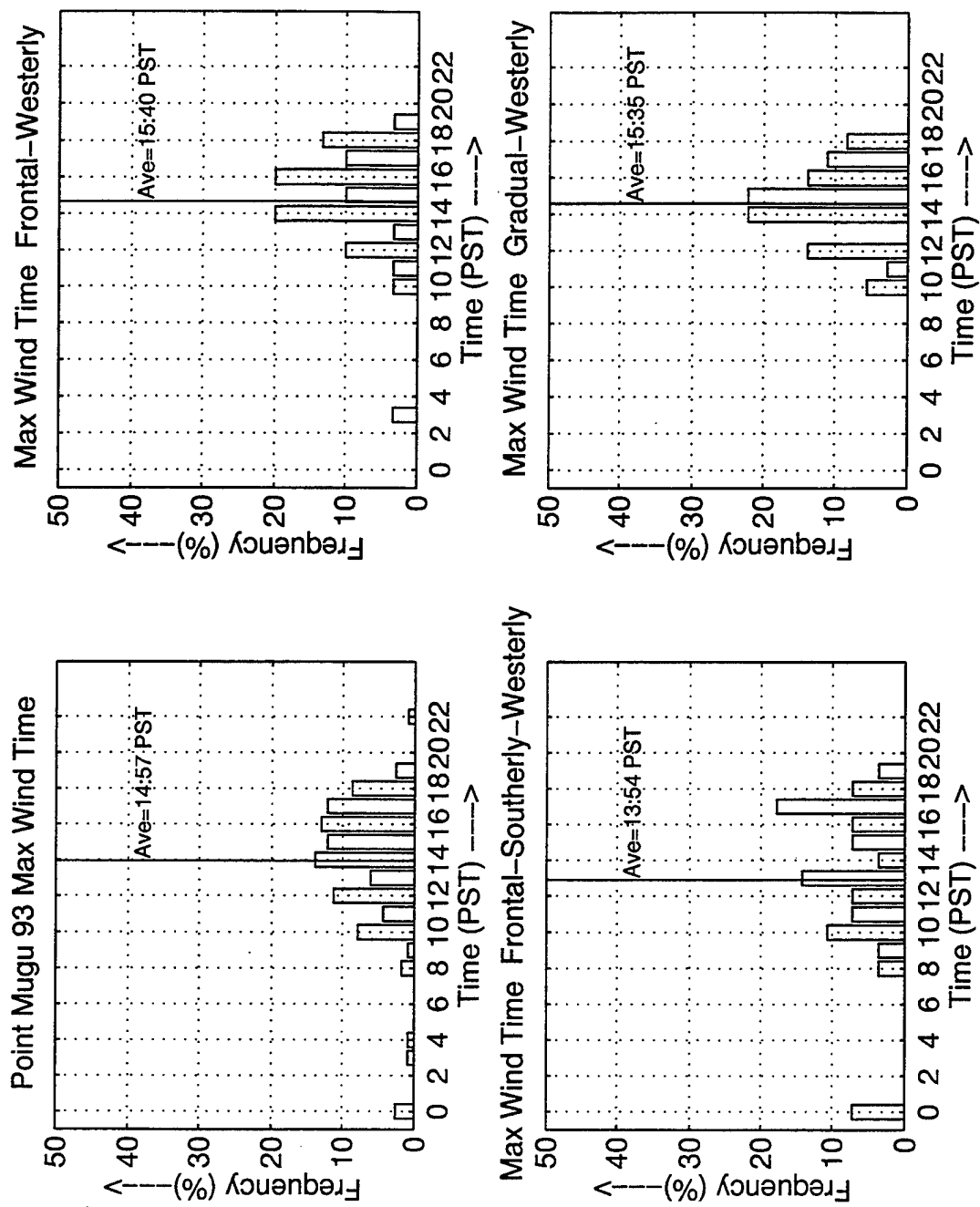


Figure 33. As Figure 32, except time of maximum wind.

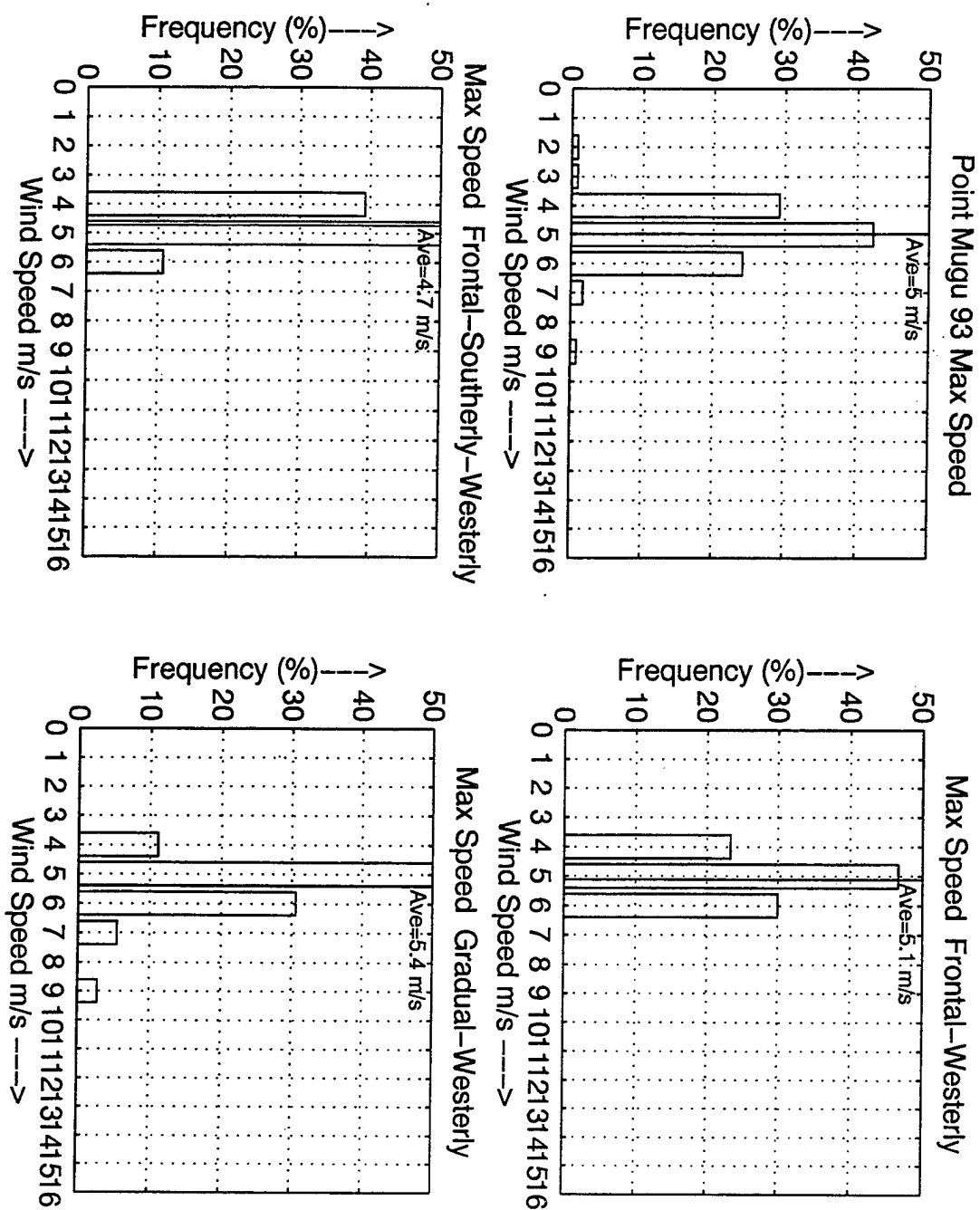


Figure 34. As Figure 32, except maximum wind speed.

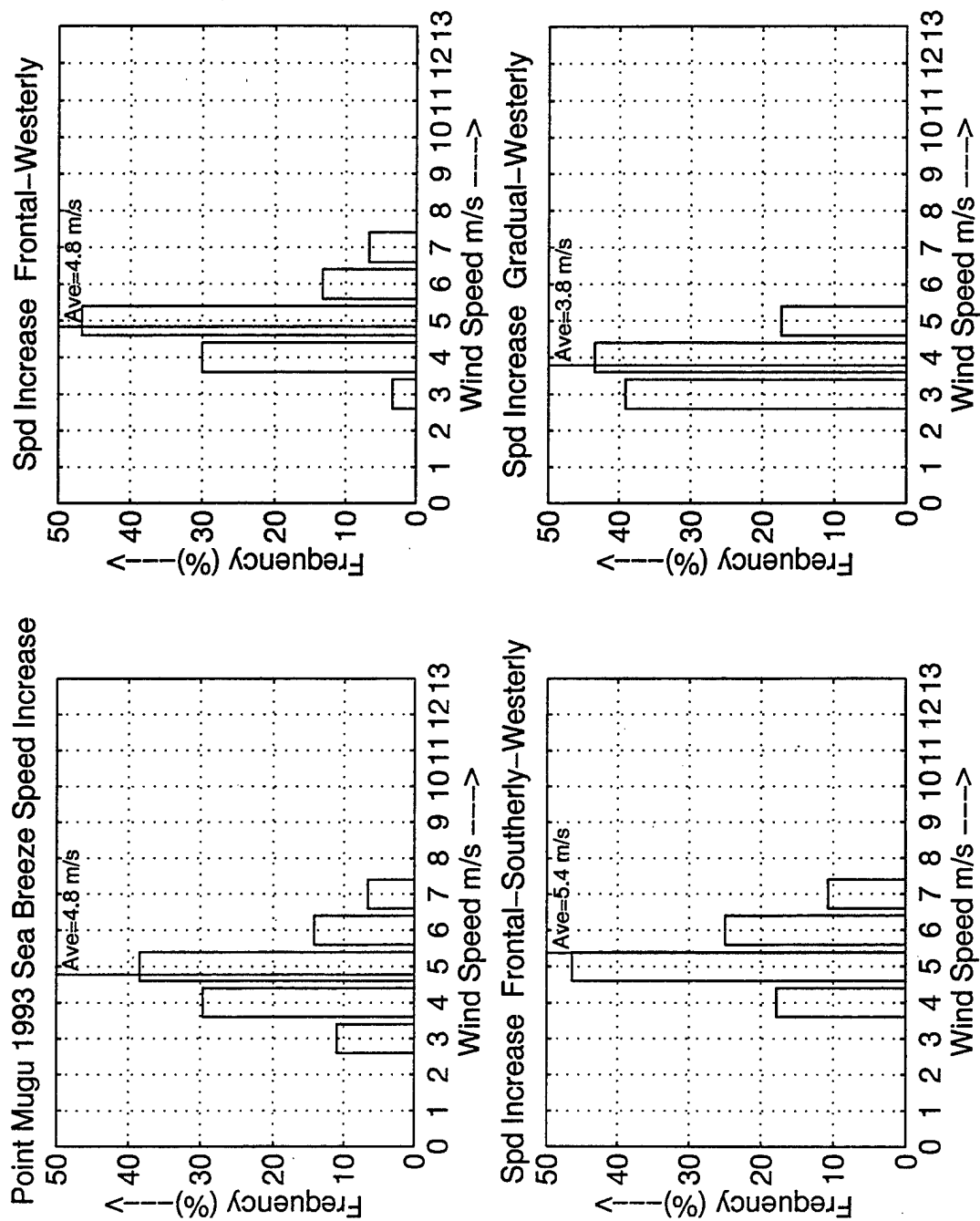


Figure 35. As Figure 32, except wind speed increase associated with sea breeze.

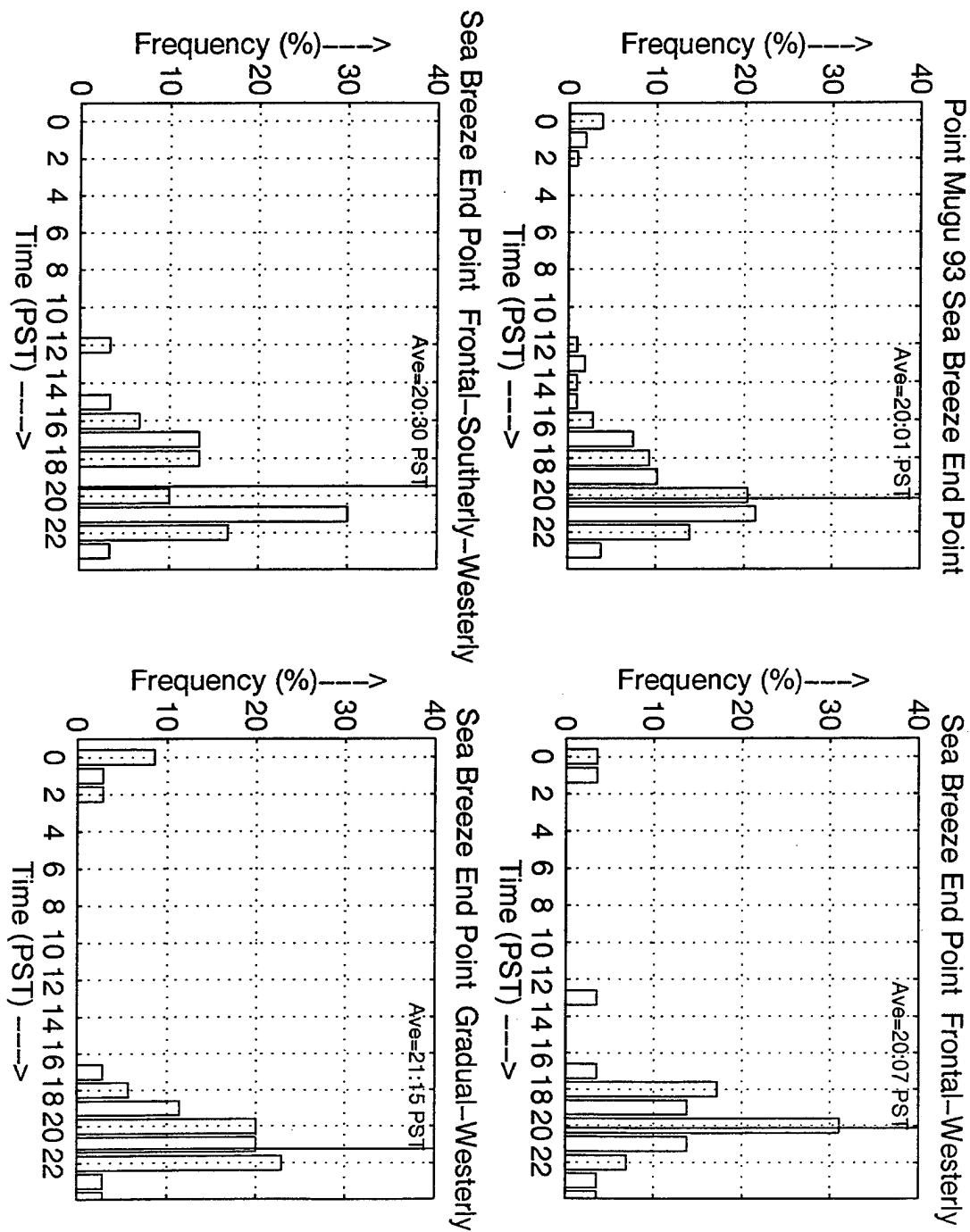


Figure 36. As Figure 32, except time of sea breeze end point.

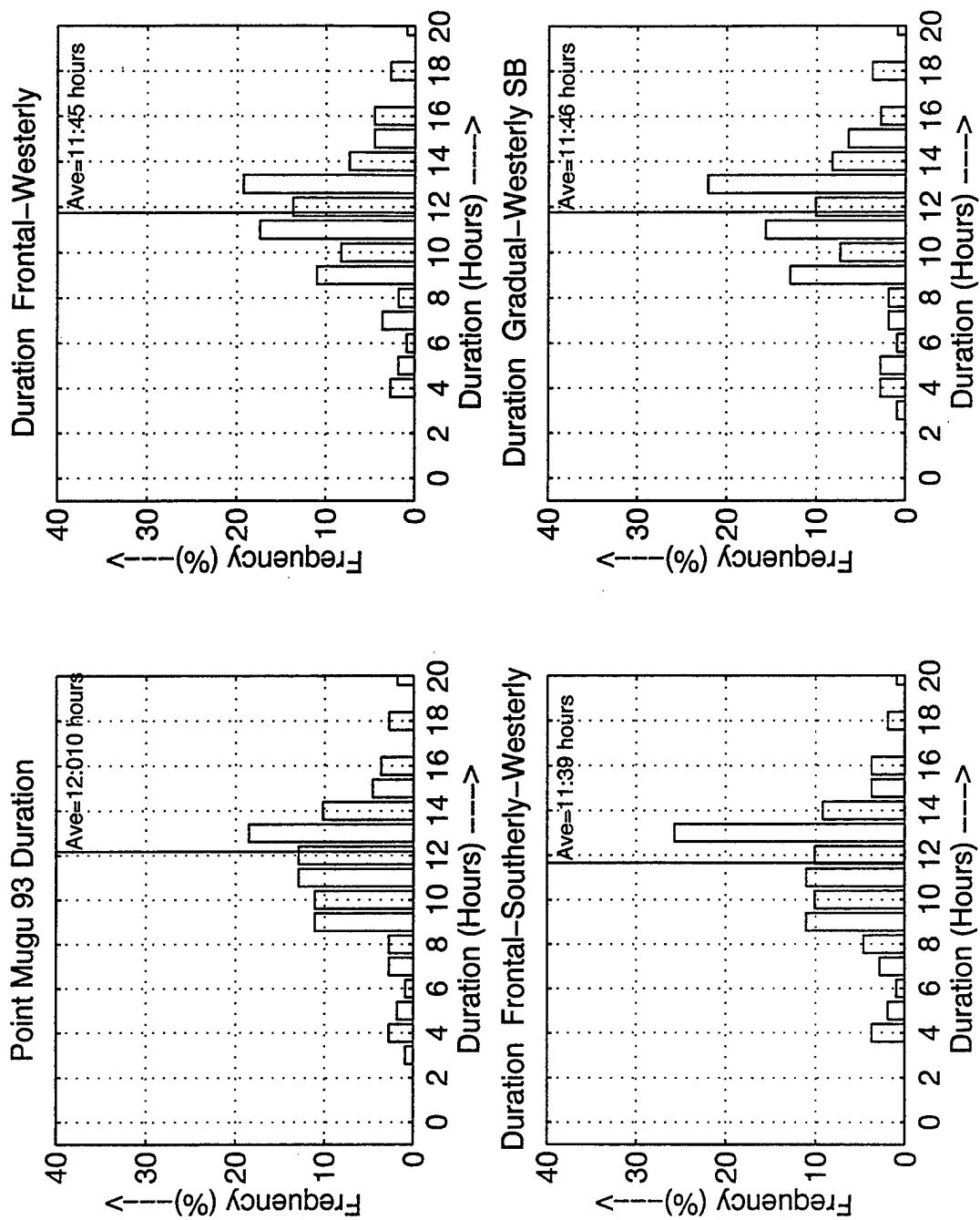
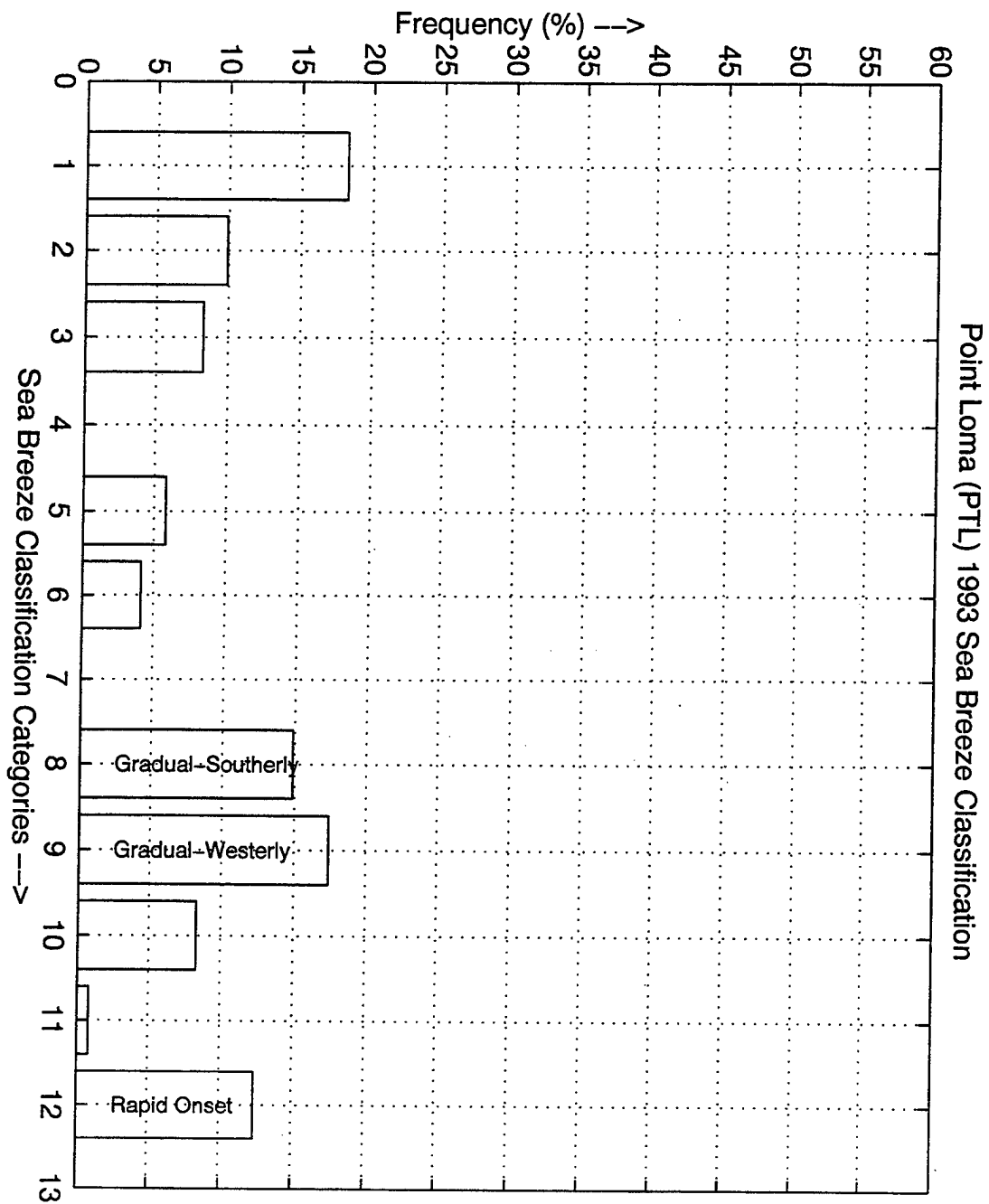


Figure 37. As Figure 32, except duration of sea breeze.





**Figure 38.** Sea breeze distribution for Point Loma for the summer of 1993. Sea breeze classification as Figure 18.

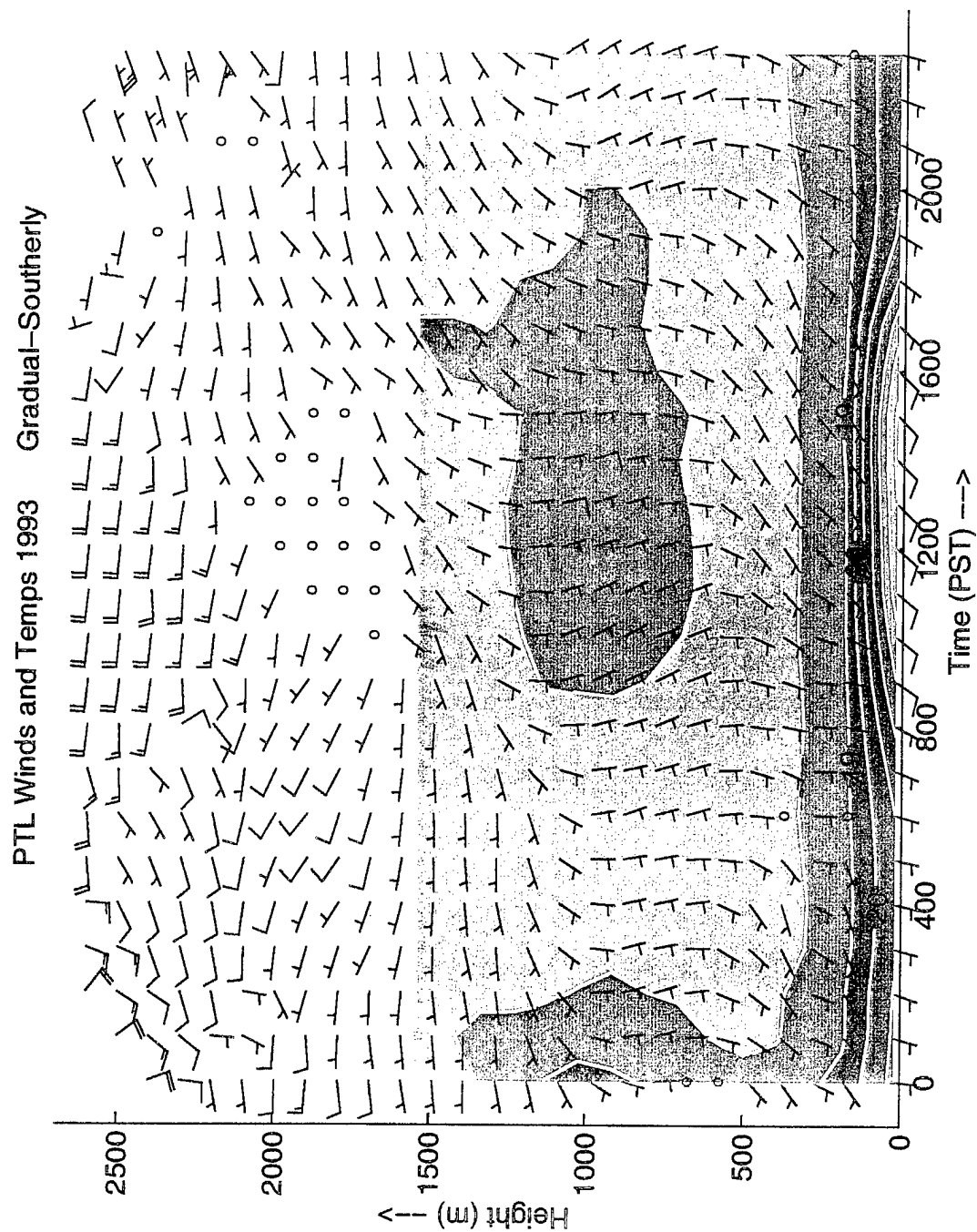
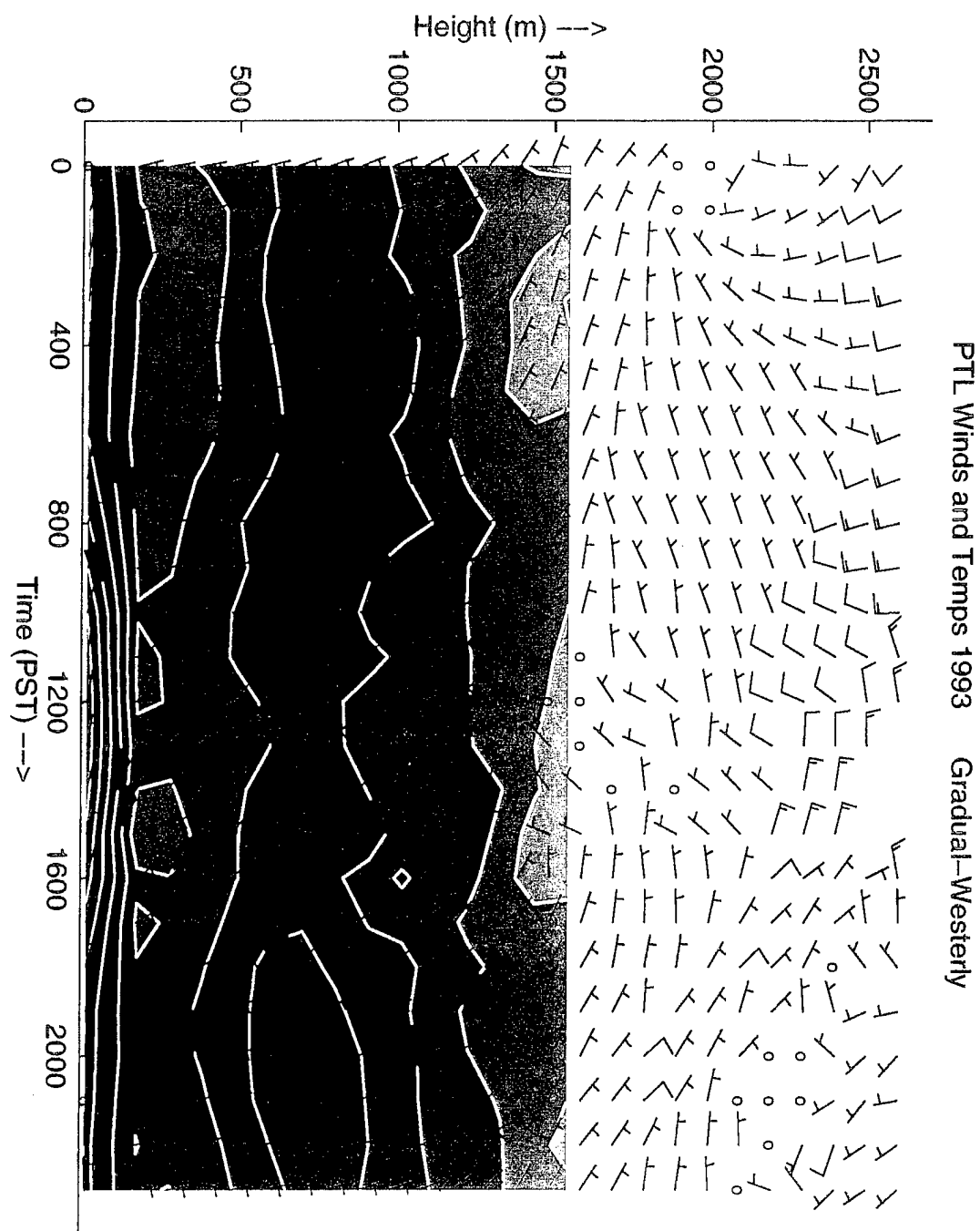


Figure 39. Composite of Point Loma winds and virtual temperature structure for 18 gradual-southerly sea breeze days.



**Figure 40.** As Figure 39, except 21 gradual-westerly sea breeze days.

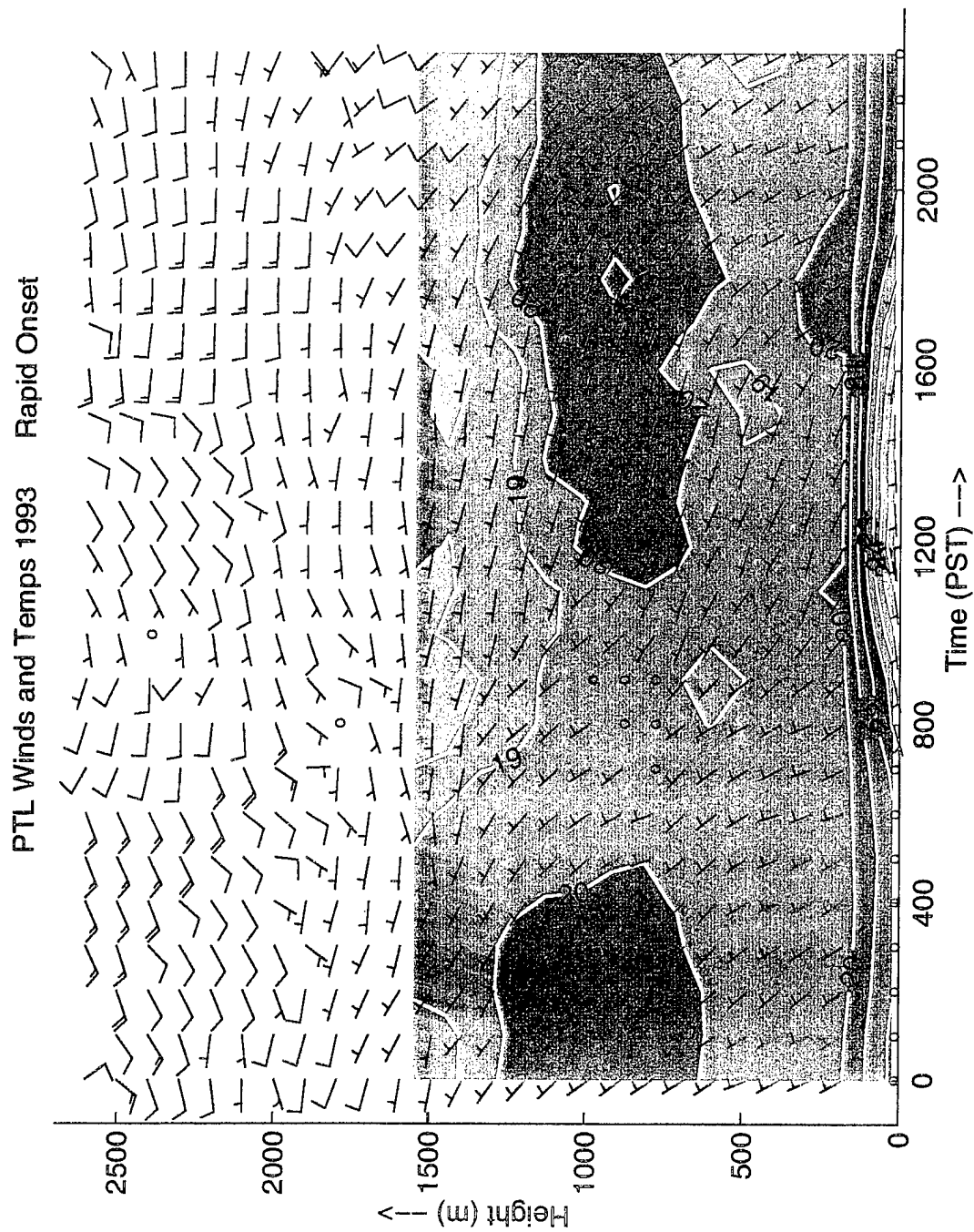
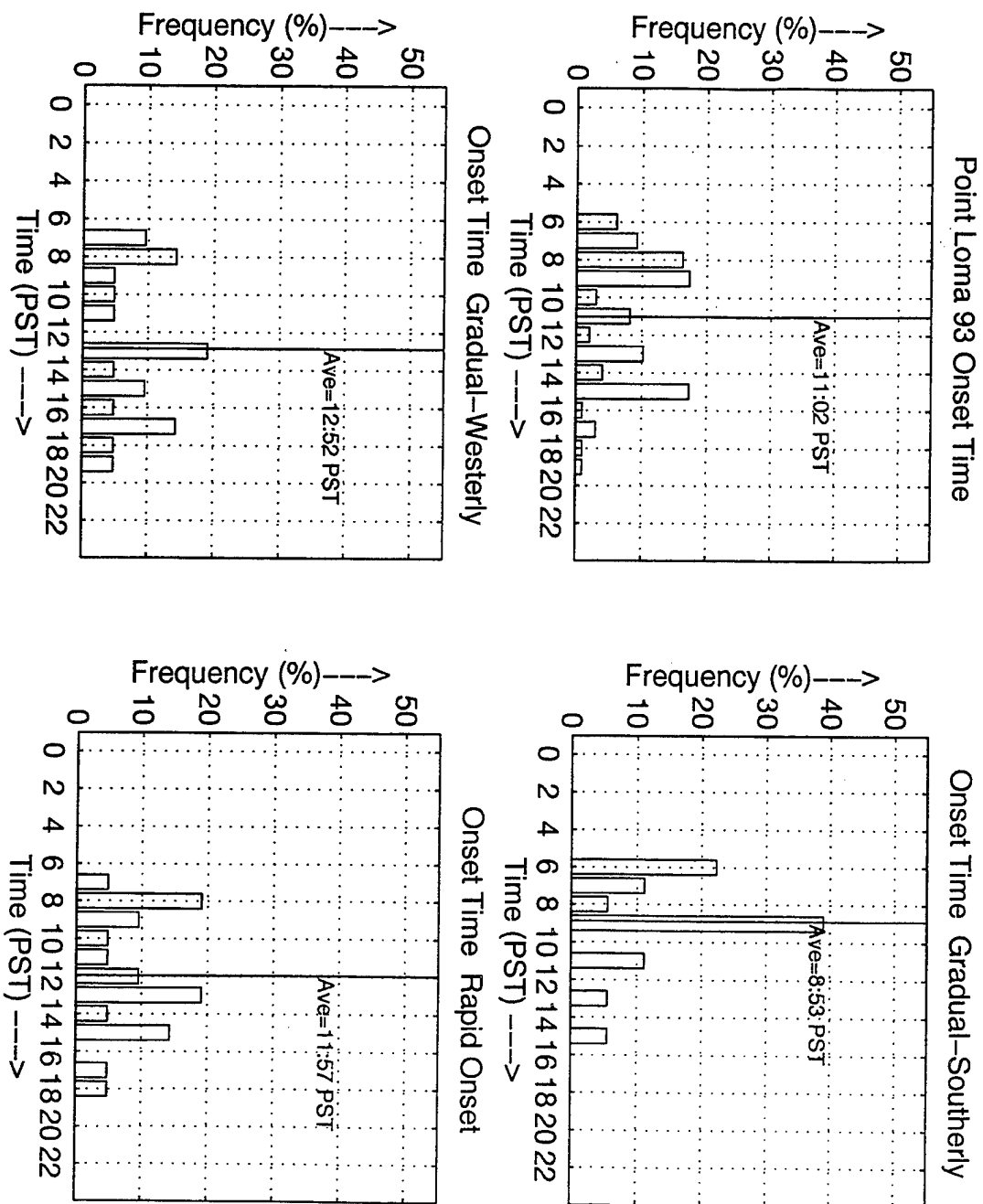


Figure 41. Distribution of sea breeze onset times for summer of 1993 at Point Loma: a) all sea breeze days, b) gradual-southerly days, c) gradual-westerly days, and d) rapid onset days.



**Figure 42.** As Figure 39, except 15 rapid onset sea breeze days.

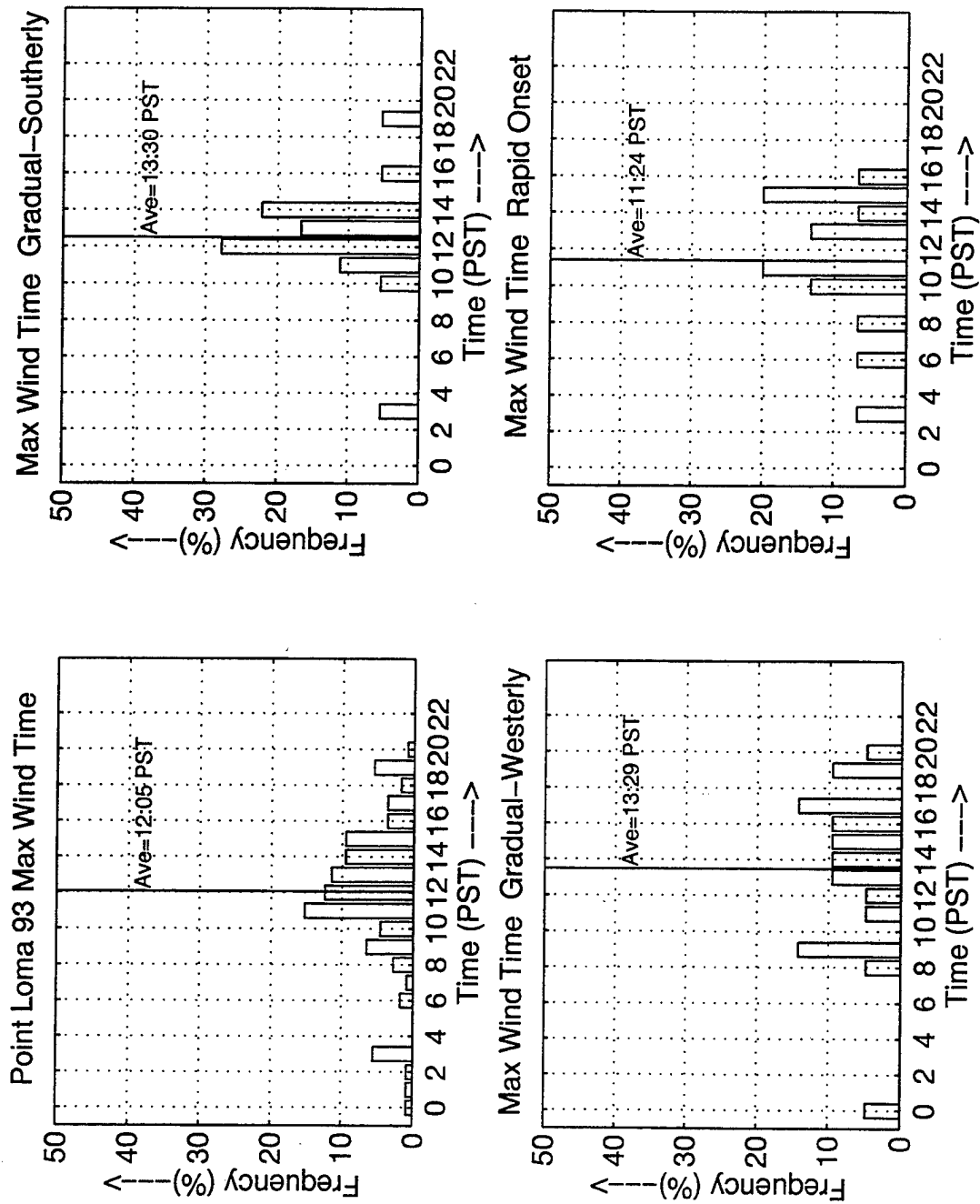
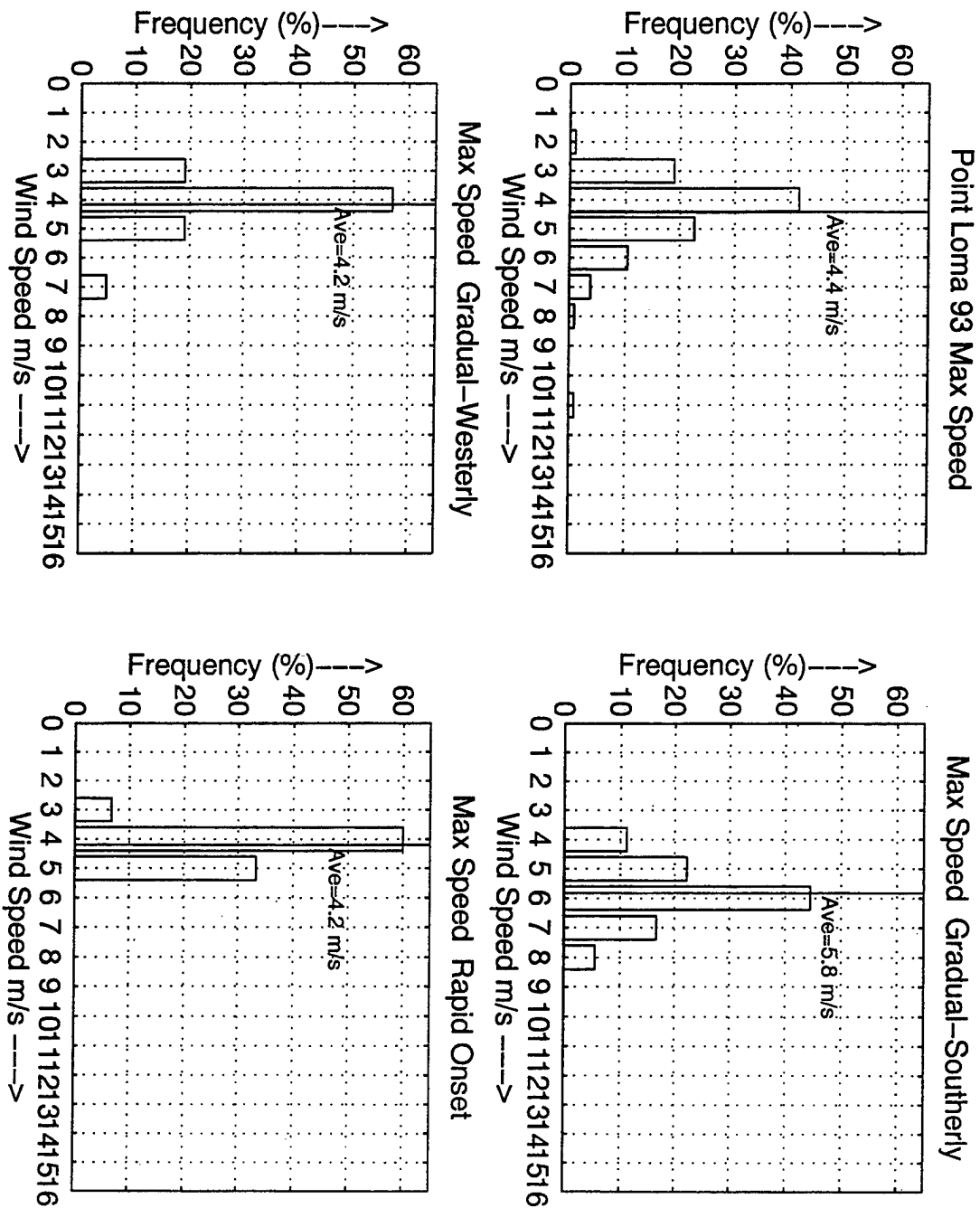


Figure 43. As Figure 42, except time of maximum wind.



**Figure 44.** As Figure 42, except maximum wind speed.

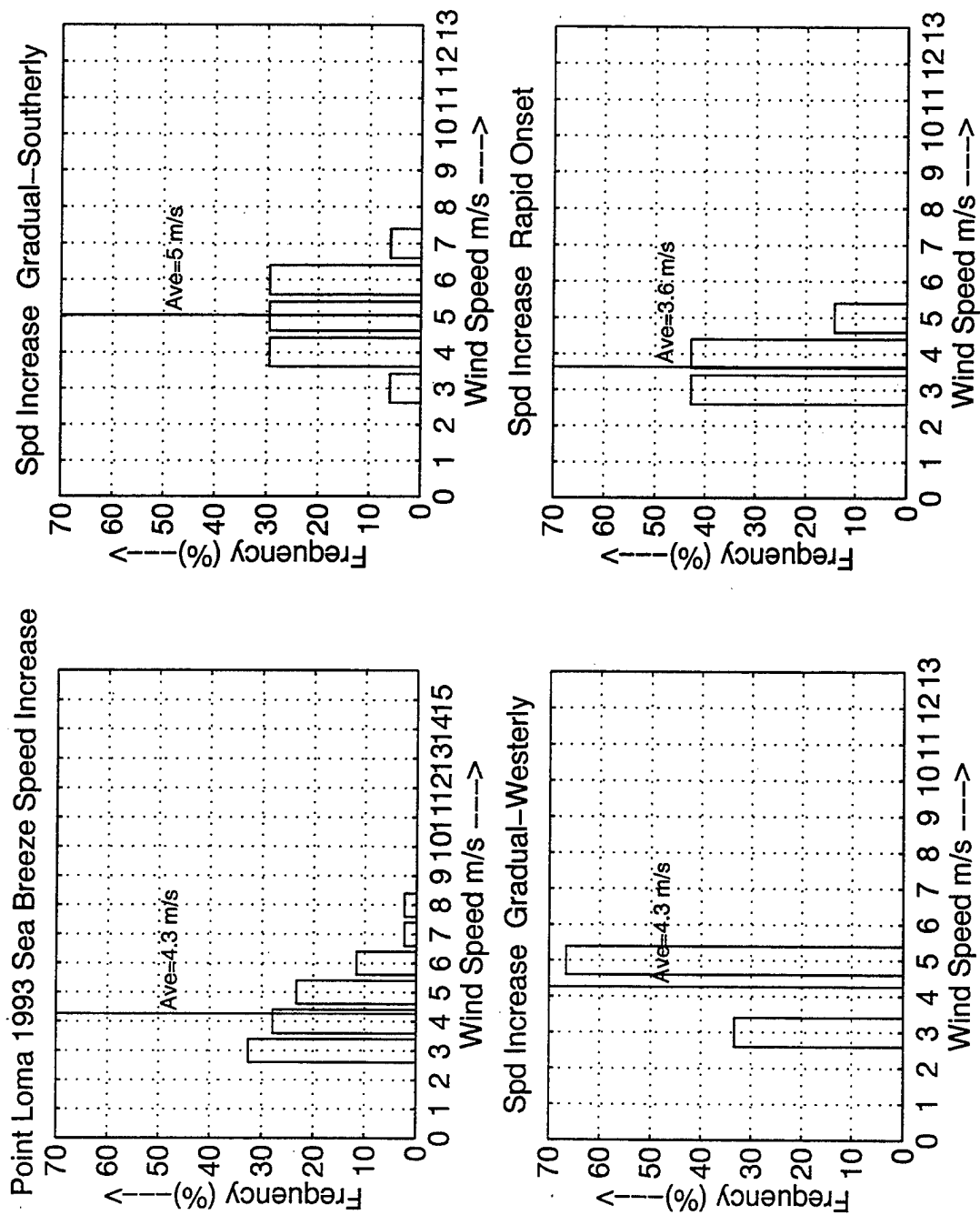


Figure 45. As Figure 42, except wind speed increase associated with sea breeze.



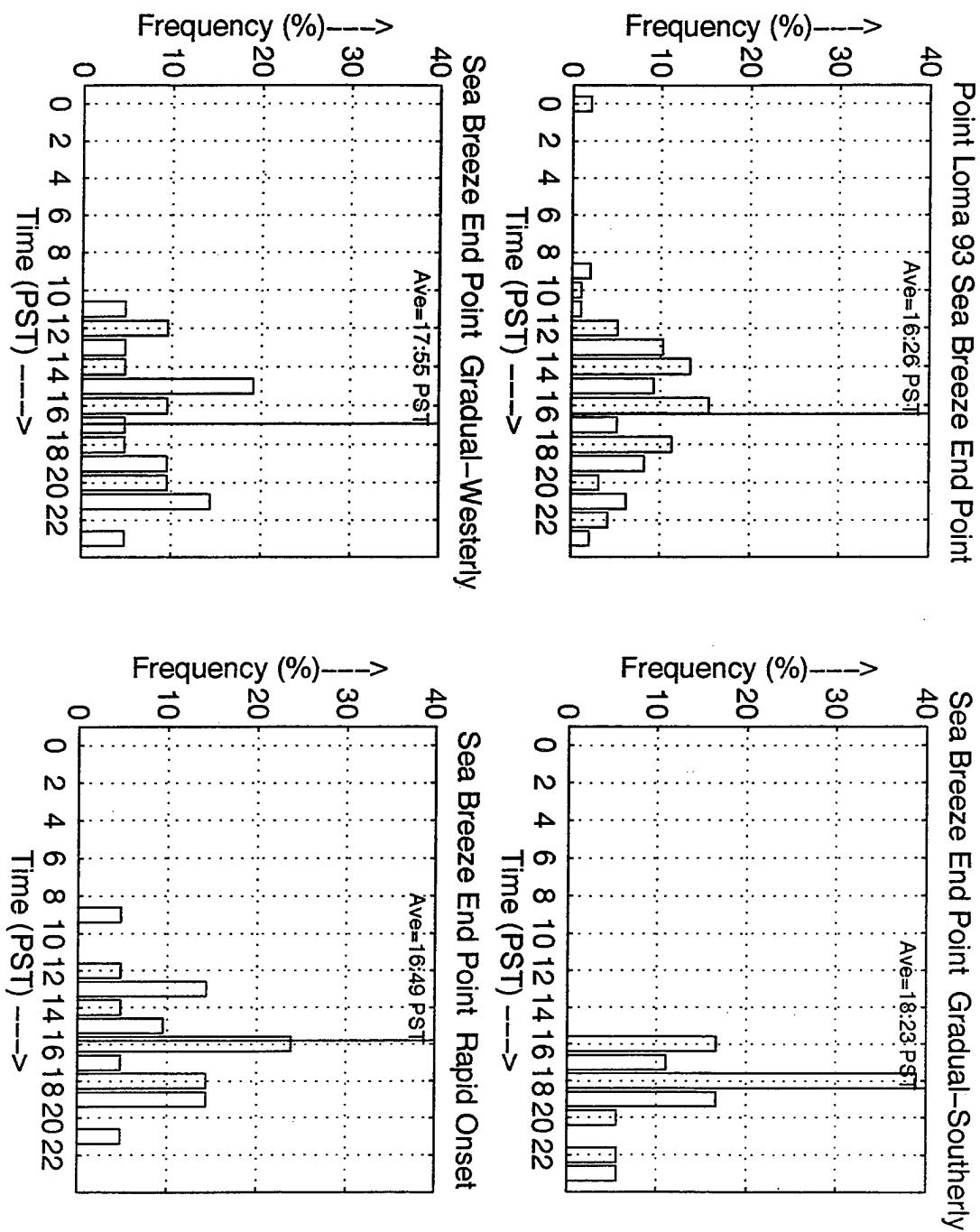


Figure 46. As Figure 42, except time of sea breeze end point.

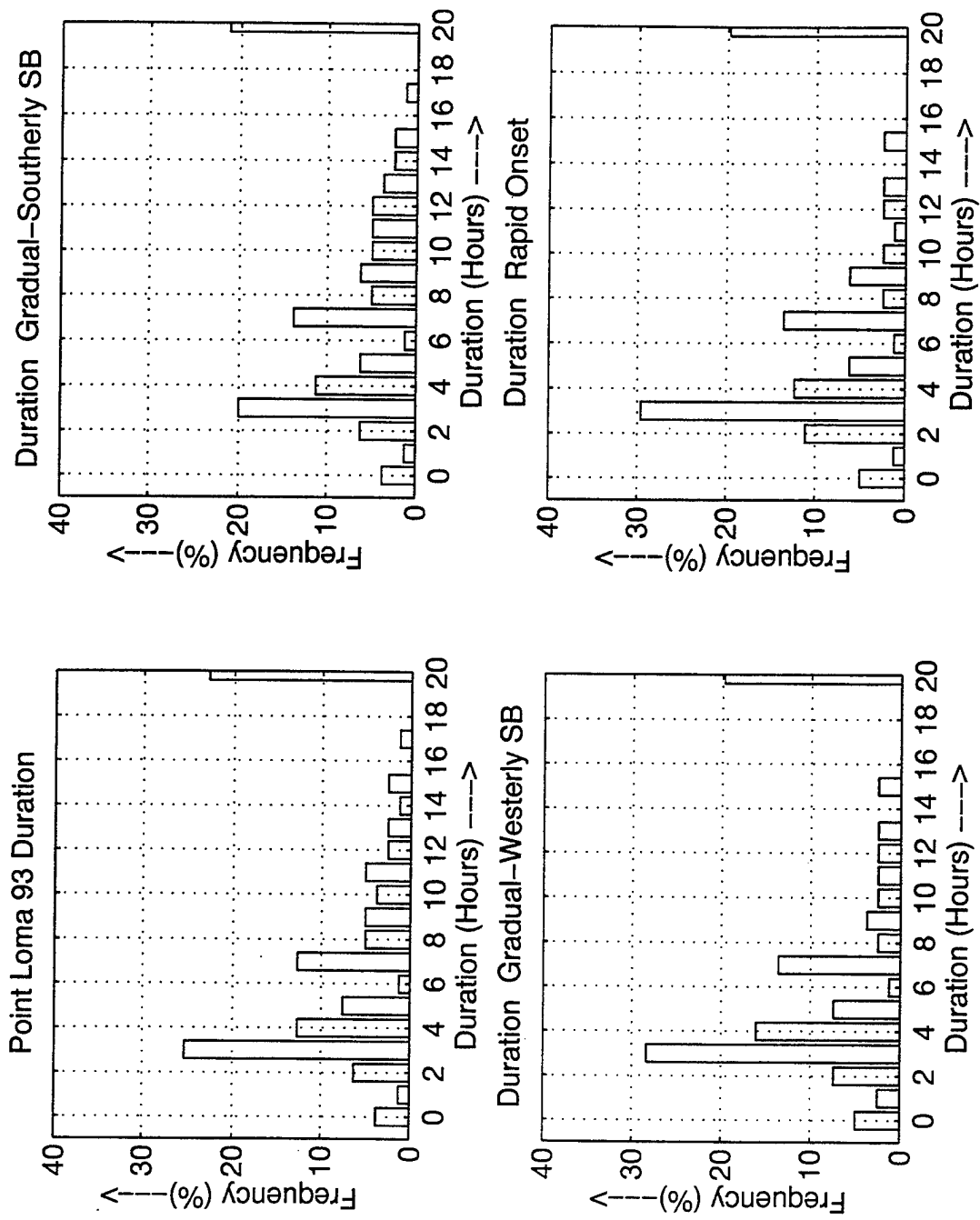
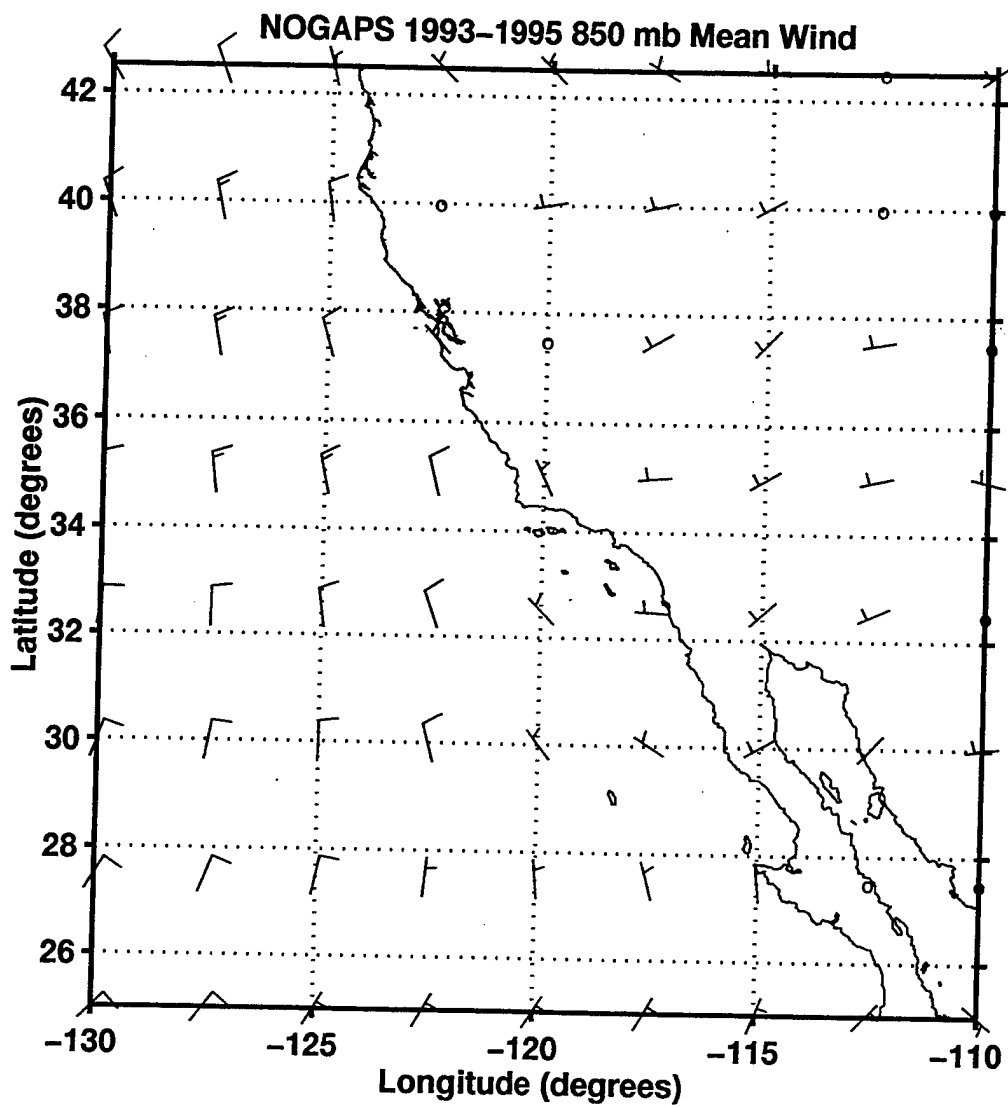
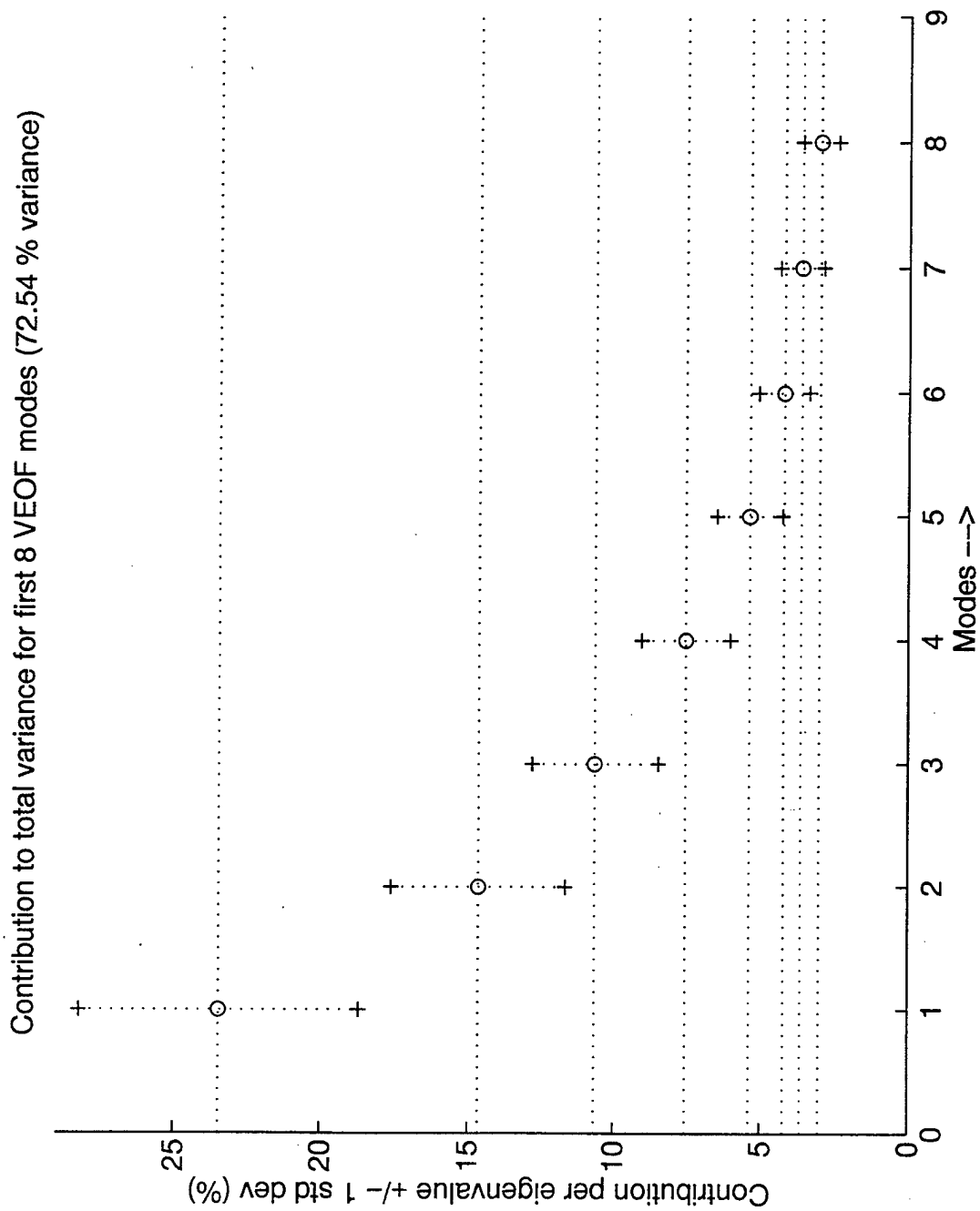


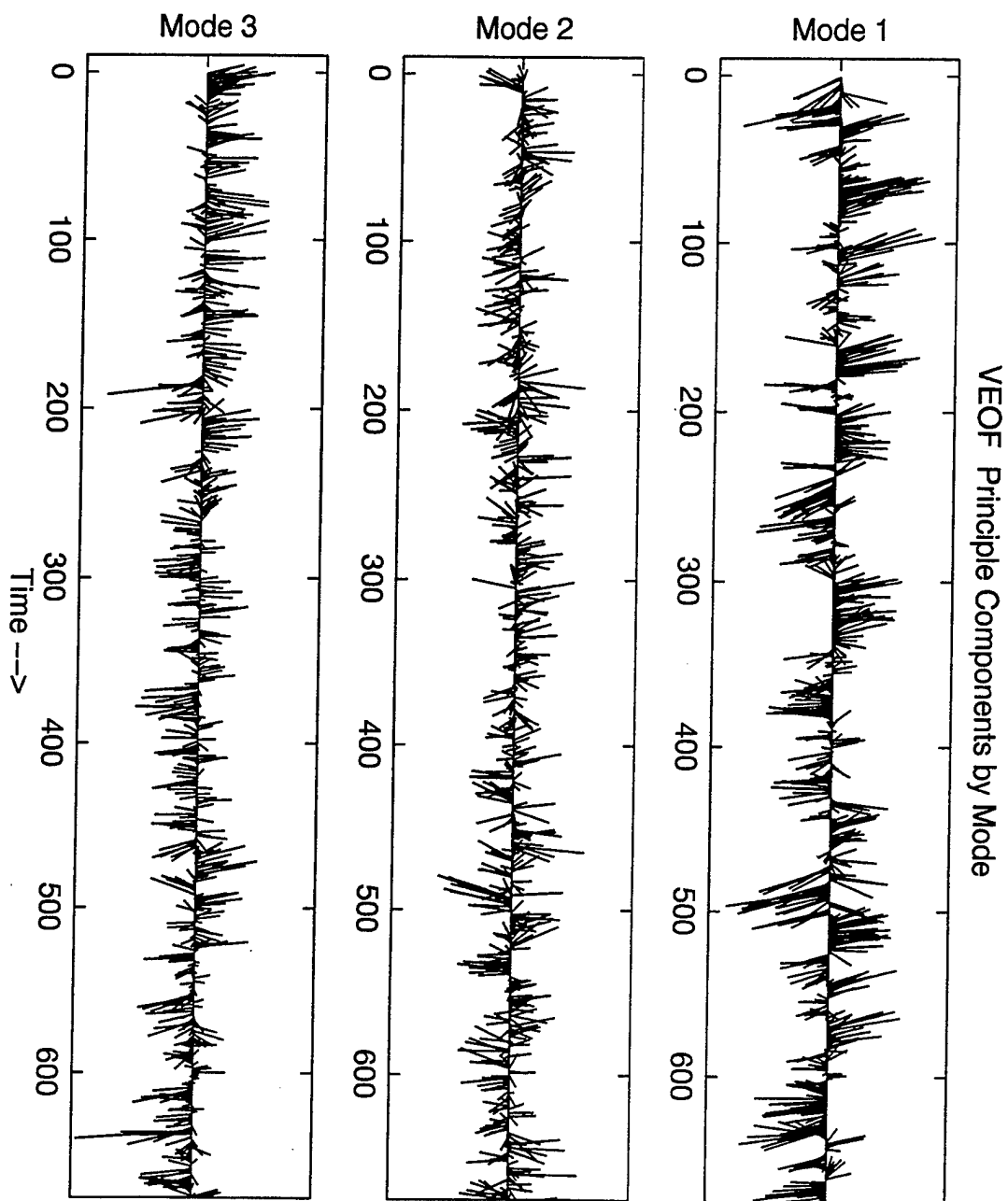
Figure 47. As Figure 42, except duration of sea breeze.



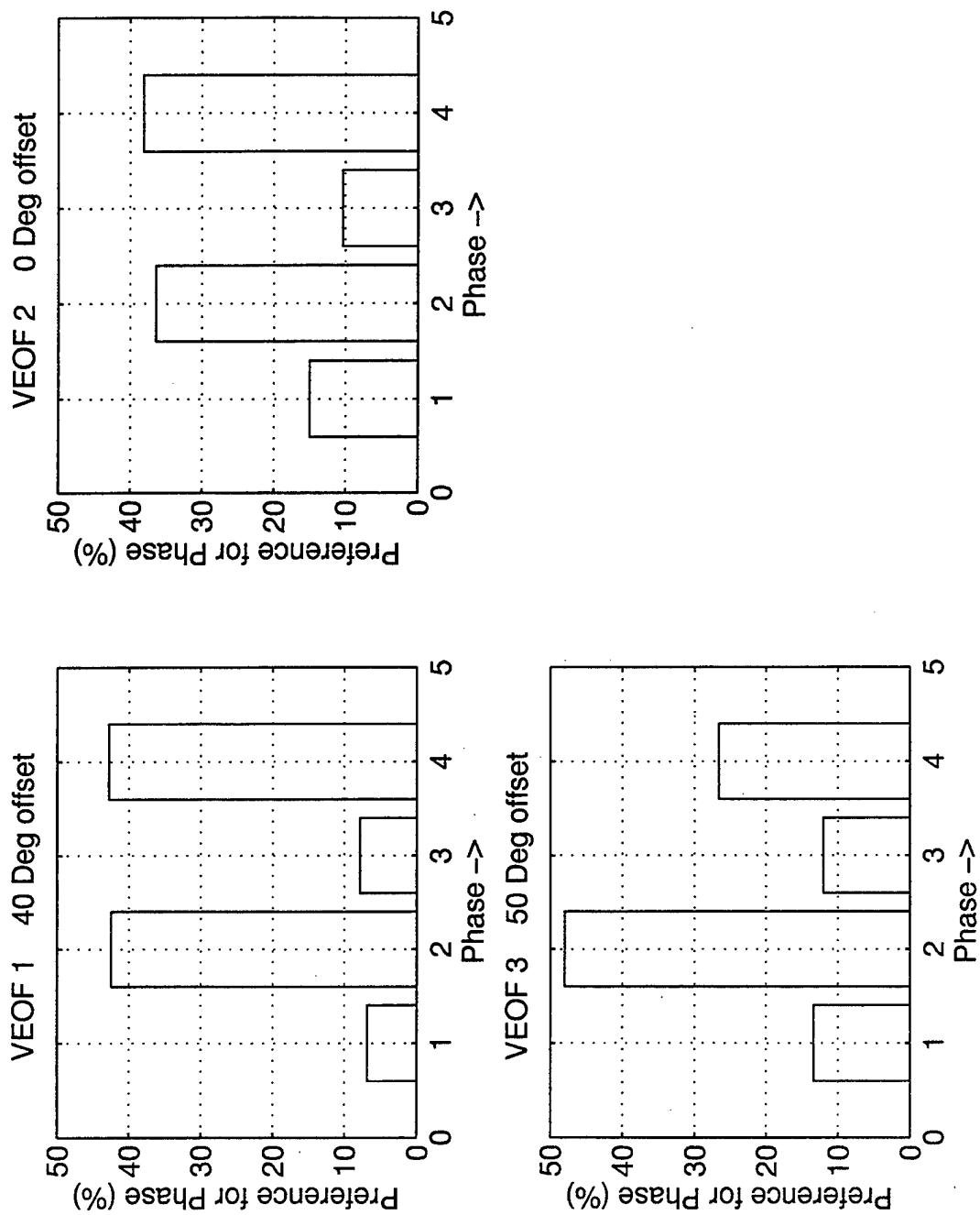
**Figure 48.** NOGAPS 850 mb mean winds for the summers of 1993-1995. One wind barb equals  $5 \text{ m s}^{-1}$ .



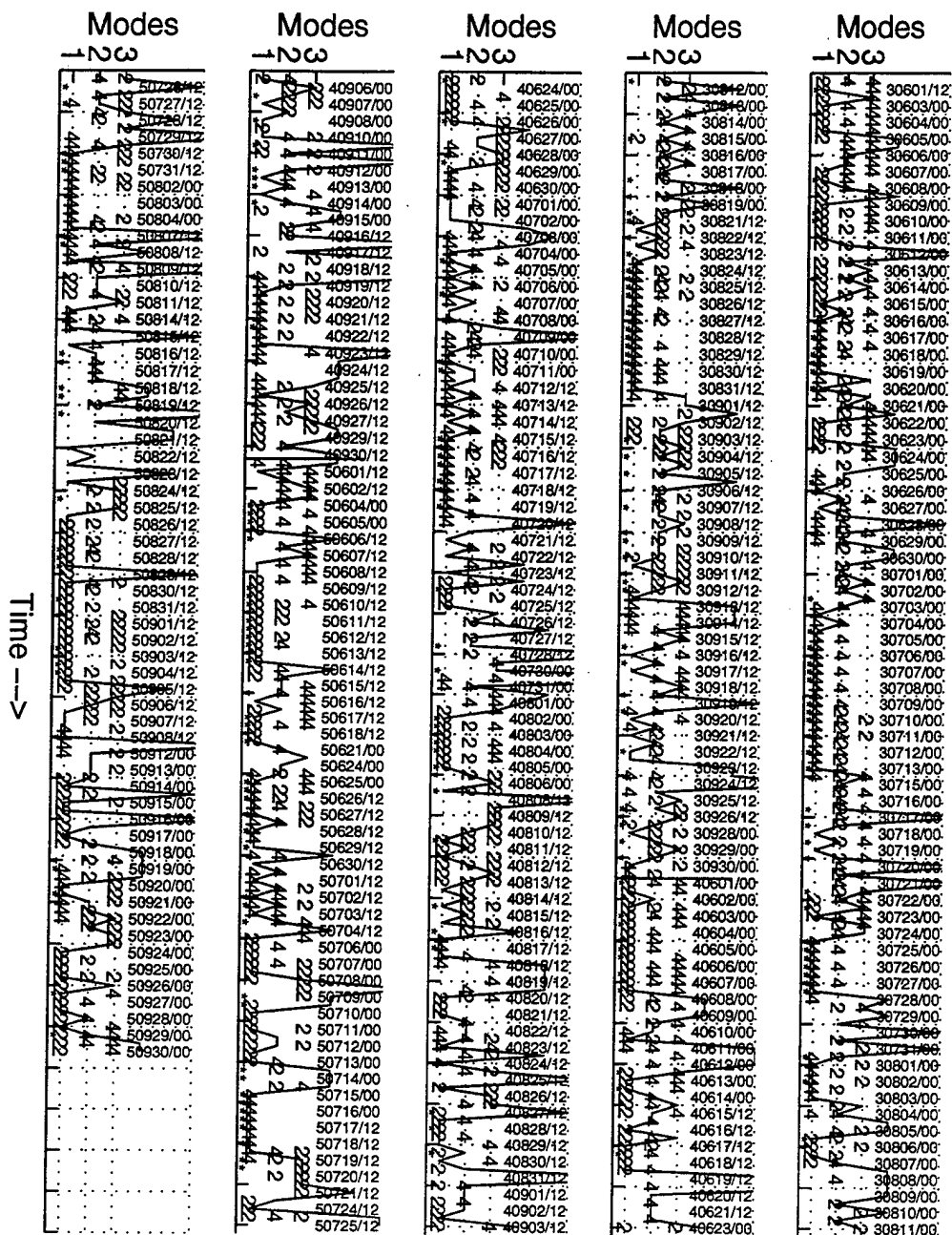
**Figure 49.** Contribution of VEOF modes 1-8 to the total variance by mode.  $\pm$  standard error is plotted as '+'s.



**Figure 50.** Plot of the VEOF mode 1-3 principal components.

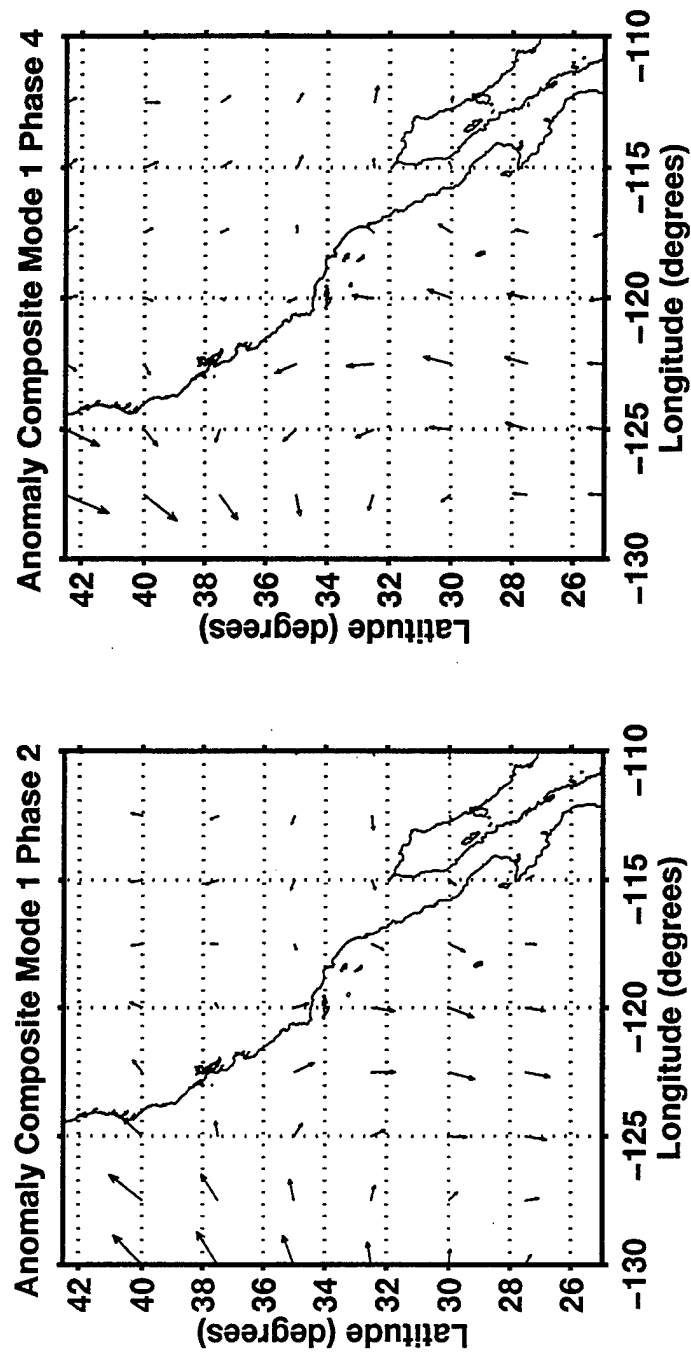


**Figure 51.** Histograms of the distribution of the principal components of VEOF modes 1-3 into 90° sectors (phases). The offset represents the amount of rotation of the first sector from 0°.



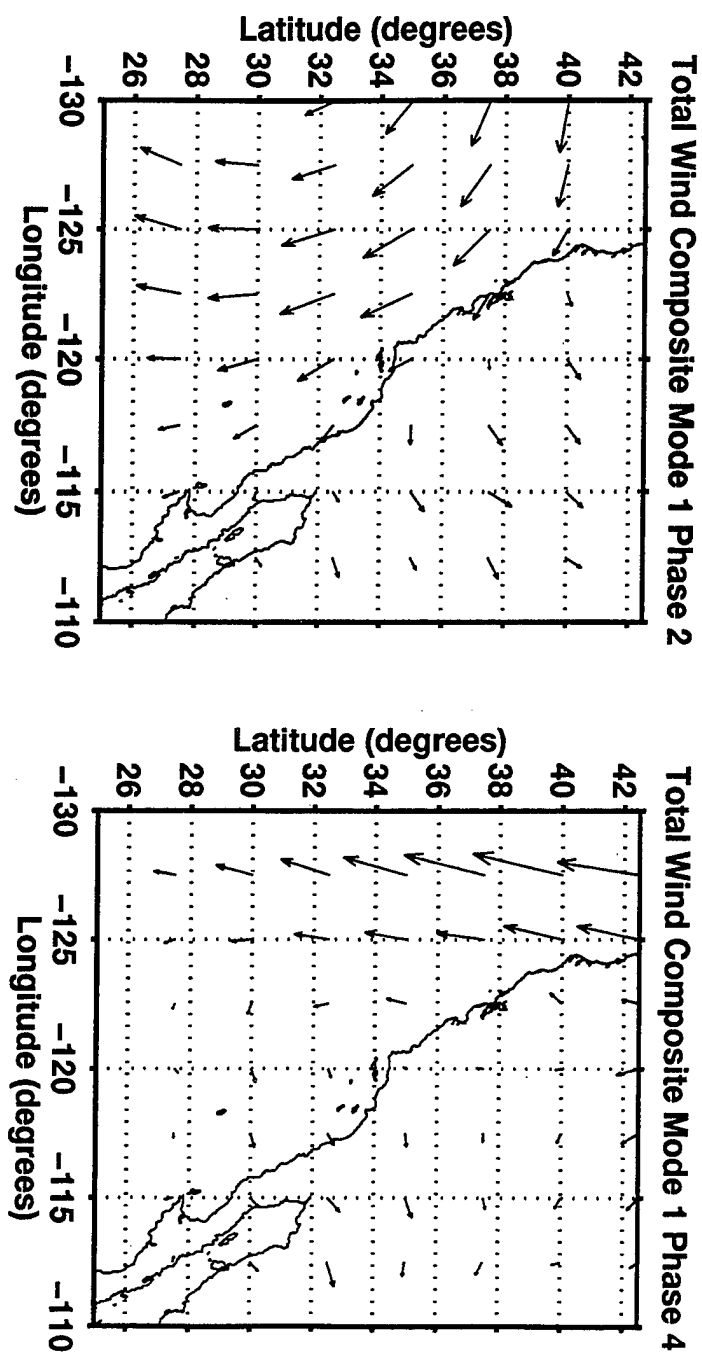
Contribution of VEOF 850 mb Wind Modes 1:3

Figure 52. Plot of the distributions of the primary phases of VEOF modes 1-3 for every 12 hours. Plots of 2 and 4 in each mode represents principal components in the primary phases, while blanks represent components in the minor 1 and 3 phases. The solid line connects the magnitudes of the largest VEOF mode for each time period.



**Figure 53.** Anomaly 850 mb wind composites of the primary VEOF mode 1 phase 2 (southerly ridge regime - 130 members) and mode 1 phase 4 (northerly ridge regime - 131 members).





**Figure 54.** Total 850 mb wind composites of the primary VEOF mode 1 phase 2 (southerly ridge regime - 130 members) and mode 1 phase 4 (northerly ridge regime - 131 members).

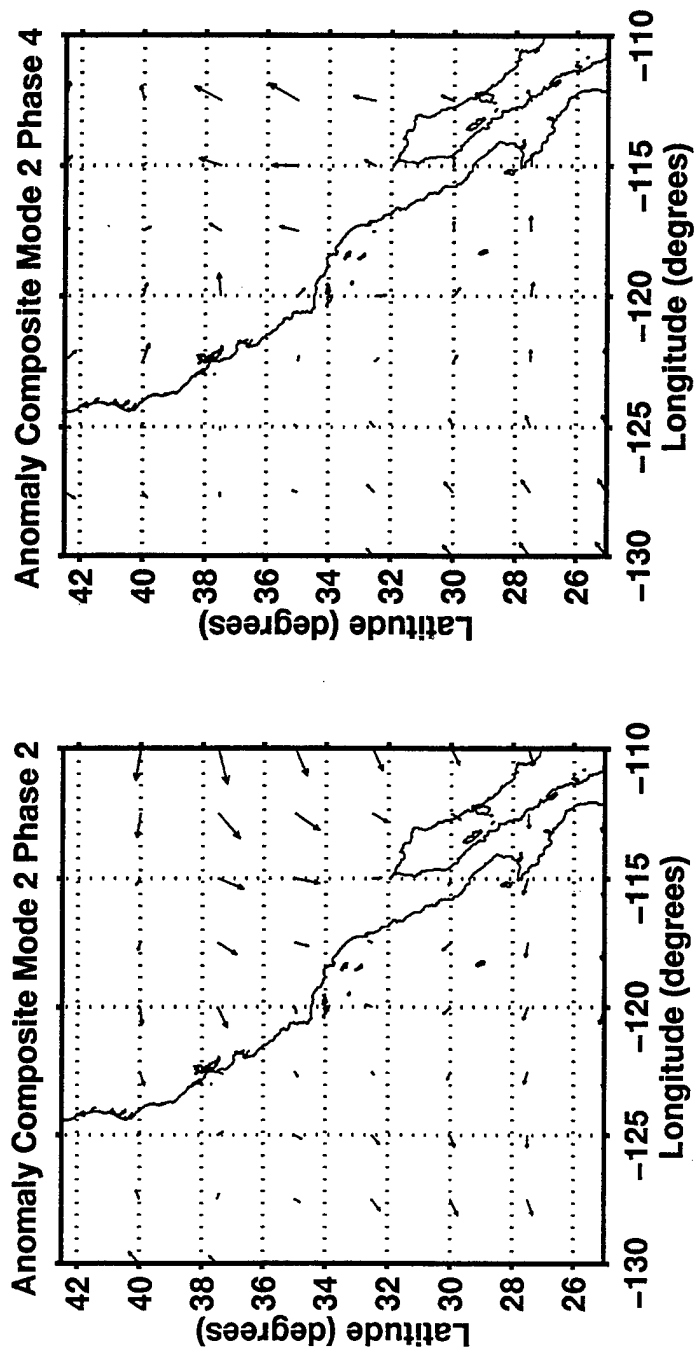


**Figure 55.** Anomaly 850 mb wind composites of the primary VEOF mode 2 phase 2 (continental land breeze regime - 77 members) and mode 2 phase 4 (continental sea breeze regime - 79 members).

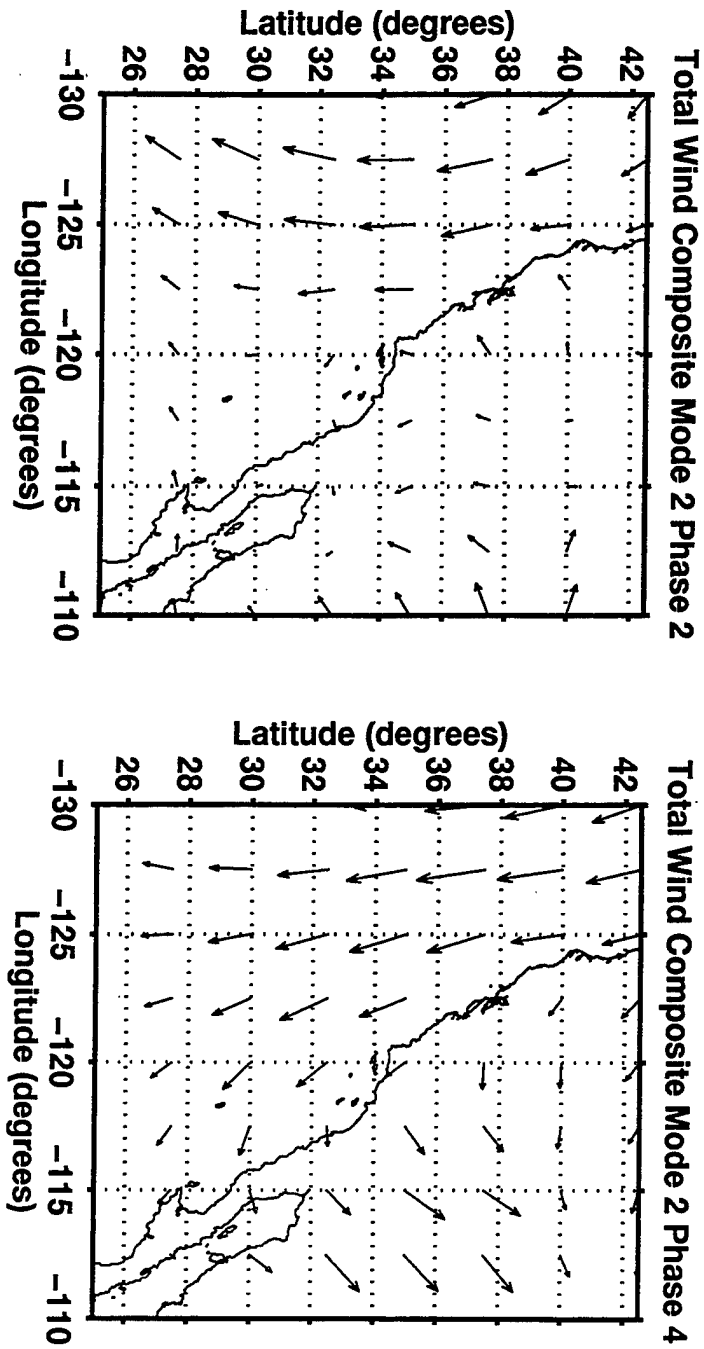


**Figure 56.** Total 850 mb wind composites of the primary VEOF mode 2 phase 2 (continental land breeze regime - 77 members) and mode 2 phase 4 (continental sea breeze regime - 79 members).

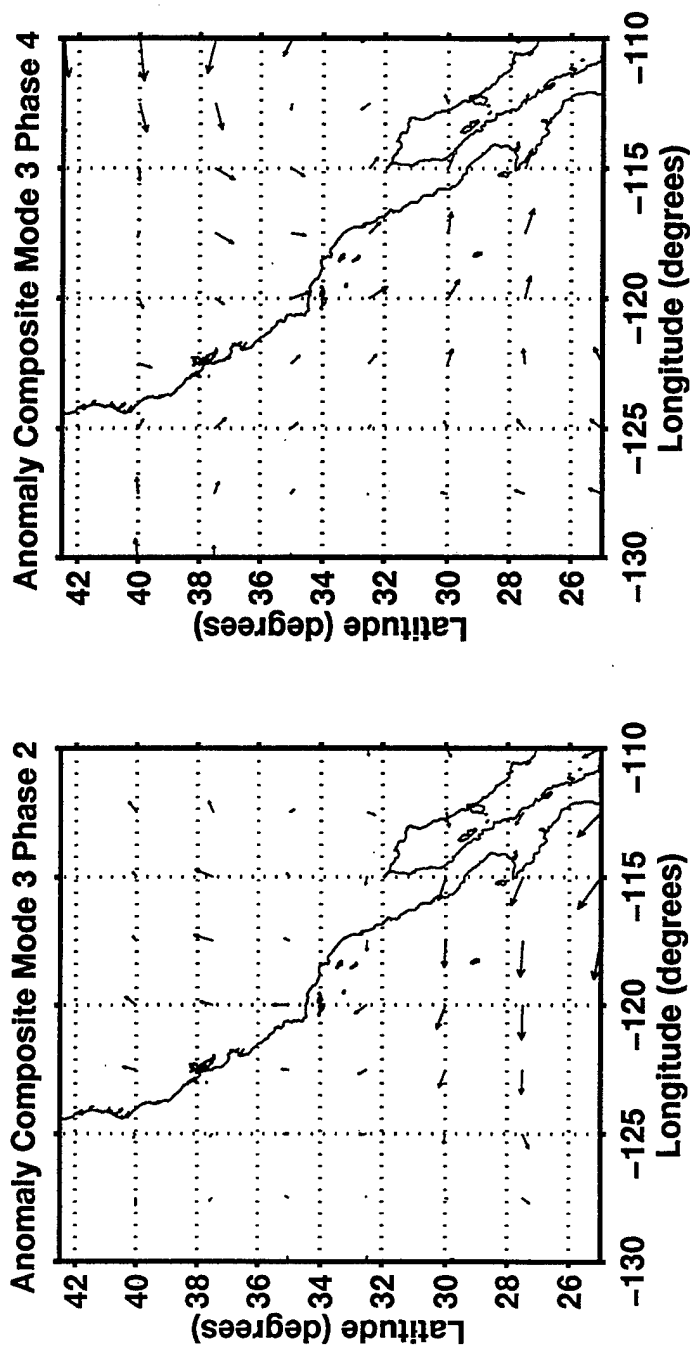


**Figure 57.** Anomaly 850 mb wind composites of the primary VEOF mode 3 phase 2 (reduced alongshore winds regime - 36 members) and mode 3 phase 4 (enhanced alongshore winds regime - 20 members).

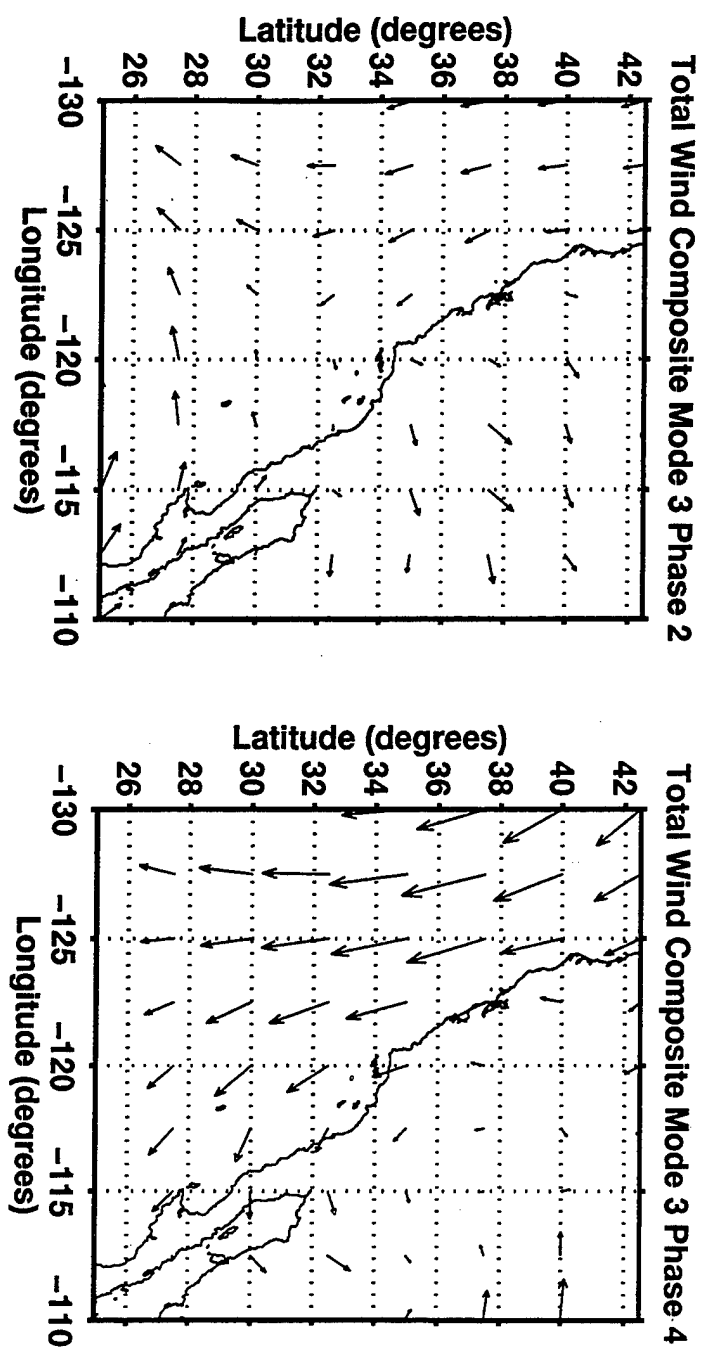


**Figure 58.** Total 850 mb wind composites of the primary VEOF mode 3 phase 2 (reduced alongshore wind regime - 36 members) and mode 3 phase 4 (enhanced alongshore wind regime - 20 members).

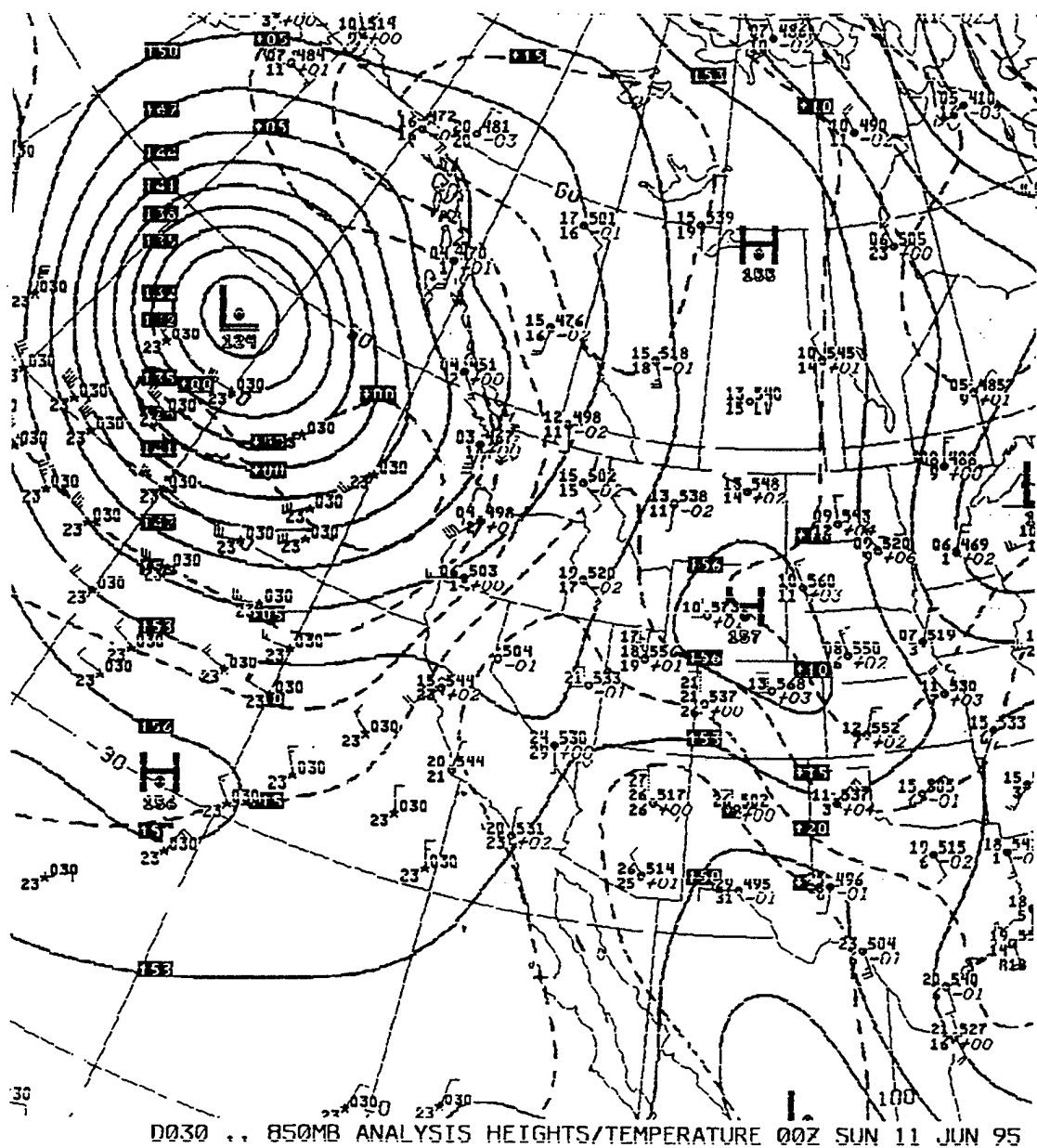
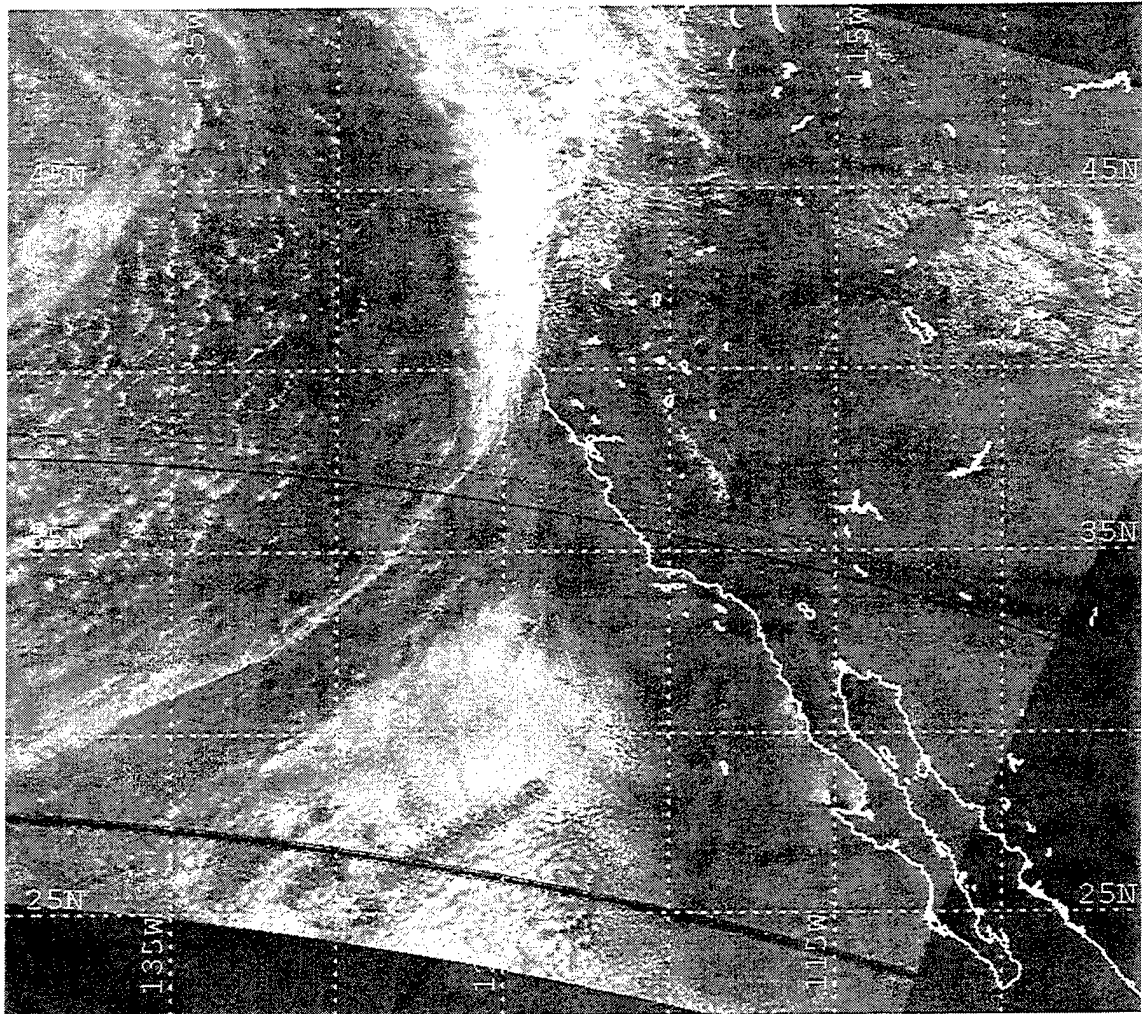


Figure 59. NMC 850 mb height analysis for June 11, 1995, corresponds to southerly ridge regime.



**Figure 60.** DMSP satellite image for 18:06 UTC June 10, 1995 (corresponds to southerly ridge regime in Figure 59).





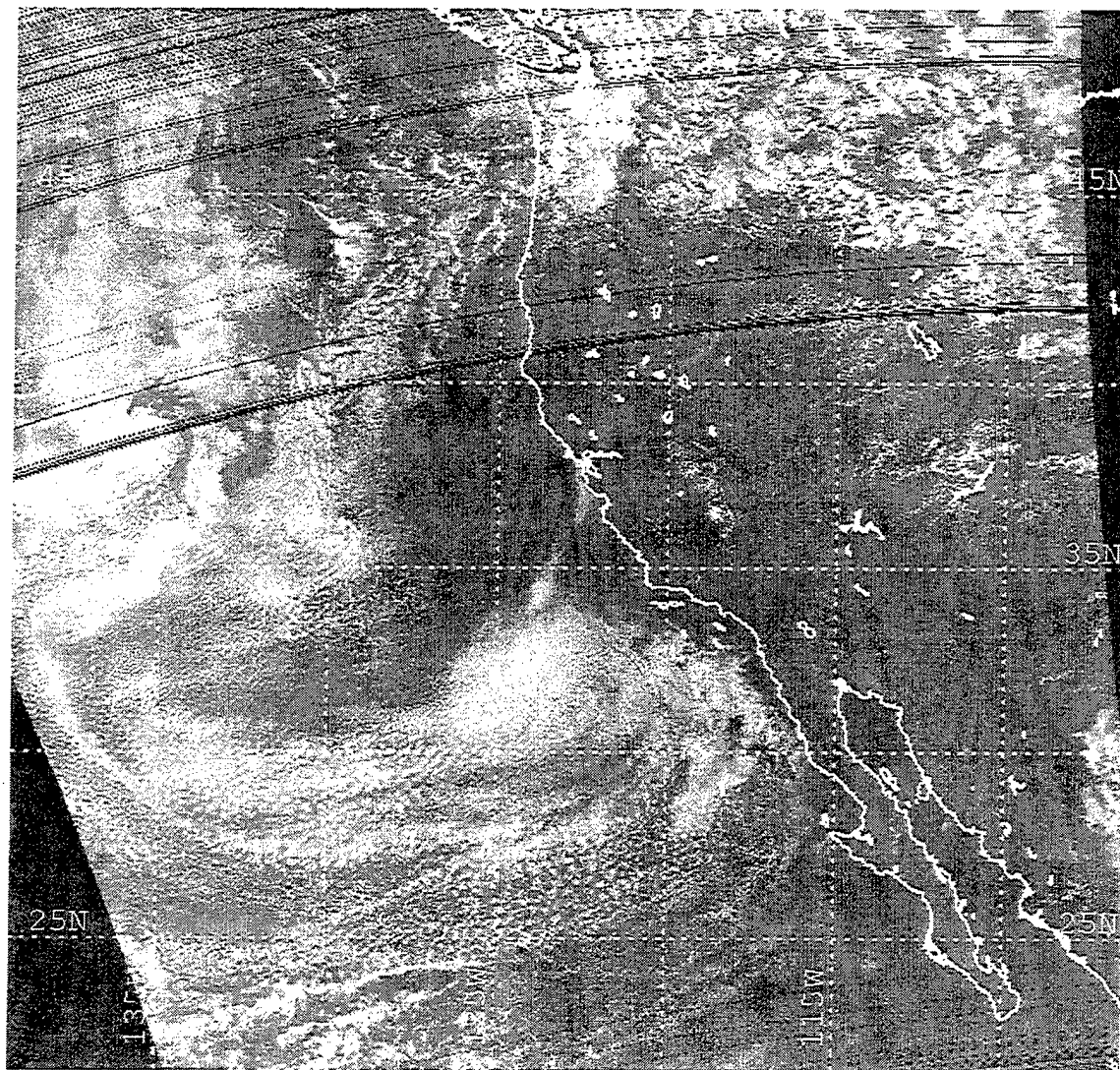


Figure 62. DMSP satellite image for 23:43 UTC July 24, 1993 (corresponds to northerly ridge regime in Figure 61).

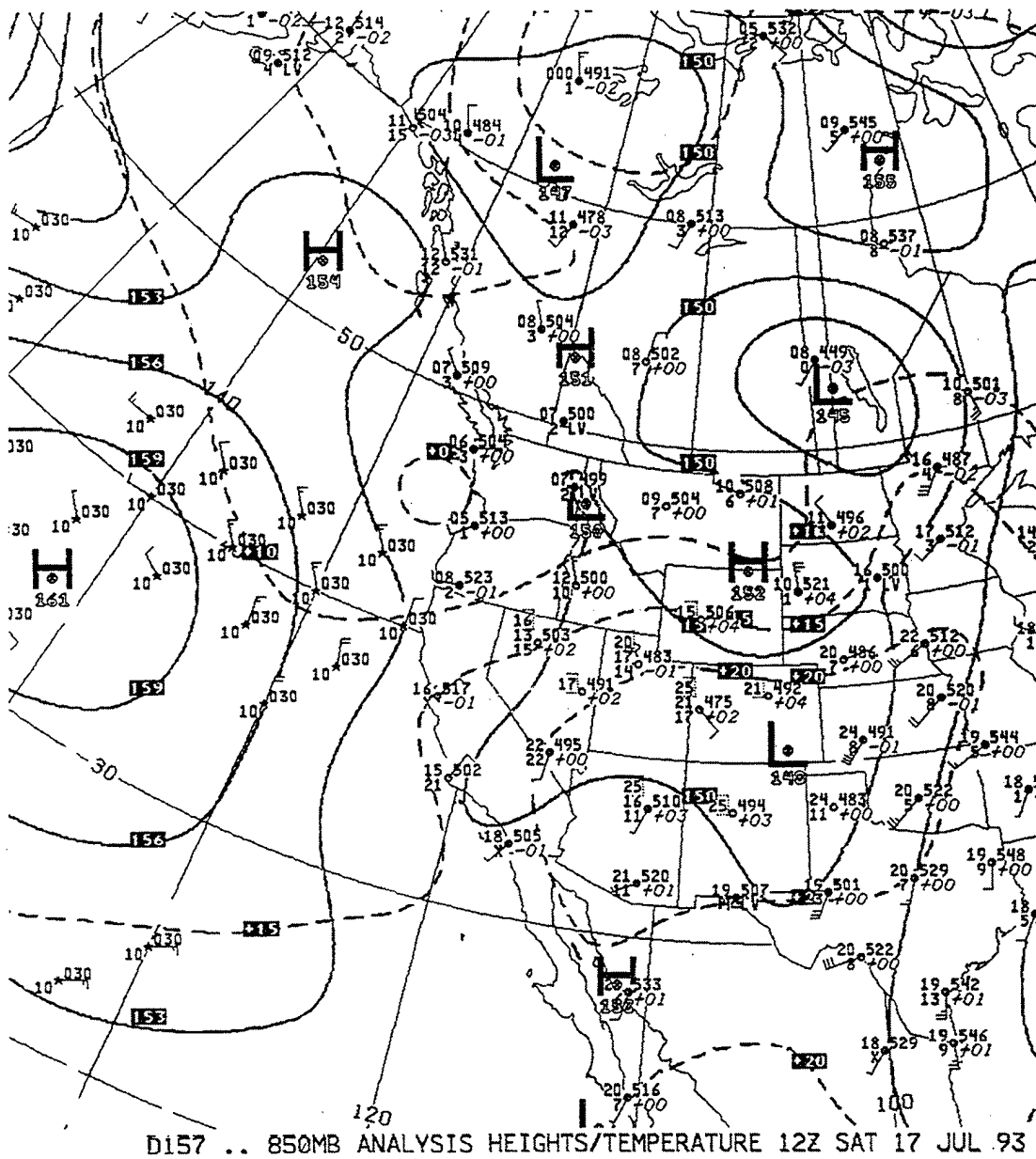
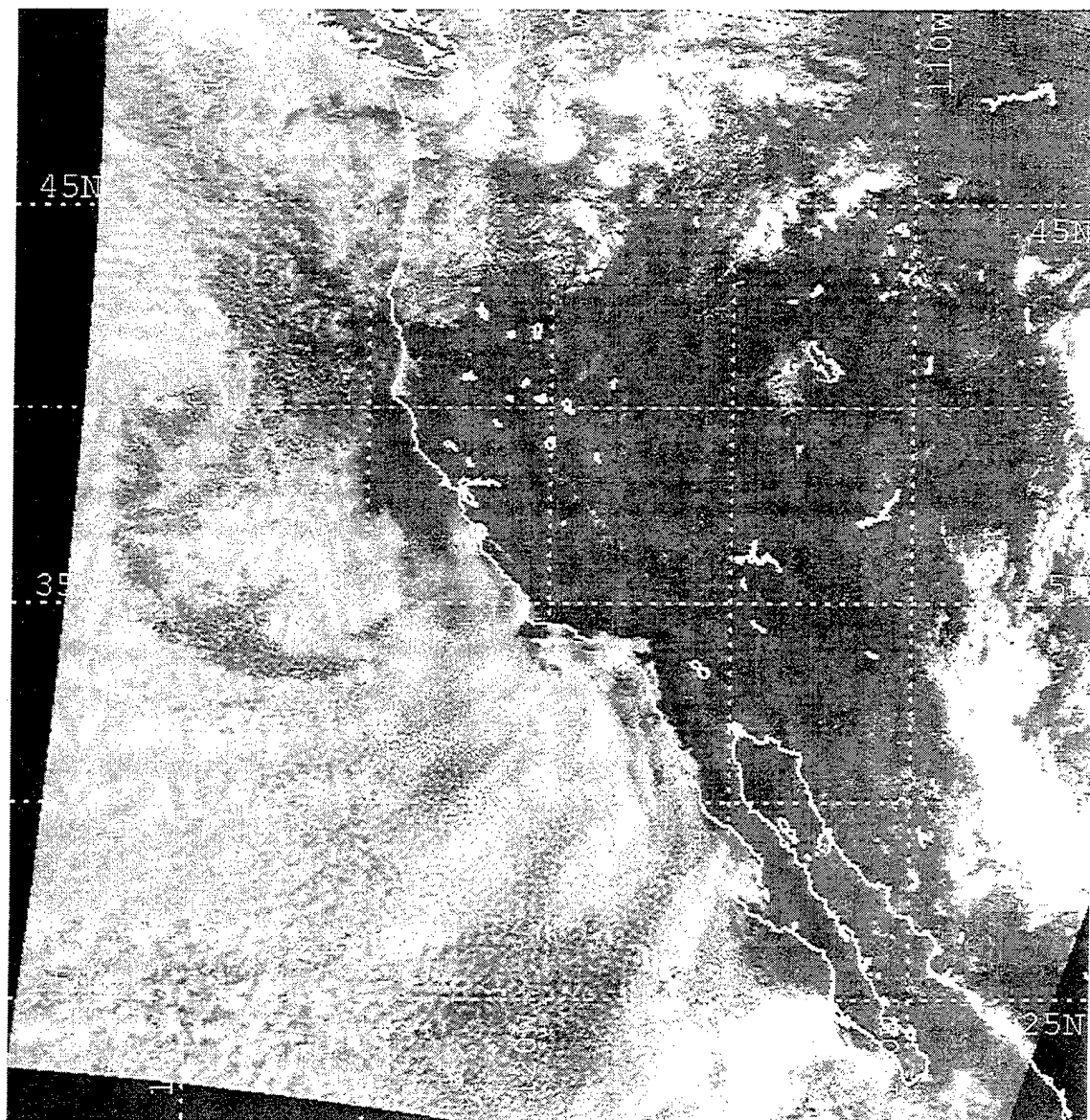


Figure 63. NMC 850 mb height analysis for July 17, 1993, corresponds to continental land/sea breeze regime.



**Figure 64.** DMSP satellite image for 15:41 UTC July 17, 1993 (corresponds to continental land/sea breeze regime in Figure 63).

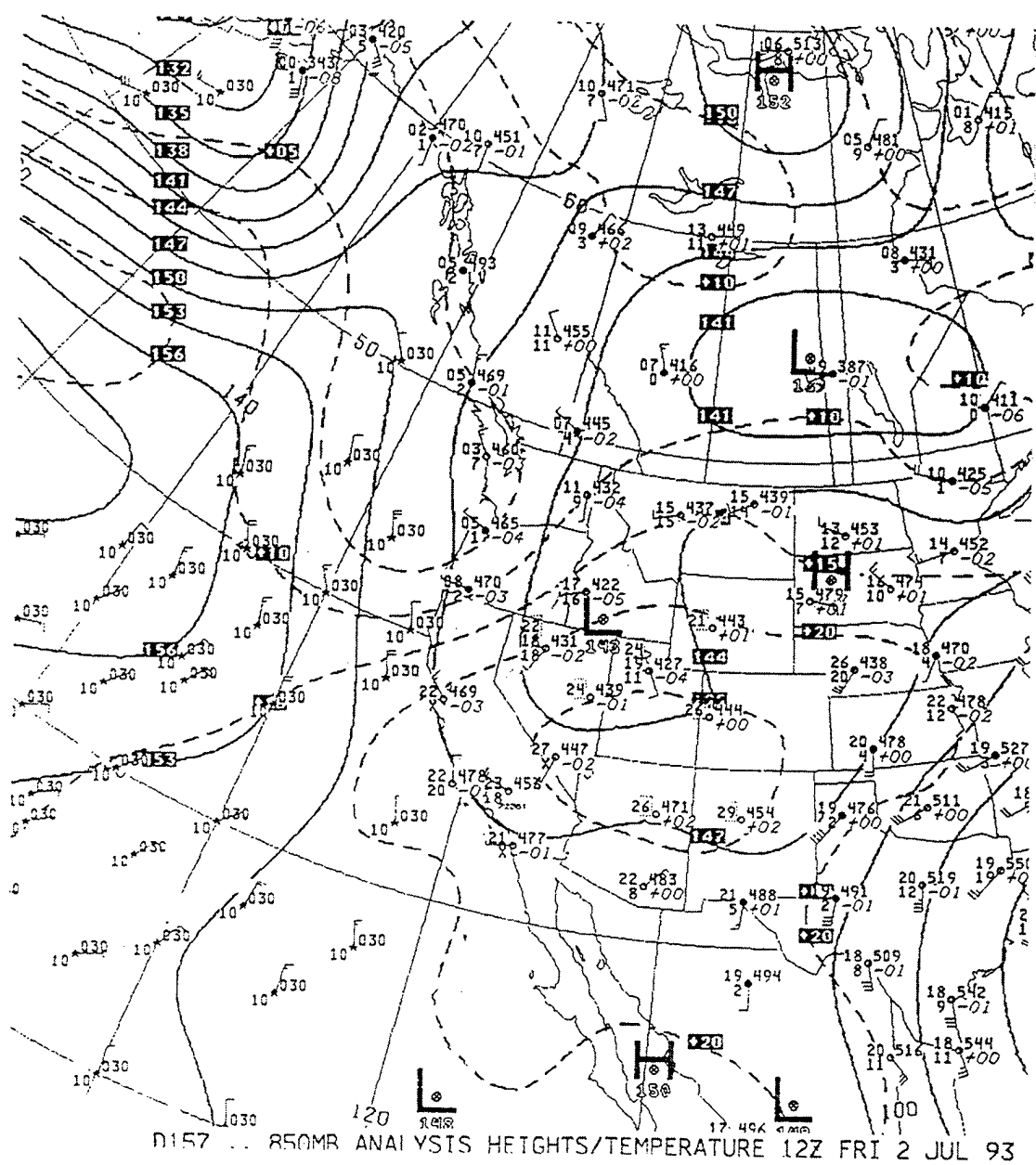
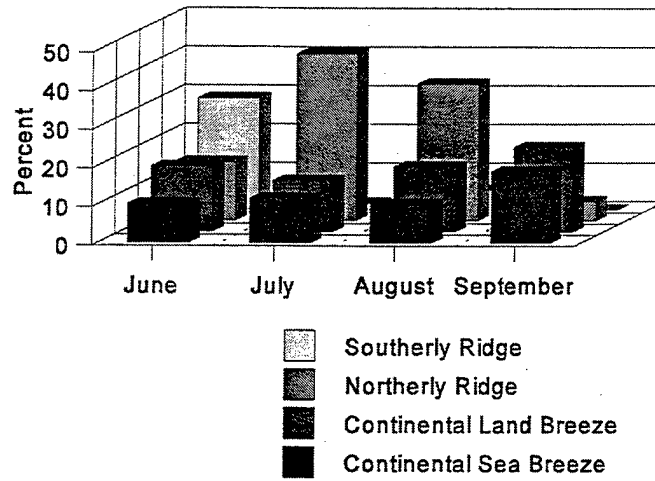
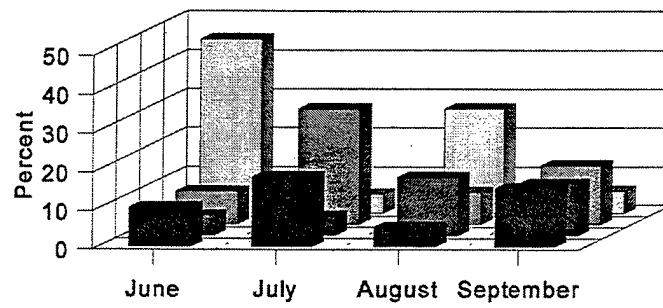


Figure 65. NMC 850 mb height analysis for July 2, 1993, corresponds to enhanced alongshore winds regime.

1993



1994



1995

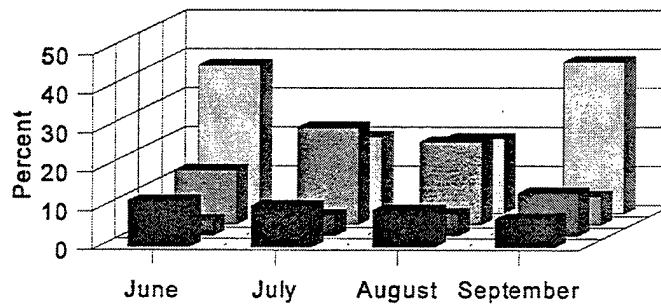


Figure 66. Contribution of strongest mode synoptic regimes by month for a) 1993, b) 1994, and c) 1995.

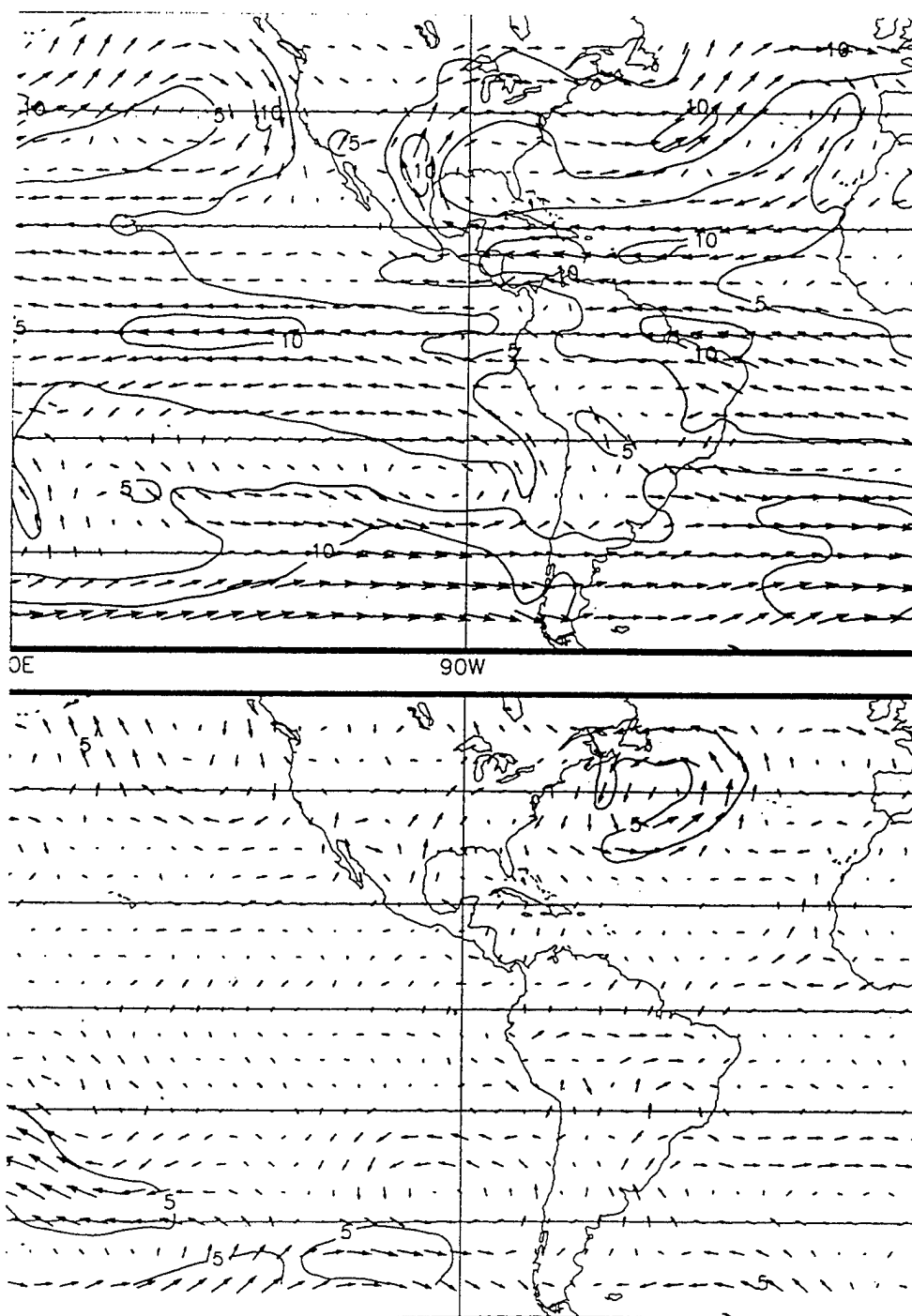


Figure 67. a) Mean monthly (top) and b) anomalous 850 mb winds for July 1993 (CDB 1993b).

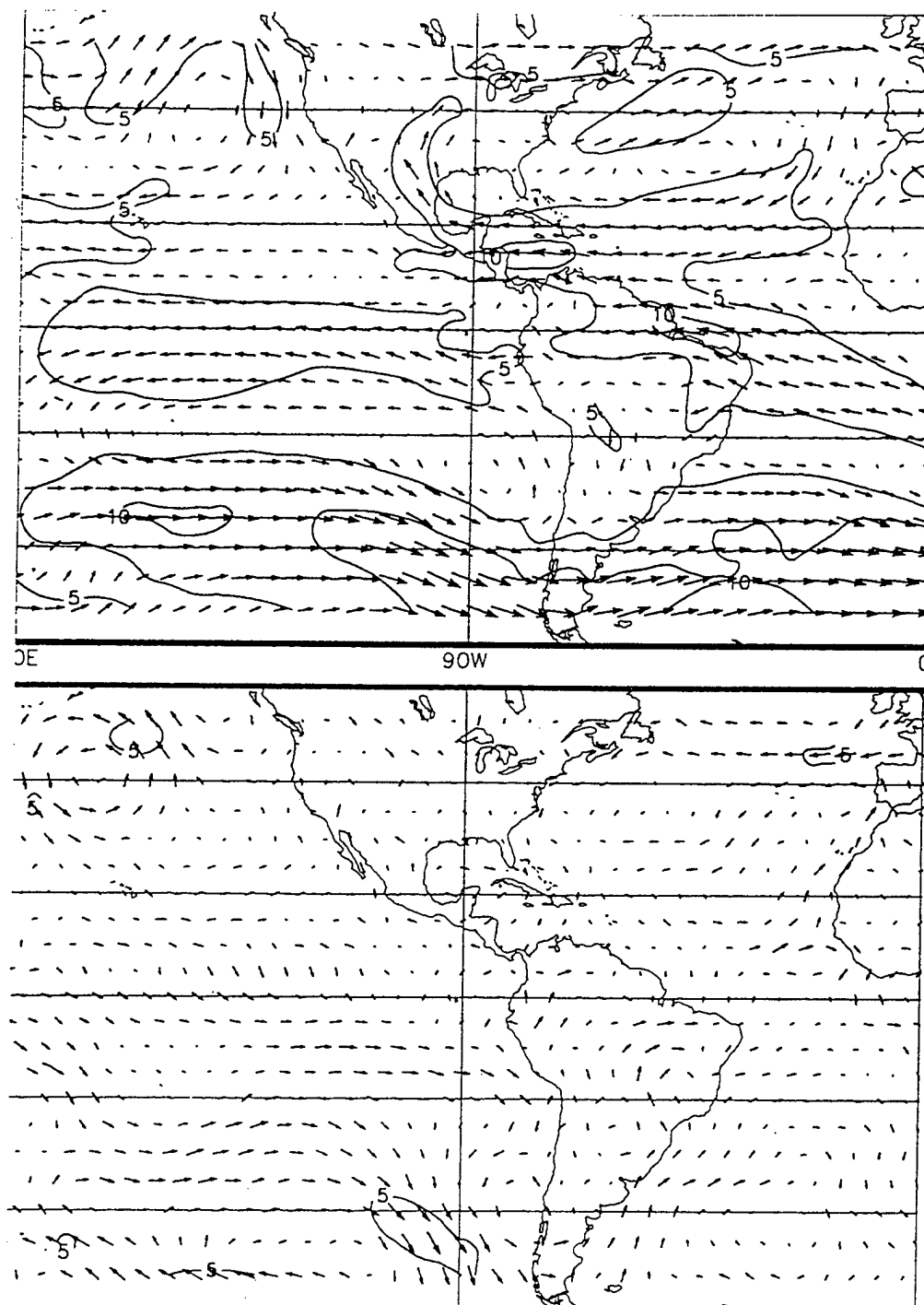


Figure 68. As Figure 67, except August 1993 (CDB 1993c).

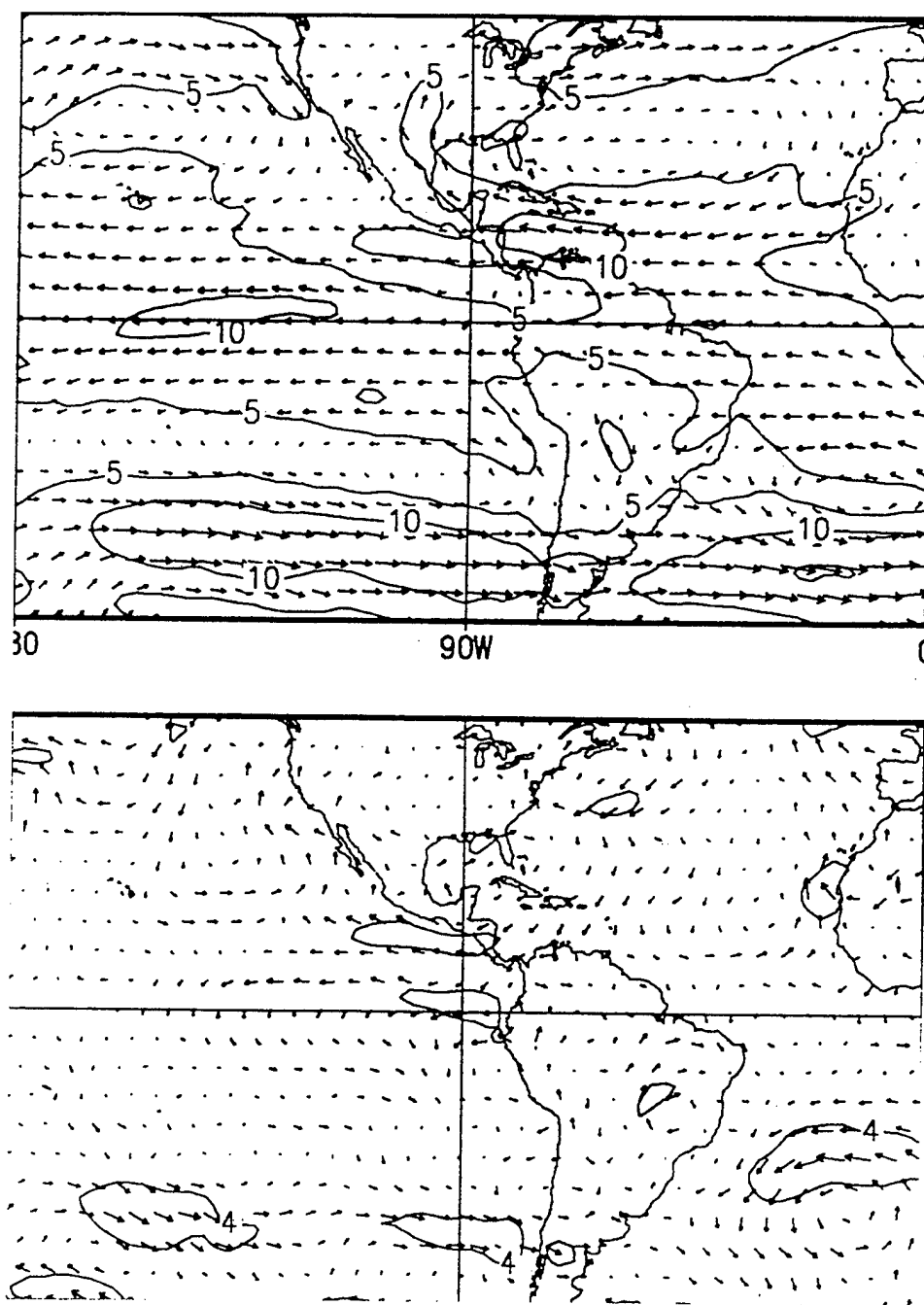
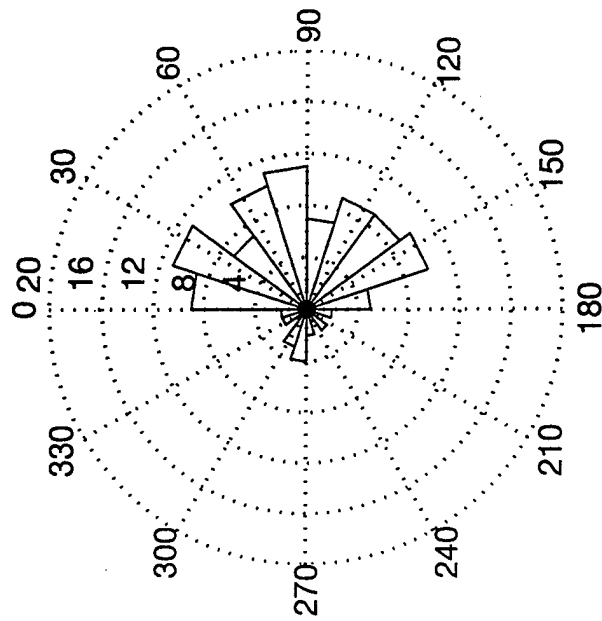


Figure 69. As Figure 67, except June 1994 (CDC 1994a).



ORD 12 UTC Winds & Frontal SB



ORD 12 UTC Winds & Gradual SB

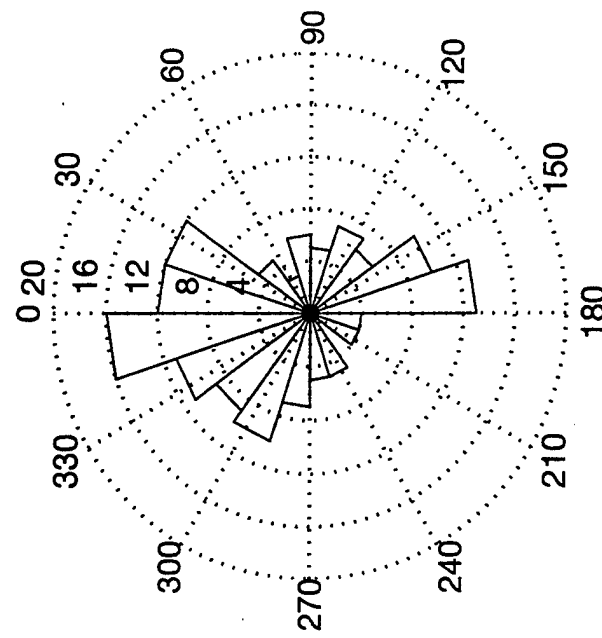


**Figure 70.** Wind rose of the 12:00 UTC observed NOGAPS anomalous winds at Fort Ord for 1993-1995 from frontal and gradual sea breeze days (directions winds are from).

## **APPENDIX. STANDARD DEVIATION AND MEAN WIND ANOMALY PLOTS**

Standard deviation plots corresponding to vertical wind and virtual temperature composites for frontal-westerly and gradual-westerly sea breeze types are shown in Figures A1 to A4.

Figures A5-A7 plot the eigenvectors associated with VEOF modes 1-2.

Figures A8-A16 show the mean monthly 850 mb wind averages and departures from the 1979-1988 base period for the summers of 1993, 1994, and 1995.

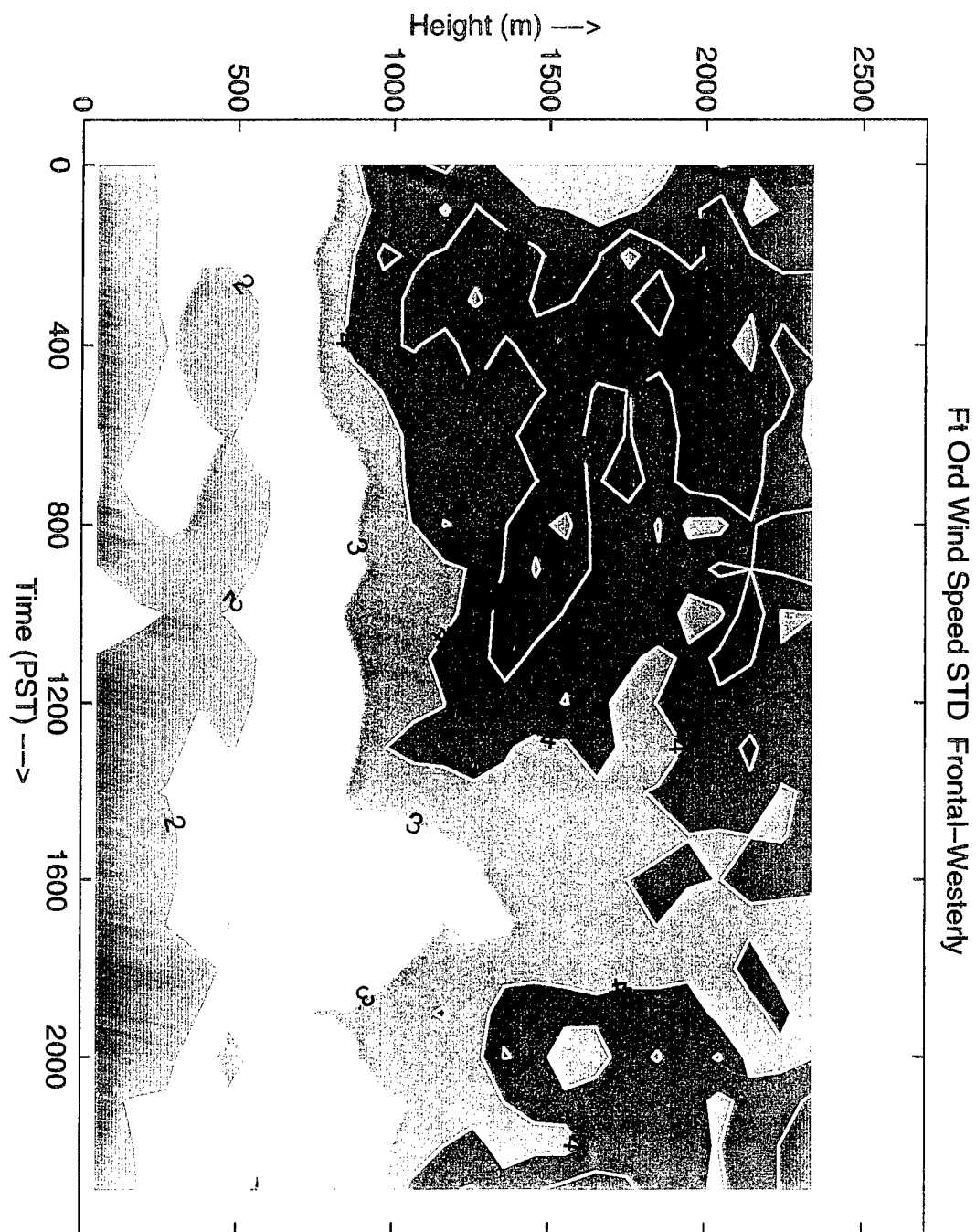


**Figure A1.** Wind speed standard deviations (m/s) associated with frontal-westerly sea breezes at Fort Ord.

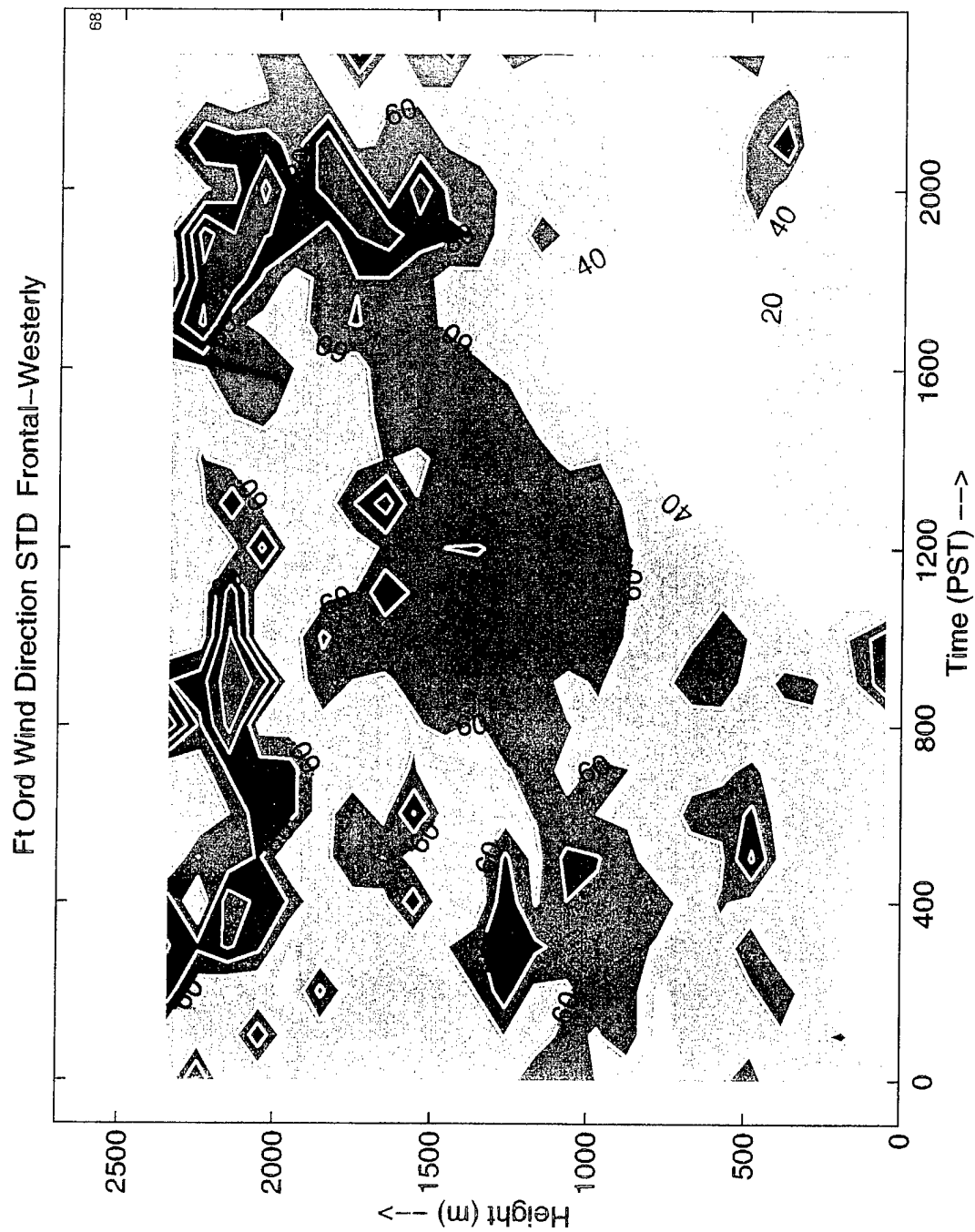


**Figure A2.** Wind direction standard deviations (degrees) associated with frontal-westerly sea breezes at Fort Ord.

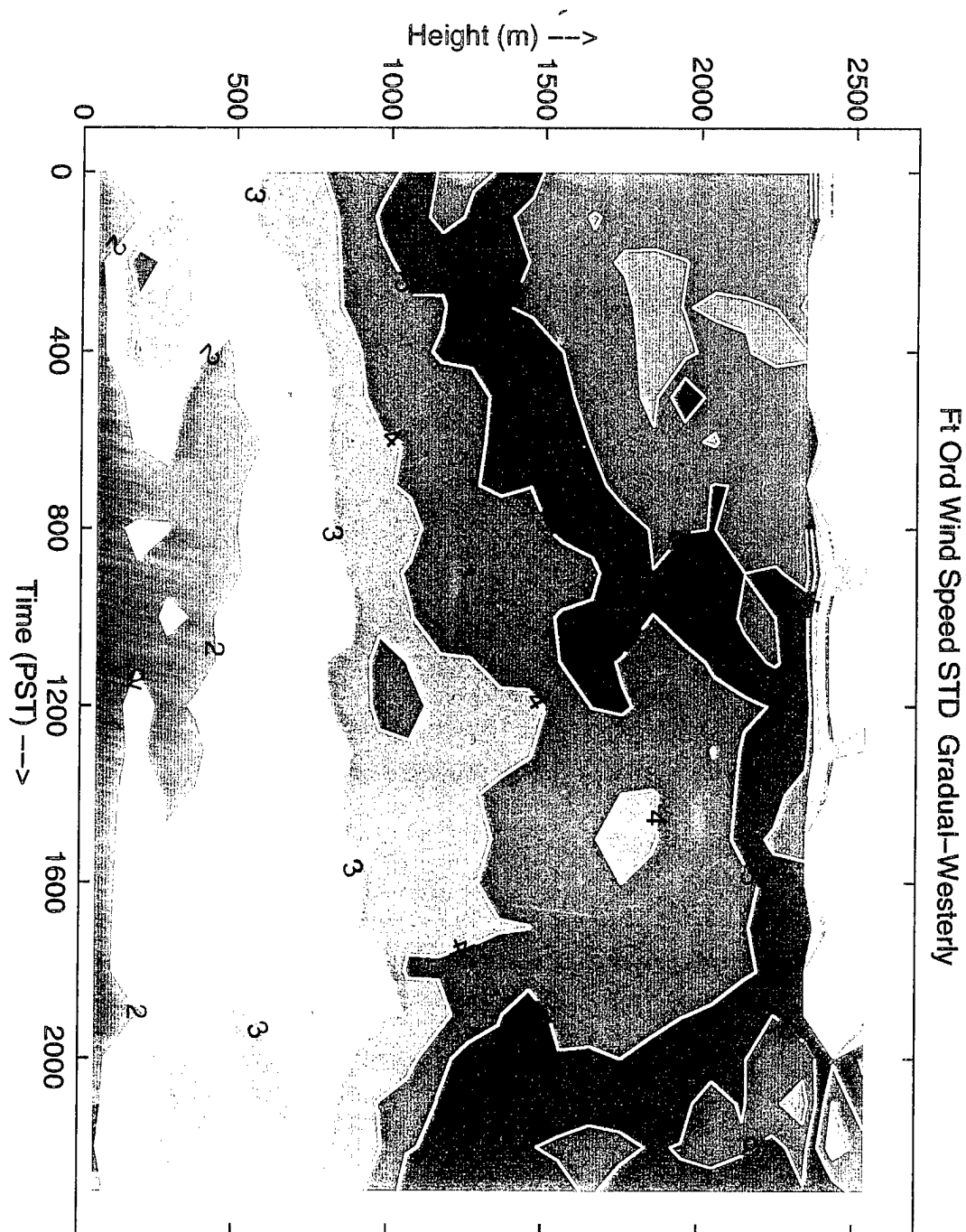


Figure A3. As Figure A1, except gradual-westerly sea breeze.

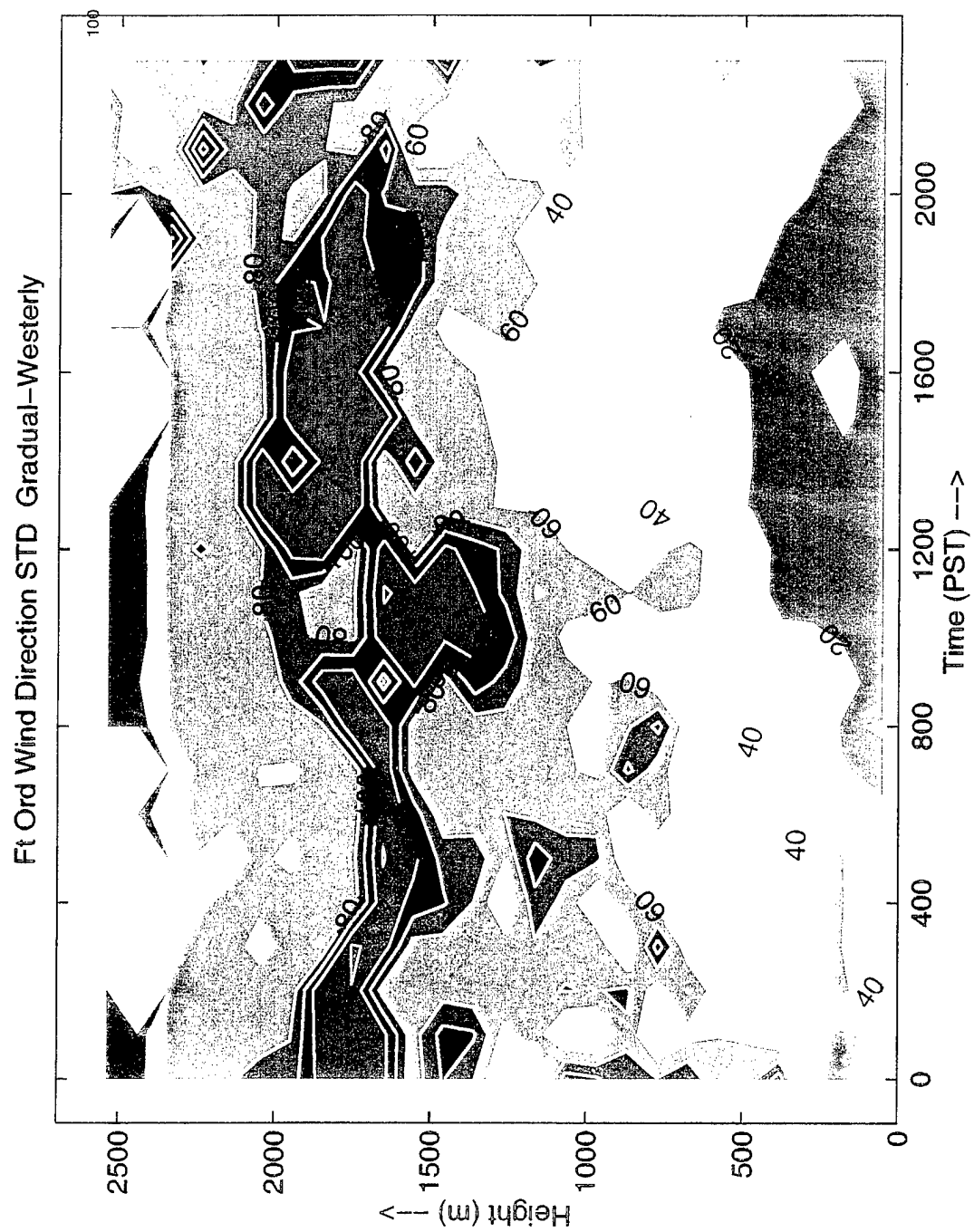


Figure A4. As Figure A2, except gradual-westerly sea breeze.

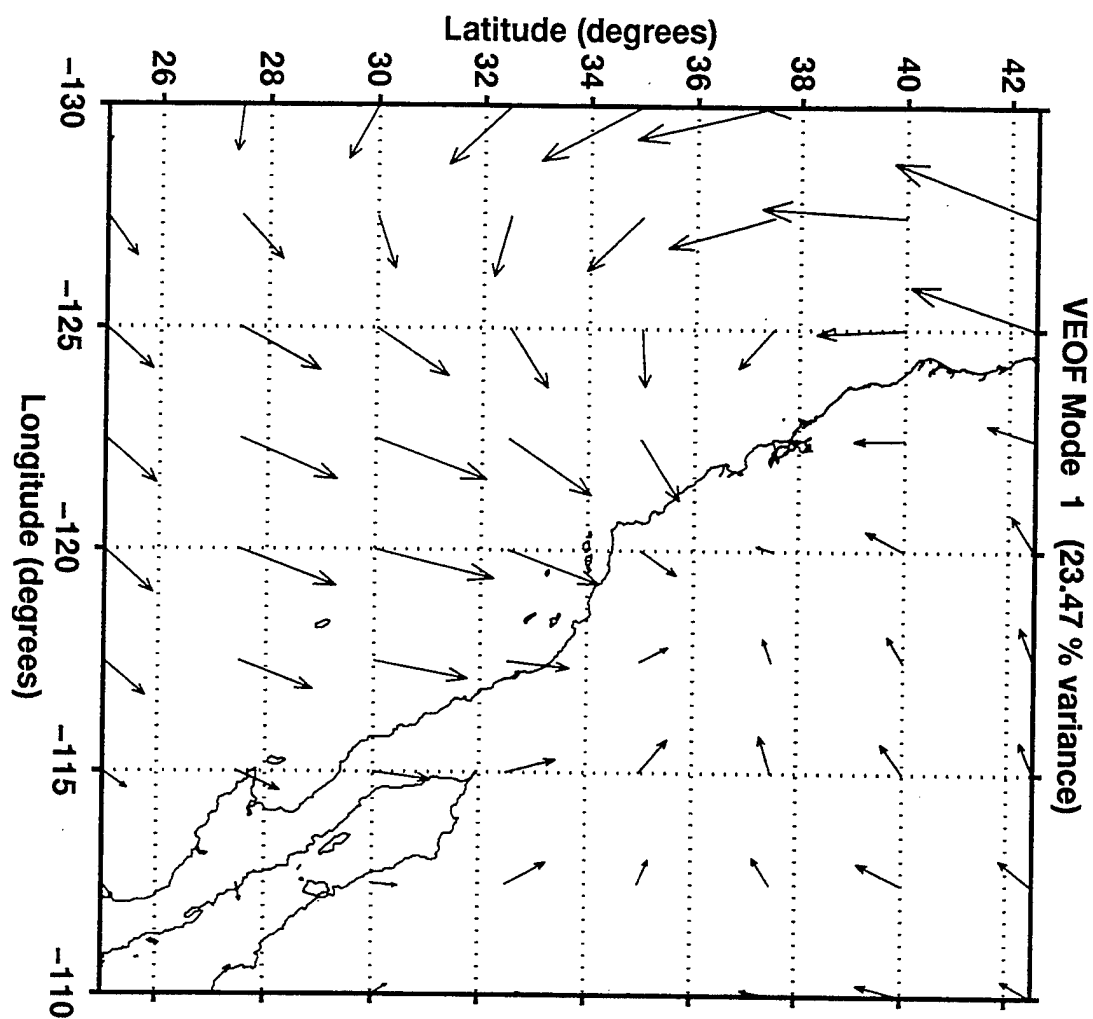


Figure A5. Plot of eigenvectors associated with VEOF mode 1.

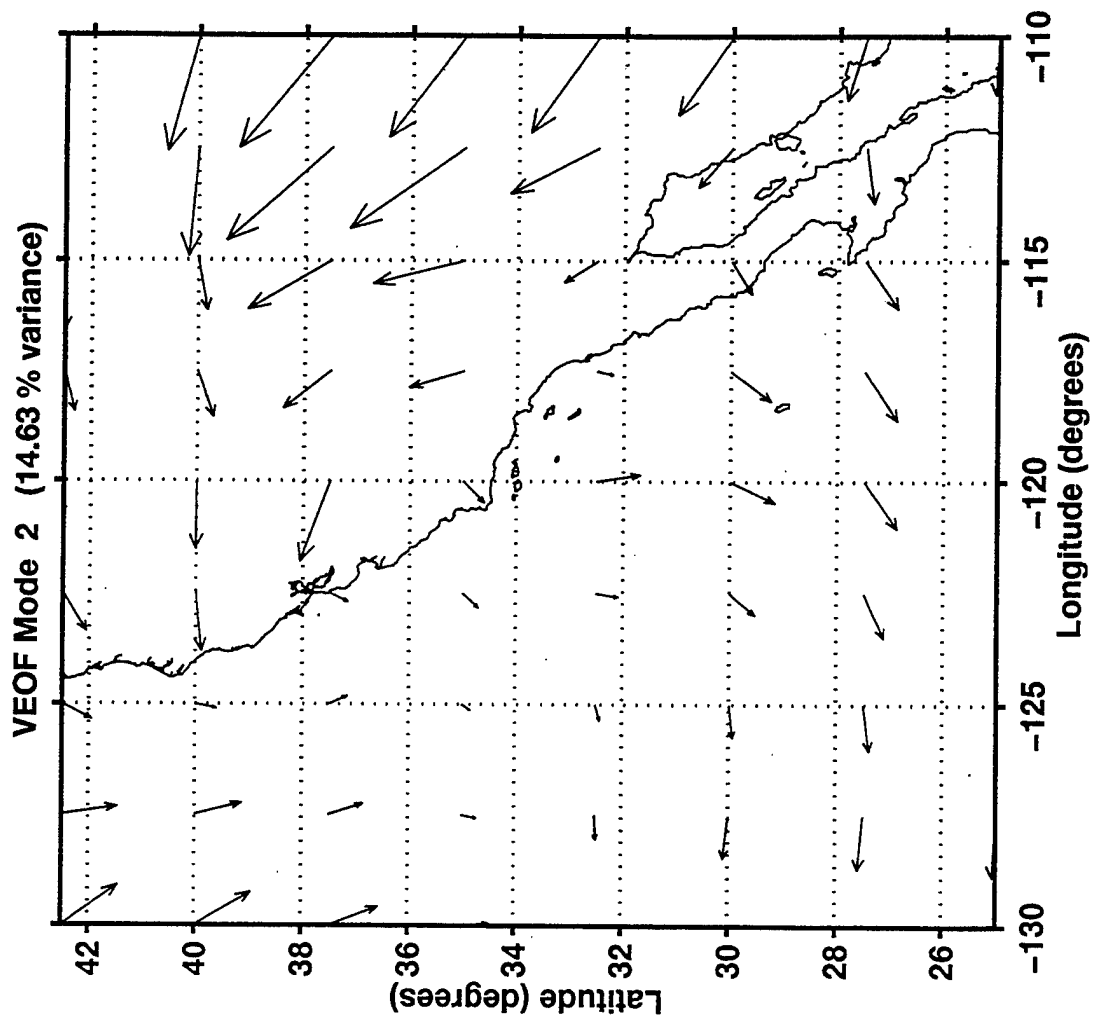


Figure A6. As Figure A5, except VEOF mode 2.



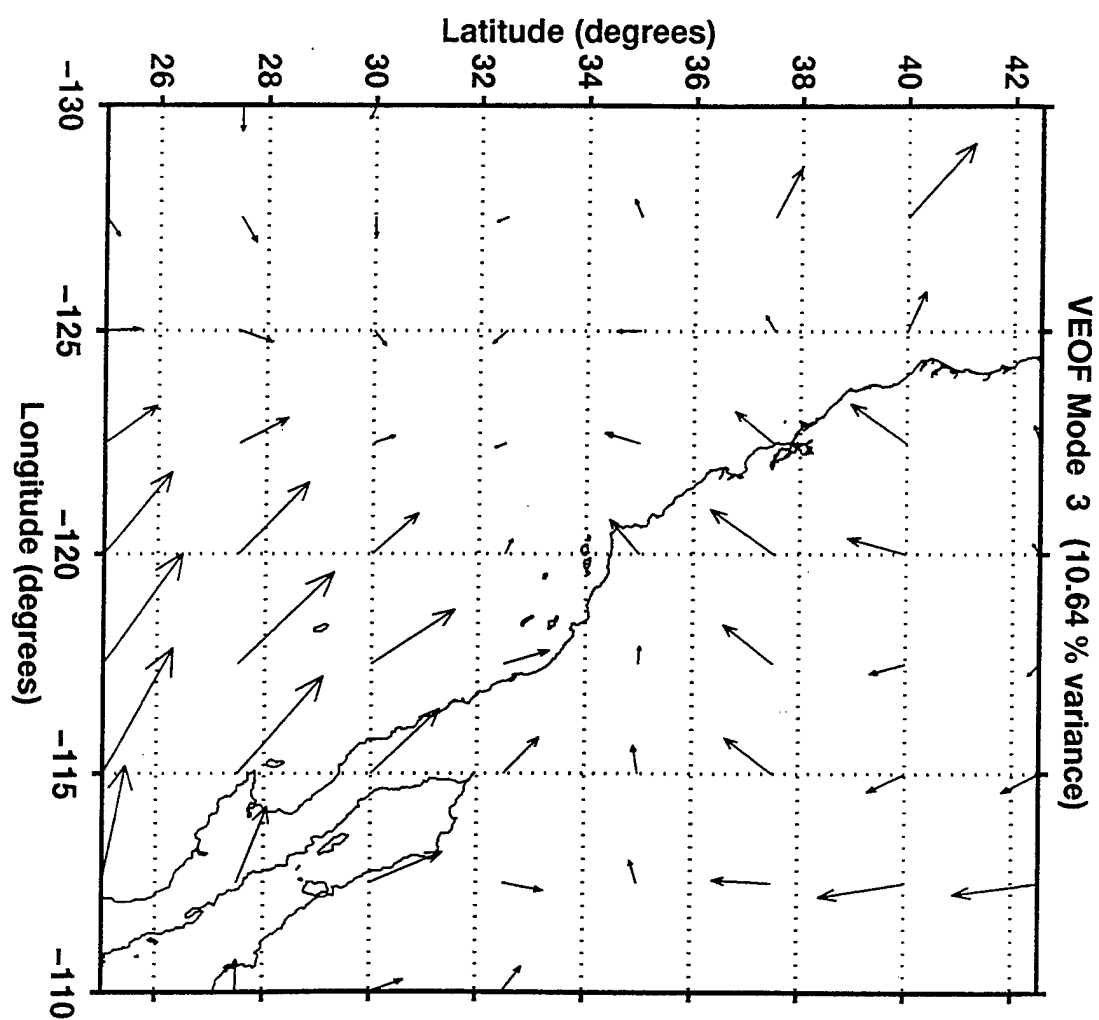
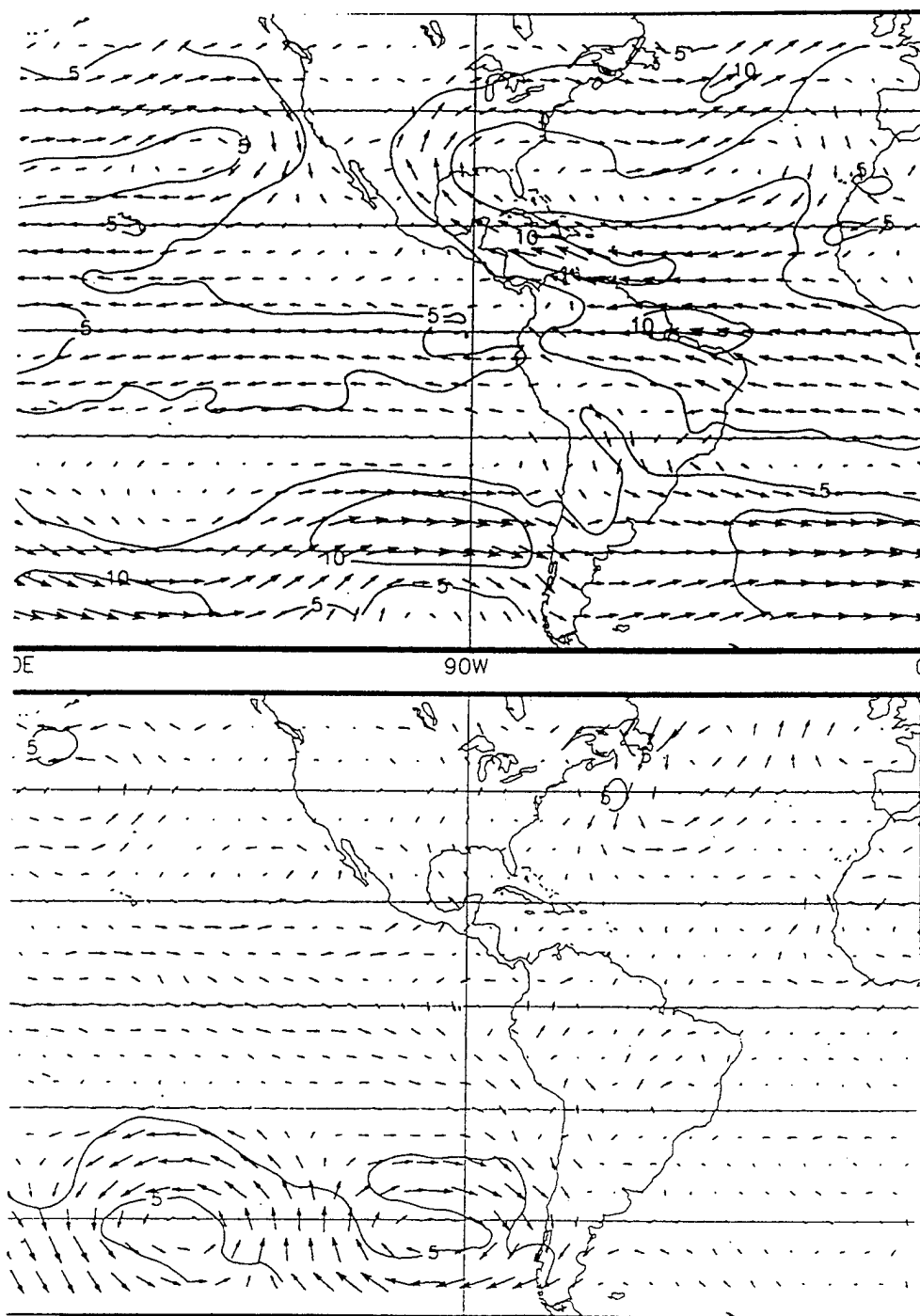


Figure A7. As Figure A5, except VEOF mode 3.



**Figure A8.** a) Mean monthly (top) and b) anomalous (bottom) 850 mb winds for June 1993 (CBD 1993a).

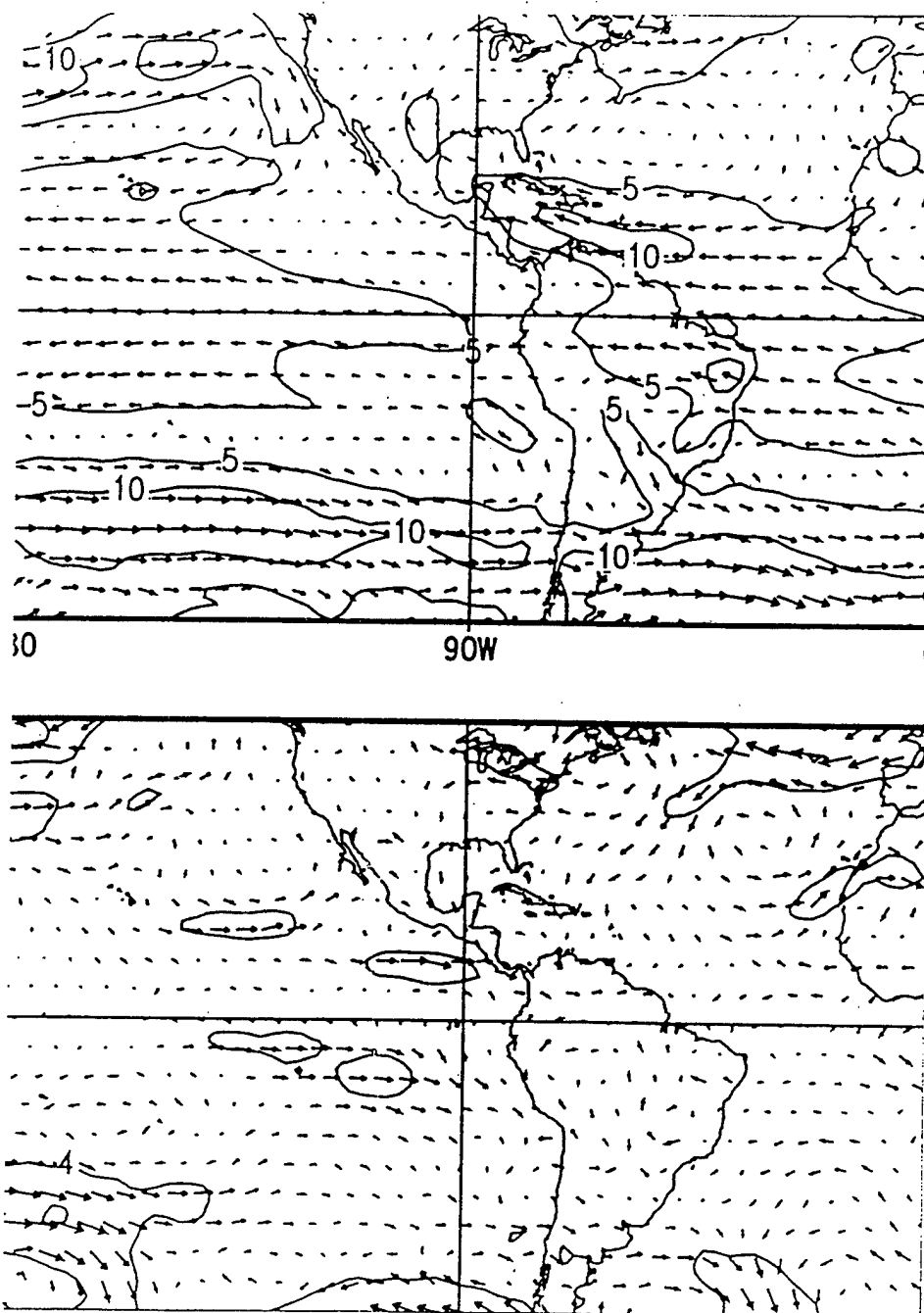
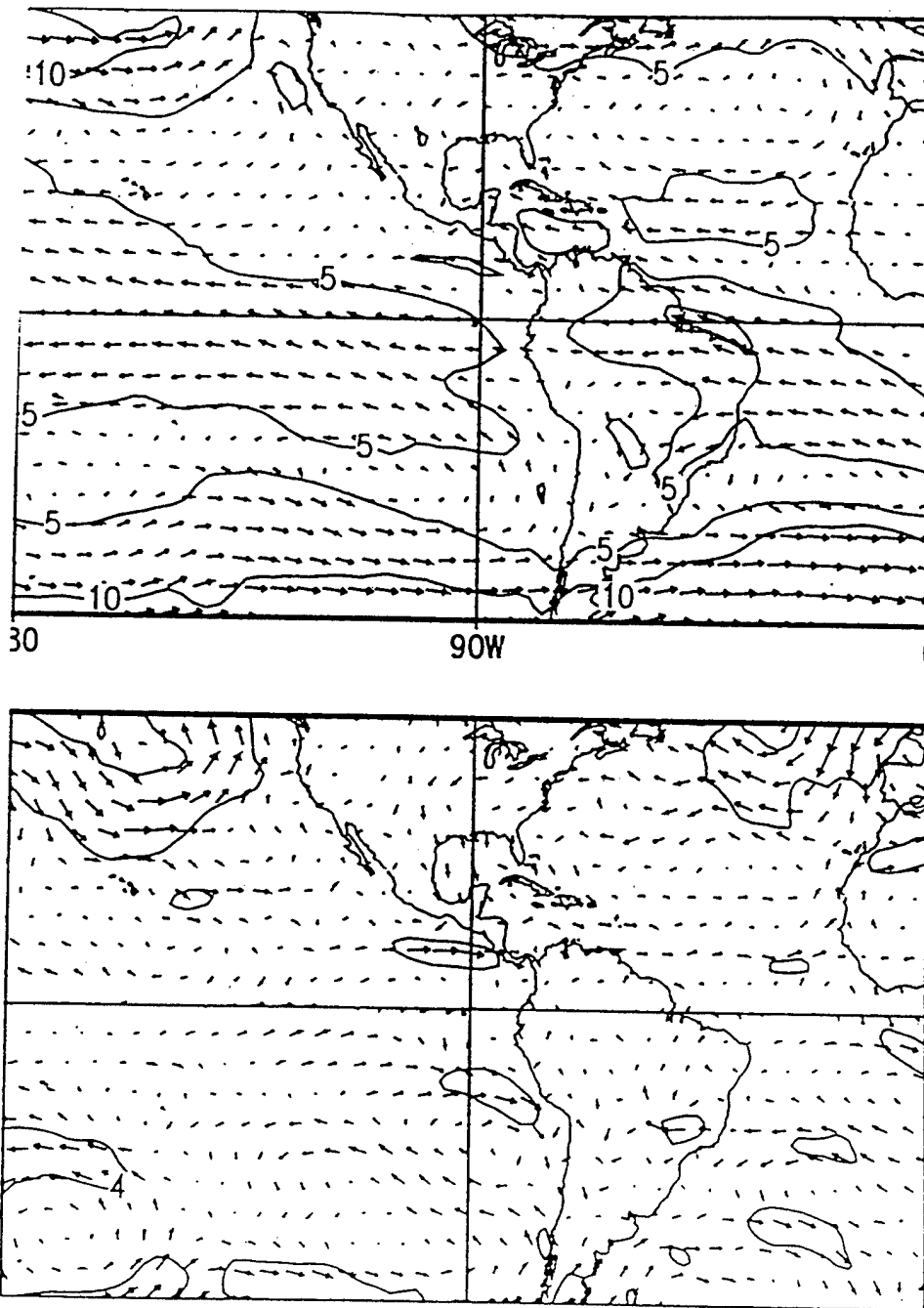
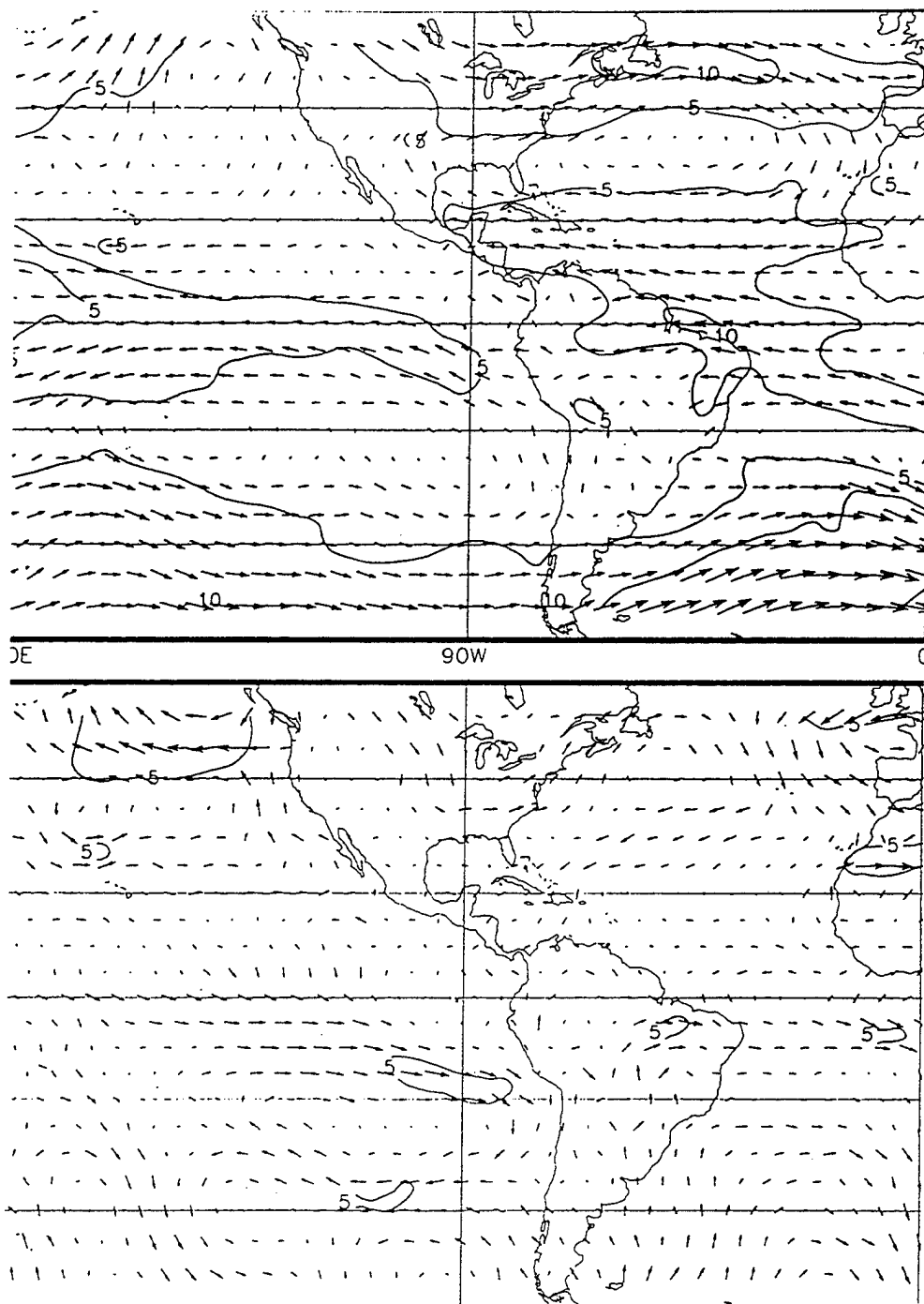


Figure A9. As Figure A8, except June 1995 (CDB 1995a).



**Figure A10.** As Figure A8, except September 1995 (CDB 1995d).



**Figure A11.** As Figure A8, except September 1993 (CDB 1993d).

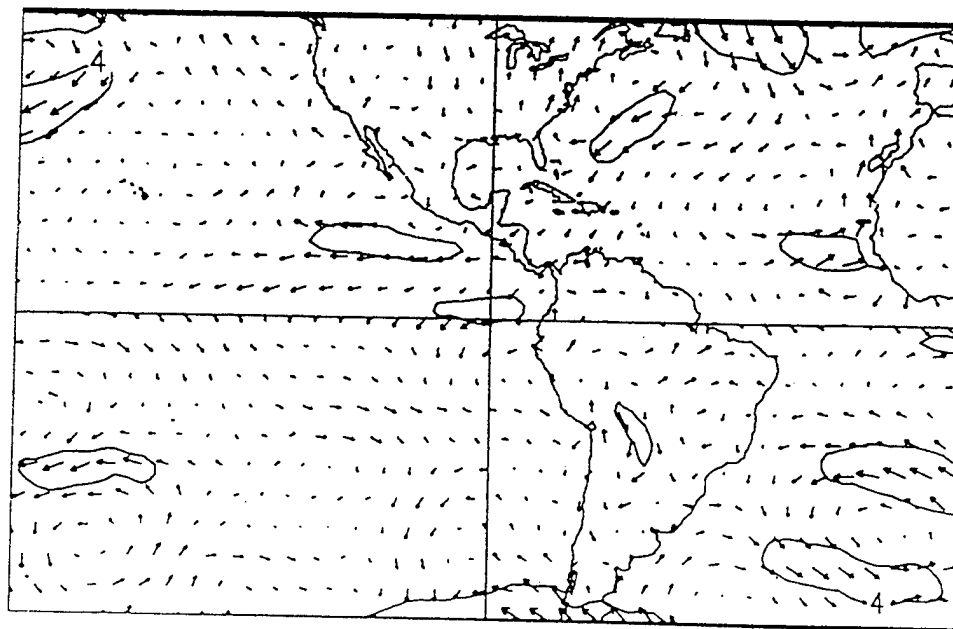
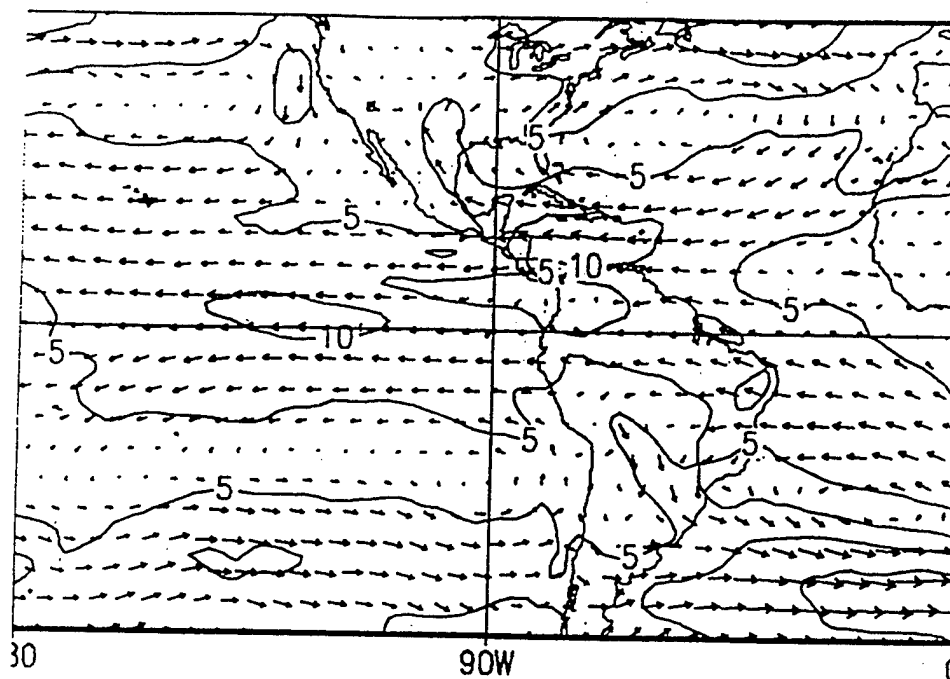


**Figure A12.** As Figure A8, except July 1994 (CDB 1994b).

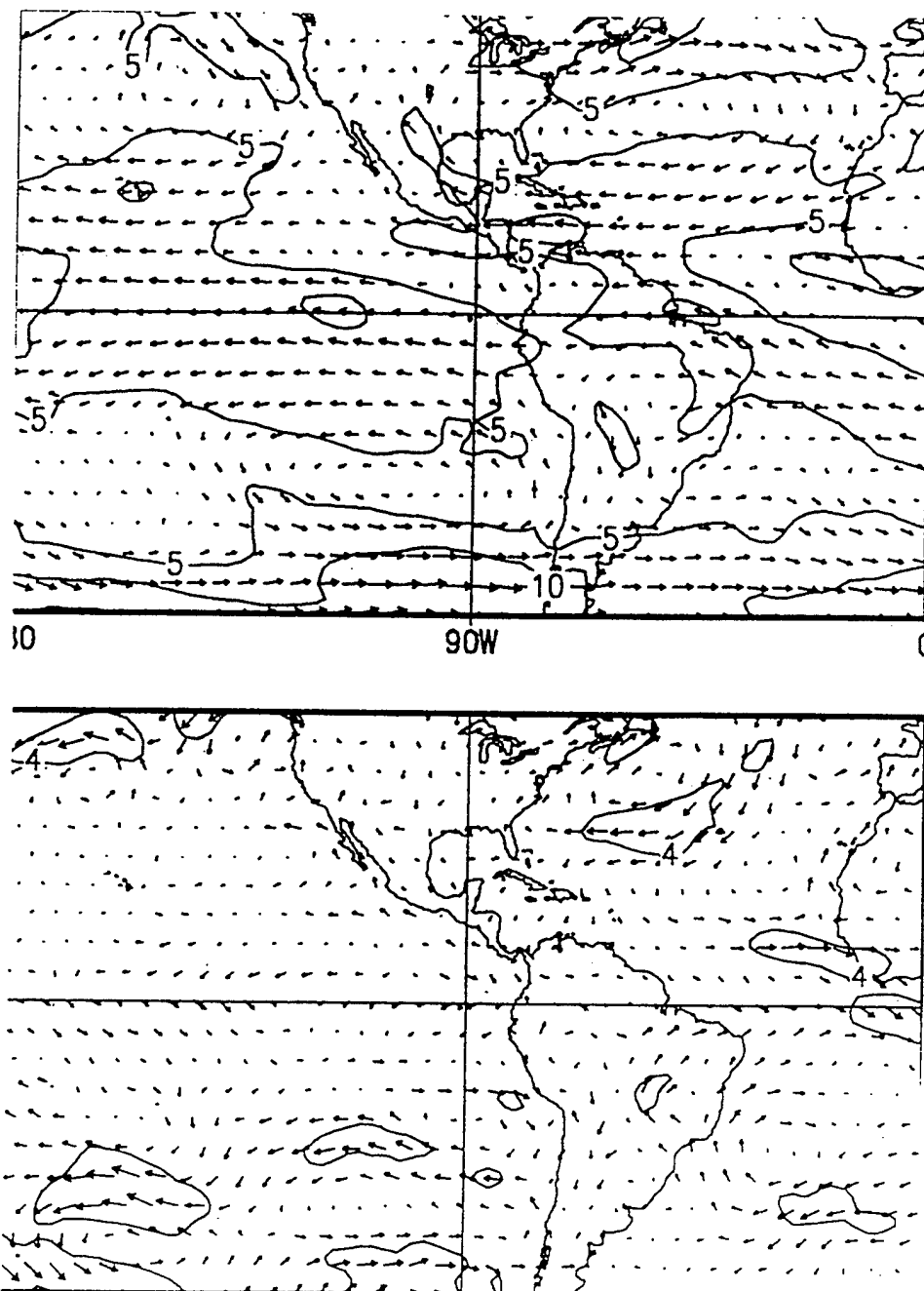


**Figure A13.** As Figure A8, except August 1994 (CDB 1994c).

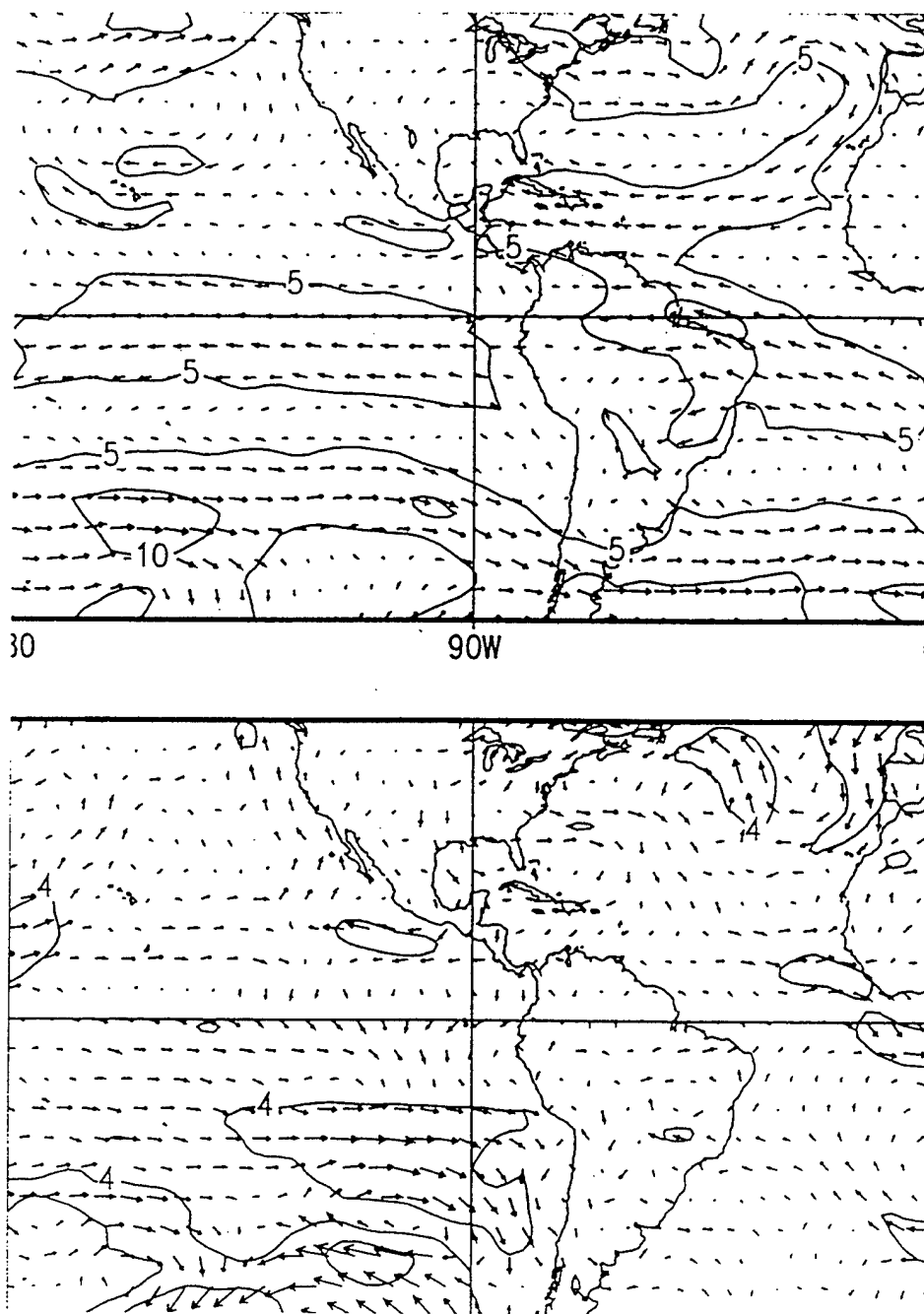


**Figure A14.** As Figure A8, except September 1994 (CDB 1994d).



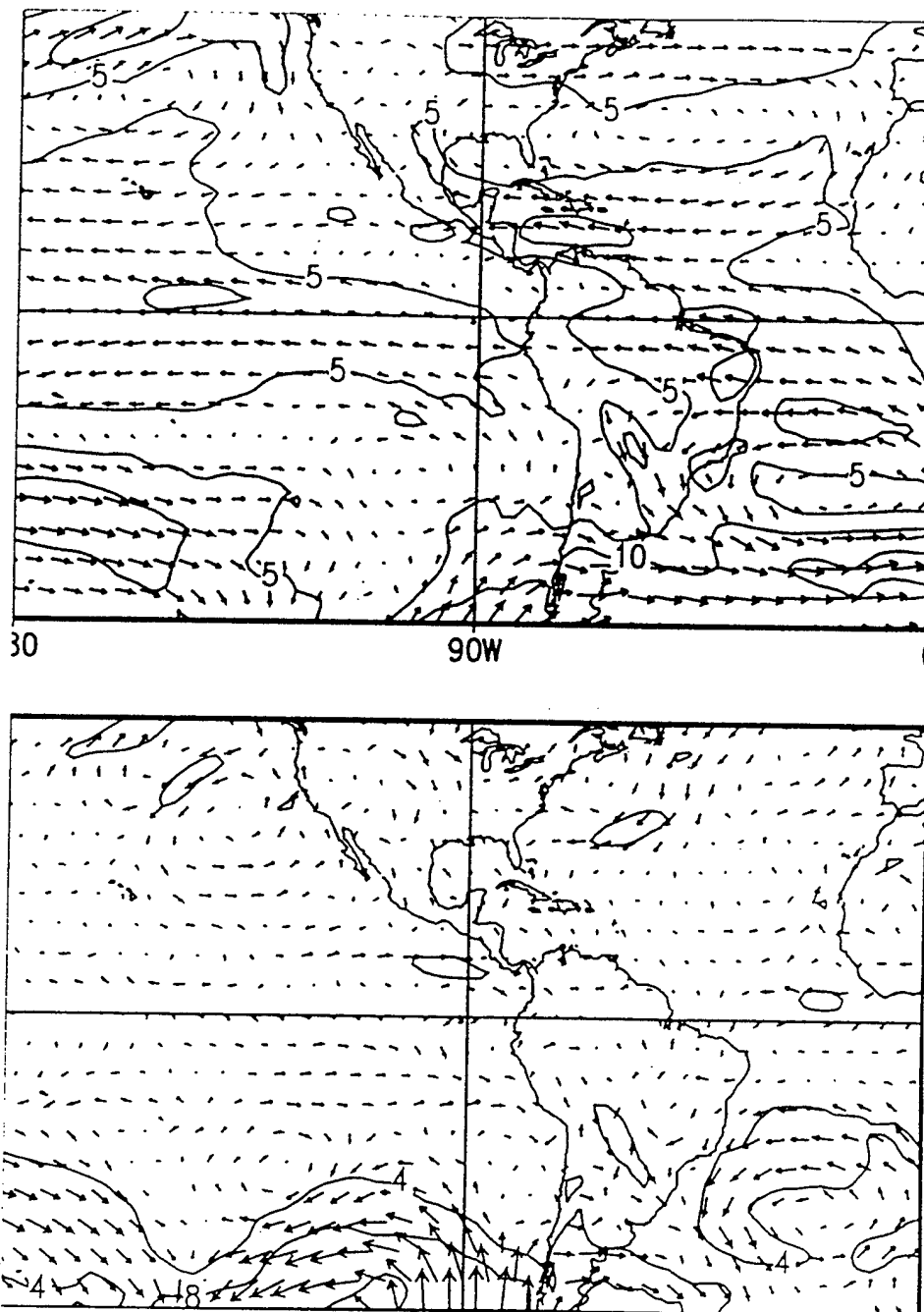


Figure A15. As Figure A8, except July 1995 (CDB 1995b).

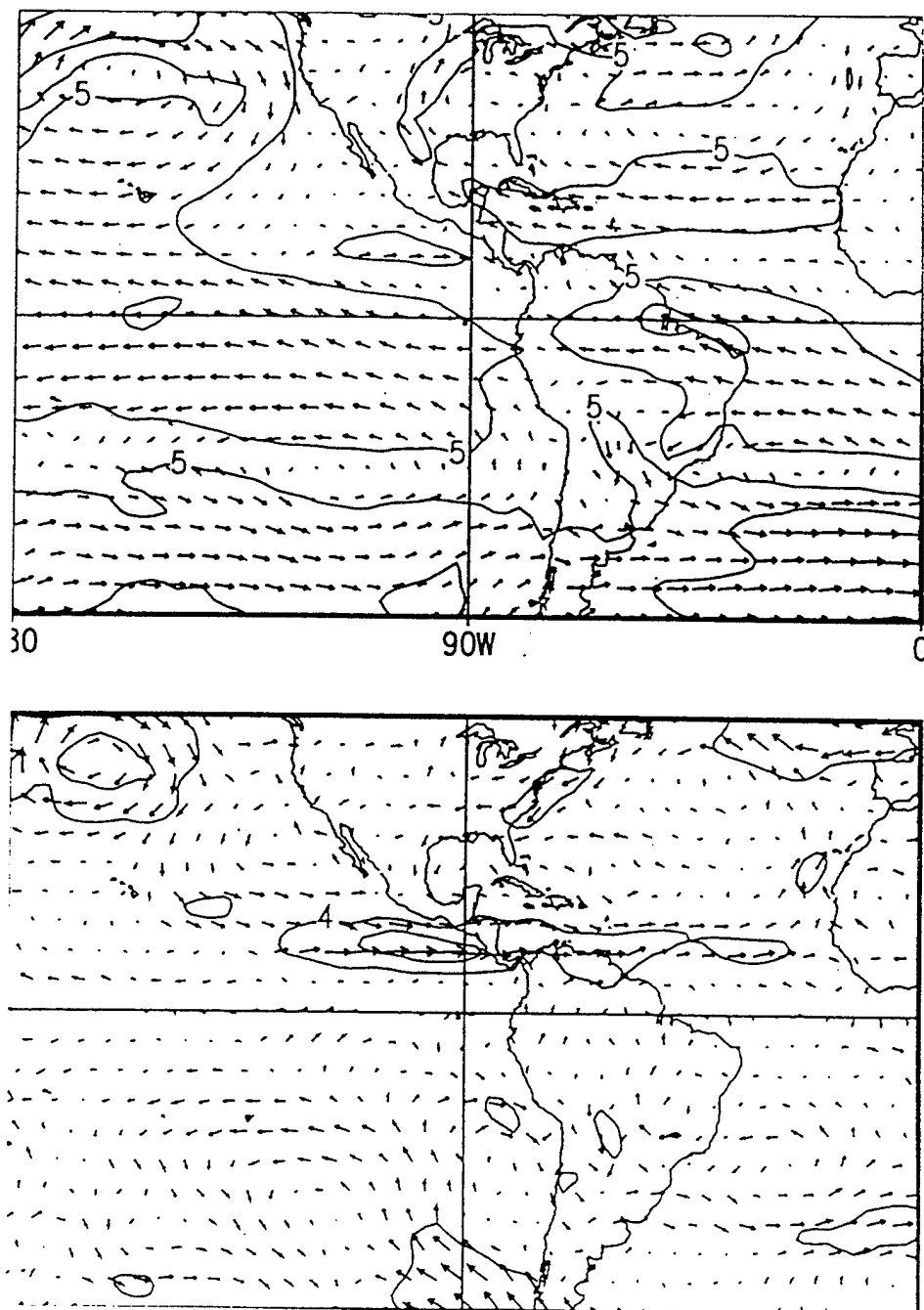


Figure A16. As Figure A8, except August 1995 (CDB 1995c).



## LIST OF REFERENCES

- Arritt, R.W., 1993: Effects of the large-scale flow on characteristic features of the sea breeze. *J. Appl. Meteor.*, **32**, 116-125.
- Atkinson, B.W., 1981: *Meso-scale Atmospheric Circulations*, Academic Press. 495 pp.
- Banta, R.M., 1995: Sea breezes shallow and deep on the California coast. *Mon. Wea. Rev.*, **123**, 3614-3622.
- , L.D. Oliver, and D.H. Levinson, 1993: Evolution of the Monterey Bay sea-breeze layer as observed by pulsed Doppler lidar. *J. Atmos. Sci.*, **50**, 3959-3982.
- Beardsley, R.C., C.E. Dorman, C.A. Friehe, L.K. Rosenfeld, and C.D. Winant, 1987: Local atmospheric forcing during Coastal Ocean Dynamics Experiment: A description of the marine boundary layer and atmospheric conditions over a northern California upwelling region. *J. Geophys. Res.*, **92**, 1467-1488.
- Blanchard, D.O., and R.E. López, 1985: Spatial patterns of convection in south Florida. *Mon. Wea. Rev.*, **113**, 1282-1299.
- Bridger, A.F.C., W.C. Brick, and P.F. Lester, 1993: The structure of the marine inversion layer off the central California coast: Mesoscale conditions. *Mon. Wea. Rev.*, **121**, 335-351.
- CDB, 1993a: *Climate Diagnostic Bulletin 93/6*, Climate Analysis Center, NOAA, Washington, DC., 76 pp.
- , 1993b: *Climate Diagnostic Bulletin 93/7*, Climate Analysis Center, NOAA, Washington, DC., 82 pp.
- , 1993c: *Climate Diagnostic Bulletin 93/8*, Climate Analysis Center, NOAA, Washington, DC., 78 pp.
- , 1993d: *Climate Diagnostic Bulletin 93/9*, Climate Analysis Center, NOAA, Washington, DC., 74 pp.
- , 1994a: *Climate Diagnostic Bulletin 94/6*, Climate Analysis Center, NOAA, Washington, DC., 86 pp.
- , 1994b: *Climate Diagnostic Bulletin 94/7*, Climate Analysis Center, NOAA, Washington, DC., 86 pp.
- , 1994c: *Climate Diagnostic Bulletin 94/8*, Climate Analysis Center, NOAA, Washington, DC., 86 pp.
- , 1994d: *Climate Diagnostic Bulletin 94/9*, Climate Analysis Center, NOAA, Washington, DC.,

86 pp.

—, 1995a: *Climate Diagnostic Bulletin 95/6*, Climate Analysis Center, NOAA, Washington, DC., 84 pp.

—, 1995b: *Climate Diagnostic Bulletin 95/7*, Climate Analysis Center, NOAA, Washington, DC., 78 pp.

—, 1995c: *Climate Diagnostic Bulletin 95/8*, Climate Analysis Center, NOAA, Washington, DC., 82 pp.

—, 1995d: *Climate Diagnostic Bulletin 95/9*, Climate Analysis Center, NOAA, Washington, DC., 78 pp.

Elliott, D.L., and J.J. O'Brien, 1977: Observational studies of the marine boundary layer over an upwelling region. *Mon. Wea. Rev.*, **105**, 86-98.

Estoque, M.A., 1961: A theoretical investigation of the sea breeze. *Quart. J. Roy. Met. Soc.*, **87**, 136-146.

—, 1962: The sea breeze as a function of the prevailing synoptic situation. *J. Atmos. Sci.*, **19**, 244-250.

Fagen, M., 1988: The sea breeze circulation during the land sea breeze experiment (LASBEX) in central California, M.S. Thesis, Naval Postgraduate School, Monterey, California, 127 pp.

Fisher, E.L., 1960: An observational study of the sea breeze. *J. Meteor.*, **17**, 645-660.

Foster, M.D., 1993: *Evolution of diurnal surface winds and surface currents for Monterey Bay*. M.S. Thesis, Naval Postgraduate School, Monterey, California, 100 pp.

Gould, K.J., and H.E. Fuelberg, 1996: The use of GOES-8 imagery and RAMSDIS to develop a sea climatology over the Florida panhandle. Preprint: Eighth Conference on Satellite Meteorology and Oceanography, Atlanta, Georgia, 100-104.

—, C.G. Herbster, J.D. Korotky, P.H. Ruscher, 1996: WSR-88D, GOES-8, and MM5 mesoscale model observations of the Florida panhandle sea breeze circulation under different synoptic flow regimes. Preprint: Conference on Coastal Oceanic and Atmospheric Prediction, Atlanta, Georgia, 364-369.

Hardy, D.M., 1977: Empirical eigenvector analysis of vector observations. *Geophys. Res. Lett.*, **4**, 319-320.

Harr, P.A., 1993: *Large-scale Circulation Regimes and Tropical Cyclone Characteristics over the Western Pacific Ocean*. Ph.D. Dissertation, Naval Postgraduate School, Monterey, California, 275 pp.

Haurwitz, B., 1947: Comments on the sea breeze circulation. *J. Meteor.*, **4**, 1-8.

Hogan, T.F., 1996: Personal communication.

—, and L.R. Brody, 1993: Sensitivity studies for the Navy's global forecast model parameterizations and evaluation of the improvements to NOGAPS. *Mon. Wea. Rev.*, **121**, 2373-2395.

Holton, J.R., 1979: *An Introduction to Dynamic Meteorology*, Academic Press. 391 pp.

Hsu, S.A., 1988: *Coastal Meteorology*, Academic Press. 260 pp.

Intrieri, J.M., C.G. Little, W.J. Shaw, R.M. Banta, P.A. Durkee, and R.M. Hardesty, 1990: The land/sea breeze experiment (LASBEX). *Bull. Amer. Meteor. Soc.*, **71**, 656-664.

Johnson, A. Jr., J.J. O'Brien, 1973: A study of an Oregon sea breeze event. *J. Appl. Meteor.*, **12**, 1267-1283.

Klink, K., and C.J. Willmott, 1989: Principle components of the surface wind field in the United States: A comparison of analyses based upon wind velocity, direction, and speed. *J. Climatol.*, **9**, 293-308.

Knapp, M.C., 1994: *Synoptic-scale influence on the Monterey Bay sea-breeze*. M.S. Thesis, Naval Postgraduate School, Monterey, California, 98 pp.

Kondo, J., 1975: Air-sea bulk transfer coefficients in diabatic conditions. *Boundary Layer Met.*, **9**, 91-112.

Koschmieder, H., and K. Hornickel, 1936: Dansiger seewind studien I. *Danziger Meteorol., Forschungs-arbeiten*, **8**.

—, 1941: Dansiger seewind studien II. *Danziger Meteorol., Forschungs-arbeiten*, **10**.

—, 1942: Dansiger seewind studien III. *Danziger Meteorol., Forschungs-arbeiten*, **11**.

Kutzbach, J.E., 1967: Empirical eigenvectors of sea-level pressure, surface temperature, and precipitation complexes over North America. *J. Appl. Meteor.*, **6**, 791-802.

Leith, C.E., 1973: The standard error of time-average estimates of climatic means. *J. Appl. Meteor.*, **12**, 1066-1069.

- Lorenz, E.N., 1956: Empirical orthogonal functions and statistical weather prediction. Science Report 1, Statistical Forecasting Project, Department of Meteorology, Massachusetts Institute of Technology. [NTIS AD 110268} 49 pp.
- May, P.T., and J.M. Wilczak, 1993: Diurnal and seasonal variations of boundary-layer structure observed with a radar wind profiler and RASS. *Mon. Wea. Rev.*, **121**, 673-682.
- , K.P. Moran, and R.G. Strauch, 1989: The accuracy of RASS Temperature Measurements. *J. Appl. Meteor.*, **28**, 1329-1335.
- McCumber, M.C., 1980: *A Numerical Simulation of the Influence of Heat and Moisture Fluxes upon Mesoscale Circulations*. Ph.D. Dissertation, Department of Environmental Science, University of Virginia, Charlottesville, 255 pp.
- Moran, J.M., and M.D. Morgan, 1986: *Meteorology: The Atmosphere and the Science of Weather*, Burgess Press. 502 pp.
- North, G.R., T.L. Bell, R.F. Cahalan, and F.J. Moeng, 1982: Sampling errors in the estimation of Empirical Orthogonal Functions. *Mon. Wea. Rev.*, **110**, 699-706.
- Nuss, W.A., 1993: *Lecture Notes for MR4800, Coastal Meteorology*, Naval Postgraduate School, Monterey, California.
- Paulus, R.A., 1992: Personal communication.
- Pielke, R.A., 1984: *Mesoscale Meteorological Modelling*, Academic Press. 612 pp.
- Richman, M.B., 1986: Rotation of principle components. *J. Climatol.*, **6**, 293-335.
- Round, R.D., 1993: *Climatology and analysis of the Monterey Bay sea breeze*. M.S. Thesis, Naval Postgraduate School, Monterey, California, 113 pp.
- Segal, M., and R.W. Arritt, 1992: Nonclassical mesoscale circulations caused by surface sensible heat-flux gradients. *Bull. Amer. Meteor. Soc.*, **73**, 1593-1604.
- , R. Avissar, M.C. McCumber, and R.A. Pielke, 1988: Evaluating vegetation effects on the generation and modification of mesoscale circulations. *Bull. Amer. Meteor. Soc.*, **45**, 2268-2291.
- Schroeder, M.J., M.A. Fosberg, O.P. Cramer, and C.A. O'Dell, 1967: Marine air invasion of the Pacific coast: a problem analysis. *Bull. Amer. Meteor. Soc.*, **48**, 802-808.
- Simpson, J.E., 1995: Diurnal changes in sea-breeze direction. *J. Appl. Meteor.*, **35**, 1166-1169.
- , 1994: *Sea Breeze and Local Wind*, Cambridge University Press. 234 pp.

Stec, J.D., 1996: *Wind profiler study of the central California sea/land breeze*. M.S. Thesis, Naval Postgraduate School, Monterey, California, 98 pp.

Weber, B.L., and D.B. Wuertz, 1990: Comparison of rawinsonde and wind profiler radar measurements. *J. Atmos. Oceanic. Technol.*, **7**, 157-174.

Wexler, R., 1946: Theory and Observations of land and sea breezes. *Bull. Amer. Met. Soc.*, **27**, 272-287.

Zhong, S., and E.S. Takle, 1993: The effects of large-scale winds on the sea-land-breeze circulations in an area of complex coastal heating. *J. Appl. Meteor.*, **32**, 1181-1195.





# INITIAL DISTRIBUTION LIST

	No. Copies
1. Defense Technical Information Center 8725 John J. Kingman Rd., STE 0944 Ft. Belvoir, VA 22060-6218	2
2. Dudley Knox Library Naval Postgraduate School 411 Dyer Rd. Monterey, CA 93943-5101	2
3. Dr. Carlyle H. Wash (Code MR/Wx) Department of Meteorology Naval Postgraduate School Monterey, CA 93943-5000	4
4. Dr. Kenneth L. Davidson (Code MR/Ds) Department of Meteorology Naval Postgraduate School Monterey, CA 93943-5000	1
5. Dr. Wendell A. Nuss (Code MR/Nu) Department of Meteorology Naval Postgraduate School Monterey, CA 93943-5000	1
6. Dr. Philip A. Durkee (Code MR/De) Department of Meteorology Naval Postgraduate School Monterey, CA 93943-5000	1
7. Dr. Patrick A. Harr (Code MR/Hp) Department of Meteorology Naval Postgraduate School Monterey, CA 93943-5000	1
8. Dr. Jeffery D. Paduan (Code OC/Pd) Department of Oceanography Naval Postgraduate School Monterey, CA 93943-5000	1

- |   |   |
|---|---|
| 9. Dr. Craig Rasmussen (Code MA/Ra)<br>Department of Mathematics<br>Naval Postgraduate School<br>Monterey, CA 93943-5000    | 1 |
| 10. Dr. Roger T. Williams (Code MR/Wu)<br>Department of Meteorology<br>Naval Postgraduate School<br>Monterey, CA 93943-5000 | 1 |
| 11. Dr. Qing Wang (Code MR/Qg)<br>Department of Meteorology<br>Naval Postgraduate School<br>Monterey, CA 93943-5000         | 1 |
| 12. Richard J. Lind (Code MR/Ln)<br>Department of Meteorology<br>Naval Postgraduate School<br>Monterey, CA 93943-5000       | 1 |
| 13. Mary S. Jordan (Code MR/Jr)<br>Department of Meteorology<br>Naval Postgraduate School<br>Monterey, CA 93943-5000        | 1 |
| 14. Mike Cook (Code OC/Ck)<br>Department of Oceanography<br>Naval Postgraduate School<br>Monterey, CA 93943-5000            | 1 |
| 15. LCDR Michael D. Foster, USN<br>2196 Cheshire Drive<br>Birmingham, AL 35235  | 3 |
| 16. Oceanographer of the Navy<br>Naval Observatory<br>34th and Massachusetts Avenue NW<br>Washington, DC 20390              | 1 |
| 17. Commander<br>Naval Oceanography Command<br>Stennis Space Ctr, MS 39529-5000   | 1 |
| 18. Commanding Officer<br>Naval Oceanographic Office<br>Stennis Space Ctr<br>Bay St. Louis, MS 39522-5001                   | 1 |